

**A RADIOMETRIC STUDY OF
SEDIMENT ACCUMULATION AND ACCRETION IN
TIDAL MARSHES OF
DELAWARE AND NEW JERSEY**

by

Brandon Michael Boyd

A dissertation submitted to the Faculty of the University of Delaware in partial fulfillment of the requirements for the degree of Doctor of Philosophy in Oceanography

Summer 2016

© 2016 Brandon M. Boyd
All Rights Reserved

ProQuest Number: 10190928

All rights reserved

INFORMATION TO ALL USERS

The quality of this reproduction is dependent upon the quality of the copy submitted.

In the unlikely event that the author did not send a complete manuscript and there are missing pages, these will be noted. Also, if material had to be removed, a note will indicate the deletion.



ProQuest 10190928

Published by ProQuest LLC (2016). Copyright of the Dissertation is held by the Author.

All rights reserved.

This work is protected against unauthorized copying under Title 17, United States Code
Microform Edition © ProQuest LLC.

ProQuest LLC.
789 East Eisenhower Parkway
P.O. Box 1346
Ann Arbor, MI 48106 - 1346

**A RADIOMETRIC STUDY OF
SEDIMENT ACCUMULATION AND ACCRETION IN
TIDAL MARSHES OF
DELAWARE AND NEW JERSEY**

by

Brandon Michael Boyd

Approved: _____
Mark A. Moline, Ph.D.
Director of the School of Marine Science and Policy

Approved: _____
Moshen Badiey, Ph.D.
Acting Dean of the College of Earth, Ocean, and Environment

Approved: _____
Ann L. Ardis, Ph.D.
Senior Vice Provost for Graduate and Professional Education

I certify that I have read this dissertation and that in my opinion it meets the academic and professional standard required by the University as a dissertation for the degree of Doctor of Philosophy.

Signed:

Christopher K. Sommerfield, Ph.D.
Professor in charge of dissertation

I certify that I have read this dissertation and that in my opinion it meets the academic and professional standard required by the University as a dissertation for the degree of Doctor of Philosophy.

Signed:

William J. Ullman, Ph.D.
Member of dissertation committee

I certify that I have read this dissertation and that in my opinion it meets the academic and professional standard required by the University as a dissertation for the degree of Doctor of Philosophy.

Signed:

Joanna K. York, Ph.D.
Member of dissertation committee

I certify that I have read this dissertation and that in my opinion it meets the academic and professional standard required by the University as a dissertation for the degree of Doctor of Philosophy.

Signed:

Joseph Z. Gailani, Ph.D.
Member of dissertation committee

I certify that I have read this dissertation and that in my opinion it meets the academic and professional standard required by the University as a dissertation for the degree of Doctor of Philosophy.

Signed:

Joseph T. Kelley, Ph.D.
Member of dissertation committee

I certify that I have read this dissertation and that in my opinion it meets the academic and professional standard required by the University as a dissertation for the degree of Doctor of Philosophy.

Signed:

Tracy E. Quirk, Ph.D.
Member of dissertation committee

ACKNOWLEDGMENTS

This research was supported primarily by a U.S. Department of Defense Science, Math, and Research for Transformation Fellowship and partly by a National Oceanic and Atmospheric Administration National Estuarine Research Reserve Graduate Research Fellowship. The data used in this dissertation were generated during a New Jersey SeaGrant study (NJSG/NOAA Grant #6210-0011) awarded to D. Velinsky (The Academy of Natural Sciences of Drexel University) and T. Quirk (Louisiana State University).

TABLE OF CONTENTS

LIST OF TABLES	x
LIST OF FIGURES	xii
ABSTRACT	xviii
Chapter	
1 INTRODUCTION	1
1.1 Tidal Marsh Accumulation and Accretion	1
1.2 Geochronology using ¹³⁷ Cs and ²¹⁰ Pb	2
1.3 Contributions of this dissertation.....	4
REFERENCES	6
2 HYDROGEOMORPHIC INFLUENCES ON SALT MARSH SEDIMENT ACCUMULATION AND ACCRETION IN TWO ESTUARIES OF THE U.S. MID-ATLANTIC COAST.....	9
2.1 Abstract.....	9
2.2 Introduction	10
2.3 Study Area.....	12
2.3.1 Delaware Bay Estuary	14
2.3.2 Barnegat Bay-Little Egg Harbor Estuary	15
2.4 Methods	16
2.4.1 Hydrogeomorphic analysis	16
2.4.2 Marsh core sampling	18
2.4.3 Soil physical properties	18
2.4.4 Radionuclide measurements	21
2.4.5 Marsh accretion and mass accumulation rates	21
2.5 Results and Interpretation.....	23
2.5.1 Marsh hydrogeomorphic characteristics.....	23
2.5.2 Marsh soil properties	27

2.5.3	Marsh accretion and mass accumulation rates	30
2.5.4	Inter-estuary comparison	36
2.6	Discussion.....	37
2.6.1	Hydrogeomorphic controls on sediment accumulation and accretion	37
2.6.2	Potential feedbacks between mass accumulation and accretion..	42
2.6.3	Marsh accretion and inundation potential	45
2.7	Conclusions	47
REFERENCES		48
3	ASSESSMENT OF ²¹⁰ Pb AND ¹³⁷ Cs CHRONOLOGICAL MODELS FOR TIDAL MARSH DEPOSITS	56
3.1	Abstract.....	56
3.2	Introduction	57
3.2.1	Tidal marsh geochronology	57
3.2.2	¹³⁷ Cs sources and geochronology	58
3.2.3	²¹⁰ Pb geochronology	61
3.2.4	²¹⁰ Pb chronological models	62
3.2.5	Objectives	66
3.3	Methods	66
3.3.1	Soil core collection	66
3.3.2	Radionuclide analysis	67
3.3.3	Calculation of radionuclide inventories.....	68
3.3.4	¹³⁷ Cs and ²¹⁰ Pb geochronologies and mass accumulation rates...	68
3.4	Results	70
3.4.1	¹³⁷ Cs activities and inventories	70
3.4.2	Excess ²¹⁰ Pb activities and inventories	74
3.4.3	²¹⁰ Pb chronologies and accumulation rates	79
3.5	Discussion.....	83
3.5.1	Application of ¹³⁷ Cs and ²¹⁰ Pb geochronology.....	83
3.5.2	Summary.....	84
3.6	Conclusions	87

REFERENCES	89
4 CAPTURE AND BURIAL OF ²¹⁰ PB AND ¹³⁷ CS IN SALT MARSHES.....	93
4.1 Abstract.....	93
4.2 Introduction and Background	94
4.2.1 Sources of ²¹⁰ Pb _u and ¹³⁷ Cs in tidal marsh systems.....	96
4.2.2 ²¹⁰ Pb and ¹³⁷ Cs accumulation by plants and soils.....	99
4.3 Methods	101
4.3.1 Sample collection and processing	101
4.3.2 Separation of soil solids.....	103
4.3.3 Aboveground biomass samples	104
4.3.4 Plant-radionuclide standard preparation.....	107
4.3.5 Radionuclide analysis	108
4.4 Results	109
4.4.1 Aboveground activities.....	109
4.4.2 Marsh soil composition and radionuclide activity.....	114
4.4.3 Soil inventories of excess ²¹⁰ Pb.....	118
4.5 Discussion.....	123
4.5.1 Plant capture and burial of excess ²¹⁰ Pb in marsh soils.....	123
4.5.2 Implications to marsh geochronology	125
4.5.3 Methodological and analytical considerations	126
4.6 Conclusions	126
REFERENCES	128
5 POTENTIAL USE OF ²⁴¹ AM AS A SEDIMENT CHRONOMETER IN NORTH AMERICAN TIDAL MARSHES	133
5.1 Abstract.....	133
5.2 Introduction	134
5.2.1 Motivation	134
5.2.2 Sources of ²⁴¹ Am in the environment	134
5.2.3 ²⁴¹ Am as a particle tracer and chronometer	136
5.3 Methods	137

5.3.1	Measurement of radionuclides and soil physical properties.....	137
5.3.2	Fallout and theoretical ²⁴¹ Am inventory	138
5.4	Results	139
5.4.1	Activities and profiles of ²⁴¹ Am and ¹³⁷ Cs	139
5.4.2	Soil inventory of ²⁴¹ Am.....	141
5.5	Discussion.....	143
5.5.1	Attribution of ²⁴¹ Am to AWT fallout	143
5.5.2	Advantages of ²⁴¹ Am as a geochronometer.....	144
5.6	Conclusions	145
REFERENCES.....		146
6	SUMMARY AND CONCLUSIONS.....	149
6.1	Summary.....	149
6.2	Conclusions	151
6.3	Implications and applications	152
6.4	Future work	153
REFERENCES.....		155
Appendix		
A	SOIL PHYSICAL PROPERTIES AND RADIONUCLIDE ACTIVITIES ..	172
B	SOIL VOLUME PROFILES.....	196
C	RADIONUCLIDE PROFILES	199

LIST OF TABLES

Table 2.1:	Hypsometric and tidal flooding characteristics for the marsh coring sites. See Figure 2.1 for names and location of tide gauges used to calculate flooding characteristics. Lidar elevations used in calculation of the hypsometric integral (HI) were from the USGS and USACE and were retrieved from the Digital Coast Data Access Viewer (https://coast.noaa.gov/dataviewer/#).....	17
Table 2.2:	Location, length, and physical properties for cores collected for this study. Standard deviation of the down-core mean is shown in parentheses. Physical properties determined gravimetrically and by loss-on-ignition (LOI).	19
Table 2.3:	Summary of accretion, mineral sediment accumulation (MSA), and organic matter accumulation (OMA) rates determined using ^{137}Cs and excess ^{210}Pb ($^{210}\text{Pb}_u$) methods for this study. The ^{137}Cs rates were based on the 1963 year-depth corresponding to peak ^{137}Cs activity.	34
Table 3.1:	Equations and assumptions for the CFCS, CRS, and CIC ^{210}Pb models described in the text.....	63
Table 3.2:	Core ^{137}Cs inventories, depth horizons, and peak activities. The inventory due to atmospheric flux (Figure 3.1) is 1.8 kBq m^{-2} . Dividing the 1954 depth and 1963 depth by 58 years (2012 – 1954) and 49 years (2012 – 1963), respectively, will give the mass accumulation rate based on that age-depth. The standard deviations are shown in parentheses.....	72
Table 3.3:	Summary of the inputs, surface activity (A_0) and inventory (I), and resulting mass accumulation rates (ω) for the CFCS, CRS, and CIC ^{210}Pb models. The constant $^{210}\text{Pb}_u$ flux (P) is calculated from the product of I and λ . The P for the CIC model (P_{CIC}) can be variable (Table 3.1) and the core average is shown. The ω shown for the CIC and CRS models can be variable (Table 3.1) and the core average is shown. Standard deviations are shown in parentheses.....	76
Table 4.1:	Core locations and bulk soil properties and radionuclide activities for the 0–6 cm surface soils from Chapter 2.....	102

Table 4.2:	Aboveground biomass concentrations and radionuclide activities. Hyphens indicate where samples were not analyzed.	105
Table 4.3:	Massic activities (Bq kg^{-1}) for the soil size-fractions. Activity error is shown in parentheses. The size fractions are as follows: clay ($<2\mu\text{m}$), silt ($>2\mu\text{m}$ and $<63\mu\text{m}$), sand ($>63\mu\text{m}$ and $<125\mu\text{m}$), micro-organic ($>125\mu\text{m}$ and $<1\text{mm}$), and macro-organic ($>1\text{mm}$).	110

LIST OF FIGURES

- Figure 2.1: Map of the U.S. central Mid-Atlantic coast showing the locations of the (A) Delaware Bay and (B) Barnegat Bay estuaries. The six marsh systems studied are shown in solid-lined boxes. See Table 2.1 and Figures 2.3 and 2.4 for core locations. The USGS tide gauges referred to in the text are numbered (1=Maurice River at Bivalve, 2=Sluice Creek near South Dennis, 3=Little Egg Inlet near Tuckerton, 4=Barnegat Bay at Waretown, 5=Barnegat Bay at Mantoloking). Tidal marshland is denoted by gray shading (USFWS, 2010). 13
- Figure 2.2: Plots of marsh flood frequency (A) and duration (B) versus elevation for Delaware Bay and Barnegat Bay study areas. The curves were produced using 6-minute water level records (2000–2015) for the USGS tide gauges listed in the legend. 24
- Figure 2.3: Lidar-based elevation maps and hypsometric curves for the Delaware Bay marsh systems. The horizontal extent of each map corresponds to the solid bounding boxes in Figure 2.1. The hypsometric curves were computed from elevations within a 100 m radius of each coring site, which are numbered 1–3 in the maps and plotted as solid circles on the curves. Mean high water (MHW) was calculated as the average of high waters from the nearest USGS tide gauge shown in Figure 2.1 and listed in Table 2.1. 25
- Figure 2.4: Lidar-based elevation maps and hypsometric curves for the Barnegat Bay marsh systems. The horizontal extent of each map corresponds to the solid bounding boxes in Figure 2.1. The hypsometric curves were computed from elevations within a 100 m radius of each coring site, which are numbered 1–3 in the maps and plotted as a solid circles on the curves. Mean high water (MHW) was calculated as the average of high waters from the nearest USGS tide gauge shown in Figure 2.1 and listed in Table 2.1. 26
- Figure 2.5: Scatterplot of tidal flood duration versus the hypsometric integral, the elevation relief ratio for a given site. For both the Delaware Bay (blue) and Barnegat Bay (red) marsh sites, there was an inverse relationship between flood duration and hypsometric integral. See text for further description. 27

- Figure 2.6: Box-and-whisker plots of organic and mineral solids concentration and density for Delaware Bay (n = 284) and Barnegat Bay (n = 204) marsh soils. The lower whisker is the minimum value excluding outliers (lower than 1.5 x interquartile range), bottom line of the box is the lower quartile, the solid line inside the box represents the median, the upper line of the box is the upper quartile, the upper whisker is the maximum excluding outliers (larger than 1.5 x the interquartile range), and outliers are represented by open circles. Soil organic densities are similar between the two estuaries, but mineral sediment densities are twofold larger in the Delaware Bay marshes. 29
- Figure 2.7: Representative marsh soil profiles for the Delaware and Barnegat bay estuaries showing the volumetric contributions of mineral sediment, organic matter, and water-filled pore space to the total soil volume. The location of the 1963 year-depth is marked by a dashed line. Inventories of mineral sediment and organic matter relative to 1963 are calculated by dividing mass accumulation divided by accretion using the values presented in Table 2.3..... 30
- Figure 2.8: Depth profiles of ^{137}Cs activity for Delaware and Barnegat bay marsh cores. The dashed line represents the 1963 activity peak used to calculate accretion and mass accumulation rates (Table 2.3). Note that a ^{137}Cs activity peak was not present in the profile for core MR-3. 32
- Figure 2.9: Depth profiles of $^{210}\text{Pb}_u$ for the Delaware and Barnegat bay marsh cores. The dashed line is based on the least-squares regression used to calculate accretion and accumulation rates (Table 2.3). The coefficient of determination for each regression is shown and p was less than 0.05. 33
- Figure 2.10: Scatterplots of accretion versus distance to tide water (A) and surface elevation (B) and mineral sediment accumulation versus distance to tide water (C) and surface elevation (D) for the Delaware Bay (blue) and Barnegat Bay (red) marsh sites. While these regressions for Barnegat Bay marsh sites were found to be significant, no significant relationship was found for Delaware Bay marsh sites. Note that the accretion and sediment accumulation rates are referenced to the ^{137}Cs 1963 age-depth horizon in cores. 38

Figure 2.11: Scatterplots of accretion rate versus accumulated mineral mass (a) and accumulated organic mass (b), and accumulated mineral mass versus accumulated organic mass (c) for the Delaware Bay (blue) and Barnegat Bay (red) marsh sites. Note that the accretion rates and accumulated mass values are referenced to the ^{137}Cs 1963 age-depth horizon in cores.	44
Figure 2.12: Range of ^{137}Cs -based accretion rates for the Delaware Bay and Barnegat Bay marsh sites plotted with the range (cm y^{-1}) of relative sea level rise (RSLR) reported for nearby NOAA tide gauges. See text for further discussion.	46
Figure 3.1: Ground-level record of ^{137}Cs fallout based on measured fallout of ^{90}Sr (data from Global Fallout Deposition Program, EML, http://www.wipp.energy.gov/NAMP/EMLLegacy/databases.htm). The dashed line is the original flux (solid line) decay-corrected to 2012. See text for further discussion.	59
Figure 3.2: Selected profiles of ^{137}Cs activity for cores MR-3 (A), DV-2 (B), and IB-2 (C) showing different characteristics. Core MR-3 had no identifiable 1954 onset (dotted line) or 1963 peak (dashed line) in ^{137}Cs ; core DV-2 had good agreement between 1954 and 1963 horizons; and core IB-2 had poor agreement between 1954 and 1963 age-depths.	71
Figure 3.3: Regression of ^{137}Cs soil inventory and accumulated mass for the coring sites. The direct relationship suggests that sediment focusing contributes to the measured inventory of ^{137}Cs at some of the marsh sites.	74
Figure 3.4: Correlation of $^{210}\text{Pb}_u$ soil inventory and accumulated mass for the coring sites. The direct relationship suggests that sediment focusing rather than boundary scavenging contributes $^{210}\text{Pb}_u$ inventory at some of the marsh sites.	78
Figure 3.5: Scatterplot of $^{210}\text{Pb}_u$ surface activity versus ^{137}Cs -based mass accumulation rates for the coring sites. Data from Delaware Bay marshes are shown in blue and Barnegat Bay marshes shown in red. See text for further discussion.	79
Figure 3.6: Delaware Bay ^{210}Pb chronologies showing age in years before 2012. The lines represent chronologies generated from the CIC (solid), CRS (dashed), and CFCS (dotted) models. The 1963 ^{137}Cs age-depths are shown (triangle), if identified.	81

Figure 3.7: Barnegat Bay ^{210}Pb chronologies showing age in years before 2012. The lines represent chronologies generated from the CIC (solid), CRS (dashed), and CFCS (dotted) models. The 1963 (triangle) ^{137}Cs age-depths are shown (triangle). 82

Figure 3.8: Example profiles of $^{210}\text{Pb}_u$ and CFCS model age for cores DV-2 (A) and DN-2 (B) showing good correspondence with 1963 age dates (red dots) derived from ^{137}Cs data for the same cores. While the CFCS and ^{137}Cs dates agree for DV-2, examination of the $^{210}\text{Pb}_u$ profile shows the CFCS assumption of linearity is violated and the model should not be used for detailed chronology 85

Figure 4.1. Conceptualized model of ^{210}Pb delivery to tidal marshes and methods of incorporation into marsh soils..... 97

Figure 4.2: The excess ^{210}Pb activities of aboveground biomass – standing and litter – and the underlying bulk soil (0–6 cm). 112

Figure 4.3: Bar plot showing the percent mass contribution of the soil-size fractions to the bulk soil (0-6cm). The top row are sites from marshes in Delaware Bay and the bottom row from marshes in Barnegat Bay. The volume contribution showed higher organic contribution and lower mineral contribution due to the low particle density of organic matter (1.14 g cm^{-3}) relative to mineral sediment (2.61 g cm^{-3}). 113

Figure 4.4: Regression of the mass contribution of organic soil-fraction (macro- and micro-) and the organic fraction of the bulk sediment sample. Data from Delaware Bay is shown in blue and from Barnegat Bay in red. Confidence in the physical separation used in size fraction methods is supported by the good agreement between the physical separation and the loss-on-ignition (LOI) method use on the bulk soil. The dashed line represents a 1:1 relationship..... 114

Figure 4.5: The excess ^{210}Pb activities of the clay, silt, sand, micro-organic, and macro-organic size fractions from 0–6 cm depth. Note the different scales for the top row, sites from marshes in Delaware Bay, and the bottom row, sites from marshes in Barnegat Bay. 115

Figure 4.6: The percent of the bulk excess ^{210}Pb inventory held by each soil fraction. The top row are sites from marshes in Delaware Bay and the bottom row from marshes in Barnegat Bay..... 116

Figure 4.7:	The ^{137}Cs activity of the clay, silt, sand, micro-organic, and macro-organic soil size fractions from 0–6 cm depth. The top row are sites from marshes in Delaware Bay and the bottom row are sites from marshes in Barnegat Bay.	117
Figure 4.8:	The percent of the bulk ^{37}Cs inventory held by each soil fraction. The top row are sites from marshes in Delaware Bay and the bottom row from marshes in Barnegat Bay.	118
Figure 4.9:	The excess ^{210}Pb activities of aboveground biomass – canopy and litter – and the underlying organic soil (sand + micro- + macro-organic; 0–6 cm).....	119
Figure 4.10:	Theoretical and measured partial (0–6 cm) inventories of excess ^{210}Pb . The theoretical inventories are based on the age of the surface layer from ^{137}Cs dating (Chapter 1) and an average literature ^{210}Pb flux of $165 \text{ Bq m}^{-2} \text{ y}^{-1}$ (Turekian et al. 1983; Kim et al. 2000). All measured inventories were found to be enriched compared to theoretical inventories except for sites IB-1 and IB-2.....	120
Figure 4.11:	The theoretical excess ^{210}Pb inventory that could be explained by the clay, silt, sand, micro-organic, and macro-organic soil size fractions. The theoretical inventory (Figure 4.10) was calculated based on atmospheric flux of ^{210}Pb ($165 \text{ Bq m}^{-2} \text{ y}^{-1}$) and soil layer (0–6 cm) age (Table 4.1). Note the different scales for the top row, sites from marshes in Delaware Bay, and the bottom row, sites from marshes in Barnegat Bay.	121
Figure 4.12:	Regression of the excess ^{210}Pb activities of the organic soil-fraction (sand + macro- + micro-organic) and total aboveground biomass (standing + litter). Data from Delaware Bay is shown in blue and from Barnegat Bay in red. The positive direct relationship suggests that the activity of the plant biomass aboveground has some influence on the activity of organic matter belowground, possibly through burial of decomposed leaf and stem litter.	122
Figure 5.1:	Energy spectrum showing gamma photopeaks generated from a sediment sample from core RC-3 at 14-16 cm depth. Photopeaks produced by ^{210}Pb , ^{241}Am , and ^{137}Cs are shown in red.	138

- Figure 5.2: Scatterplot of ^{241}Am and ^{137}Cs activities ($n = 83$) measured in 2-cm depth intervals from eighteen marsh cores collected in marshes located in the Delaware and Barnegat bays. The direct relationship, higher ^{241}Am activity associated with higher ^{137}Cs activity, suggests that these radionuclides have a similar input function, likely Northern Hemisphere atmospheric weapons testing fallout. 140
- Figure 5.3: Depth profiles of ^{137}Cs and ^{241}Am activity measured in marsh cores from the Delaware (DN-2 and DV-3) and Barnegat (IB-2 and RC-3) bay estuaries. The depth of the ^{137}Cs and ^{241}Am activity peaks is attributed to the 1963-1964 maximum fallout of Northern Hemisphere atmospheric weapons testing. Note different scales for ^{137}Cs and ^{241}Am 141
- Figure 5.4: Fallout history of ^{241}Pu and ^{137}Cs due to atmospheric weapons testing. The record is based on the ^{90}Sr fallout measured at New York, New York, USA and the concentrations of ^{241}Pu and ^{137}Cs in fallout debris. See text for further discussion. 142
- Figure 5.5: Theoretical soil inventories of ^{241}Pu , ^{137}Cs , and ^{241}Am from the time these radionuclides were introduced to the environment in 1954 to 2075. The inventory record for ^{241}Pu and ^{137}Cs is based on the estimated atmospheric flux (Figure 5.4) and radioactive decay. The ^{241}Am inventory is based on ingrowth from ^{241}Pu and decay. Note the different scale (right) for ^{241}Am 143

ABSTRACT

The goal of this dissertation research was to develop new insight into the application of radionuclide methods (^{210}Pb , ^{137}Cs , ^{241}Am) in tidal marshes for studies of geochronology and geomorphology. A comprehensive radionuclide dataset was generated by gamma spectroscopy of samples from eighteen marsh soil cores collected in two Mid-Atlantic estuaries, the Delaware Bay and the Barnegat Bay. The research was carried out in four separate studies, all of which involved different aspects of radionuclide measurements as applied to tidal marsh deposits.

The mineral-rich estuarine marshes of the Delaware Bay provided a contrast to the organic-rich coastal marshes of the Barnegat Bay. The close proximity of these sites in southern and central New Jersey minimized climatic and oceanographic variation that must be taken into account when comparing marsh accretionary processes for different regions. Additionally, the atmospheric flux of ^{210}Pb , ^{137}Cs , ^{241}Am to the marshes can be assumed to be nearly identical considering the proximity of the study sites, which allowed for direct comparison of radionuclide inventories and chronologies. Marsh sites in both estuaries were dominated by the halophyte *Spartina alterniflora* minimizing biotic variations in the soil forming process.

The marshes of Delaware Bay were found to have higher rates of mineral sediment accumulation compared to the Barnegat Bay marshes. This difference was at least partly due to the larger supply of mineral sediment in Delaware Bay, a consequence of the estuarine turbidity maximum and its entrapment of sediment supplied to the estuary. Barnegat Bay had more frequent and longer flooding but

mineral sediment accumulation in marshes there was low. Barnegat Bay marsh accretion rates were found to be equal to or less than rates of relative sea-level rise, whereas Delaware Bay marshes were found to outpace relative sea-level rise.

The applicability of radionuclide chronology models (^{210}Pb , ^{137}Cs), originally developed for marine and lacustrine deposits, were objectively tested for salt marshes in the study area. The biophysical nature of marsh accretion – the in situ accumulation of organic matter and tidal deposition of mineral sediments – requires careful consideration of the models' assumptions. The range of soil compositions from sites sampled for this research provided a unique case study of model performance in both organic- and mineral-rich marshes, and recommendations for best practices were offered. Part of this analysis involved separation and radionuclide analysis of size-fractions of marsh surface soils, the results of which raise questions concerning traditional assumptions of how ^{210}Pb and ^{137}Cs are delivered to the marsh surface. Detection of ^{241}Am in marsh deposits, a consequence of the decay of fallout ^{241}Pu , provides a new chronological tool that will become increasingly useful as ^{137}Cs decays to extinction.

The results of this study have implications for numerical modeling of marsh accretion, chronology of mixed sediments, and contaminant transport and burial in the marsh-estuary system.

Chapter 1

INTRODUCTION

1.1 Tidal Marsh Accumulation and Accretion

Tidal marsh accretion is the vertical growth of the marsh surface resulting from mass accumulation of organic and mineral solids. There are a variety of mechanisms of sediment and organic accumulation in tidal marshes (Friedrichs and Perry, 2001; Nyman et al., 2006). Deposition of allochthonous material and accumulation of autochthonous organic matter contribute to the accretion, or upward growth, of the marsh surface. Mineral sediment is sourced from either terrigenous sources, marine sources, or some combination of the two. Clays, silts, and sands can be transported via rivers, tides, flood waters, wind waves, wind, and ice. Organic matter accumulates through belowground macrophyte and microbial production, burial of litter and detritus, and the living structures of the plant contribute soil volume by trapping water and gases with potential for expansion.

Aboveground plant structures reduce fluid velocity allowing particle settling and trapping that would otherwise be entrained in the flow (Bouma et al., 2010). Mineral deposition on the marsh surface leads to upward migration of plants to prevent burial. Sediment elevation is affected by the belowground expansion or contraction of living root volume. The relative contributions of organic matter and mineral sediment to measured overall accretion rates has been investigated through short-term plot experiments (e.g., Cahoon and Turner, 1989; Reed et al., 1997; Calvo-Cubero et al., 2013), and by regression analysis of radiometrically determined mass

accumulation rates (Bricker-Urso et al., 1989; Chmura and Hung, 2004; Neubauer, 2008; Nyman et al., 1993; Turner et al., 2000).

The following generalizations of salt marsh accretion can be made from the collective findings of these studies: (1) marsh accretion is dependent on organic matter accumulation and mineral sediment accumulation or more dependent on organic matter accumulation in some marshes; (2) variations in organic matter accumulation explains more of the variation in overall accretion rates than does variation in mineral sediment accumulation; (3) mineral and organic mass accumulation are related through time-dependent feedbacks between physical and biotic factors that moderate plant growth. For example, a youthful marsh that develops on a mudflat and builds elevation within the tidal frame will trap a decreasing amount of mineral sediment due a reduction in hydroperiod (Allen, 2000). Also, as the marsh matures and reaches an optimal tidal elevation for plant growth belowground organic matter production and accumulation increases (Morris et al., 2002).

1.2 Geochronology using ^{137}Cs and ^{210}Pb

The radionuclides ^{137}Cs and ^{210}Pb are delivered to the marsh platform via atmospheric deposition (wet and dry), tidal or ground water transport (dissolved), and deposition of waterborne particles (particulate). The input of radionuclides from difference sources produces an inventory that represents a balance between inputs and radioactive decay. Prior studies have described and documented the formation of radionuclide inventory in marsh soils, which sequester radionuclides transported in tidal waters (Church et al., 1981; Olsen et al., 1985). Due to the association of many radionuclides with particles, radionuclides can be used as tracers to quantify sediment

deposition, reworking, and erosion (Zhang and Walling, 2005), and to isolate sediment sources (Matisoff et al., 1999).

Use of ^{137}Cs and ^{210}Pb inventories as particle tracers is common in sediment erosion and transport studies. The relative radionuclide inventories of bottom sediments in lakes have been used to describe redeposition of shallow-water sediments to sites deeper in the lake, a process generally referred as "focusing" (Crusius and Anderson, 1995). In tidal marshes, focusing of radionuclide activity can indicate remobilization and redeposition of mineral sediment (Morris et al., 2000).

Atmospheric ^{210}Pb , produced by the decay of ^{222}Rn , is deposited through wet and dry deposition on plants, sediments, or water. This excess ^{210}Pb becomes buried as sediment accumulates. Additional excess ^{210}Pb can be imported into the marsh on particles eroded or formed elsewhere in the estuary. The total ^{210}Pb is the sum of this excess and the supported ^{210}Pb , generated from the *in situ* decay of ^{238}U and its progeny. Deviation from the atmospherically-sourced ^{210}Pb inventory is indicative of addition or removal of ^{210}Pb via particle deposition or erosion.

Analysis of the canopy is usually not a component of radionuclide studies in marshes, even though some activity is trapped on plant leaves and stems. For example, in a study of ^{210}Pb and ^7Be deposition by Olsen et al. (1985) it was shown that marsh plant structures indeed sequester radionuclide activity, thereby contributing to the belowground inventory. Although plant litter is thought not to be a contributing factor to organic accumulation, studies have shown that the extent of accumulation and decay of litter is species specific (Windham, 2001) and can lead to differential rates of accretion over intermediate (days to years) time scales (Rooth et al., 2003). Ideally, the

association of radionuclides with organic matter should be quantified both above and below the surface.

The radionuclides ^{210}Pb and ^{137}Cs are not a "fingerprint" of sediment sources to marshes, but rather provide a time-averaged (~50-100 y) indicator of radionuclide and sediment transport pathways by association. At the scale of a marsh platform, spatial comparison of at-site inventories can be used to assess where sediment is focused (e.g., Crusius and Anderson, 1995). This method has implications for coastal sediment management as it has potential to identify sites of sediment surpluses and deficiencies. At the estuary scale, radionuclide inventories can help identify patterns of sediment accumulation associated with estuarine circulation, turbidity maximum processes, and estuary-to-wetland exchanges.

1.3 Contributions of this dissertation

Chapter 2 describes the mass accumulation and accretion rates for marshes in the Delaware Bay and Barnegat Bay estuaries and defines the differences between the estuaries using their characteristic hydrogeomorphic setting. These rates were determined using ^{137}Cs and ^{210}Pb geochronology of the sediment record. Long-term water-level records and digital elevation models were analyzed to characterize marsh hydrology and topography. The relationship between geomorphic variables, sediment accumulation, and accretion is discussed.

Chapter 3 investigates the assumptions of ^{137}Cs and ^{210}Pb dating models concerning their application in tidal marshes. The atmospheric flux of ^{137}Cs was used to determine the theoretical depth profile and soil inventory. The assumptions of three commonly used ^{210}Pb dating models were tested and the model output chronologies compared with the ^{137}Cs age-model results. Best practices for radiochronology in tidal

marshes are discussed and suggestions for the most appropriate ^{210}Pb dating model based on marsh type are made.

Chapter 4 quantifies the contribution of soil components to the soil radionuclide inventory. Mineral sediment is often considered the main vector for radionuclide transport and burial. Plant canopy, litter, and belowground organic matter were analyzed for ^{137}Cs and ^{210}Pb to determine their role, if any, in radionuclide capture and burial. The aboveground biomass holds some percentage of the annual atmospheric ^{210}Pb flux and is related through regression to near-surface belowground organic matter.

Chapter 5 demonstrates the current and future applications of fallout-sourced ^{241}Am to geochronology and particle tracing in the estuarine setting. The ingrowth of ^{241}Am due to the decay its parent, ^{241}Pu , is quantified to estimate apparent inventories of ^{241}Am in tidal marsh soils. Future use of this radionuclide for marsh soil chronology, in conjunction with and independent of ^{137}Cs , is discussed.

REFERENCES

- Allen, J.R.L., 2000. Morphodynamics of Holocene salt marshes: a review sketch from the Atlantic and Southern North Sea coasts of Europe. *Quat. Sci. Rev.* 19, 1155–1231. doi:10.1016/S0277-3791(99)00034-7
- Bouma, T.J., De Vries, M.B., Herman, P.M.J., 2010. Comparing ecosystem engineering efficiency of two plant species with contrasting growth strategies. *Ecology* 91, 2696–704.
- Bricker-Urso, S., Nixon, S.W., Cochran, J.K., Hirschberg, D.J., Hunt, C., 1989. Accretion rates and sediment accumulation in Rhode Island salt marshes. *Estuaries* 12, 300–317. doi:10.2307/1351908
- Cahoon, D.R., Turner, R.E., 1989. Accretion and canal impacts in a rapidly subsiding wetland II. feldspar marker horizon technique. *Estuaries* 12, 260–268. doi:10.2307/1351905
- Calvo-Cubero, J., Ibáñez, C., Rovira, A., Sharpe, P.J., Reyes, E., 2013. Mineral versus organic contribution to vertical accretion and elevation change in restored marshes (Ebro Delta, Spain). *Ecol. Eng.* 61, 12–22. doi:10.1016/j.ecoleng.2013.09.047
- Chmura, G.L., Hung, G.A., 2004. Controls on salt marsh accretion: a test in salt marshes of Eastern Canada. *Estuaries* 27, 70–81. doi:10.1007/BF02803561
- Church, T., Lord III, C., Somayajulu, B., 1981. Uranium, thorium and lead nuclides in a Delaware salt marsh sediment. *Estuar. Coast. Shelf Sci.* 13, 267–275. doi:10.1016/S0302-3524(81)80025-4
- Crusius, J., Anderson, R.F., 1995. Sediment focusing in six small lakes inferred from radionuclide profiles. *J. Paleolimnol.* 13, 143–155. doi:10.1007/BF00678103
- Friedrichs, C.T., Perry, J.E., 2001. Tidal salt marsh morphodynamics: a synthesis. *J. Coast. Res.* 81, 7–37.

- He, Q., Walling, D., 1996. Interpreting particle size effects in the adsorption of ^{137}Cs and unsupported ^{210}Pb by mineral soils and sediments. *J. Environ. Radioact.* 30, 117–137. doi:10.1016/0265-931X(96)89275-7
- Matisoff, G., Bonniwell, E.C., Whiting, P.J., 1999. Soil erosion and sediment sources in an Ohio watershed using beryllium-7, cesium-137, and lead-210. *J. Environ. Qual.* 31, 54–61. doi:10.2134/jeq2002.5400
- Morris, J.T., Sundareshwar, P. V., Nietch, C.T., Kjerfve, B., Cahoon, D.R., 2002. Responses of Coastal Wetlands To Rising Sea Level. *Ecology* 83, 2869–2877. doi:10.1890/0012-9658(2002)083[2869:ROCWTR]2.0.CO;2
- Neubauer, S., 2008. Contributions of mineral and organic components to tidal freshwater marsh accretion. *Estuar. Coast. Shelf Sci.* 78, 78–88. doi:10.1016/j.ecss.2007.11.011
- Nyman, J., DeLaune, R., Roberts, H., Patrick Jr., W., 1993. Relationship between vegetation and soil formation in a rapidly submerging coastal marsh. *Mar. Ecol. Prog. Ser.* 96, 269–279.
- Nyman, J.A., Walters, R.J., Delaune, R.D., Patrick Jr., W.H., 2006. Marsh vertical accretion via vegetative growth. *Estuar. Coast. Shelf Sci.* 69, 370–380. doi:10.1016/j.ecss.2006.05.041
- Olsen, C.R., Larsen, I.L., Lowry, P.D., Cutshall, N.H., Todd, J.F., Wong, G.T.F., Casey, W.H., 1985. Atmospheric fluxes and marsh-soil inventories of ^7Be and ^{210}Pb . *J. Geophys. Res.* 90, 10487–10495. doi:10.1029/JD090iD06p10487
- Reed, D.J., de Luca, N., Foote, A.L., 1997. Effect of Hydrologic Management on Marsh Surface Sediment Deposition in Coastal Louisiana. *Estuaries* 20, 301. doi:10.2307/1352345
- Rooth, J.E., Stevenson, J.C., Cornwell, J.C., 2003. Increased sediment accretion rates following invasion by *Phragmites australis*: The role of litter. *Estuaries* 26. doi:10.1007/BF02823724
- Turner, R.E., Swenson, E.M., Milan, C.S., 2000. Organic and inorganic contributions to vertical accretion in salt marsh sediments, in: Weinstien, M.P., Kreeger, D.A. (Eds.), *Concepts and Controversies in Tidal Marsh Ecology*. Kluwer Academic Publishers, Dordrecht, pp. 583–595. doi:10.1007/0-306-47534-0_27
- Windham, L., 2001. Comparison of biomass production and decomposition between *Phragmites australis* (common reed) and *Spartina patens* (salt hay grass) in

brackish tidal marshes of New Jersey, USA. *Wetlands* 21, 179–188.
doi:10.1672/0277-5212(2001)021[0179:COBPAD]2.0.CO;2

Zhang, X., Walling, D., 2005. Characterizing land surface erosion from cesium-137 profiles in lake and reservoir sediments. *J. Environ. Qual.* 34, 514–523.
doi:10.2134/jeq2005.0514

Chapter 2

HYDROGEOMORPHIC INFLUENCES ON SALT MARSH SEDIMENT ACCUMULATION AND ACCRETION IN TWO ESTUARIES OF THE U.S. MID-ATLANTIC COAST

2.1 Abstract

Salt marshes in two estuaries of the U.S. Mid-Atlantic coast, Barnegat Bay and Delaware Bay, were investigated to identify relationships between rates of sedimentation and hydrogeomorphology. Barnegat Bay is a microtidal lagoonal estuary with back-barrier and mainland coastal marshes, whereas Delaware Bay is a micro-mesotidal coastal plain estuary with sediment-rich estuarine marshes. Salt marshes of both estuaries are dominated by *Spartina alterniflora*. A hydrogeomorphic analysis was performed to characterize marsh hypsometry and tidal flooding, and a coring study was conducted to measure rates of mineral sediment accumulation, organic matter accumulation, and vertical accretion using ^{137}Cs and ^{210}Pb chronology at nine sites in both estuaries. Mineral sediment and organic matter accumulation rates were significantly higher in Delaware Bay marshes (mineral mean and 1σ : 2.57 ± 2.03 $\text{kg m}^{-2} \text{y}^{-1}$; organic: 0.65 ± 0.26 $\text{kg m}^{-2} \text{y}^{-1}$) than in Barnegat Bay (mineral: 0.31 ± 0.27 $\text{kg m}^{-2} \text{y}^{-1}$; organic: 0.29 ± 0.08 $\text{kg m}^{-2} \text{y}^{-1}$). Marsh accretion rates in both estuaries (Delaware Bay: 0.79 ± 0.06 cm y^{-1} ; Barnegat Bay: 0.28 ± 0.06 cm y^{-1}) were positively correlated with sediment and organic accumulation, but the upper limit of accretion was set by sediment accumulation rate. Flood duration did not influence accumulation and accretion rates thus suspended sediment concentration, not flood duration, appears

to be the overarching control on rates of mass accumulation and accretion in marshes of Delaware Bay and Barnegat Bay. If true, natural and (or) human influences on suspended-sediment production and transport in these estuaries has potential to impact marsh accretionary status and stability, independent of sea-level rise.

2.2 Introduction

The classical conceptual model of tidal marsh development involves tidal flooding of intertidal flats, organic matter production by halophytic vegetation, and allochthonous mineral sedimentation (Redfield, 1972), which promote vertical accretion and lateral expansion of the marsh in space and time. Describing and parameterizing these processes toward a predictive capability has become a universal goal in marsh ecology and geomorphology, in light of rapid and widespread loss of tidal wetlands worldwide (Nicholls et al., 1999). Numerous researchers have examined the relative contributions of mineral and organic mass to measured rates of marsh accretion for insight on mechanisms of marsh accretion (Chmura and Hung, 2004; Neubauer et al., 2002; Nyman et al., 2006; Turner et al., 2000), whereas others have investigated linkages between accretion and various biotic and abiotic factors (French, 2006; Mudd et al., 2009). While there have been significant advances in our understanding of marsh geomorphology (see reviews by Allen, 2000; Friedrichs and Perry, 2000; Fagherazzi et al., 2012), generalizations of how rates of marsh sediment accumulation and accretion scale across the full range of marsh types, and how these rates are influenced by local processes in the wetland complex versus those related to regional coastal and estuarine dynamics remain to be well constrained.

Although highly variable in form and function, tidal marshes can be divided into coastal and estuarine subtypes on the basis of genesis, morphodynamics,

vegetation, and soil properties. Coastal marshes are found in bar-built or lagoon-type estuaries, either on the back-barrier or mainland shore of the lagoon, and form as a result of tides and storms (Nichols, 1989). On the U.S. Atlantic margin, coastal marshes are most often dominated by the halophytes *Spartina alterniflora* and *Spartina patens*, emerging from sandy tidal flats and barrier overwash deposits. Estuarine marshes form in coastal plain estuaries on the flanks of tidal channels and creeks, and may range from salt marshes at the estuary mouth to tidal freshwater marshes at the head (Odum, 1988). Estuarine marshes exhibit a diverse range of marsh vegetation and platform morphology, and have soils enriched with mud-sized sediments derived from fluvial input and erosional sources within the estuary. Although outwardly similar in appearance, coastal and estuarine marshes have distinctive soil properties related to local hydrogeomorphic properties, vegetative growth factors, and larger scale estuarine dynamics (Darmody and Foss, 1979).

The objective of this study is to compare patterns and rates of mass accumulation (mineral sediment and organic matter) and accretion in archetype coastal and estuarine marshes for insight on relationships between hydrogeomorphic properties and accretionary processes. To meet this objective, salt marshes in two different types of estuaries on the U.S. Mid-Atlantic coast, Barnegat Bay and Delaware Bay, were investigated using identical methods. Barnegat Bay is a microtidal lagoon estuary with coastal marshes, whereas Delaware Bay is a micro-mesotidal sediment-rich coastal plain estuary with estuarine marshes. At the outset it was hypothesized that rates of mineral sediment accumulation and accretion in the estuarine marshes of Delaware Bay were higher than in the coastal Barnegat Bay because of the larger source of allochthonous mineral sediment and higher tidal range

in Delaware Bay. To test this hypothesis, a hydrogeomorphic analysis was performed to characterize marsh topography and tidal flooding characteristics, and a coring study was conducted to measure rates of sediment accumulation, organic matter accumulation, and vertical accretion using ^{137}Cs and ^{210}Pb chronology. Barnegat Bay and Delaware Bay are located on the same segment of the U.S. Mid-Atlantic coast, minimizing variations in marsh accretionary processes related to regional oceanographic and climatic factors. Additionally, salt marshes in these estuaries are characterized by the same halophytic vegetation, reducing some of the variability associated with species-specific biotic factors. By elucidating internal versus external influences on marsh sedimentation rates, the findings of this study have potential to inform conceptual and numerical models of tidal marsh morphodynamics.

2.3 Study Area

The Delaware Bay and Barnegat Bay-Little Egg Harbor estuaries are located in New Jersey (USA) and fall within the New Jersey Coastal Plain province (Figure 2.1). Sea-level rise and coastal transgression following the Wisconsin deglaciation was a major influence on the development of tidal wetlands in this region. Widespread expansion of coastal and estuarine marshes took place after 6 ky partly in response to decelerating rates of eustatic sea level rise (Fletcher et al., 1990). Salt marshes became established on the present-day coast around 1–3 ky in response to relative sea level rise and inundation of coastal lowlands (Fletcher, III et al., 1992; Oertel and Kraft, 1994). For the southern New Jersey coast and eastern Delaware Bay, the rate of relative sea-level rise between 2 ky and 1900 CE was 1.3 mm y^{-1} , primarily due to subsidence with relaxation of the proglacial forebulge (Horton et al., 2013; Nikitina et al., 2015). Local tide gauge records indicate post-1900 rates of $3.4\text{--}4.6 \text{ mm y}^{-1}$

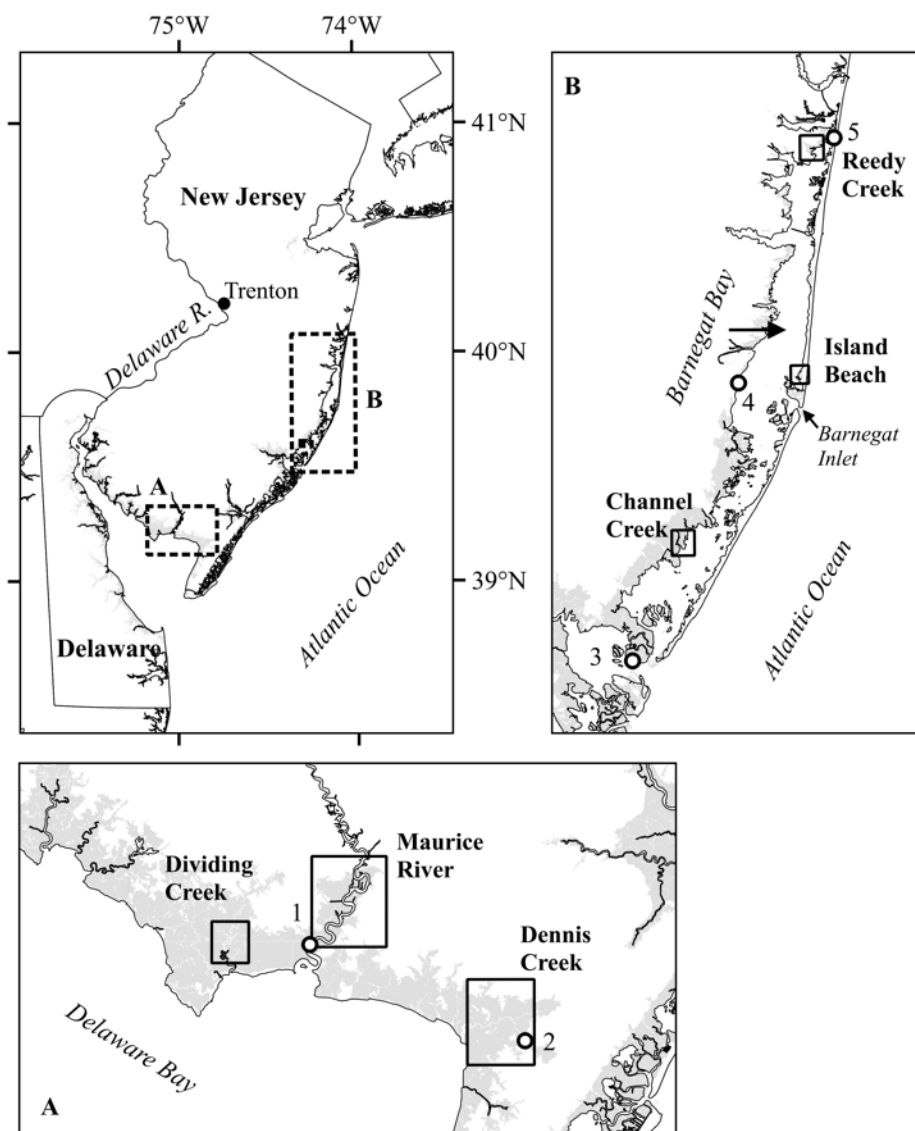


Figure 2.1: Map of the U.S. central Mid-Atlantic coast showing the locations of the (A) Delaware Bay and (B) Barnegat Bay estuaries. The six marsh systems studied are shown in solid-lined boxes. See Table 2.1 and Figures 2.3 and 2.4 for core locations. The USGS tide gauges referred to in the text are numbered (1=Maurice River at Bivalve, 2=Sluice Creek near South Dennis, 3=Little Egg Inlet near Tuckerton, 4=Barnegat Bay at Waretown, 5=Barnegat Bay at Mantoloking). Tidal marshland is denoted by gray shading (USFWS, 2010).

(NOAA, 2013), which are higher than the global average due to the aforementioned subsidence and regional ocean dynamics (Ezer et al., 2013).

2.3.1 Delaware Bay Estuary

The Delaware Bay estuary is a 2000 km² coastal plain estuary extending 215 km from the head of tides in Trenton, New Jersey, to the bay mouth (Figure 2.1) with a 35,000 km² watershed (NOAA, 1985). Holocene sea level flooding of the ancestral Delaware River valley along with landward migration of sediment depocenter contributed to the emergence of tidal wetlands that fringe the estuary and its numerous sub-estuaries (Fletcher et al., 1992). The upper estuary floor is composed of mud and sandy muds whereas the lower estuary has a sand and gravelly sand bottom (Biggs and Beasley, 1988). The estuary exhibits classical gravitational circulation driven by freshwater outflow with seaward and landward mean flows in the upper and lower water column, respectively. Associated with the two-layer circulation is a broad turbidity maximum that serves as an internal source of fine-grained sediment to the estuary floor and fringing tidal wetlands (Cook et al., 2007). Suspended-sediment concentrations are high within the turbidity maximum zone and reach several 10s to 100s of mg l⁻¹ (Sommerfield and Wong, 2011). Cross-estuary circulations along with shoaling wind waves contribute to high suspended-sediment concentrations over the broad subtidal flats flanking the axial channel (McSweeney et al., 2016).

Estuarine marshes selected for this study were located on the wetland coast of lower eastern Delaware Bay and are associated with the sub-estuaries Dividing Creek (DV), Maurice River (MR), and Dennis Creek (DN) (Figure 2.1). These marshes are dominated by the halophyte *S. alterniflora*. In this area, Delaware Bay is shallow (<4

m depths) and separated from the tidal wetlands by a narrow barrier beach. Locally the spring tidal range is ~1.6 m.

2.3.2 Barnegat Bay-Little Egg Harbor Estuary

The Barnegat Bay-Little Egg Harbor estuary is a 264 km² back-barrier, lagoon-type estuary on the coast of New Jersey (Figure 2.1). The bay was formed during the late Holocene (5–7 ky) following the development of wave-dominated barrier islands (Oertel and Kraft, 1994). The estuary is 67 km in length and separated from the Atlantic Ocean by a barrier island (Figure 2.1). The estuary has a 1,716 km² watershed (Kennish, 2001). Tide water is exchanged through three inlets: one in the north; one near the center of the island; and one in the south. The largest tidal flow occurs at the central Barnegat Inlet (Kennish, 2001). Transport in the estuary is influenced by tides and local wind forcing (Defne and Ganju, 2015). The bottom composition of the Barnegat Bay lagoon is predominantly muddy sand with sediment fining along an east to west gradient (Rogers et al., 1990 as cited in Kennish, 2001).

The salt marshes investigated were located in north and central Barnegat Bay at Reedy Creek (RC), Island Beach (IB), and Channel Creek (CC) (Figure 2.1). Island Beach marsh, located on the back barrier island adjacent to Barnegat Inlet, was established on an overwash fan, whereas the mainland marshes at Reedy Creek and Channel Creek emerged from muddy and sandy tidal flat deposits. Barnegat Bay marshes are similarly dominated by *S. alterniflora*. Spring tide range in this region of the bay is 0.66 m.

2.4 Methods

2.4.1 Hydrogeomorphic analysis

Recent (2008–2013) lidar-based digital elevation models (DEMs) produced by the United State Geological Survey (USGS) and the United States Army Corps of Engineers (USACE) for the marsh locations were retrieved from the online Digital Coast Data Access Viewer (<https://coast.noaa.gov/dataviewer/#>). From these DEMs, hypsometric curves (percent area above a given elevation) for a 100-m radius around each coring site were generated following the methods of Luo (1998). For this purpose, the marsh platform was isolated by masking nearby marsh edges and waterways below mean tide level, determined by analysis of local water-level data. The hypsometric integral (*HI*), a dimensionless index of topography, was calculated for each 0.03-km² area as follows:

$$HI = \frac{h_{mean} - h_{min}}{h_{max} - h_{min}} \quad (2.1)$$

where h_{mean} , h_{min} , and h_{max} are the mean, minimum, and maximum elevation, respectively. This index is a dimensionless number between 0 and 1 that represents the ratio between elevation and relief. Often used to characterize age and erosional nature of drainage basins, the hypsometric integral can be used as a relative value of slope steepness when comparing land areas (Strahler, 1952).

Water-level data (6-minute interval, 2000–2015) from five USGS gauges were used to determine tidal flooding characteristics and datums (Figure 2.1 and Table 2.1). Flood frequency, the number of times the marsh is flooded within a specific time period, was calculated as the percentage of high water events exceeding the present coring site elevation relative to the total number of high waters during the 15-year period of record. Flood duration, the amount of time that the marsh is covered with

Table 2.1: Hypsometric and tidal flooding characteristics for the marsh coring sites. See Figure 2.1 for names and location of tide gauges used to calculate flooding characteristics. Lidar elevations used in calculation of the hypsometric integral (HI) were from the USGS and USACE and were retrieved from the Digital Coast Data Access Viewer (<https://coast.noaa.gov/dataviewer/#>).

Estuary	Marsh system	Core	Elevation, RTK-GPS (m NAVD88)	HI	Flooding frequency (%)	Flooding duration (%)	USGS Tide Gauge
Delaware Bay	Dennis Creek	1	0.733	0.64	59	13	2
		2	0.757	0.71	51	11	
		3	0.514	0.36	95	34	
	Dividing Creek	1	0.871	0.59	49	9	1
		2	0.657	0.53	81	20	
		3	0.629	0.59	84	21	
	Maurice River	1	0.679	0.60	78	19	1
		2	0.352	0.49	98	35	
		3	0.724 ^a	0.44	72	16	
Barnegat Bay	Channel Creek	1	0.279	0.71	80	25	3
		2	0.284	0.66	80	24	
		3	0.312	0.60	76	22	
	Island Beach	1	0.083	0.27	73	46	4
		2	0.146	0.29	57	30	
		3	0.126	0.39	62	35	
Reedy Creek	1	0.104	0.24	71	46	5	
	2	-0.103	0.11	96	88		
	3	-0.070	0.30	94	84		

^a Lidar-based

tide water, was calculated as the percentage of the total time the water height was equal to, or in excess of, the site elevation. Relative sea-level trends for the study area are available from NOAA tide gauging stations (NOAA, 2013).

2.4.2 Marsh core sampling

In summer 2012 three coring sites were selected in three different marshes within both estuaries (see Table 2.2 for geographic positions). At each site, one 15-cm diameter core 0.5–1 m in length was retrieved. In the laboratory, cores were extruded vertically and sectioned in 2-cm intervals. One half of each 2-cm soil interval was used for a related study of organic carbon accumulation (Unger et al., submitted), whereas the remaining half was used in this study for gravimetric analysis of soil properties and gamma spectroscopy. Real-time kinematic (RTK) GPS elevations were taken at each coring site except for MR-3, where lidar-based elevation was used.

2.4.3 Soil physical properties

A total of 488 subsamples from the 18 cores were analyzed for soil physical properties. Water content, dry bulk density, and organic content were measured continuously at 2-cm intervals. Water content (W) was determined gravimetrically from the wet and dry weights of oven-dried samples, and organic content was determined by loss-on-ignition (LOI) by combusting 4 g of sediment powder in a muffle furnace at 550°C for 4 hours (Heiri et al., 2001). The mass of the residual ash was taken as the amount of non-combustible mineral sediment in the sample. Dry bulk density (ρ_d) was computed as follows:

$$\rho_d = \frac{1-W}{\frac{W}{\rho} + \frac{1-W}{\rho_s}} \quad (2.2)$$

where ρ is the average density of pore fluid (1020 kg m⁻³), ρ_s is the density of unconsolidated solids, calculated as $(1-LOI \times 2610) + (LOI \times 1140)$, and 2610 and 1140 are the average particle densities (kg m⁻³) of mineral and organic solids in salt marsh soils (Callaway et al., 1997).

Table 2.2: Location, length, and physical properties for cores collected for this study. Standard deviation of the down-core mean is shown in parentheses. Physical properties determined gravimetrically and by loss-on-ignition (LOI).

Estuary	Marsh	Core	Latitude (DMS, N)	Longitude (DMS, W)	Core length (cm)	Water content (% mass)	LOI (% solid mass)	Bulk density (kg m ⁻³)	Organic density (kg m ⁻³)	Mineral density (kg m ⁻³)
Delaware Bay	Dennis Creek (DN)	1	39° 10' 18.46"	74° 52' 32.80"	50	80 (8)	42 (10)	219 (106)	82 (20)	137 (89)
		2	39° 10' 34.41"	74° 51' 43.84"	60	73 (3)	26 (3)	315 (48)	81 (10)	233 (42)
		3	39° 10' 51.83"	74° 50' 19.04"	62	70 (4)	22 (4)	354 (69)	75 (6)	279 (71)
	Dividing Creek (DV)	1	39° 13' 31.09"	75° 06' 27.67"	76	73 (4)	23 (4)	295 (53)	69 (12)	227 (50)
		2	39° 13' 56.52"	75° 06' 59.90"	60	72 (5)	25 (7)	326 (83)	77 (9)	249 (80)
		3	39° 14' 25.89"	75° 06' 12.80"	60	87 (3)	52 (6)	150 (32)	78 (14)	72 (22)
	Maurice River (MR)	1	39° 14' 32.30"	75° 00' 40.59"	74	60 (1)	16 (3)	517 (28)	84 (18)	433 (33)
		2	39° 15' 58.79"	74° 59' 45.43"	78	61 (4)	15 (3)	494 (68)	74 (8)	420 (72)
		3	39° 17' 00.47"	74° 59' 10.15"	76	61 (2)	14 (1)	492 (42)	72 (5)	420 (43)

Table 2.2 continued

Barnegat Bay	Channel Creek (CC)	1	39° 37' 35.10"	74° 15' 25.70"	42	70 (6)	26 (9)	359 (101)	88 (14)	270 (105)
		2	39° 37' 44.45"	74° 15' 27.95"	52	72 (7)	31 (9)	301 (90)	89 (16)	212 (91)
		3	39° 37' 58.70"	74° 15' 33.10"	42	71 (6)	28 (9)	335 (92)	88 (12)	247 (96)
	Island Beach (IB)	1	39° 47' 55.35"	74° 06' 08.90"	46	82 (3)	44 (14)	198 (43)	84 (16)	113 (47)
		2	39° 47' 57.49"	74° 06' 05.92"	74	73 (12)	38 (16)	253 (94)	83 (11)	171 (96)
		3	39° 47' 58.74"	74° 05' 57.66"	42	79 (4)	44 (19)	226 (54)	95 (34)	131 (71)
	Reedy Creek (RC)	1	40° 01' 49.35"	74° 04' 44.37"	42	82 (6)	45 (9)	195 (79)	82 (17)	113 (65)
		2	40° 01' 43.86"	74° 05' 03.67"	64	75 (10)	40 (16)	269 (137)	89 (14)	180 (131)
		3	40° 01' 51.80"	74° 05' 09.39"	42	79 (9)	45 (16)	233 (123)	88 (6)	146 (119)

2.4.4 Radionuclide measurements

Profiles of excess ^{210}Pb ($^{210}\text{Pb}_u$) and ^{137}Cs activity and were constructed from cores to determine rates of mass accumulation and vertical accretion at marsh coring sites. These radionuclide chronometers average accumulation and accretion over 50–100 years and thus provide long-term rates relative to short-term estimates based on data from particle collection devices or marker beds. A total of 485 samples were analyzed for 24 hours for ^{137}Cs , ^{210}Pb , and ^{214}Bi activity via gamma-ray spectroscopy using Canberra low-energy planar Germanium detectors. Activity efficiencies for marsh soil samples were determined by analysis of a natural matrix standard (SRM Rocky Flats Soil; Nour et al., 2008). The minimum detectable activity for ^{210}Pb and ^{137}Cs was 0.533 and 0.087 Bq, respectively. Uncertainties were calculated as the 1σ counting error. Activity of $^{210}\text{Pb}_u$ was calculated by subtracting the ^{214}Bi activity, the ^{226}Ra -produced supported ^{210}Pb activity, from the total ^{210}Pb activity ($^{210}\text{Pb}_u = ^{210}\text{Pb}_{\text{total}} - ^{214}\text{Bi}$). The $^{210}\text{Pb}_u$ activity uncertainty was computed as the sum of ^{210}Pb and ^{214}Bi activity uncertainties. Because the cores were collected within a period of several weeks and the radionuclide analysis completed within a year of collection, decay corrections were not applied to the ^{210}Pb and ^{137}Cs data.

2.4.5 Marsh accretion and mass accumulation rates

Rates of accretion and mass accumulation (mineral sediment and organic matter) were computed by linear regression of the entire $^{210}\text{Pb}_u$ activity-depth profile for the cores. At steady state $^{210}\text{Pb}_u$ decreases exponentially with soil depth following:

$$A_z = A_0 e^{-\lambda z} \quad (2.3)$$

where A_z is the excess activity (Bq kg^{-1}) of $^{210}\text{Pb}_u$ at depth z (m), A_0 is the initial activity at the core top, λ is the decay constant (0.0311 y^{-1}), and S is the accretion rate (cm y^{-1}). The corresponding mass accumulation rate ($\text{kg m}^{-2} \text{ y}^{-1}$) was computed by regression of $^{210}\text{Pb}_u$ activity versus cumulative mass (kg m^{-2}), which is the product of dry bulk density and the interval thickness.

Mass accumulation and accretion rates were also computed by assigning the ^{137}Cs activity peak as an indicator of the year of maximum atmospheric fallout (1963; Ritchie and McHenry, 1990). The depth (or accumulated mass) of the activity peak divided by the time interval between the year of core collection (2012) and 1963 gives the accretion rate (or mass accumulation rate). Average organic matter accumulation (OMA in kg m^{-2}) since 1963 was determined as follows:

$$OMA = \sum_{i=0m}^{1963 \text{ depth}} (OM_i \cdot \rho_{di} \cdot x_i) \quad (2.4)$$

where OM_i is the mass concentration ($\text{kg organic matter/kg soil sample}$) of combustible organic matter ($LOI/100$) for the i th depth interval, ρ_d is the dry bulk density (kg m^{-3}), and x_i is the interval thickness (m). Similarly, mineral sediment accumulation (MSA in kg m^{-2}) were calculated according to:

$$MSA = \sum_{i=0m}^{1963 \text{ depth}} (MM_i \cdot \rho_{di} \cdot x_i) \quad (2.5)$$

where MM_i is the mass concentration ($\text{kg mineral matter/kg soil sample}$) of incombustible solids ($(1-LOI)/100$) for the i th depth interval, and the other terms are described above. Implicit in ^{210}Pb and ^{137}Cs dating methods are the following assumptions: 1) particle mixing by burrowing organisms has not altered the initial age-depth relationship; 2) the radionuclide is chemically immobile; and 3) the sedimentary record is complete and not punctuated by significant non-depositional or erosional episodes. As discussed later, these assumptions were verified in this study.

To identify differences in marsh soil properties and accretion and accumulation within and between the two estuaries, two-sample t-tests ($\alpha = 0.05$) were conducted. While the hierarchical design of this study may lend itself to a nested analysis of variance approach to hypotheses testing, a two-sample t-test is both simpler and, for this design, mathematically equivalent (e.g., Murtaugh, 2007). Rates of mass accumulation and accretion derived using ^{137}Cs and $^{210}\text{Pb}_u$ methods were compared using paired t-tests. Normality was achieved using simple log or inverse transformations, if necessary. All analyses were conducted using the *R stats* package (<http://cran.r-project.org/>).

2.5 Results and Interpretation

2.5.1 Marsh hydrogeomorphic characteristics

Tidal flooding duration and frequency curves computed for the Delaware Bay and Barnegat Bay study areas are shown in Figure 2.2. The Delaware Bay marshes fell in the mid- to upper tidal frame whereas the Barnegat Bay marshes fell within the full range of the tidal frame. The average frequency of marsh flooding estimated was similar at $74\pm 18\%$ (1σ , $n=9$) and $76\pm 13\%$ (1σ , $n=9$) for Delaware Bay and Barnegat Bay marshes, respectively. The duration of tidal flooding was less similar at $20\pm 9\%$ and $44\pm 25\%$ of the time for Delaware Bay and Barnegat Bay, respectively.

As indicated by the hypsometric curves plotted in Figures 2.3 and 2.4, there was considerably more inter-site variability in marsh platform hypsometry among the three marsh systems in Delaware Bay than in Barnegat Bay. Overall the hypsometric integral averaged 0.55 ± 0.11 (1σ , $n=9$) and 0.40 ± 0.21 for Delaware Bay and Barnegat Bay marshes, respectively (Table 2.1), indicating that marshes in Delaware Bay have

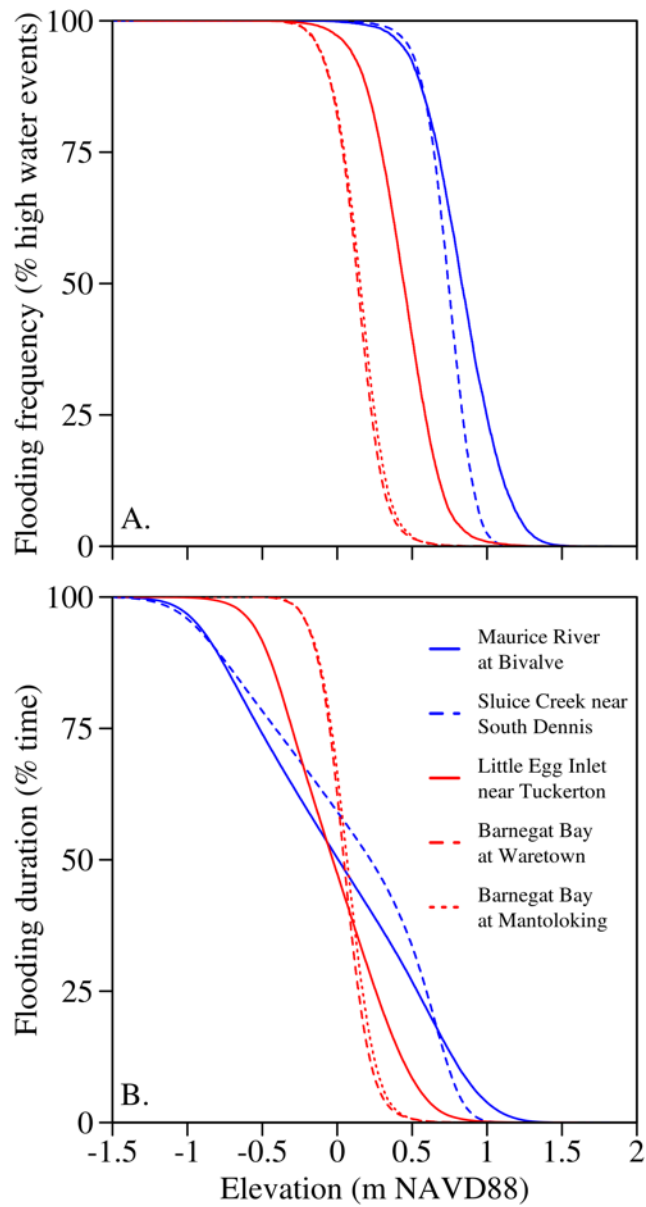


Figure 2.2: Plots of marsh flood frequency (A) and duration (B) versus elevation for Delaware Bay and Barnegat Bay study areas. The curves were produced using 6-minute water level records (2000–2015) for the USGS tide gauges listed in the legend.

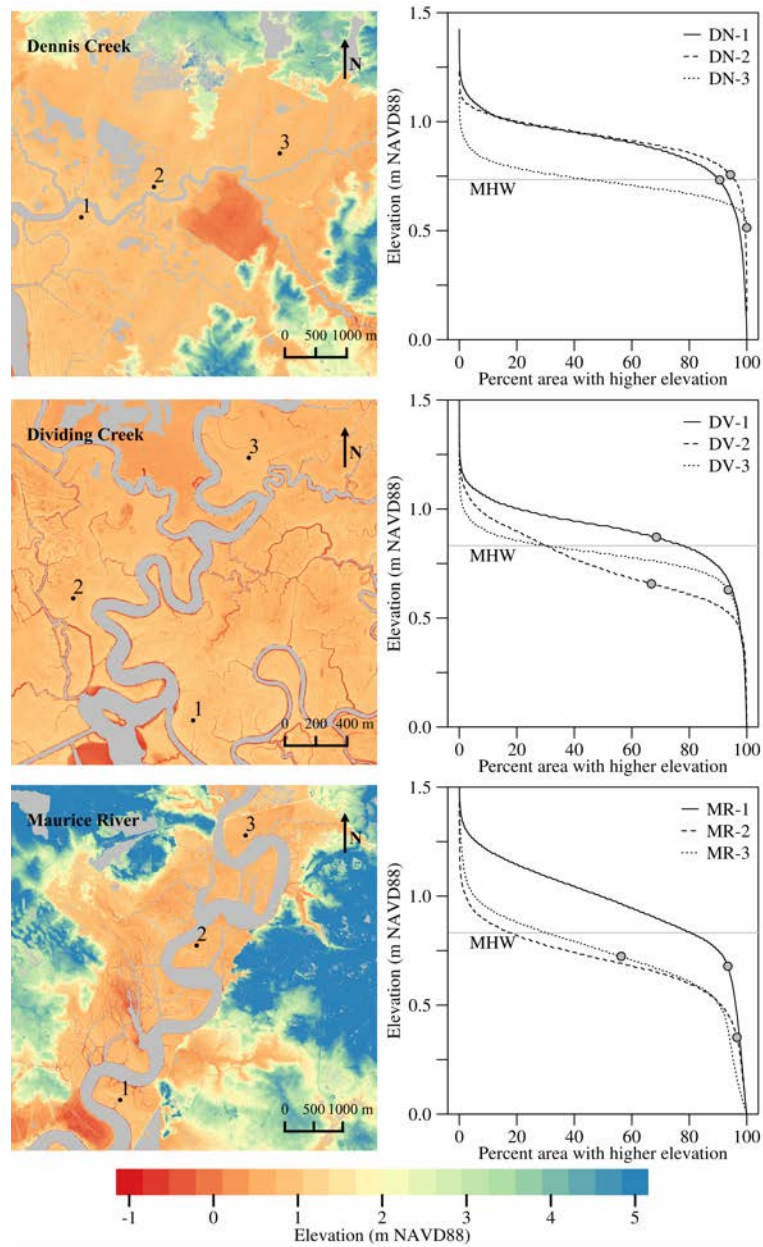


Figure 2.3: Lidar-based elevation maps and hypsometric curves for the Delaware Bay marsh systems. The horizontal extent of each map corresponds to the solid bounding boxes in Figure 2.1. The hypsometric curves were computed from elevations within a 100 m radius of each coring site, which are numbered 1–3 in the maps and plotted as solid circles on the curves. Mean high water (MHW) was calculated as the average of high waters from the nearest USGS tide gauge shown in Figure 2.1 and listed in Table 2.1.

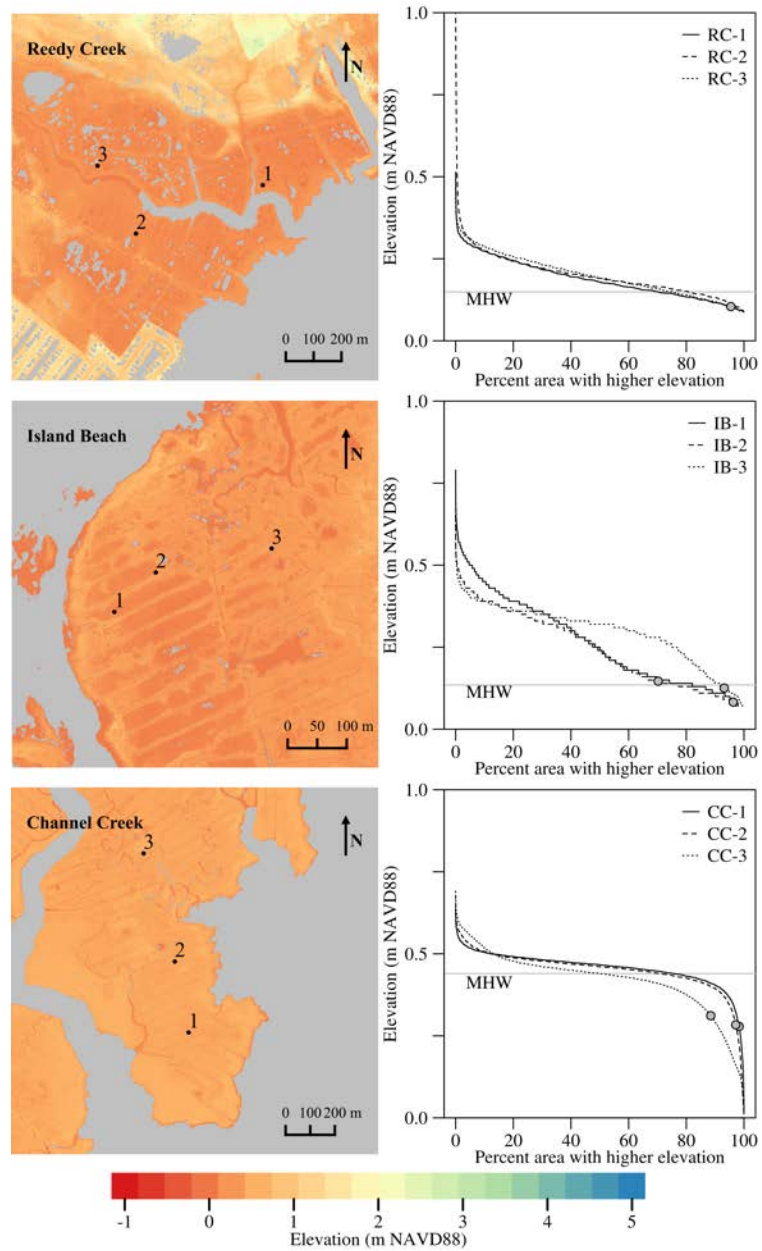


Figure 2.4: Lidar-based elevation maps and hypsometric curves for the Barnegat Bay marsh systems. The horizontal extent of each map corresponds to the solid bounding boxes in Figure 2.1. The hypsometric curves were computed from elevations within a 100 m radius of each coring site, which are numbered 1–3 in the maps and plotted as a solid circles on the curves. Mean high water (MHW) was calculated as the average of high waters from the nearest USGS tide gauge shown in Figure 2.1 and listed in Table 2.1.

more relief. Tidal flooding duration and hypsometric integral were inversely correlated (Figure 2.5), demonstrating that marsh areas with more relief have shorter periods of tidal flooding. Hence, although marshes in both estuaries have similar tidal flooding frequencies, the steeper platforms of Delaware Bay marshes have shorter hydroperiods than shallower sloped platforms of Barnegat Bay marshes.

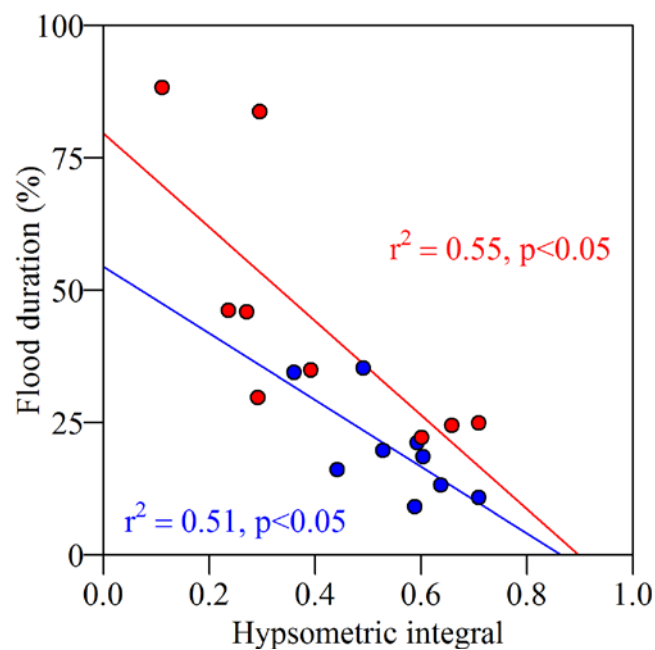


Figure 2.5: Scatterplot of tidal flood duration versus the hypsometric integral, the elevation relief ratio for a given site. For both the Delaware Bay (blue) and Barnegat Bay (red) marsh sites, there was an inverse relationship between flood duration and hypsometric integral. See text for further description.

2.5.2 Marsh soil properties

Down-core values of marsh soil water content, *LOI*, and density are presented in Table 2.2. Soil water content ranged 60–87 and 70–82 % mass, *LOI*

ranged 14–52 and 26–45 % solid mass, and dry bulk density ranged 150–517 and 195–359 kg m⁻³ in Delaware Bay and Barnegat Bay, respectively. Marsh soils from Barnegat Bay had a larger amount of organic matter than mineral sediment by mass, whereas Delaware Bay marsh soils had a larger amount of mineral sediment than organic matter (Figure 2.6). Dry bulk density generally varied inversely with water content and organic matter content (*LOI*) and directly with mineral sediment content ($1/LOI$), as is frequently observed for marsh soils (Bricker-Urso et al., 1989; Callaway et al., 2012). Tabulated soil properties for all core samples are presented in Appendix A.

Profiles of soil volume composition were used to examine the relative contributions of mineral sediment and organic matter to the total, because the volume of mineral and organic solids is more closely related to soil structure and vertical accretion than mass. As shown in Figure 2.7, the volume of marsh soils in both estuaries consists mostly of water volume (>80%) with considerably lesser amounts made up of mineral and organic solids. Mineral sediment comprises a larger fraction of the total volume of the Delaware Bay marsh soil than the marsh soil of Barnegat Bay, whereas the volume of organic matter is more comparable. Integrated above the 1963 year-depth, Barnegat and Delaware Bay marsh soils have similar organic volume (7%) but Barnegat Bay soils are composed of three times less mineral volume (3%) than Delaware Bay soils (9%). These results make clear that soils of estuarine marshes in Delaware Bay are more minerogenic than the comparatively organogenic soils of Barnegat Bay coastal marshes, consistent with the physiographic soils classification of Darmody and Foss (1979). Soil profiles for all cores are presented in Appendix B.

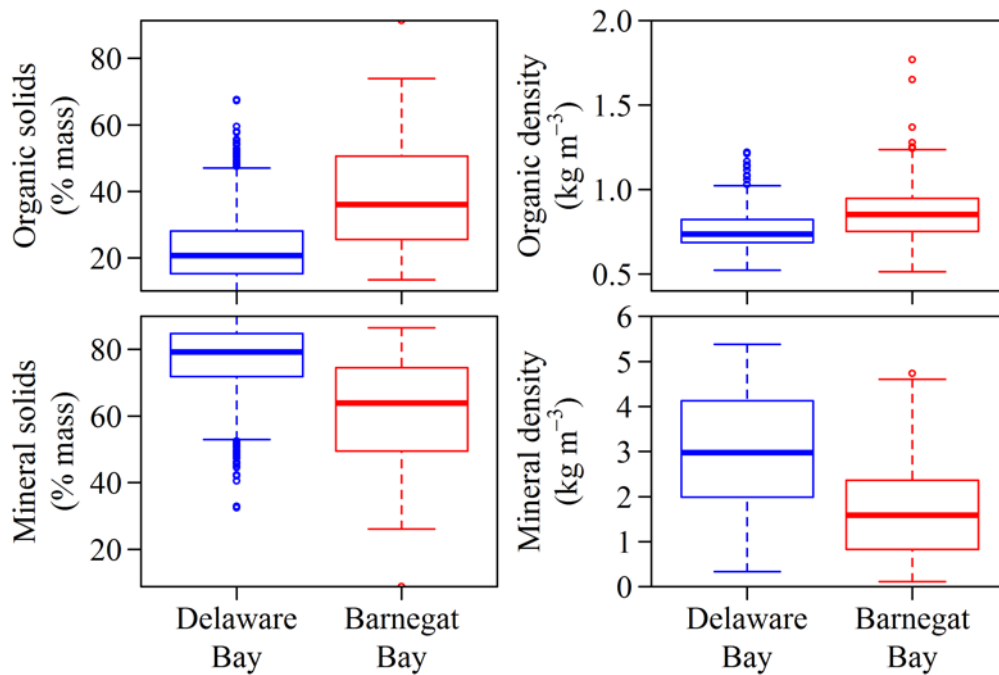


Figure 2.6: Box-and-whisker plots of organic and mineral solids concentration and density for Delaware Bay (n = 284) and Barnegat Bay (n = 204) marsh soils. The lower whisker is the minimum value excluding outliers (lower than 1.5 x interquartile range), bottom line of the box is the lower quartile, the solid line inside the box represents the median, the upper line of the box is the upper quartile, the upper whisker is the maximum excluding outliers (larger than 1.5 x the interquartile range), and outliers are represented by open circles. Soil organic densities are similar between the two estuaries, but mineral sediment densities are twofold larger in the Delaware Bay marshes.

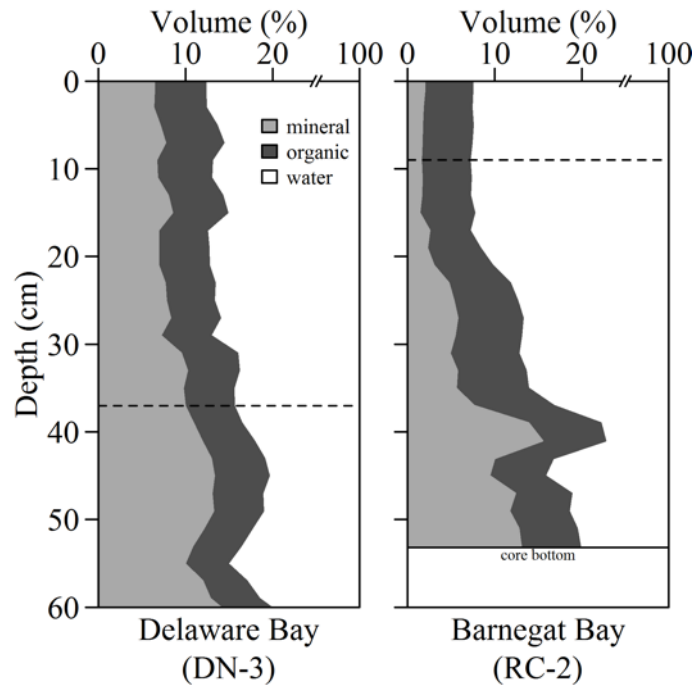


Figure 2.7: Representative marsh soil profiles for the Delaware and Barnegat bay estuaries showing the volumetric contributions of mineral sediment, organic matter, and water-filled pore space to the total soil volume. The location of the 1963 year-depth is marked by a dashed line. Inventories of mineral sediment and organic matter relative to 1963 are calculated by dividing mass accumulation divided by accretion using the values presented in Table 2.3.

2.5.3 Marsh accretion and mass accumulation rates

A ^{137}Cs activity peak, corresponding to maximum atmospheric fallout in 1963, was present in all cores with the exception of MR-3 (Figure 2.8). Tabulated radionuclide activities for all core samples are presented in Appendix A. In all cores ^{137}Cs was detectable in the uppermost sample (0–2 cm), which, given that global fallout has been negligible since about 1990, suggests that there are sources of legacy ^{137}Cs in the study areas. These sources may include wash-in of ^{137}Cs -laden soils from watershed and sediment eroded from marsh edges and redeposited on the marsh

platform. The ^{137}Cs activity peaks are distinct and suggest that these profiles have not been subjected to significant physical or biological mixing. The depth of the ^{137}Cs peak in cores ranged from 9 to 51 cm overall, consistent with vertical accretion rates of 0.19 to 1.06 cm y^{-1} (Table 2.3). Accretion rates for the Delaware Bay marshes averaged 0.70 cm y^{-1} ($n=8$) compared to 0.28 cm y^{-1} ($n=9$) for Barnegat Bay.

Profiles of $^{210}\text{Pb}_u$ activity were used to calculate accretion rates for the eighteen cores following Equation 2.3 (Figure 2.9). Tabulated radionuclide activities for all core samples are presented in Appendix A. Core profiles of ^{210}Pb and ^{214}Bi activity are presented in Appendix C. With a few exceptions activities decreased monotonically with depth in the soil profile, and the linear regressions were significant ($p<0.05$) with correlation coefficients of $r^2=0.52-0.94$ (Figure 2.9). Accretion rates averaged 0.81 cm y^{-1} ($n=9$) and 0.28 cm y^{-1} ($n=9$) for Delaware Bay and Barnegat Bay marshes, respectively (Table 2.3). There was no significant difference in at-site rates of accretion determined by ^{137}Cs and $^{210}\text{Pb}_u$ chronometry (paired t-test, $t(16) = -0.55$, $p = 0.59$). Marsh accretion rates in Delaware Bay were more spatially variable than in Barnegat Bay marshes, presumably on account of the relatively larger spatial variation in mineral sediment and organic matter accumulation.

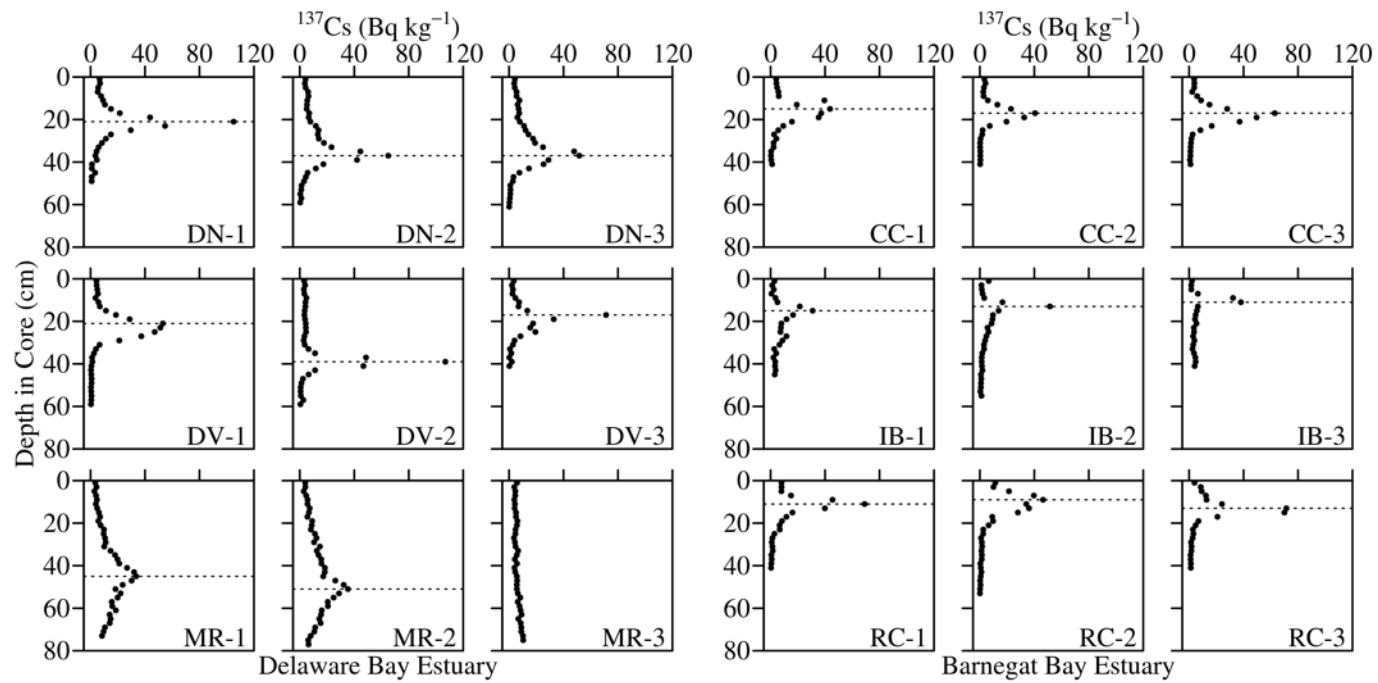


Figure 2.8: Depth profiles of ^{137}Cs activity for Delaware and Barnegat bay marsh cores. The dashed line represents the 1963 activity peak used to calculate accretion and mass accumulation rates (Table 2.3). Note that a ^{137}Cs activity peak was not present in the profile for core MR-3.

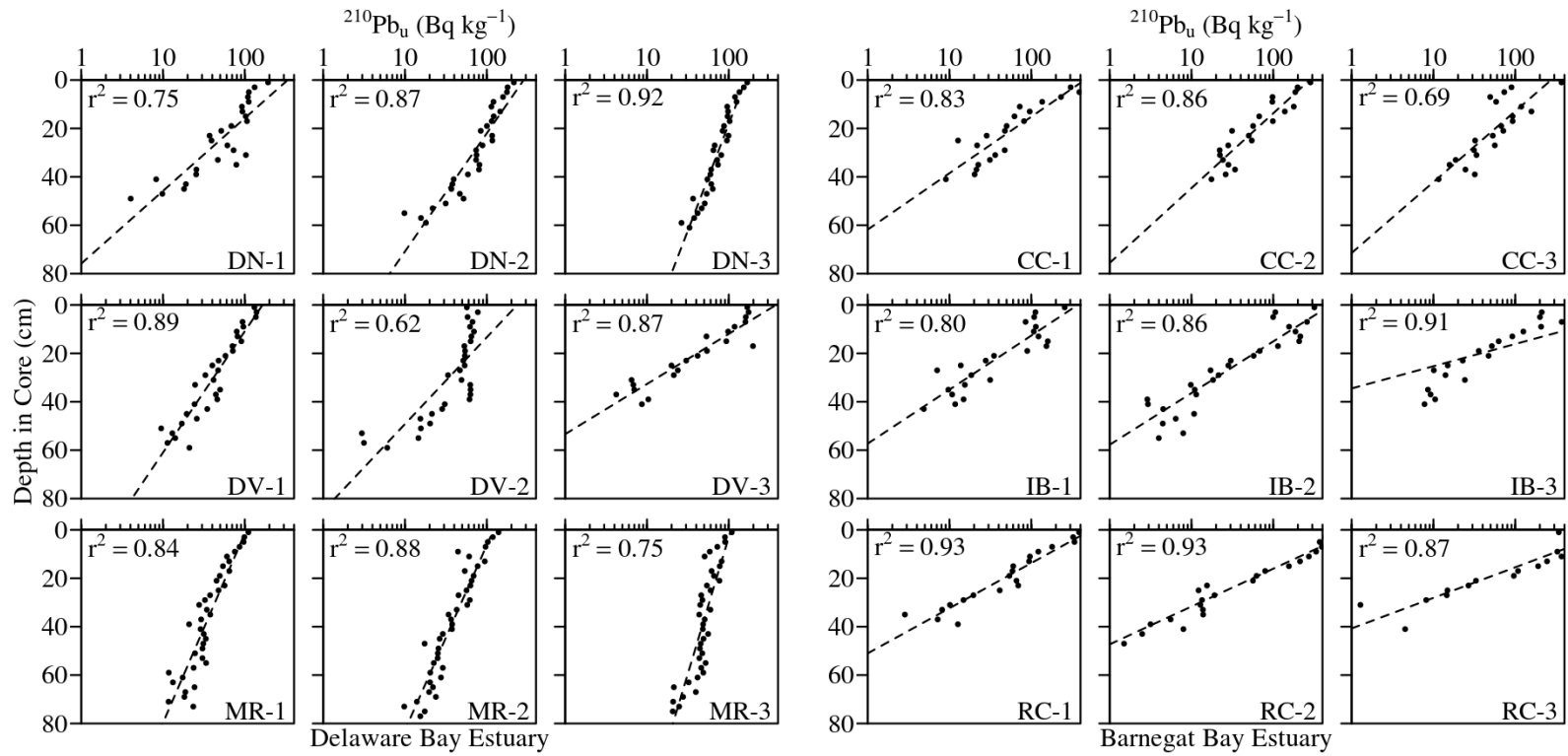


Figure 2.9: Depth profiles of $^{210}\text{Pb}_u$ for the Delaware and Barnegat bay marsh cores. The dashed line is based on the least-squares regression used to calculate accretion and accumulation rates (Table 2.3). The coefficient of determination for each regression is shown and p was less than 0.05.

Table 2.3: Summary of accretion, mineral sediment accumulation (MSA), and organic matter accumulation (OMA) rates determined using ^{137}Cs and excess ^{210}Pb ($^{210}\text{Pb}_u$) methods for this study. The ^{137}Cs rates were based on the 1963 year-depth corresponding to peak ^{137}Cs activity.

Estuary	Marsh	Core	^{137}Cs			$^{210}\text{Pb}_u$		
			Accretion (cm y^{-1})	MSA ($\text{kg m}^{-2}\text{y}^{-1}$)	OMA ($\text{kg m}^{-2}\text{y}^{-1}$)	Accretion (cm y^{-1})	MSA ($\text{kg m}^{-2}\text{y}^{-1}$)	OMA ($\text{kg m}^{-2}\text{y}^{-1}$)
Delaware Bay	Dennis Creek	1	0.44	1.01	0.44	0.41	0.57	0.34
		2	0.77	1.87	0.66	0.66	1.57	0.54
		3	0.77	1.83	0.62	1.19	3.37	0.91
	Dividing Creek	1	0.44	1.12	0.38	0.68	1.54	0.48
		2	0.81	2.29	0.63	-	-	-
		3	0.35	0.31	0.33	0.28	0.21	0.22
	Maurice River	1	0.94	4.05	0.89	1.06	4.66	0.90
		2	1.06	4.20	0.83	1.03	4.38	0.77
		3	-	-	-	1.52	6.47	1.10
means $\pm 1\sigma$			0.70 \pm 0.26	2.08 \pm 1.40	0.60 \pm 0.20	0.81 \pm 0.41	2.66 \pm 2.15	0.63 \pm 0.30

Table 2.3 continued

		1	0.31	0.57	0.34	0.31	0.86	0.28
	Channel Creek	2	0.35	0.72	0.38	0.42	0.91	0.38
		3	0.35	0.59	0.36	0.40	1.01	0.36
		1	0.31	0.21	0.31	0.30	0.35	0.26
Barnegat Bay	Island Beach	2	0.27	0.15	0.25	0.29	0.50	0.24
		3	0.23	0.15	0.36	0.27	0.36	0.26
		1	0.23	0.19	0.21	0.28	0.32	0.24
	Reedy Creek	2	0.19	0.11	0.16	0.23	0.42	0.21
		3	0.27	0.15	0.24	0.17	0.25	0.15
	means $\pm 1\sigma$		0.28 \pm 0.06	0.31 \pm 0.24	0.29 \pm 0.08	0.30 \pm 0.08	0.55 \pm 0.29	0.27 \pm 0.07

Sediment and organic accumulation rates determined by ^{137}Cs chronometry averaged $2.1 \text{ kg m}^{-2} \text{ y}^{-1}$ and $0.60 \text{ kg m}^{-2} \text{ y}^{-1}$, respectively, for Delaware Bay marshes and $0.31 \text{ kg m}^{-2} \text{ y}^{-1}$ and $0.29 \text{ kg m}^{-2} \text{ y}^{-1}$ for marshes in Barnegat Bay (Table 2.3). Sediment and organic accumulation rates based on $^{210}\text{Pb}_u$ chronometry were similar, averaging $2.7 \text{ kg m}^{-2} \text{ y}^{-1}$ and $0.63 \text{ kg m}^{-2} \text{ y}^{-1}$, respectively, for Delaware Bay and $0.56 \text{ kg m}^{-2} \text{ y}^{-1}$ and $0.27 \text{ kg m}^{-2} \text{ y}^{-1}$ for Barnegat Bay. As was the case with accretion rates, there was no significant difference in at-site rates of sediment (paired t-test, $t(16) = 0.19$) and organic (paired t-test, $t(16) = -0.95$, $p = 0.35$) accumulation derived by ^{137}Cs and $^{210}\text{Pb}_u$ chronometry.

It is worth noting that rates of marsh accretion and mass accumulation based on ^{137}Cs activity profiles can be somewhat higher than rates derived from $^{210}\text{Pb}_u$ geochronology when the ^{137}Cs peak is located in the living root zone of marsh soil, and when the $^{210}\text{Pb}_u$ profile extends well below this zone (Mudd et al., 2009). This difference may arise because the $^{210}\text{Pb}_u$ profile averages over a broader range of soil conditions within and below the root zone. In the present case it would appear that $^{210}\text{Pb}_u$ activity did not extend far enough below the root zone to yield accretion and accumulation rates that were significantly different from the ^{137}Cs -derived rates.

2.5.4 Inter-estuary comparison

A goal of this study was to determine if sedimentation rates were significantly different between the two estuaries using simple statistical tests. This was accomplished using a balanced experimental design (*estuary* → *marsh system* → *coring site*) and aggregated, two-sample t-tests. This design accounts for inter-estuary variability observed in the marshes while comparing the rates from Delaware Bay to Barnegat Bay. The ^{137}Cs -based accretion and accumulation rates were used for these

tests except for core MR-3, which did not exhibit a ^{137}Cs activity peak; instead, the $^{210}\text{Pb}_u$ -based rates were used. Test results indicated that mean rates of marsh accretion ($t(4) = -3.79$, $p = 0.019$), mineral sediment accumulation ($t(4) = -3.41$, $p = 0.027$), and organic matter accumulation ($t(4) = -2.87$, $p = 0.045$) were significantly different between the two estuaries. This finding suggests that marshes of coastal plain and lagoon-type estuaries may exhibit distinctive rates of long-term mass accumulation and accretion mostly because of high rates of sediment accumulation in estuarine-type marshes of coastal plain estuaries. Overall, accretion rates measured in this study are comparable to similarly determined rates for other salt marsh systems in the U.S. Mid-Atlantic region (Kemp et al., 2013; Kraft et al., 1992; Nikitina et al., 2014; Velinsky et al., 2011).

2.6 Discussion

2.6.1 Hydrogeomorphic controls on sediment accumulation and accretion

The notion that mineral sediment accumulation and accretion are inversely related to marsh elevation and distance to the nearest tidal waterway (sediment source) was not supported by the results of this study (Figure 2.10). Barnegat Bay marshes are flooded at similar frequencies but for longer durations than Delaware Bay marshes (Table 2.1). Following Equation 2.6, this implies that the Barnegat Bay marshes have greater potential to accumulate mineral sediment, all other factors being equal. Accumulation of sediment should be highest at sites that fall lowest within the tide frame where longer duration of flooding creates the longest time available for deposition. However, an inverse relationship between mineral sediment accumulation and marsh elevation was not

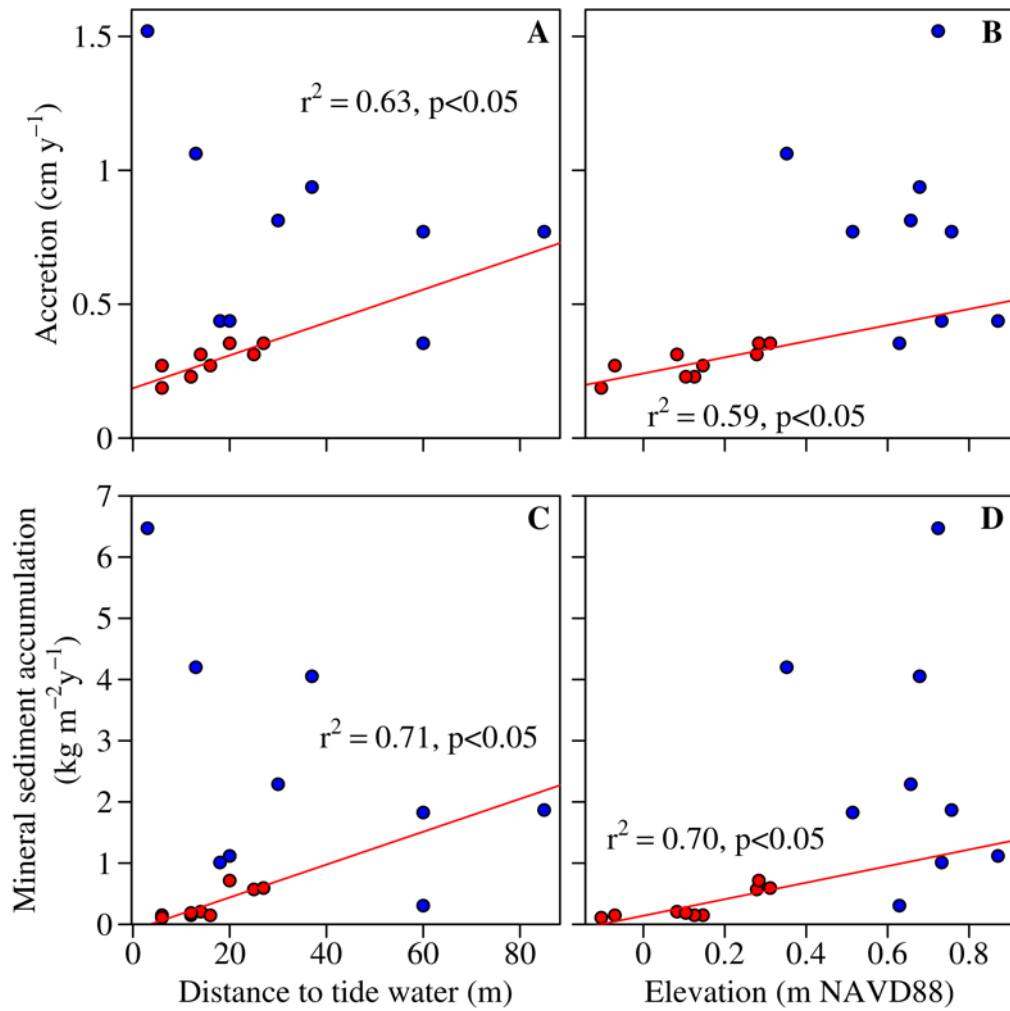


Figure 2.10: Scatterplots of accretion versus distance to tide water (A) and surface elevation (B) and mineral sediment accumulation versus distance to tide water (C) and surface elevation (D) for the Delaware Bay (blue) and Barnegat Bay (red) marsh sites. While these regressions for Barnegat Bay marsh sites were found to be significant, no significant relationship was found for Delaware Bay marsh sites. Note that the accretion and sediment accumulation rates are referenced to the ¹³⁷Cs 1963 age-depth horizon in cores.

found in this study—the opposite was observed (Figure 2.10). Rates of sediment accumulation were 2–3 times higher in Delaware Bay marshes than in Barnegat Bay,

which, lacking a relationship with tidal flood frequency or duration, implies that higher depositional fluxes are responsible for the higher rates of accumulation and accretion on the long term. Intuitively, these higher depositional fluxes reflect the higher concentration and larger resident suspended inventory of Delaware Bay waters compared to Barnegat Bay.

As first proposed by Pethick (1981), accumulation and accretion rates are controlled by the relationship between the depth and duration of tidal flooding and marsh platform elevation such that longer periods of flooding promote sedimentation of particulates by gravitational settling. According to Pethick (1981) and furthered by French (1993), the rate of accretion decreases over time as the marsh builds elevation within the tidal frame, eventually reaching a steady-state value that approaches the local rate of relative sea-level rise. Results of this study illustrate that sediment availability and deposition are primary drivers of accretion over landscape scales, while elevation and proximity to sediment source can influence local variability in sedimentation rate.

Differences in scale and local variability may explain why the Pethick's conceptual model has mixed support by observations (see reviews by Allen, 2000; Fagherazzi et al., 2012; Friedrichs and Perry, 2001). A convincing inverse relationship between marsh elevation and tidal sediment deposition rate is indicated for some marshes (Cahoon and Reed, 1995; French and Spencer, 1993; Temmerman et al., 2003), but not all (van Proosdij et al., 2006), and the same can be concluded for sediment deposition rate as a function of distance to tidal waterways. Relationships between elevation or distance and long-term, radiometrically based rates of accumulation and accretion are more tenuous (Chmura and Hung, 2004; Temmerman

et al., 2004). In fact, there is evidence to suggest that a given marsh can exhibit different patterns of deposition depending on how and when sampling is conducted.

For example, French and Spencer (1993) observed inverse *and* direct correlations between elevation and accretion rates for the same salt marsh sampled at different spatial scales. For a Scheldt Estuary salt marsh, Oenema and DeLaune (1988) reported inverse *and* direct relationships between elevation and accretion rate for the same locations sampled at different times of the year. Given the wide range of biotic (e.g., Gleason et al., 1979; Nepf, 1999) and physical properties (e.g., Sanford and Halka, 1993; Voulgaris and Meyers, 2004) that influence particle transport and particle trapping on the marsh platform, it is likely that spatiotemporal variability complicates Pethick's paradigm of salt marsh accretion.

A range of simplified models have been used to up-scale rates of tidal deposition to annual and longer-term sediment accumulation for insight on rates of accretion and elevation change (Allen, 1990; French, 1993; Krone, 1987; Temmerman et al., 2004). An example is shown the following equation, which gives an annual rate of sediment accumulation (S) from the product of suspended-sediment concentration (C) and settling velocity (w_s), integrated over the tidal period and integrated again over the number of tidal flooding events per year:

$$\frac{dS}{dt} = \int_{year} \int_{tide} C(t) \cdot w_s dt \quad (2.6)$$

where the product of C and w_s is the depositional flux ($M/L^2/T$). A probability term to estimate sediment resuspension during the period of tidal flooding can be included in Equation 2.6 (French, 1993), and variations in C over the tidal cycle can be parameterized through a relationship with water depth (Temmerman et al., 2004). At steady state, and when applied to a sloping marsh platform, the time integrals in

Equation 2.6 produce an inverse relationship between marsh elevation and sediment deposition rate. Despite its simplicity, Equation 2.6 is capable of yielding realistic rates of sediment accumulation and accretion in minerogenic marshes where creation of soil volume occurs predominantly through aboveground processes (French, 1993; Temmerman et al., 2004).

Two limitations of simple models analogous to Equation 2.6 are that they (1) do not include a threshold stress condition for deposition and erosion but rather assume deposition is continuous, and (2) do not consider time-dependent settling velocity. As such these models cannot capture the condition of concurrent deposition and resuspension of different-sized particle aggregates with different settling velocities (Sanford and Halka, 1993), which has been observed in marsh creeks (Voulgaris and Meyers, 2004). Hence, the oft-assumed decrease in sediment deposition rate within increasing marsh elevation, while frequently interpreted to reflect decreasing C with increasing hydroperiod, could be explained by differential settling of particles of different size along the flow pathway. For example, in a study of tidal deposition in a Delaware salt marsh, Moskalski and Sommerfield (2012) found that creek-to-marsh depositional patterns were better explained by spatial variations in mudfloc size and settling velocity than variations in flood frequency and duration. Particle aggregation-disaggregation influences tidal deposition and thereby complicates simple upscaling of deposition rates to longer-term sediment accumulation.

Episodic sediment deposition during storms is a further limitation of tidal up-scaling models such as Equation 2.6. In U.S. Mid-Atlantic marshes, patterns rates of fair-weather sediment deposition are overprinted by the effects of meteorologically enhanced tides, particularly northeaster storms, which flood the low–high marsh

platform with high-turbidity water (Moskalski and Sommerfield, 2013; Roman and Daiber, 1984; Stumpf, 1983). Northeasters are much more frequent and generally longer-lived than tropical cyclones regionally and capable of super-elevating marsh water levels over several tidal cycles. Rainfall runoff, enhanced tidal currents, and wind-waves in wetland waterways of the Delaware Bay coast contribute to suspended sediment concentrations during northeasters, and are directly relevant to marsh sedimentation (Moskalski et al., 2011). Models of marsh sedimentation that do not account for episodic deposition by storms are not likely to produce realistic estimates of longer-term accretion and elevation change.

2.6.2 Potential feedbacks between mass accumulation and accretion

Regression-based relationships between marsh accretion and mass accumulation (mineral and organic) are frequently used for insight on biotic and abiotic processes of soil formation (Callaway et al., 2012; Chmura and Hung, 2004; Nyman et al., 2006; Turner et al., 2000). Comparison of accretion and mass accumulation rates invalidates the assumption of independence because the accumulation rate is derived from the accretion rate. Rather, accumulated mass (kg m^{-2}) can be compared to accretion independently. In the present study, accumulated mass and accretion were strongly correlated in marshes of both estuaries (Figure 2.11a,b). For Delaware Bay marshes, variation in accumulated mineral sediment and organic matter explained 94% of the variation in marsh accretion rate compared to 60–69% for marshes in Barnegat Bay (Figure 2.11a,b). Whereas mineral sediment explained more of this variation for Barnegat Bay marshes, both mineral sediment and organic matter explained variations in accretion similarly in Delaware Bay. Based on the trendline slopes, marsh accretion in Delaware Bay was relatively more sensitive to

variations in mineral and organic accumulation. Hence, although organic matter accumulation clearly influences vertical accretion rate in these marshes, the upper limit of accretion is set by the rate of mineral sediment accumulation. These results are broadly consistent with relationships reported for U.S. Gulf Coast (Nyman et al., 2006; Turner et al., 2000) and West Coast tidal marshes (Callaway et al., 2012).

As shown in Figure 2.11c, there were significant correlations between accumulated mineral and organic mass in Delaware Bay and in Barnegat Bay. This relationship likely signifies a biogeomorphic feedback between mineral sedimentation and plants on the marsh platform, a well-known process that is incorporated within numerical models of tidal marsh sedimentation (Fagherazzi et al., 2012). Surface feedbacks include reduction of flow velocity and direct capture of suspended matter by the canopy leading to increased mineral sedimentation (Gleason et al., 1979; Nepf, 1999). Additional feedbacks between plants and mass accumulation could include: reduced surface-sediment resuspension by root encapsulation (Langlois et al., 2001), increased soil shear strength and erosion resistance by roots (Watts et al., 2003), stimulated root growth by mineral sediment (DeLaune et al., 1981), and burial of the plant itself (Deng et al., 2008; Langlois et al., 2001). Soil organic matter in the *Spartina* marshes in this study was composed of almost exclusively belowground biomass in the form of root and rhizome material (as opposed to leaves and stems), and sedimentation may have enhanced root growth (Boorman et al., 2001). In Barnegat Bay, the weaker relationship between accumulated mineral sediment and organic matter may have been associated with the relatively low range of sedimentation rates (Figure 2.11c). Since 1963, sediment delivery to Barnegat Bay marshes resulted in less than 40 kg m⁻² of mineral sediment, which correlates with a

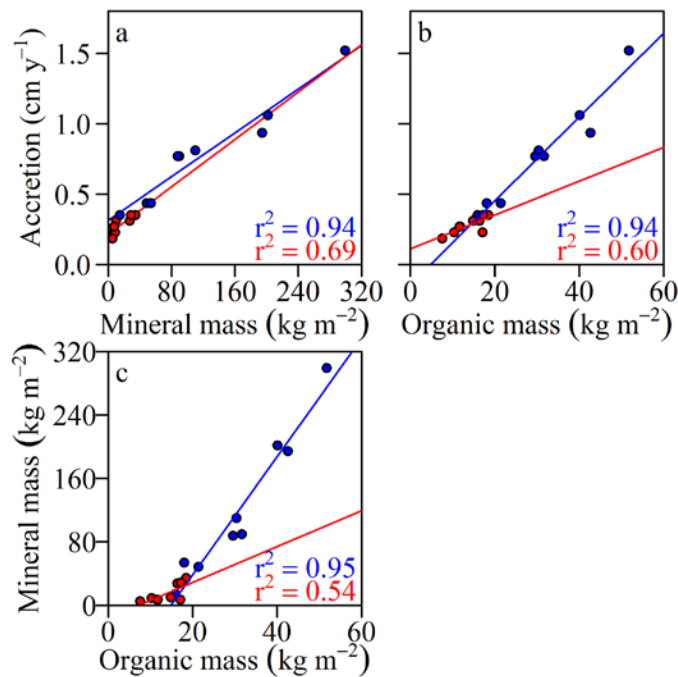


Figure 2.11: Scatterplots of accretion rate versus accumulated mineral mass (a) and accumulated organic mass (b), and accumulated mineral mass versus accumulated organic mass (c) for the Delaware Bay (blue) and Barnegat Bay (red) marsh sites. Note that the accretion rates and accumulated mass values are referenced to the ¹³⁷Cs 1963 age-depth horizon in cores.

relatively low accumulation of organic matter (< 20 kg m⁻²) in both estuaries. It is only when mineral sediment accumulated above 80 kg m⁻² that the amount of organic matter increased. This threshold could be indicative of either an enhancement of belowground production and/or litter burial by mineral deposition. However, identification the exact mechanisms and feedbacks was not possible from analysis of the soil record in this study.

2.6.3 Marsh accretion and inundation potential

While geographically proximal, Delaware Bay and Barnegat Bay represent endmember estuarine environments with regard to tidal wetland stability and adaptability in the face of climatic and anthropogenic impacts. Indeed, results of this study indicate that rates of mass accumulation and accretion in sediment-rich marshes of Delaware Estuary are significantly higher than rates for Barnegat Bay marshes (Table 2.3). In an assessment of U.S. Mid-Atlantic marsh vulnerability to sea-level rise, Reed et al. (2008) concluded that marshes might convert to open water should rates of sea level rise accelerate in the future. To further address inundation potential, accretion rates measured for this study were compared to rates of relative sea-level rise rates from local tide gauges (Figure 2.12). This comparison is reasonable since the radionuclide-based rates of accretion average over the same timespan (50–100 y) as the gauged record of sea level. However, it assumes that the marsh landscape and tide gauges are subsiding at the same rate, when in fact differential subsidence associated with different processes and on different time scales (i.e., crustal isostatic adjustment, compaction of marsh soil) can lead to differences (Cahoon, 2015).

At current rates of local relative sea-level rise ($3.4\text{--}4.6\text{ mm y}^{-1}$) the Barnegat Bay marshes examined in this study are at risk of inundation, and more so the risk increases if sea-level rise were to accelerate in the future (Figure 2.12). In contrast, the Delaware Bay marshes are accreting at to above rates of relative sea-level rise and do not appear to be in jeopardy of submergence at current rates. In a review of marsh accretion and elevation change for US Atlantic and Gulf coast tidal marshes, Kirwan et al. (2016) suggest that comparisons of accretion and sea-level rise rates overestimate vulnerability as this does not take into account landward migration of the marsh and biophysical feedbacks between plant growth and sedimentation. However,

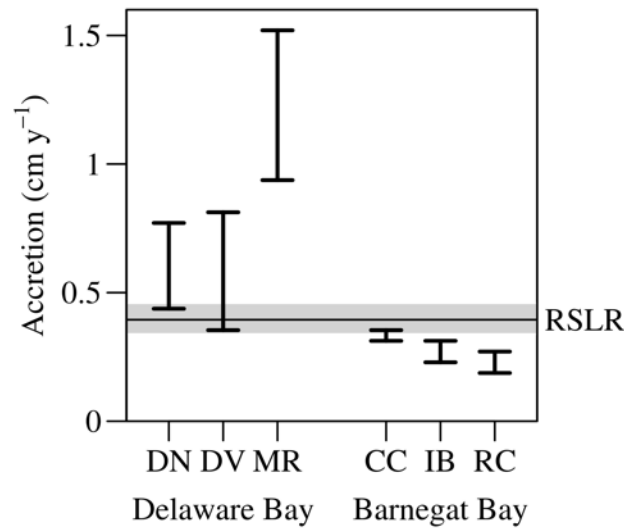


Figure 2.12: Range of ¹³⁷Cs-based accretion rates for the Delaware Bay and Barnegat Bay marsh sites plotted with the range (cm y⁻¹) of relative sea level rise (RSLR) reported for nearby NOAA tide gauges. See text for further discussion.

such feedbacks require a minimum level of mineral sediment input that may not exist in some wetland systems. In the case of Barnegat Bay, marsh accretion rates are at or below current rates of relative sea-level rise, partly because of low rates of sediment accumulation. Being primarily organogenic, Barnegat Bay marshes will be prone to reduced plant productivity due to water logging associated with land subsidence and sea-level inundation (Kirwan et al., 2010; Snedden et al., 2015) relative to the rapidly accreting minerogenic marshes in Delaware Bay. Moreover, the relative paucity of suspended sediment in the Barnegat estuarine system fundamentally limits the ways in which the marshes can adjust to increases in tidal flood frequency and duration. Based on the findings of this study, it can be concluded that accretion deficits that cannot be offset by increased organic accumulation must be accompanied by increased sediment

accumulation to avert marsh submergence. In Barnegat Bay 36% of the shoreline is hardened and 70% of the landward buffer developed (Lathrop Jr. and Bognar, 2001); hence, even if the marshes are capable of adjustment, the potential for landward migration is limited.

2.7 Conclusions

In this study, rates of mineral and organic accumulation in estuarine marshes of Delaware Bay coastal marshes of Barnegat Bay marshes were determined via ^{137}Cs and $^{210}\text{Pb}_u$ radionuclide methods to gain insight on accretionary dynamics with regard to geomorphic setting. Accretion rates in marshes of both estuaries were correlated with rates of organic matter and mineral sediment accumulation, as has been observed in other salt marsh systems. However, accretion and sediment accumulation rates did not exhibit the oft-assumed inverse relationships with marsh elevation and distance to nearest sediment source. Hence, it would appear that hydroperiod is less of a determinant on sediment accumulation and accretion than rates of tidal deposition mediated by suspended-sediment concentration in estuarine waters. Sediment accumulation and accretion rates were significantly higher in Delaware Bay marshes ($2.57 \pm 2.03 \text{ kg m}^{-2} \text{ y}^{-1}$ and $0.79 \pm 0.06 \text{ cm y}^{-1}$) than those in Barnegat Bay ($0.31 \pm 0.27 \text{ kg m}^{-2} \text{ y}^{-1}$ and $0.28 \pm 0.06 \text{ cm y}^{-1}$). This difference is a direct reflection of estuarine geomorphic setting, i.e., a sediment-rich, mesotidal coastal plain estuary versus a sediment-limited, microtidal lagoon estuary, and will factor into the ability of the marshes to adjust to sea-level rise and human pressures.

REFERENCES

- Allen, J.R.L., 2000. Morphodynamics of Holocene salt marshes: a review sketch from the Atlantic and Southern North Sea coasts of Europe. *Quat. Sci. Rev.* 19, 1155–1231. doi:10.1016/S0277-3791(99)00034-7
- Allen, J.R.L., 1990. Salt-marsh growth and stratification: a numerical model with special reference to the Severn Estuary, southwest Britain. *Mar. Geol.* 95, 77–96. doi:10.1016/0025-3227(90)90042-I
- Biggs, R.B., Beasley, E.L., 1988. Bottom and suspended sediments in the Delaware River and Estuary, in: Majumdar, S.K., Miller, E.W., Sage, L.E. (Eds.), *Ecology and Restoration of the Delaware River Basin*. The Pennsylvania Academy of Science, pp. 116–131.
- Boorman, L.A., Hazelden, J., Boorman, M. 2001. The effect of rates of sedimentation and tidal submersion regimes on the growth of salt marsh plants. *Cont. Shelf Res.* 21, 2155-2165.
- Bricker-Urso, S., Nixon, S.W., Cochran, J.K., Hirschberg, D.J., Hunt, C., 1989. Accretion rates and sediment accumulation in Rhode Island salt marshes. *Estuaries* 12, 300–317. doi:10.2307/1351908
- Cahoon, D.R., 2015. Estimating relative sea-level rise and submergence potential at a coastal wetland. *Estuaries and Coasts* 38, 1077–1084. doi:10.1007/s12237-014-9872-8
- Cahoon, D.R., Reed, D.J., 1995. Relationships among marsh surface topography, hydroperiod, and soil accretion in a deteriorating Louisiana salt marsh. *J. Coast. Res.* 11, 357–369.
- Callaway, J.C., Borgnis, E.L., Turner, R.E., Milan, C.S., 2012. Carbon sequestration and sediment accretion in San Francisco Bay tidal wetlands. *Estuaries and Coasts* 35, 1163–1181. doi:10.1007/s12237-012-9508-9
- Callaway, J.C., DeLaune, R., Patrick Jr., W., 1997. Sediment accretion rates from four coastal wetlands along the Gulf of Mexico. *J. Coast. Res.* 13, 181–191.

- Chmura, G.L., Hung, G.A., 2004. Controls on salt marsh accretion: a test in salt marshes of Eastern Canada. *Estuaries* 27, 70–81. doi:10.1007/BF02803561
- Cook, T.L., Sommerfield, C.K., Wong, K.-C., 2007. Observations of tidal and springtime sediment transport in the upper Delaware Estuary. *Estuar. Coast. Shelf Sci.* 72, 235–246. doi:10.1016/j.ecss.2006.10.014
- Darmody, R.G., Foss, J.E., 1979. Soil-landscape relationships of the tidal marshes of Maryland. *Soil Sci. Soc. Am. J.* 43, 534–541.
- Defne, Z., Ganju, N.K., 2015. Quantifying the residence time and flushing characteristics of a shallow, back-barrier estuary: application of hydrodynamic and particle tracking models. *Estuaries and Coasts* 38, 1719–1734. doi:10.1007/s12237-014-9885-3
- DeLaune, R., Reddy, C.N., Patrick Jr., W., 1981. Accumulation of plant nutrients and heavy metals through sedimentation processes and accretion in a Louisiana salt marsh. *Estuaries* 4, 328. doi:10.2307/1352157
- Deng, Z., An, S., Zhao, C., Chen, L., Zhou, C., Zhi, Y., Li, H., 2008. Sediment burial stimulates the growth and propagule production of *Spartina alterniflora* Loisel. *Estuar. Coast. Shelf Sci.* 76, 818–826. doi:10.1016/j.ecss.2007.08.008
- Ezer, T., Atkinson, L.P., Corlett, W.B., Blanco, J.L., 2013. Gulf Stream's induced sea level rise and variability along the U.S. Mid-Atlantic coast. *J. Geophys. Res. Ocean.* 118, 685–697. doi:10.1002/jgrc.20091
- Fagherazzi, S., Kirwan, M.L., Mudd, S.M., 2012. Numerical models of salt marsh evolution: Ecological, geomorphic, and climatic factors. *Rev. Geophys.* 50, 1–28. doi:10.1029/2011RG000359.1.INTRODUCTION
- Fletcher, III, C., Knebel, H., Kraft, J.C., 1992. Holocene depocenter migration and sediment accumulation in Delaware Bay: a submerging marginal marine sedimentary basin. *Mar. Geol.* 103, 165–183.
- Fletcher, III, C.H., Knebel, H.J., Kraft, J.C., 1990. Holocene evolution of an estuarine coast and tidal wetlands. *Geol. Soc. Am. Bull.* 102, 283–297. doi:10.1130/0016-7606(1990)102<0283:HEOAEC>2.3.CO;2
- French, J.R., 2006. Tidal marsh sedimentation and resilience to environmental change: Exploratory modelling of tidal, sea-level and sediment supply forcing in predominantly allochthonous systems. *Mar. Geol.* 235, 119–136. doi:10.1016/j.margeo.2006.10.009

- French, J.R., 1993. Numerical simulation of vertical marsh growth and adjustment to accelerated sea-level rise, North Norfolk, U.K. *Earth Surf. Process. Landforms* 18, 63–81. doi:10.1002/esp.3290180105
- French, J.R., Spencer, T., 1993. Dynamics of sedimentation in a tide-dominated backbarrier salt marsh, Norfolk, UK. *Mar. Geol.* 110, 315–331. doi:10.1016/0025-3227(93)90091-9
- Friedrichs, C.T., Perry, J.E., 2001. Tidal salt marsh morphodynamics: a synthesis. *J. Coast. Res.* 81, 7–37.
- Gleason, M.L., Elmer, D.A., Pien, N.C., Fisher, J.S., 1979. Effects of Stem Density upon Sediment Retention by Salt Marsh Cord Grass, *Spartina alterniflora* Loisel. *Estuaries* 2, 271. doi:10.2307/1351574
- Heiri, O., Lotter, A.F., Lemcke, G., 2001. Loss on ignition as a method for estimating organic and carbonate content in sediments: reproducibility and comparability of results. *J. Paleolimnol.* 25, 101–110. doi:10.1023/A:1008119611481
- Horton, B.P., Engelhart, S.E., Hill, D.F., Kemp, A.C., Nikitina, D., Miller, K.G., Peltier, W.R., 2013. Influence of tidal-range change and sediment compaction on Holocene relative sea-level change in New Jersey, USA. *J. Quat. Sci.* 28, 403–411. doi:10.1002/jqs.2634
- Kemp, A.C., Horton, B.P., Vane, C.H., Bernhardt, C.E., Corbett, D.R., Engelhart, S.E., Anisfeld, S.C., Parnell, A.C., Cahill, N., 2013. Sea-level change during the last 2500 years in New Jersey, USA. *Quat. Sci. Rev.* 81, 90–104. doi:10.1016/j.quascirev.2013.09.024
- Kennish, M.J., 2001. Physical description of the Barnegat Bay—Little Egg Harbor estuarine system. *J. Coast. Res.* SI 32, 13–27.
- Kirwan, M.L., Guntenspergen, G.R., D’Alpaos, A., Morris, J.T., Mudd, S.M., Temmerman, S., 2010. Limits on the adaptability of coastal marshes to rising sea level. *Geophys. Res. Lett.* 37, 1–5. doi:10.1029/2010GL045489
- Kirwan, M.L., Temmerman, S., Skeeahan, E.E., Guntenspergen, G.R., Fagherazzi, S., 2016. Overestimation of marsh vulnerability to sea level rise. *Nat. Clim. Chang.* 6, 253–260. doi:10.1038/nclimate2909
- Kraft, J.C., Yi, H., Khalequzzaman, M., 1992. Geologic and human factors in the decline of the tidal salt marsh lithosome: the Delaware estuary and Atlantic coastal zone. *Sediment. Geol.* 80, 233–246. doi:10.1016/0037-0738(92)90043-Q

- Krone, R., 1987. A method for simulating historic marsh elevations, in: Krause, N. (Ed.), *Coastal Sediments '87*. American Society of Civil Engineers, New York, New York, pp. 316–323.
- Langlois, E., Bonis, A., Bouzillé, J.B., 2001. The response of *Puccinellia maritima* to burial: a key to understanding its role in salt-marsh dynamics? *J. Veg. Sci.* 12, 289–297. doi:10.2307/3236613
- Lathrop Jr., R., Bognar, J., 2001. Habitat loss and alteration in the Barnegat Bay region. *J. Coast. Res.* 212–228.
- Luo, W., 1998. Short note hypsometric analysis with a geographic information system. *Comput. Geosci.* 24, 815–821. doi:10.1016/S0098-3004(98)00076-4
- McSweeney, J.M., Chant, R.J., Sommerfield, C.K., 2016. Lateral variability of sediment transport in the Delaware Estuary. *J. Geophys. Res. Ocean.* 121, 725–744. doi:10.1002/2015JC010974
- Moskalski, S.M., Sommerfield, C.K., 2013. Effects of northeaster storms on water level and turbidity in a Delaware Bay subestuary. *J. Coast. Res.* doi:10.2112/JCOASTRES-D-12-00222.1
- Moskalski, S.M., Sommerfield, C.K., 2012. Suspended sediment deposition and trapping efficiency in a Delaware salt marsh. *Geomorphology* 139-140, 195–204. doi:10.1016/j.geomorph.2011.10.018
- Moskalski, S.M., Sommerfield, C.K., and Wong, K.C., 2011. Oceanic and hydrologic influences on flow and water properties in the St. Jones River Estuary, Delaware. *Estuaries and Coasts*, doi: 10.1007/s12237-011-9407-5.
- Mudd, S.M., Howell, S.M., Morris, J.T., 2009. Impact of dynamic feedbacks between sedimentation, sea-level rise, and biomass production on near-surface marsh stratigraphy and carbon accumulation. *Estuar. Coast. Shelf Sci.* 82, 377–389. doi:10.1016/j.ecss.2009.01.028
- Murtaugh, P.A., 2007. Simplicity and complexity in ecological data analysis. *Ecology* 88, 56–62. doi:10.1890/0012-9658(2007)88[56:SACIED]2.0.CO;2
- National Oceanic and Atmospheric Administration (NOAA), 1985. National estuarine inventory: data atlas. Volume 1: physical and hydrologic characteristics. Washington, D.C.

- National Oceanic and Atmospheric Administration (NOAA) /National Ocean Service (NOS)/Center for Operational Oceanographic Products and Services(CO-OPS), 2013. Sea levels online: sea level variations of the United States derived from National Water Level Observation Network stations.
<http://tidesandcurrents.noaa.gov/sltrends/sltrends.html> (accessed 1.1.2014).
- Nepf, H.M., 1999. Drag, turbulence, and diffusion in flow through emergent vegetation. *Water Resour. Res.* 35, 479–489. doi:10.1029/1998WR900069
- Neubauer, S., Anderson, I., Constantine, J., Kuehl, S., 2002. Sediment deposition and accretion in a mid-Atlantic (USA) tidal freshwater marsh. *Estuar. Coast. Shelf Sci.* 54, 713–727. doi:10.1006/ecss.2001.0854
- Nicholls, R.J., Hoozemans, F.M.J., Marchand, M., 1999. Increasing flood risk and wetland losses due to global sea-level rise: regional and global analyses. *Glob. Environ. Chang.* 9. doi:10.1016/S0959-3780(99)00019-9
- Nichols, M.M., 1989. Sediment accumulation rates and relative sea-level rise in lagoons. *Mar. Geol.* 88, 201–219. doi:10.1016/0025-3227(89)90098-4
- Nikitina, D., Kemp, A.C., Engelhart, S.E., Horton, B.P., Hill, D.F., Kopp, R.E., 2015. Sea-level change and subsidence in the Delaware Estuary during the last ~2200 years. *Estuar. Coast. Shelf Sci.* 164, 506–519. doi:10.1016/j.ecss.2015.08.012
- Nikitina, D.L., Kemp, A.C., Horton, B.P., Vane, C.H., van de Plassche, O., Engelhart, S.E., 2014. Storm erosion during the past 2000 years along the north shore of Delaware Bay, USA. *Geomorphology* 208, 160–172.
 doi:10.1016/j.geomorph.2013.11.022
- Nour, S., Inn, K., Filliben, J., 2008. Development of the NIST Rocky Flats Soil Standard. *J. Radioanal. Nucl. Chem.* 277, 161–168. doi:10.1007/s10967-008-0725-4
- Nyman, J.A., Walters, R.J., Delaune, R.D., Patrick Jr., W.H., 2006. Marsh vertical accretion via vegetative growth. *Estuar. Coast. Shelf Sci.* 69, 370–380.
 doi:10.1016/j.ecss.2006.05.041
- Odum, W., 1988. Comparative ecology of tidal freshwater and salt marshes. *Annu. Rev. Ecol. Syst.* 19, 147–176.
- Oenema, O., DeLaune, R.D., 1988. Accretion rates in salt marshes in the Eastern Scheldt, South-west Netherlands. *Estuar. Coast. Shelf Sci.* 26, 379–394.
 doi:10.1016/0272-7714(88)90019-4

- Oertel, G.F., Kraft, J.C., 1994. New Jersey and Delmarva Barrier Islands, in: Davis, R.A. (Ed.), *Geology of Holocene Barrier Island Systems*. Springer, Berlin, pp. 207–232. doi:10.1007/978-3-642-78360-9_6
- Pethick, J.S., 1981. Long-term accretion rates on tidal salt marshes. *J. Sediment. Petrol.* 51, 0571–0577. doi:10.1306/212F7CDE-2B24-11D7-8648000102C1865D
- Redfield, A.C., 1972. Development of a New England Salt Marsh. *Ecol. Monogr.* 42, 201–237. doi:10.2307/1942263
- Reed, D.J., Bishara, D.A., Cahoon, D.R., Donnelly, J.P., Kearney, M.S., Kolker, A.S., Leonard, L.L., Orson, R.A., Stevenson, J.C., 2008. Site-Specific Scenarios for Wetlands Accretion as Sea Level Rises in the Mid-Atlantic Region, in: Titus, J.G., Strange, E.M. (Eds.), *Background Documents Supporting Climate Change Science Program Synthesis and Assessment Product 4.1*. U.S. EPA, Washington, D.C., pp. 134–174.
- Ritchie, J.C., McHenry, J.R., 1990. Application of Radioactive Fallout Cesium-137 for Measuring Soil Erosion and Sediment Accumulation Rates and Patterns: A Review. *J. Environ. Qual.* 19, 215. doi:10.2134/jeq1990.00472425001900020006x
- Rogers, Golden, Halpern, 1990. Profile of the Barnegat Bay: final report for the Barnegat Bay Study Group. New Jersey Dept. of Environmental Protection, Trenton, New Jersey.
- Roman, C.T., Daiber, F.C., 1984. Aboveground and belowground primary production dynamics of two Delaware Bay tidal marshes. *Bull. Torrey Bot. Club* 111, 34–41. doi:10.2307/2996208
- Sanford, L.P., Halka, J.P., 1993. Assessing the paradigm of mutually exclusive erosion and deposition of mud, with examples from upper Chesapeake Bay. *Mar. Geol.* 114, 37–57. doi:10.1016/0025-3227(93)90038-W
- Snedden, G.A., Cretini, K., Patton, B., 2015. Inundation and salinity impacts to above- and belowground productivity in *Spartina patens* and *Spartina alterniflora* in the Mississippi River deltaic plain: implications for using river diversions as restoration tools. *Ecol. Eng.* 81, 133–139. doi:10.1016/j.ecoleng.2015.04.035
- Sommerfield, C.K., Wong, K.-C., 2011. Mechanisms of sediment flux and turbidity maintenance in the Delaware Estuary. *J. Geophys. Res.* 116, 1–16. doi:10.1029/2010JC006462

- Strahler, A.N., 1952. Hypsometric (area-altitude) analysis of erosional topography. *Geol. Soc. Am. Bull.* 63, 1117. doi:10.1130/0016-7606(1952)63[1117:HAAOET]2.0.CO;2
- Stumpf, R.P., 1983. The process of sedimentation on the surface of a salt marsh. *Estuar. Coast. Shelf Sci.* 17, 495–508. doi:10.1016/0272-7714(83)90002-1
- Temmerman, S., Govers, G., Meire, P., Wartel, S., 2003. Modelling long-term tidal marsh growth under changing tidal conditions and suspended sediment concentrations, Scheldt estuary, Belgium. *Mar. Geol.* 193, 151–169. doi:10.1016/S0025-3227(02)00642-4
- Temmerman, S., Govers, G., Wartel, S., Meire, P., 2004. Modelling estuarine variations in tidal marsh sedimentation: response to changing sea level and suspended sediment concentrations. *Mar. Geol.* 212, 1–19. doi:10.1016/j.margeo.2004.10.021
- Turner, R.E., Swenson, E.M., Milan, C.S., 2000. Organic and inorganic contributions to vertical accretion in salt marsh sediments, in: Weinstien, M.P., Kreeger, D.A. (Eds.), *Concepts and Controversies in Tidal Marsh Ecology*. Kluwer Academic Publishers, Dordrecht, pp. 583–595. doi:10.1007/0-306-47534-0_27
- Unger, V., Elsey-Quirk, T., Sommerfield, C.K., and Velinsky, D.J. Stability of organic carbon accumulating in *Spartina alterniflora*-dominated salt marshes of the Mid-Atlantic U.S. Manuscript in review.
- U. S. Fish and Wildlife Service (USFWS), 2010. National Wetlands Inventory. <http://www.fws.gov/wetlands/> (accessed 1.1.2014)
- van Proosdij, D., Davidson-Arnott, R.G.D., Ollerhead, J., Vanproosdij, D., 2006. Controls on spatial patterns of sediment deposition across a macro-tidal salt marsh surface over single tidal cycles. *Estuar. Coast. Shelf Sci.* 69, 64–86. doi:10.1016/j.ecss.2006.04.022
- Velinsky, D.J., Sommerfield, C.K., Enache, M., Charles, D.F., 2011. Nutrient and ecological histories in Barnegat Bay, New Jersey. New Jersey Depart. of Environmental Protection PCER Report No. 10-05. Philadelphia, PA.
- Voulgaris, G., Meyers, S.T., 2004. Temporal variability of hydrodynamics, sediment concentration and sediment settling velocity in a tidal creek. *Cont. Shelf Res.* 24, 1659–1683. doi:10.1016/j.csr.2004.05.006

Watts, C.W., Tolhurst, T.J., Black, K.S., Whitmore, A.P., 2003. In situ measurements of erosion shear stress and geotechnical shear strength of the intertidal sediments of the experimental managed realignment scheme at Tollesbury, Essex, UK. *Estuar. Coast. Shelf Sci.* 58, 611–620. doi:10.1016/S0272-7714(03)00139-2

Chapter 3

ASSESSMENT OF ^{210}Pb AND ^{137}Cs CHRONOLOGICAL MODELS FOR TIDAL MARSH DEPOSITS

3.1 Abstract

Geochronology of sediments and soils using the radionuclides ^{210}Pb and ^{137}Cs has been applied in a wide range of terrestrial and aquatic environments, and the underlying transport models have been reviewed in numerous publications. However, an objective analysis of the assumptions associated with ^{210}Pb and ^{137}Cs geochronology has not been conducted for tidal marsh deposits, which are unique in terms of radionuclide supply pathways and soil composition. The Constant Flux – Constant Supply (CFCS), Constant Rate of Supply (CRS), and Constant Initial Concentration (CIC) models for ^{210}Pb chronology were applied to eighteen marsh soil cores from two different U.S. Mid-Atlantic estuaries. Age-depth relationships based on the onset and peak fallout of ^{137}Cs were determined to verify the ^{210}Pb geochronologies and to calculate mass accumulation rates for testing ^{210}Pb model assumptions. The different hydrogeomorphic settings for the nearby marsh study areas provided a means to test model assumptions with regard to tidal delivery of ^{210}Pb to the soils, while reducing geographical variations in the atmospheric fluxes of the radionuclides. Detection of ^{137}Cs in recent sediments suggests import of ^{137}Cs from elsewhere in the marsh-estuary system. A positive direct relationship between accumulated soil mass and inventories of excess ^{210}Pb and ^{137}Cs suggests that sediment focusing could be occurring in these marshes and has implications for ^{210}Pb

model selection. No relationship between surface excess ^{210}Pb activity and mass accumulation was observed, invalidating the assumptions of the CRS model. The CIC model often dated younger sediments below older sediments indicating that either changes in activity or soil composition at the surface could be occurring over time. No one ^{210}Pb model appears to be more suited for tidal marshes in general. The CFCS model resulted in chronologies with the least amount of agreement with ^{137}Cs chronology. This disagreement and the violation of other CFCS assumptions suggests that the use of the CFCS model to generate chronologies for marsh deposits should be applied with caution, if at all. Based on the agreement with ^{137}Cs chronology, the CIC model was best suited for chronology in the mineral-rich marshes of the Delaware Bay whereas the CRS model was best suited for use in the organic-rich marshes in the Barnegat Bay. These observations result in new hypotheses concerning the mechanisms of radionuclide delivery and burial that have implications for model development and particle transport in soils varying in organic and mineral composition. Further work on quantifying mineral- and organic-particle capture of radionuclides and partitioning of the soil radionuclide inventory is needed to better apply these models to tidal marsh deposits.

3.2 Introduction

3.2.1 Tidal marsh geochronology

As stated by Robbins (1978), the conditions needed for geochronology of sediment and soils are “growth or accumulation ordered in time, spatial localization of the time marker, and known time variations in marker supply rate (preferably constant).” The radioisotopes ^{137}Cs and ^{210}Pb meet these conditions. Originally

developed to age-date glacier and lake deposits, these radionuclides and related dating models have been applied to a variety of terrestrial, estuarine, and marine environments. One such environment, tidal marshes, are highly variable systems with multiple sources of water, sediment, and ^{210}Pb and ^{137}Cs . As such, there remain questions concerning the assumptions of ^{210}Pb and ^{137}Cs models as originally developed for other depositional environments.

Accretionary process in tidal marshes differs from that of other environments in that marshes accrete through both physical and biotic processes. *In-situ* growth of aquatic plants results in both the volumetric expansion of the root zone and accumulation of organic matter. Additionally, suspended sediments delivered to the marsh surface by tidal flooding are deposited and contribute soil volume. These two processes form soils that can range from mineralogenic to organogenic composition over small geographical areas (Chapter 2). The unique accretionary process and variable composition of marsh soils bring into question the mechanisms of radionuclide delivery (atmospheric versus tidal) and sequestration, and thus the underlying assumptions of radionuclide models. This chapter presents a critical evaluation of ^{137}Cs and ^{210}Pb chronological models as applied to tidal marsh deposits for purposes of age dating and deriving rates of vertical accretion and mass accumulation.

3.2.2 ^{137}Cs sources and geochronology

The artificial nuclide ^{137}Cs ($t_{1/2} = 30.2$ y) is a ^{235}U fission product released in the environment largely through atmospheric nuclear weapons testing in the 1950s and 1960s. Using gamma-ray spectroscopy, the activity of ^{137}Cs can be quantified by the gamma photon emission associated with the beta decay of its metastable daughter

$^{137\text{m}}\text{Ba}$ ($t_{1/2} = 153\text{s}$). Nuclear reactor releases, such as the 1986 Chernobyl accident and authorized effluent releases such as from the Sellafield Reprocessing Plant in the U.K., can be significant regional or local sources (Callaway et al., 1996; Thomson et al., 2002). The ^{137}Cs cation has a strong affinity for clay minerals and is readily adsorbed on fine-grained sediments where it becomes more-or-less geochemically fixed (Wahlberg and Fishman, 1962; Davis, 1963). The measured fallout record of ^{137}Cs since the early 1950s compared to activity-depth concentration profiles in soils and sediments is the basis for use of ^{137}Cs as an absolute time tracer (Ritchie and McHenry, 1990).

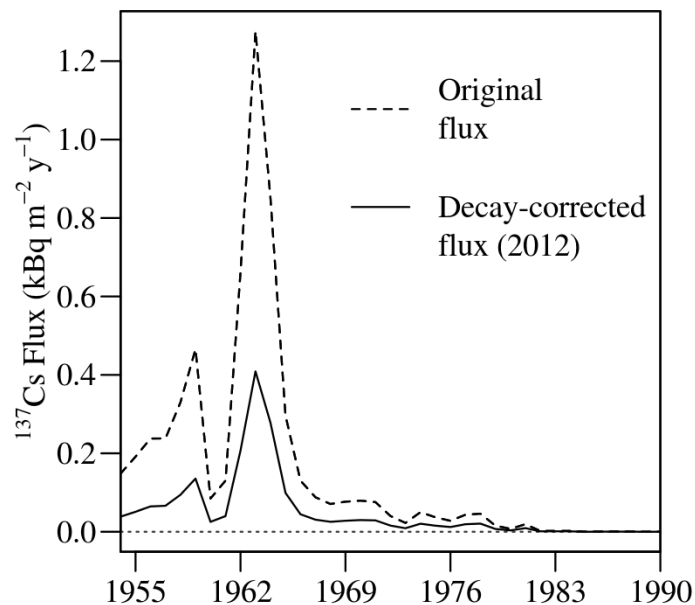


Figure 3.1: Ground-level record of ^{137}Cs fallout based on measured fallout of ^{90}Sr (data from Global Fallout Deposition Program, EML, <http://www.wipp.energy.gov/NAMP/EMLLegacy/databases.htm>). The dashed line is the original flux (solid line) decay-corrected to 2012. See text for further discussion.

Beginning in 1952, ^{137}Cs produced by weapons testing was dispersed globally via atmospheric circulation and was detectable worldwide starting in 1954 (Perkins and Thomas, 1980). Atmospheric fallout of ^{137}Cs measured at New York, New York, (1955 – 1990) is shown in Figure 3.1. Atmospheric weapons testing peaked in 1962-1964, during when 48% of the total fallout was deposited (Figure 3.1). Fallout quickly declined in the Northern Hemisphere due to adoption of the Limited Test Ban Treaty of 1963 by the US, UK, and USSR; thereafter only France conducted atmospheric weapons testing in the Southern Hemisphere (Perkins and Thomas, 1980). Atmospheric testing of nuclear weapons testing by China began in late 1964 and continued until the last test by any nation in 1980 (Norris, 1996), after which fallout declined to below detection limits (Monetti, 1996).

Geochronology using ^{137}Cs provides absolute age dates based on the atmospheric fallout record established for a particular region. Since there are no natural sources of ^{137}Cs in the environment, the first occurrence (depth of penetration) and peak of ^{137}Cs activity in a column of sediment are concordant with the years of initial (1954) and peak (1963-64) fallout resulting from weapons testing, assuming ^{137}Cs activity is not mixed after deposition. Several factors can alter the absolute year-depth relationship in sediments and soils, for example, post-depositional bioturbation of particle-associated ^{137}Cs and chemical migration of desorbed, dissolved ^{137}Cs in pore water. Numerical modeling has shown that diffusive-type biological mixing can broaden the activity peak and deepen the position of first occurrence in sediment, but it does not offset or completely smear the peak (Olsen et al., 1981), which is why ^{137}Cs chronology can be effective even in bioturbated sediments. In tidal marsh soils, it has been shown that downward “tailing” of ^{137}Cs activity by root bioturbation can deepen

the apparent depth ^{137}Cs first occurrence (DeLaune et al., 1978). For this reason and others (see Leslie and Hanock, 2008), assigning the depth of ^{137}Cs first-occurrence in a core profile the year 1954 is inadvisable in many cases.

3.2.3 ^{210}Pb geochronology

Lead-210 ($t_{1/2}=22.3$ y) occurs naturally and is a member of the ^{238}U decay series. Chronological application of ^{210}Pb arises from disequilibrium between ^{210}Pb and its immediate parent ^{226}Ra ($t_{1/2}=1600$ y). Radium-226 decays directly to the inert gas ^{222}Rn ($t_{1/2}=3.8$ d) which then decays quickly (< 1 h) to several intermediary nuclides to ^{210}Pb . In natural waters, rocks, and sediments, decay of ^{238}U -sourced ^{226}Ra produces “supported” ^{210}Pb activity ($^{210}\text{Pb}_s$) at low activity concentrations. Radon-222 diffuses from Earth’s surface to the atmosphere where it decays to ^{210}Pb via a series of non-gaseous daughter nuclides. The ^{210}Pb so produced returns to Earth’s surface in rainfall and dry (aerosol) deposition, and is known as “unsupported” ^{210}Pb ($^{210}\text{Pb}_u$) as it is not directly sourced *in situ* from minerogenic ^{226}Ra . In summary, the ^{210}Pb activity supported by in-situ decay of ^{222}Rn is the “supported” ($^{210}\text{Pb}_s$), whereas atmospherically derived ^{210}Pb is “unsupported” ($^{210}\text{Pb}_u$).

Activity concentrations of $^{210}\text{Pb}_u$ are generally higher to much higher than $^{210}\text{Pb}_s$ activities because $^{210}\text{Pb}_u$ becomes concentrated in the atmosphere with ^{222}Rn emanation from Earth’s surface. In a column of sediment or soil, the total activity of ^{210}Pb ($^{210}\text{Pb}_{\text{total}}$) present consists of $^{210}\text{Pb}_s$ and $^{210}\text{Pb}_u$ activity, the difference of which is sometimes referred to as “excess” ^{210}Pb activity. Put another way, assuming there is no ^{222}Rn loss from collected samples, $^{210}\text{Pb}_{\text{total}} = ^{210}\text{Pb}_s + ^{210}\text{Pb}_u$ and $^{210}\text{Pb}_s = ^{226}\text{Ra}$. Over time $^{210}\text{Pb}_u$ activity decays to levels below $^{210}\text{Pb}_s$ and eventually decays completely.

As detailed below, the down-core profile of $^{210}\text{Pb}_u$ activity, along with the knowledge of its half-life, provides the information required for ^{210}Pb geochronology.

3.2.4 ^{210}Pb chronological models

The ^{210}Pb chronological models most often employed in marine, estuarine, and lacustrine studies are Constant Flux – Constant Sedimentation (CFCS), Constant Rate of Supply (CRS), and Constant Initial Concentration (CIC). The assumptions and general applications of these models have been reviewed by Robbins (1978), Appleby (2001), Sanchez-Cabeza and Ruiz-Fernández (2012), and Corbett and Walsh (2015). Descriptive equations for these models are presented in Table 3.1. In all three of these models the flux (P , $\text{Bq m}^{-2} \text{y}^{-1}$) of $^{210}\text{Pb}_u$ to the sediment or soil surface divided by the sediment mass accumulation rate (ω , $\text{kg m}^{-2} \text{y}^{-1}$) gives the initial activity concentration of $^{210}\text{Pb}_u$ (A_o , Bq kg^{-1}). Where these models differ lies in the assumption of how ^{210}Pb is delivered to the sediment surface, as either a constant P or A_o . Depending on the particular application, the decay profile of ^{210}Pb downcore is used along with a model to either age-date the sediment column or determine sedimentation rates, expressed as a linear sedimentation rate (s , cm yr^{-1}) or ω . Theoretically, when ω is constant the CFCS, CIC, and CRS models should yield identical age dates and sedimentation rates for the dated sediment column. Regardless of the ^{210}Pb model employed, it has become common practice to use another radionuclide, such as ^{137}Cs , to validate ^{210}Pb -based age dates or ω .

The CFCS or “simple” ^{210}Pb model assumes that P and ω are constant such that A_o at the sediment-water or sediment-air interface is constant (Table 3.1). In a plot of the natural log of $^{210}\text{Pb}_u$ activity versus depth (z , cm), a steady-state CFCS profile is linear with monotonically decreasing activity. When depth is expressed as

accumulated mass (m , kg m^{-2}), the slope of the decay profile is given by $-\lambda/\omega$, where λ is the decay constant for ^{210}Pb (0.0311 y). An advantage of this model is that ω or s can be determined by least-squares regression of $^{210}\text{Pb}_u$ profile even when the activity profile

Table 3.1: Equations and assumptions for the CFCS, CRS, and CIC ^{210}Pb models described in the text.

Model	Decay equation	Initial activity (A_0)	Mass accumulation rate (ω)	Layer age (t)
CFCS	$A_m = A_0 e^{-\lambda t}$	$A_0 = \frac{P}{\omega}$	$\omega = \frac{-\lambda m}{\ln(A_m/A_0)}$	$t = \frac{m}{\omega}$
		Constant	Constant	
CRS	$A_m = \frac{P e^{-\lambda t}}{\omega}$	$A_0 = \frac{P}{\omega}$	$\omega_m = \frac{\lambda I_m}{A_m}$	$t_m = \frac{\ln(I_0/I_m)}{\lambda}$
		Variable	Variable	
CIC	$A_m = A_0 e^{-\lambda t}$	$A_0 = \frac{P}{\omega}$	$\omega_m = \frac{-\lambda m}{\ln(A_m/A_0)}$	$t_m = \frac{\ln(A_0/A_m)}{\lambda}$
		Constant	Variable	

is incomplete, in other words, if the full profile of $^{210}\text{Pb}_u$ is not recovered in the core sample. By extension, the age of a sediment layer (t) is computed by simply dividing

m or x by ω or s , respectively. The assumptions of the CFCS model make it suitable for a broad range of depositional environments.

The CRS model, also known as the constant flux model, was first described by Goldberg (1963). This model allows for variable ω but requires constant P (Table 3.1), and specifies that $^{210}\text{Pb}_u$ activity in the sediment column increases and decreases, respectively, with decreasing and increasing ω . Accordingly, the CRS model describes a closed system in which $^{210}\text{Pb}_u$ activity adjusts to the ambient suspended-sediment concentration. In the CRS model, t or ω are determined from the amount of $^{210}\text{Pb}_u$ accumulated at given mass depth relative to the total amount integrated over the profile, the total $^{210}\text{Pb}_u$ inventory (I_o , Bq m^{-2}). The entire inventory of $^{210}\text{Pb}_u$ at the depositional site must be recovered in the core (or otherwise inferred) for this model to be accurate. The CRS model is best suited to depositional environments in which the flux of $^{210}\text{Pb}_u$ to the sediment surface is steady-state, but it can be employed where ω is variable in time.

The CIC model, also known as the constant activity model, was also first described by Goldberg (1963). Unlike the CRS model, the CIC model allows for variability in P and ω and specifies that A_o is constant (Table 3.1). The CIC model describes an open system in which $^{210}\text{Pb}_u$ activity and ω are independent of one another. As with the CFCS model, ω and s can be computed graphically by least-squares linear regression of the $^{210}\text{Pb}_u$ activity-depth profile using the CIC model. However, to satisfy the assumption of constant A_o , $^{210}\text{Pb}_u$ activity must decrease monotonically with depth for this model to be applicable (Appleby and Oldfield, 1983), a disadvantage in depositional environments where the sediment accumulation

rate is highly variable. However, the CIC model can be used to model $^{210}\text{Pb}_u$ profiles that do not contain the full inventory of unsupported activity.

As a sediment chronometer, ^{210}Pb was pioneered for marine and lacustrine deposits and only later applied to tidal marshes, first by Armentano and Woodwell (1975) and later by McCaffrey and Thompson (1980). Given that tidal marshes fluctuate between being subaerial and submerged, and considering that the low marsh is more frequently flooded than the high marsh, it is expected that fluxes of $^{210}\text{Pb}_u$ to the marsh surface will be non-steady state and spatially variable. Indeed, the direct atmospheric flux to the marsh canopy and dry soil surface will vary with the frequency and duration of tidal flooding, whereas the indirect flux of ^{210}Pb supplied by the tides will vary with flooding frequency, suspended-sediment concentration, and particle settling velocity. Despite widespread application of ^{210}Pb geochronology in tidal marshes, how these dynamic factors influence the initial activity of $^{210}\text{Pb}_u$ and the applicability of different chronological models is not squarely addressed in the literature. Although there has been some work on ^{210}Pb model validation in lakes, coastal bays, and continental margin settings (Appleby and Oldfield, 1983; Shukla and Joshi, 1989; Binford et al., 1993; Corbett and Walsh, 2015), tidal marshes have yet to be considered in the same context. For coastal salt marshes with dominantly organogenic soils, general agreement between the CIC and CRS ^{210}Pb models has been shown (Bricker-Urso et al., 1989; Kolker et al., 2009; Kemp et al., 2012), suggesting that sediment accumulation in these systems is approximately steady state. However, it remains to test these models for a wider range of brackish and tidal freshwater marshes that trap large amounts of mineral sediment (and $^{210}\text{Pb}_u$) in tide waters.

3.2.5 Objectives

To provide an objective test of ^{210}Pb and ^{137}Cs dating models for tidal marshes, and to assess the applicability of the different ^{210}Pb models described above, chronologies were generated for eighteen soil cores collected in two adjacent estuaries of U.S. Mid-Atlantic coast, the Delaware Bay and the Barnegat Bay. As described in Chapter 2, estuarine marshes of Delaware are enriched in mineral sediment relative to the organic-rich coastal marshes of Barnegat Bay, thus these study areas make for a useful comparative study of ^{210}Pb and ^{137}Cs methods. Significantly, the colocation of these study areas minimizes variation in the atmospheric fluxes of ^{137}Cs and ^{210}Pb , which are closely tied to latitude and precipitation (Robbins, 1978; Cambray et al., 1987). Soil age-depths determined from ^{137}Cs chronology were compared to chronologies developed from the CFCS, CIC, and CRS models. The underlying assumptions of the three ^{210}Pb models were tested by comparing A_o , I , and P computed for each of the three models, constrained by ^{137}Cs chronologies, ^{210}Pb atmospheric fluxes reported in the literature, and theoretical considerations. Results of this study are intended to inform studies involving ^{137}Cs and ^{210}Pb geochronology for a wide range of tidal freshwater, brackish, and salt marshes.

3.3 Methods

3.3.1 Soil core collection

Eighteen soil cores approximately 1 m in length were collected during the summer of 2012 from salt marshes fringing Delaware Bay and Barnegat Bay (see Chapter 2 for site details, locations, and maps). Cores were sectioned at 2-cm intervals by vertical extrusion. For this chapter soil depth is expressed in units of accumulated

mass (m , kg m^{-2}), which accounts for downcore variations in porosity related to compaction and soil compositional changes.

3.3.2 Radionuclide analysis

Activities of ^{210}Pb , ^{226}Ra (as determined from its daughter, ^{214}Bi), and ^{137}Cs for a total of 485 core intervals were determined by gamma-ray spectroscopy of the 46.5 keV, 610.0 keV, and 661.7 keV photopeaks, respectively, using dry, homogenized soil for each 0–2 cm mass-depth interval. Samples were counted for 24 h on one of two Canberra Model GL2020R low-energy Germanium detectors interfaced with a Canberra Model 1720 Desktop Inspector. These detectors are affixed with low-background components and housed in a Cu-lined, low-background Pb shield to minimize background radiation. The low-radioactivity NIST Ocean Sediment standard (SRM4357; Inn et al., 1996) was used to create a calibration curve for various sample weights and geometries. This natural sediment matrix was gamma-counted in the same geometry (container and dry density) as the samples thus eliminating the need for ^{210}Pb self-absorption correction. Activity uncertainties were calculated as 1σ counting error. The minimum detectable activities (the minimum activity that one can be 95 % confident of measuring) determined for this study averaged 0.53 ± 0.19 , 0.18 ± 0.07 , 0.0025 ± 0.0007 Bq for ^{210}Pb , ^{214}Bi , and ^{137}Cs . The $^{210}\text{Pb}_u$ activity was calculated as the difference between $^{210}\text{Pb}_{\text{total}}$ and ^{214}Bi activity, and the activity uncertainty as the sum of the propagated counting errors of ^{214}Bi and ^{210}Pb . For the nine cores with complete $^{210}\text{Pb}_u$ profiles, there was good agreement between ^{210}Pb and ^{214}Bi activities in the downcore sediments assumed to contain no $^{210}\text{Pb}_u$ (Appendix C). This agreement supported use of ^{214}Bi activity as a proxy for $^{210}\text{Pb}_s$ activity for use in $^{210}\text{Pb}_u$ calculations.

3.3.3 Calculation of radionuclide inventories

Soil inventories of ^{137}Cs and $^{210}\text{Pb}_u$ are useful for comparing spatial variations in the total amount of radionuclide sequestered at a site to theoretical levels supported by the atmospheric flux. Departures between measured and theoretical inventories convey information on additional sources or sinks for radionuclides related to sedimentary processes. Total inventories for ^{137}Cs and $^{210}\text{Pb}_u$ were calculated as follows:

$$I_0 = \sum_{i=1}^z \rho_{di} x_i A_i \quad (3.1)$$

where, I_0 is the radionuclide inventory (Bq m^{-2}), ρ_d is the soil dry bulk density (kg m^{-3}), x is the thickness of the core interval (0.02 m), A is the radionuclide specific activity (Bq kg^{-1}) and i indicates the i th interval downcore. Inventory uncertainties were calculated as the standard deviation of the activity errors of the depth intervals.

As mentioned previously a complete $^{210}\text{Pb}_u$ inventory is required to apply the CRS model. Nine of the eighteen cores collected for this study (DN-2, DN-3, DV-1, MR-1, MR-2, MR-3, CC-1, CC-2, and CC-3) did not contain the full inventory, thus the inventory was computed by linear-extrapolation of the $^{210}\text{Pb}_u$ activity-depth profile. The value of the interpolated portion of the inventory amounted to $13 \pm 13\%$ of the inventory recovered in those cores. All cores were collected in a span of weeks and analyzed within one year, so the inventories were not corrected for decay. All radionuclide activities presented from other sources has been decay-corrected to 2012 for comparison with the results of this chapter.

3.3.4 ^{137}Cs and ^{210}Pb geochronologies and mass accumulation rates

Cesium-137 chronologies for the cores were constructed based on the record of Northern Hemisphere fallout of ^{137}Cs resulting from weapons testing (Figure 3.1). The

two commonly used horizons are the 1954 onset and the 1963-1964 peak fallout. These horizons were identified by visual examination of the depth profile. The depth of peak fallout was attributed to the year 1963. The 1954 onset age-depth was not used in comparison with $^{210}\text{Pb}_u$ models for reasons discussed below. Mass accumulation rates were calculated using the 1963 age-depth of ^{137}Cs and the dry bulk density of the soil (see Chapter 2). Uncertainties in computed rates were based on the difference in the mass depth between the top and bottom of the sediment layer within which the peak was located.

The CIC, CRS, and CFCS models of ^{210}Pb accumulation were used to generate chronologies and compute mass accumulation rates following the equations in Table 3.1. Uncertainties in t and ω are derived from the standard error of least-squares regression of mass depth mass versus $^{210}\text{Pb}_u$ activity. All other uncertainties presented are calculated as the standard deviation of terms unless otherwise noted. The initial activity of $^{210}\text{Pb}_u$ upon deposition on the marsh surface was determined by treating the uppermost sample (0–2 cm) as a mixed zone with an infinite mixing rate (Eq. 46 in Robbins 1978) and calculated as follows:

$$A_0 = A_{layer} \times \frac{\omega/m_{layer} + \lambda}{\omega/m_{layer}} \quad (3.2)$$

where, A_{layer} is the measured activity of the surface layer (Bq kg^{-1}), m_{layer} is the mass depth of the surface layer (kg m^{-2}), and the other terms are defined above. For independence, the value of ω determine from ^{137}Cs was used with the exception of core MR-3 (which did not have a ^{137}Cs activity peak) for which ω derived from the CFCS ^{210}Pb model was used. The value of A_0 calculated in this manner was used to test CRS and CIC model assumptions.

It is important to consider the effects of bioturbation on the marsh soil record, especially when using the vertical profiles of radionuclides for chronology (Crusius and Kenna, 2007). Fiddler crabs (*Uca spp.*) are responsible for a large portion of bioturbation in salt marshes and known to dig vertical burrows tens of centimeters long (Basan and Frey, 1977). The density of burrows is highest near the marsh edge, declining with distance inland (McCraith et al., 2003). However, the presence or absence of burrows or bioturbation could not be determined from the shapes of the radionuclide profiles alone. No burrows were observed while sampling cores and the root material formed a thick mat in the near surface of the core, both suggesting that burrowing was minimal to nonexistent in the cores used in this study. The effects of bioturbation on the radionuclide profiles was not examined further due to these observations and the agreement observed between ^{137}Cs and ^{210}Pb chronologies.

3.4 Results

3.4.1 ^{137}Cs activities and inventories

Representative ^{137}Cs profiles for three of the cores are shown in Figure 3.2. Profiles for all cores are shown in Appendix C. The ^{137}Cs activity in the surface layer averaged $5 \pm 2 \text{ Bg kg}^{-1}$. A ^{137}Cs activity peak attributed to maximum fallout in

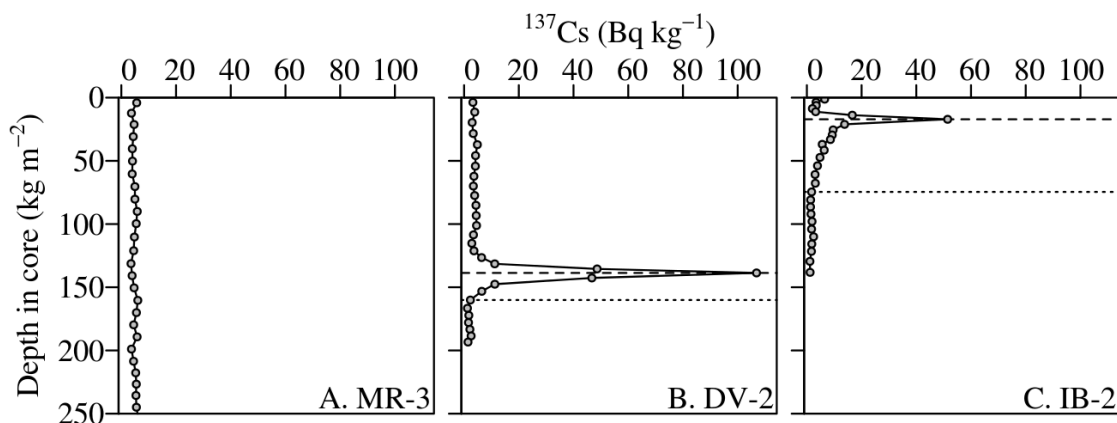


Figure 3.2: Selected profiles of ^{137}Cs activity for cores MR-3 (A), DV-2 (B), and IB-2 (C) showing different characteristics. Core MR-3 had no identifiable 1954 onset (dotted line) or 1963 peak (dashed line) in ^{137}Cs ; core DV-2 had good agreement between 1954 and 1963 horizons; and core IB-2 had poor agreement between 1954 and 1963 age-depths.

1963 was not present in one out of the eighteen cores (Figure 3.2A), averaging 55 ± 23 Bq kg^{-1} (Table 3.2). The mass depth of the peak averaged 7.3 ± 7.2 kg m^{-2} (Table 3.2). The first occurrence of ^{137}Cs in the profiles, presumably concordant with 1954, was present in fifteen of the cores at an average mass depth of 8.3 ± 4.7 kg m^{-2} (Table 3.2; Figures 3.2B and 3.2C). In six cores ^{137}Cs was detected to the bottom of the cored interval; these activities were low (<5 Bq kg^{-1}) in cores CC-1, IB-1, IB-3, but higher in all three of the MR cores. Cesium-137 was present near the top of some soil profiles, which is significant since there has been no atmospheric fallout of this radionuclide since 1980. The implication is that sediment-bound, “legacy” ^{137}Cs is being reworked and redistributed within the marsh environment.

Soil inventories of ^{137}Cs averaged 1.75 ± 0.01 kBq m^{-2} (Table 3.2). Within a given marsh system, the variability in ^{137}Cs inventory for the Delaware Bay study area was 23% (DN), 39% (DV), and 41% (MR), and for Barnegat Bay 20% (CC), 1% (IB),

Table 3.2: Core ^{137}Cs inventories, depth horizons, and peak activities. The inventory due to atmospheric flux (Figure 3.1) is 1.8 kBq m^{-2} . Dividing the 1954 depth and 1963 depth by 58 years (2012 – 1954) and 49 years (2012 – 1963), respectively, will give the mass accumulation rate based on that age-depth. The standard deviations are shown in parentheses.

Core	Soil Inventory (kBq m^{-2})	1954 depth (kg m^{-2})	1963 depth (kg m^{-2})	Measured 1963 peak activity (Bq kg^{-1})
DN-1	1.53 (0.02)	92 (2)	67 (1)	105 (2)
DN-2	2.05 (0.03)	155 (3)	118 (2)	52 (1)
DN-3	2.46 (0.03)	173 (4)	113 (3)	51 (1)
DV-1	1.64 (0.02)	96 (2)	69 (2)	48 (1)
DV-2	1.41 (0.03)	160 (3)	138 (1)	106 (2)
DV-3	0.7 (0.01)	45 (1)	28 (1)	71 (1)
HP-1	1.81 (0.03)	97 (3)	41 (2)	34 (1)
HP-2	1.22 (0.02)	82 (4)	47 (5)	40 (1)
HP-3	1.51 (0.02)	79 (4)	42 (2)	62 (1)
IB-1	0.65 (0.02)	59 (2)	22 (1)	30 (1)
IB-2	0.64 (0.02)	74 (3)	17 (1)	51 (1)
IB-3	0.65 (0.02)	29 (1)	21 (2)	38 (1)
MR-1	5.28 (0.06)	-	231 (5)	30 (1)
MR-2	5.41 (0.06)	-	236 (5)	34 (1)
MR-3	2.29 (0.05)	-	-	-
RC-1	0.7 (0.02)	39 (2)	17 (1)	69 (2)
RC-2	0.72 (0.02)	32 (2)	11 (1)	46 (2)
RC-3	0.75 (0.02)	32 (2)	17 (1)	71 (2)

and 3% and 3 % (RC). Marsh soils had measured inventories greater than (MR-1 and MR-2) or less than (DV-3, IB cores, and RC cores) the range reported for other U.S. Mid-Atlantic marshes (Graustein and Turekian, 1986) and the theoretical inventory of 1.8 kBq m^{-2} (Table 3.2). Inventories higher than the theoretical value are suggestive of boundary scavenging or sediment focusing of ^{137}Cs in these tidal marshes. Boundary scavenging involves adsorption of dissolved-phased radionuclide on particles at the sediment-water interface, increasing the activity (and inventory) of the radionuclide without accumulating sediment mass. Sediment focusing involves preferential deposition radionuclide activity where sediment accumulation rates are high, and non-deposition (or erosion) of activity at sites of sediment bypassing. This process leads heterogeneous radionuclide inventories along flow pathways that are high and low at sites of rapid deposition and erosion, respectively. Unlike boundary scavenging, sediment focusing increases the radionuclide inventory by increasing the mass of sediment deposited.

Correlation of measured ^{137}Cs inventories and accumulated mass suggested that sediment focusing contributed activity to the marsh sites and thereby increased inventories to levels above that which can be explained alone by atmospheric deposition alone (Figure 3.3). In other words, ^{137}Cs inventories tended to increase with increasing ω due to deposition of activity either not previously deposited or eroded from elsewhere in the system. Marsh sites with inventory deficits may be a source of ^{137}Cs to locations with surplus inventories; however, it cannot be determined whether these deficient inventories are a consequence of bypass or erosion.

Mass accumulation rates based on the depth of ^{137}Cs first occurrence (ca. 1954) were generally higher than rates computed from the 1963 peak (Table 3.1),

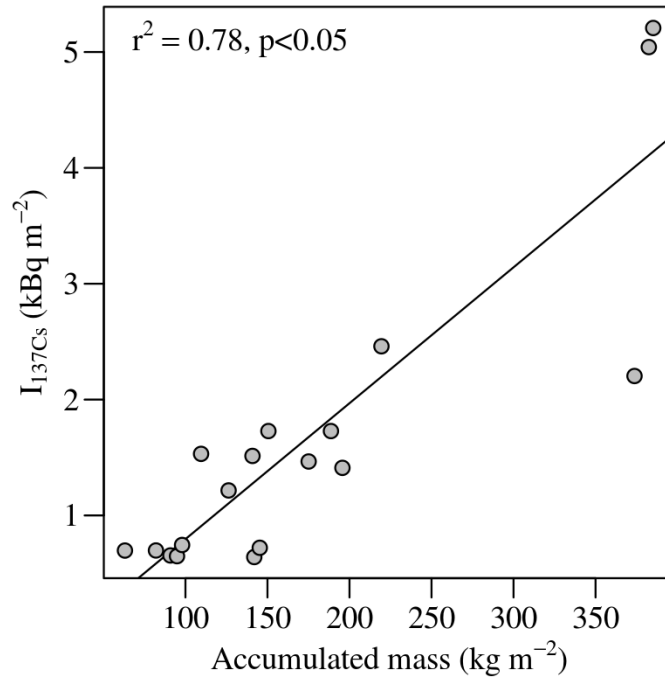


Figure 3.3: Regression of ^{137}Cs soil inventory and accumulated mass for the coring sites. The direct relationship suggests that sediment focusing contributes to the measured inventory of ^{137}Cs at some of the marsh sites.

presumably due downward transport by roots, bioturbation, chemical diffusion of dissolved-phase ^{137}Cs , or some combination of these factors (e.g., DeLaune et al., 1978; McCraith et al., 2003). Hence, for the purpose of comparison to ^{210}Pb results only the 1963 peak-based rates were used.

3.4.2 Excess ^{210}Pb activities and inventories

Overall, $^{210}\text{Pb}_u$ activity decreased monotonically with mass depth in cores from initial activities ranging from 57 to 455 Bq kg⁻¹ (Appendix C). Regression analysis of $^{210}\text{Pb}_u$ activity profiles yielded a wide range of correlation coefficients ($r^2 = 0.52$ –0.94). The low correlation coefficients imply that either P or ω are variable, which has implication to ^{210}Pb modeling assumptions.

Soil inventories of $^{210}\text{Pb}_u$ averaged $119 \pm 58 \text{ kBq m}^{-2}$ (Table 3.3). The range was similar to values determined for other U.S. Mid-Atlantic marshes by Graustein and Turekian (1986). Assuming a steady-state relationship between $^{210}\text{Pb}_u$ atmospheric flux and soil inventory defined by $P = \lambda I$, apparent atmospheric fluxes at the coring sites were $154\text{--}756 \text{ Bq m}^{-2} \text{ y}^{-1}$. These values are similar in magnitude, but mostly larger than, ^{210}Pb atmospheric fluxes measured in Connecticut ($200 \text{ Bq m}^{-2} \text{ y}^{-1}$; Turekian et al., 1983) and Maryland ($130 \text{ Bq m}^{-2} \text{ y}^{-1}$; Kim et al. 2000). While the atmospheric flux of $^{210}\text{Pb}_u$ varies geographically, it is also time-dependent, thus comparison of the soil inventory-based fluxes (100–120 year average) to shorter-term ground level records is imperfect. Nevertheless, the large values of P estimated for these marshes imply that there were non-atmospheric sources of $^{210}\text{Pb}_u$. As shown in Figure 3.4, the direct relationship between $^{210}\text{Pb}_u$ inventory and accumulated mass suggests that sediment focusing, not boundary scavenging is responsible for the high $^{210}\text{Pb}_u$ inventories as per the ^{137}Cs inventories. Significantly, sediment focusing has potential to violate the assumptions of the CRS model if it results in a non-steady flux of $^{210}\text{Pb}_u$ to the sediments.

Another test of the CRS ^{210}Pb model stems from the theoretical inverse relationship between A_o and ω caused by dilution of P by sediment mass. In other words, A_o should decrease with increasing ω in a marsh system. This assumption is often tested via regression using a ^{210}Pb -based ω ; however, the use of a ^{137}Cs -based ω maintains independence as a ^{210}Pb -based ω is derived using A_o . As shown in Figure 3.5, while there is an overall decrease in A_o with increasing ω , the correlation is weak overall and non-existent within each estuary. This result is perhaps the strongest line evidence suggesting that the flux of $^{210}\text{Pb}_u$ in the marshes is non-steady and that the

1 Table 3.3: Summary of the inputs, surface activity (A_0) and inventory (I), and resulting mass accumulation rates (ω) for
 2 the CFCS, CRS, and CIC ^{210}Pb models. The constant $^{210}\text{Pb}_u$ flux (P) is calculated from the product of I and λ . The P for the
 3 CIC model (P_{CIC}) can be variable (Table 3.1) and the core average is shown. The ω shown for the CIC and CRS models can
 4 be variable (Table 3.1) and the core average is shown. Standard deviations are shown in parentheses.

Core	A_0 (Bq kg ⁻¹)	I (kBq m ⁻²)	P (Bq m ⁻² y ⁻¹)	P_{CIC} (Bq m ⁻² y ⁻¹)	ω_{CFCS} (kg m ⁻² y ⁻¹)	ω_{CRS} (kg m ⁻² y ⁻¹)	ω_{CIC} (kg m ⁻² y ⁻¹)
DN-1	192.62 (8.05)	9.49 (0.18)	295.52 (5.73)	353.62 (539.91)	1.2 (0.18)	0.73 (0.69)	1.84 (2.77)
DN-2	260.16 (8.12)	18.49 (0.23)	575.75 (7.25)	581.4 (471.97)	2.44 (0.13)	2.18 (1.9)	2.23 (1.77)
DN-3	168.11 (7.53)	22.07 (0.3)	687.33 (9.23)	566.96 (485.51)	4.56 (0.25)	5.12 (3.79)	3.37 (2.76)
DV-1	139.97 (6.99)	12.06 (0.22)	375.66 (6.92)	316.5 (491.13)	2.25 (0.17)	1.88 (2.13)	2.26 (3.22)
DV-2	57.09 (6.5)	9.1 (0.21)	283.33 (6.67)	58.68 (1588.67)	2.66 (0.45)	1.62 (2.7)	1.03 (22.67)
DV-3	168.48 (8.29)	4.95 (0.1)	154.27 (3.11)	133.98 (264.77)	0.48 (0.04)	0.39 (0.71)	0.8 (1.45)
MR-1	109.59 (6.8)	16.78 (0.4)	522.38 (12.34)	519.96 (896.34)	6.4 (0.47)	5.44 (9.51)	4.74 (7.97)

76

5

6 Table 3.3 continued.

MR-2	95.62 (7.45)	17.11 (0.4)	532.7 (12.47)	623.53 (1021.44)	6.39 (0.41)	6.16 (10.8)	6.52 (9.94)
MR-3	101.47 (7.14)	24.3 (0.42)	756.74 (13.18)	703.31 (919.87)	9.74 (0.81)	8.49 (9.18)	6.93 (8.51)
CC-1	414.83 (10.15)	15.58 (0.24)	485.02 (7.49)	573.67 (402.99)	1.73 (0.21)	1.49 (1.25)	1.38 (0.95)
CC-2	284.74 (8.7)	11.03 (0.19)	343.37 (5.98)	358.64 (297.43)	1.52 (0.13)	1.17 (0.94)	1.26 (1.03)
CC-3	367.89 (9.7)	9.76 (0.23)	304 (7.08)	350.99 (448.15)	1.88 (0.27)	1.59 (1.46)	0.95 (1.21)
IB-1	256.23 (8.83)	5.3 (0.12)	164.92 (3.68)	175.87 (299.39)	0.73 (0.08)	0.68 (2.27)	0.69 (1.16)
IB-2	317.89 (14.36)	6.65 (0.17)	207.17 (5.16)	234.3 (1486.71)	0.89 (0.08)	1.1 (26.17)	0.74 (4.67)
IB-3	458.99 (13.51)	8.09 (0.17)	251.93 (5.2)	281.21 (565.6)	0.71 (0.06)	0.52 (1.21)	0.61 (1.23)
RC-1	384.56 (9.9)	6.35 (0.11)	197.61 (3.58)	221.32 (350.71)	0.49 (0.04)	0.43 (2.09)	0.58 (0.91)
RC-2	455.15 (11.29)	8.03 (0.16)	249.92 (5.01)	311.46 (2943.59)	0.56 (0.04)	0.57 (12.88)	0.68 (6.47)
RC-3	340.99 (11.25)	8.9 (0.13)	277.11 (3.96)	177.68 (563.51)	0.44 (0.06)	0.29 (3.08)	0.52 (1.61)

77

7

8

9

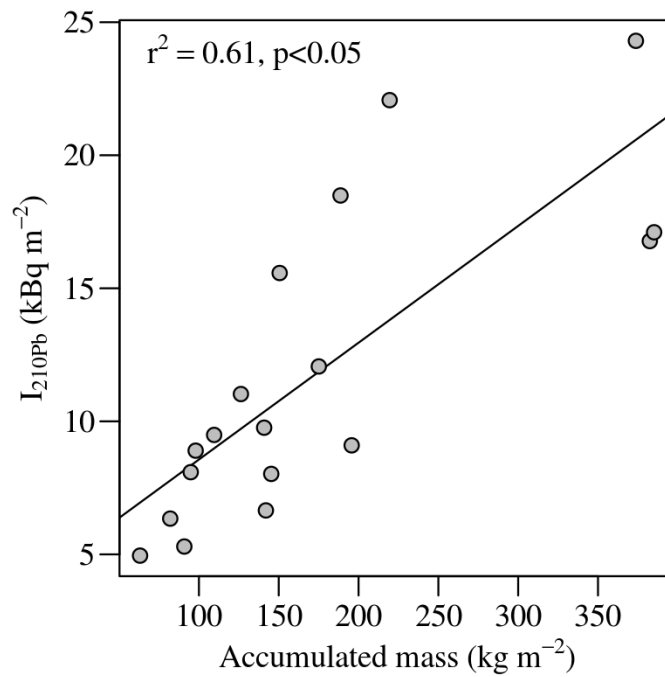


Figure 3.4: Correlation of $^{210}\text{Pb}_u$ soil inventory and accumulated mass for the coring sites. The direct relationship suggests that sediment focusing rather than boundary scavenging contributes $^{210}\text{Pb}_u$ inventory at some of the marsh sites.

CRS model is contraindicated. At the same time, it supports the underlying assumption of the CIC model, specifically, that A_o is completely independent of ω .

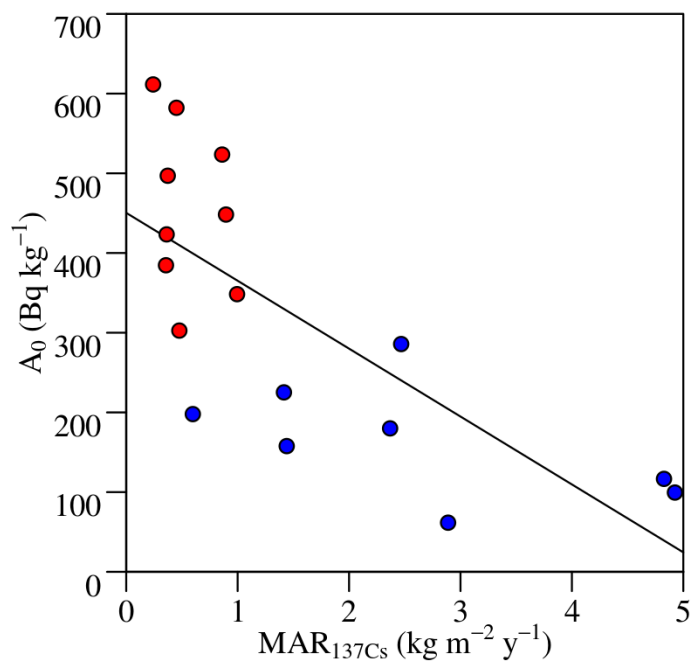


Figure 3.5: Scatterplot of $^{210}\text{Pb}_u$ surface activity versus ^{137}Cs -based mass accumulation rates for the coring sites. Data from Delaware Bay marshes are shown in blue and Barnegat Bay marshes shown in red. See text for further discussion.

3.4.3 ^{210}Pb chronologies and accumulation rates

Chronologies for the CFCS, CRS, and CIC model are presented in Figures 3.6 and 3.7. Comparison of the individual $^{210}\text{Pb}_u$ chronologies with ^{137}Cs peak was done to independently to verify the ^{210}Pb models. In some cases, one or more of the ^{210}Pb models are in reasonable agreement with the 1963 ^{137}Cs year-depth. Two cases showing disagreement are MR-3, where no ^{137}Cs peak was identified, and DN-3 (Figure 3.6). It is of interest to note that, while no ^{137}Cs peak was observed, the ^{210}Pb chronologies suggested the 1963 would be located near or just below the bottom of the retrieved record. For DN-3, the disagreement between ^{137}Cs and ^{210}Pb chronologies

could indicate a difference in capture and preservation of $^{210}\text{Pb}_u$ and ^{137}Cs activities, but no other data collected here support or refute this interpretation. In general, the CIC age-models date older layers atop younger layers in all cores. This reversal occurred where $^{210}\text{Pb}_u$ activity increased with depth and could be due to changes in A_0 over time or soil composition of the layer. Changes in the soil composition directly affect bulk density and therefore the specific activity (Bq kg^{-1}). In other words, a purely organic deposit will have a higher $^{210}\text{Pb}_u$ specific activity than that of a purely mineral deposit both receiving the same P solely due to the difference in organic and mineral particle densities. Indeed, higher A_0 were observed in the organic-rich Barnegat Bay cores than in the mineral-rich Delaware Bay cores (Figure 3.5).

For sites with log-linear $^{210}\text{Pb}_u$ profiles such as found in Core DN-2 (Appendix C), the ^{210}Pb models produce chronologies that were largely in agreement. Again the assumption of CFCS model requires that the P and ω are constant resulting in a log-linear $^{210}\text{Pb}_u$ profile. Although the CRS and CIC models allow for these terms to vary, the CRS and CIC model can still applied in situations where the P and ω are constant. In a scenario of constant P and ω , all three models would yield the same result. In cores DN-1 and DV-2, a change in the CRS and CIC depth-age trajectories signifies a change in inputs at the inflection of the profile.

The most important observation of the chronologies is that no single ^{210}Pb model agreed with ^{137}Cs dating across the range of coring sites. This observation suggests that no one chronological model is ideally suited for the full range of tidal marshes. The CFCS model had the least agreement with ^{137}Cs chronology in most cases (Figures 3.6 and 3.7). This observation suggests that marshes are not accumulating at rates fairly constant over the 100–120 year timespan of ^{210}Pb dating.

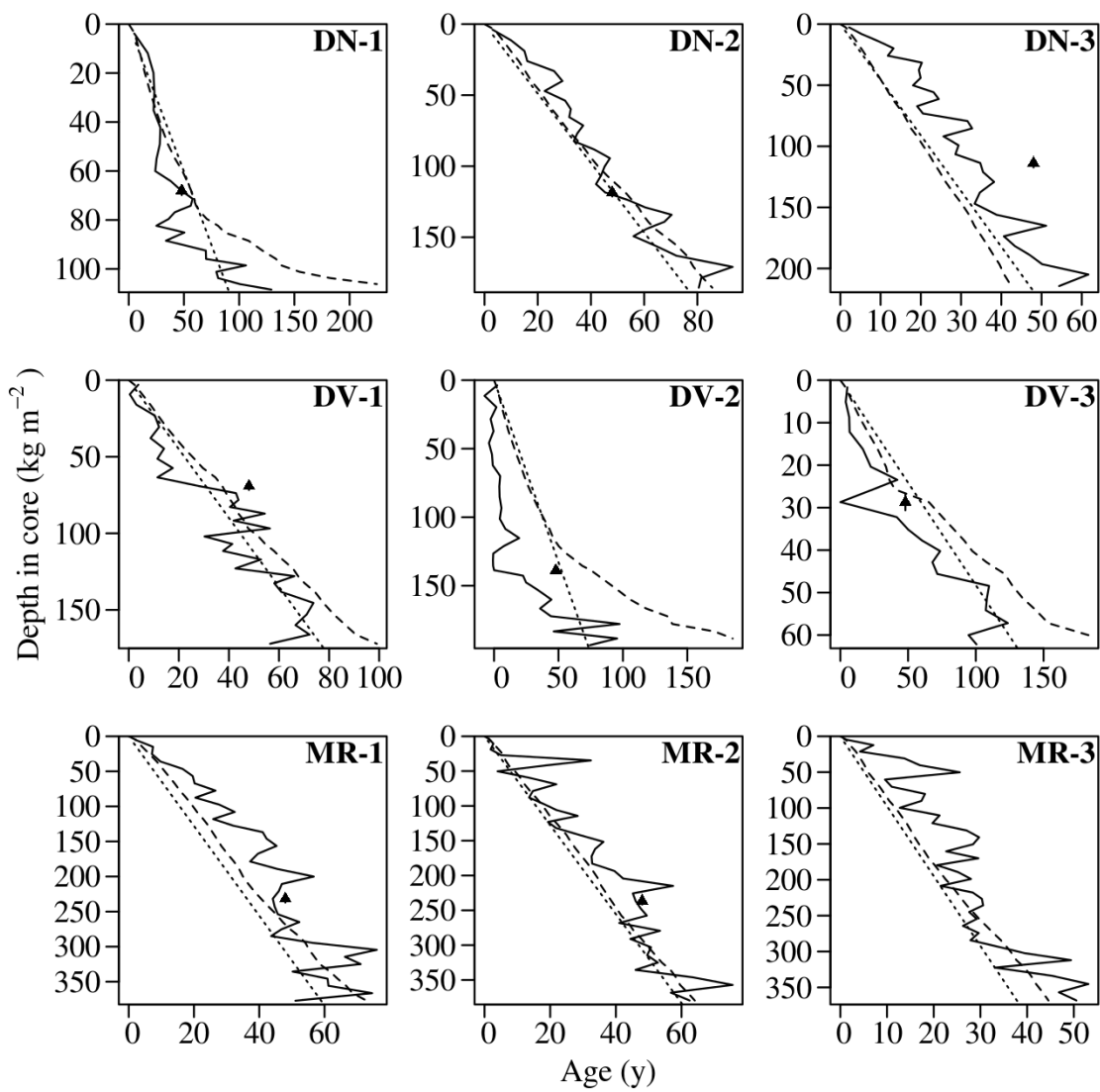


Figure 3.6: Delaware Bay ^{210}Pb chronologies showing age in years before 2012. The lines represent chronologies generated from the CIC (solid), CRS (dashed), and CFCS (dotted) models. The 1963 ^{137}Cs age-depths are shown (triangle), if identified.

However, the CIC age-depths agreed more with ^{137}Cs chronology in Delaware Bay marshes (Figure 3.6) and the CRS model with ^{137}Cs chronology in Barnegat Bay marshes (Figure 3.7). Again, the close proximity of these sites leads to the assumption

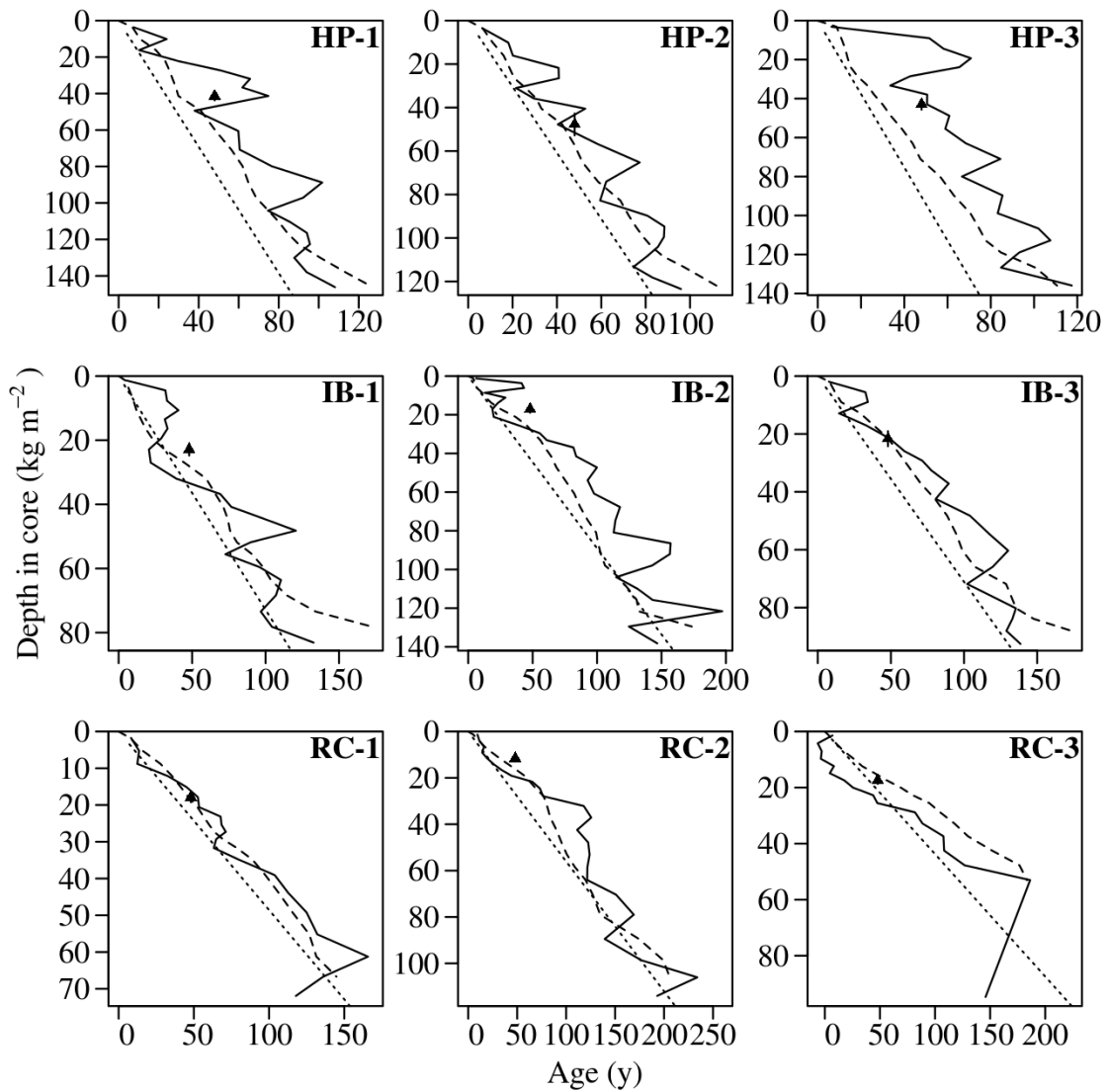


Figure 3.7: Barnegat Bay ^{210}Pb chronologies showing age in years before 2012. The lines represent chronologies generated from the CIC (solid), CRS (dashed), and CFCS (dotted) models. The 1963 (triangle) ^{137}Cs age-depths are shown (triangle).

that the atmospheric flux was the same. The composition and $^{210}\text{Pb}_u$ activity of accumulated marsh soil could explain why contrasting models perform better in one estuary type as opposed to others.

3.5 Discussion

3.5.1 Application of ^{137}Cs and ^{210}Pb geochronology

There are multiple lines of evidence for burial of ^{137}Cs activity not derived from direct atmospheric fallout over the marshes studied. Fallout of fission radionuclides such as ^{137}Cs is directly tied to precipitation and dry deposition rates (Cambray et al., 1987), so fallout variability in the study region should be minimal. As discussed previously, soil inventories of ^{137}Cs for several sites were found to be above the level supported by atmospheric fallout, possibly due to sediment focusing. Presence of ^{137}Cs in the surface layer of all cores, despite the fact that there has been no atmospheric fallout since 1980, suggest either upward mixing by particle bioturbation or deposition of ^{137}Cs redistributed from nearby erosional sites are significant processes in the studied marshes. Presence of “legacy” ^{137}Cs in the uppermost horizons of marsh soils makes clear that, while salt marshes are sinks for fine-grained sediment and particle-associated materials, there is significant internal cycling of sedimentary materials following deposition.

The assumptions of ^{210}Pb dating models can be tested by comparison of inventories, accumulation rates, and surface activities. The CFCS model assumes constant ω , P , and A_0 , resulting in a log-linear, monotonic ^{210}Pb . Profiles with deviations from this shape have one or more variable terms and invalidate the use of the CFCS model (Figure 3.8A). Profiles with a strong least-squares fit are better suited for the use of the CFCS model (Figure 3.8B). Even in core DN-2 (Figure 3.8B), there are deviations in the measured $^{210}\text{Pb}_u$ activity and the activity expected from logarithmic decay. Again, these are due to changes in aforementioned model inputs,

possibly invalidating the use of CFCS chronology. However, the CFCS model is appropriate in this case for generating core-averaged (~ 100 y) ω .

If the $^{210}\text{Pb}_u$ flux to surface sediments is constant as dictated by the CRS model, then an increase in ω would lead to a decrease in A_0 . This relationship occurs due to increasing bulk material diluting the flux and lowering surface activity. Results of linear regression showed that A_0 had no relationship with ω (Figure 3.5), thus the CRS assumption of P dilution was invalidated and the CIC assumption of A_0 independent of ω supported. Furthermore, sediment focusing was determined to occur in these marshes due to the presence of a direct relationship between inventories of ^{137}Cs and $^{210}\text{Pb}_u$ and accumulated mass (Figures 3.3 and 3.4). Sediment focusing violates the CRS assumption that atmospheric flux is the main source of $^{210}\text{Pb}_u$ to these cores and that P is not a function of ω . The large inventory-based fluxes relative to ground-level flux measurements (Table 3.3) also violate this CRS assumption.

3.5.2 Summary

Based on objective tests of model assumptions, no single ^{210}Pb model is ideally suited for all types of salt marshes. Nonetheless, based on the findings of this study, some recommendations can be made. In the organic-rich marshes of the Barnegat Bay, specifically those at IB and RC, the CRS model may be more appropriate than in more mineral-rich systems. The ^{137}Cs age-depth shows the best agreement with CRS chronology there (Figure 3.7). It may be that in these systems that the majority of $^{210}\text{Pb}_u$ is associated with organic matter in the soil. If the organic contribution to the $^{210}\text{Pb}_u$ inventory is related to or a direct resultant of atmospheric fallout, then that inventory alone may better satisfy the model assumptions. Indeed, if the radionuclide inventory associated with mineral sediment is due primarily to indirect $^{210}\text{Pb}_u$

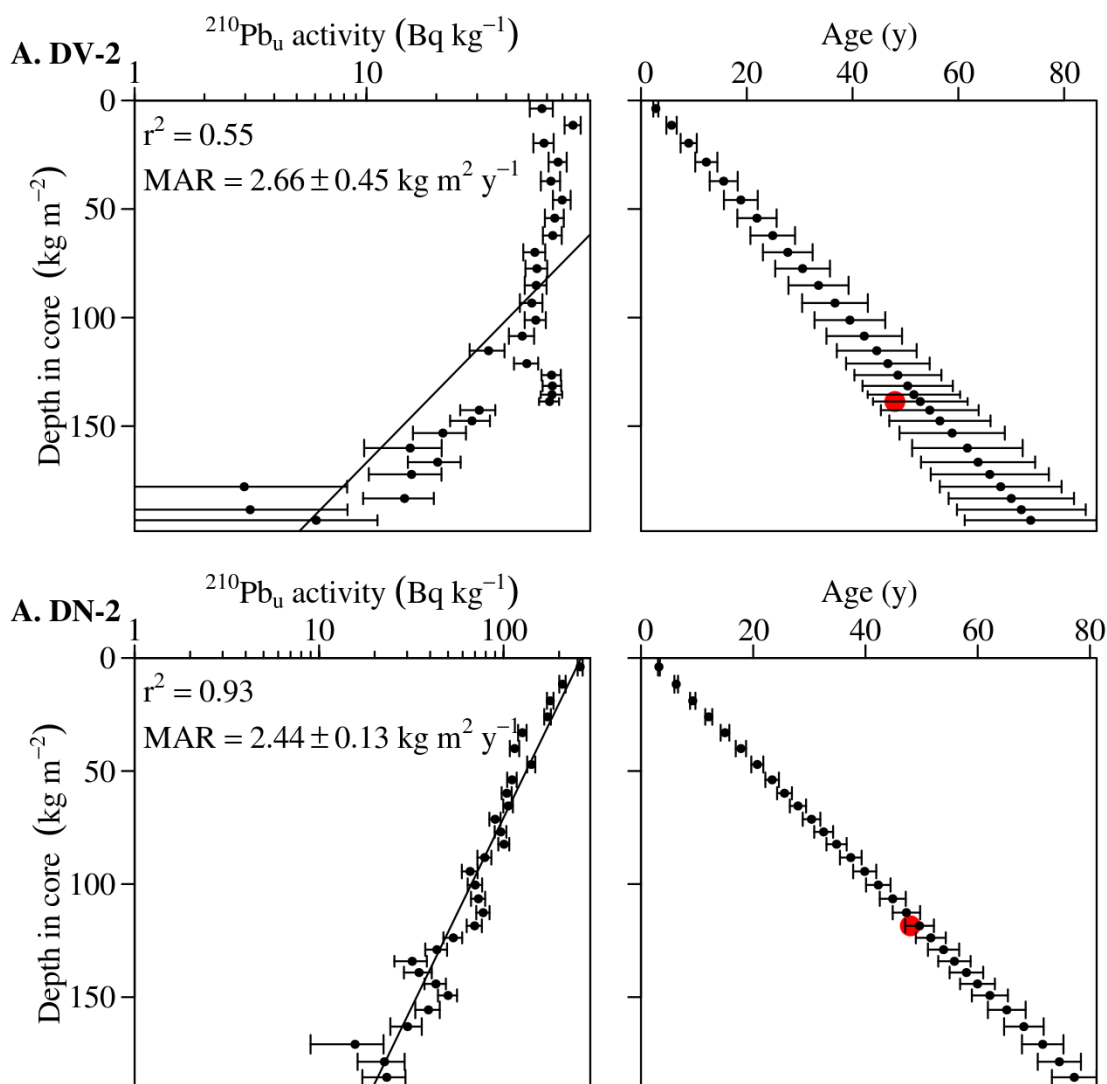


Figure 3.8: Example profiles of $^{210}\text{Pb}_u$ and CFCS model age for cores DV-2 (A) and DN-2 (B) showing good correspondence with 1963 age dates (red dots) derived from ^{137}Cs data for the same cores. While the CFCS and ^{137}Cs dates agree for DV-2, examination of the $^{210}\text{Pb}_u$ profile shows the CFCS assumption of linearity is violated and the model should not be used for detailed chronology

deposition, i.e. sediment focusing, it may be that partitioning of the inventory and use of the organically-associated inventory alone for ^{210}Pb dating may be the best practice

in organic-rich salt marsh soils. Application of the ^{210}Pb dating models in mineral-rich marshes such as those in Delaware Bay (Figure 3.6) require similar considerations regarding soil composition and radionuclide sources. In these marshes, ^{210}Pb inventories are relatively higher than Barnegat Bay inventories and enriched compared to what is expected due to atmospheric flux. If a large portion of these inventories is due to import of material, it invalidates the use of the CRS model, which would expect radionuclide inventories to be unaffected by sediment additions. The CIC model may be most appropriate for these marshes as it is less sensitive to non-atmospheric sources of $^{210}\text{Pb}_u$ as long as the resulting surface activity concentration remains the same. This recommendation is based on the assumption that the atmospheric flux is captured in a similar fashion over time and the $^{210}\text{Pb}_u$ activity of imported material remains fairly constant – both conditions requiring further research. Due to the differences in density, and possibly activity, of mineral and organic particles, it may be that some modification of the CIC model is needed to account for the composition of accumulating mass in tidal marshes. Additionally, the CIC chronologies for Delaware Bay marshes seem to have the best agreement with ^{137}Cs age-depths (Figure 3.6). The CIC age models do result in older sediments overlying younger sediments in some cases. Such a result could be due to the variation in surface activity, a violation of the main assumption of this model, or it could reflect changes in soil composition affecting the $^{210}\text{Pb}_u$ specific activities. Further work identifying the formation and preservation of the mineral and organic-associated radionuclide inventories is needed.

The contributions by organic matter, both living canopy and detrital material, to marsh soil radionuclide inventories is not clear (He and Walling, 1996). Organic incorporation of radionuclides into the soil inventory could occur through direct or

indirect mechanisms. Biological uptake could sequester radionuclides in the plant tissue. Additionally, burial of organic particle-associated radionuclides, either absorbed on surface litter or imported detritus, represent an additional indirect source. In core IB-2, $^{210}\text{Pb}_u$ was detected in organic-rich surface sediments while $^{210}\text{Pb}_s$ was not. Absence of $^{210}\text{Pb}_s$ suggests an absence of mineral sediment indicating that organic burial of radionuclides should be considered in tidal marshes.

Further research on ^{210}Pb trapping efficiency by halophytes and contributions by aboveground biomass and organic detritus to the radionuclide inventory could further these models and test several hypotheses. It may also provide insight on determining if aboveground litter (possibly with adsorbed atmospheric fallout) is buried and its significance in marsh soil formation. This information is relevant to marsh geochronology and also applicable to the transport pathways and sequestration of aerosols and other contaminants in the estuary-marsh environment. These mechanisms are discussed further in Chapter 4.

3.6 Conclusions

An assessment of ^{137}Cs and ^{210}Pb accumulation models used to date tidal salt marsh soils was conducted using cores from adjacent estuaries in the U.S. Mid-Atlantic. Multiple lines of evidence point to sediment focusing controlling the radionuclide inventories in tidal marsh deposits. Atmospheric flux alone cannot account for our observations. The lack of log-linear $^{210}\text{Pb}_u$ profiles suggested that the CFCS model should not be used for chronology of tidal marsh deposits but may be appropriate for generating a ~100 year averaged mass accumulation rate. An inverse relationship between surface activity and mass accumulation would have supported use of CRS model but such a relationship was not found. The dating of younger soils

below older soils by the CIC model suggested that either the CIC assumption of a constant surface activity was violated or changes in soil composition affected the specific activity. No single ^{210}Pb model seems appropriate to be universally applied to salt marshes. However, based on comparison with ^{137}Cs chronology, the CRS model was most appropriate in organic-rich soils where the soil mass is largely the result of *in situ* production that likely captures the atmospheric flux. In this case, utilization of the $^{210}\text{Pb}_u$ activity of organic solids in the CRS model may provide more accurate chronologies. Detection of $^{210}\text{Pb}_u$ in organic layers with little to no mineral content suggest that organic burial is possible and support further investigation of model adaption for organic-rich marsh deposits. Agreement with between ^{137}Cs and CIC model chronologies occurred in mineral-rich soils where the radionuclide inventory was believed to be enriched with $^{210}\text{Pb}_u$ activity imported on focused sediment. This interpretation assumes that the capture of atmospheric flux and activity of focused sediment is fairly constant through time – both assumptions requiring further study. The separation of the bulk marsh-soil radionuclide inventory into that adsorbed to mineral and organic solids may provide insight into mechanisms of ^{137}Cs and ^{210}Pb capture and burial. Further work is needed to determine how these soil fractions function in the capture of atmospheric fallout and serve as a vehicle for remobilization of radionuclides within the marsh-estuary system.

REFERENCES

- Appleby, P.G., 2001. Chronostratigraphic techniques in recent sediments, in: Last, W.M., Smol, J.P. (Eds.), *Tracking Environmental Change Using Lake Sediments. Volume 1: Basin Analysis, Coring, and Chronological Techniques*. Kluwer Academic Publishers, Dordrecht, The Netherlands, pp. 171–203.
- Appleby, P.G., Oldfield, F., 1983. The assessment of ^{210}Pb data from sites with varying sediment accumulation rates. *Hydrobiologia* 103, 29–35.
doi:10.1007/BF00028424
- Armentano, T., Woodwell, G., 1975. Sedimentation rates in a Long Island marsh determined by ^{210}Pb dating. *Limnol. Oceanogr.* 20, 452–456.
- Binford, M.W., Kahl, J.S., Norton, S. a., 1993. Interpretation of ^{210}Pb profiles and verification of the CRS dating model in PIRLA project lake sediment cores. *J. Paleolimnol.* 9, 275–296. doi:10.1007/BF00677218
- Bricker-Urso, S., Nixon, S.W., Cochran, J.K., Hirschberg, D.J., Hunt, C., 1989. Accretion rates and sediment accumulation in Rhode Island salt marshes. *Estuaries* 12, 300–317. doi:10.2307/1351908
- Callaway, J.C., DeLaune, R.D., Patrick, W.H., Patrick Jr., W., 1996. Chernobyl Cs-137 used to determine sediment accretion rates at selected northern European coastal wetlands. *Limnol. Oceanogr.* 41, 444–450.
doi:10.4319/lo.1996.41.3.0444
- Cambray, R.S., Cawse, P.A., Garland, J.A., Gibson, J.A.B., Johnson, P., Lewis, G.N.J., Newton, D., Salmon, L., Wade, B.O., 1987. Observations on radioactivity from the Chernobyl accident. *Nucl. Energy* 26, 77–101.
- Corbett, D.R., Walsh, J.P., 2015. ^{210}Pb -lead and ^{137}Cs -cesium: establishing a chronology for the last century, in: Shennan, I., Long, A.J., Horton, B.P. (Eds.), *Handbook of Sea-Level Research*. John Wiley and Sons, pp. 361–372.
doi:10.1002/9781118452547.ch24
- Crusius, J., Kenna, T.C., 2007. Ensuring confidence in radionuclide-based sediment chronologies and bioturbation rates. *Estuar. Coast. Shelf Sci.* 71, 537–544.
doi:10.1016/j.ecss.2006.09.006

- Davis, J.J., 1963. Cesium and its relationship to potassium in ecology, in: Schultz, V., Klement, A. (Eds.), *Radioecology*. Reinhold, New York, pp. 539–556.
- DeLaune, R.D., Patrick Jr., W.H., Buresh, R.J., 1978. Sedimentation rates determined by ^{137}Cs dating in a rapidly accreting salt marsh. *Nature* 275, 532–533. doi:doi:10.1038/275532a0
- Environmental Measurements Laboratory (EML), 1999. *Global Fallout Program*. New York, New York.
- Frey, R., Basan, P., 1985. Coastal Salt Marshes, in: Davis, R. (Ed.), *Coastal Sedimentary Environments*. Springer-Verlag, New York, p. 716. doi:10.1007/978-1-4612-5078-4
- Goldberg, E.D., 1963. Geochronology with lead-210, in: *Radioactive Dating*. IAEA, Vienna, pp. 121–131.
- Graustein, W.C., Turekian, K.K., 1986. ^{210}Pb and ^{137}Cs in air and soils measure the rate and vertical profile of aerosol scavenging. *J. Geophys. Res.* 91, 14355–143369. doi:10.1029/JD091iD13p14355
- He, Q., Walling, D., 1996. Interpreting particle size effects in the adsorption of ^{137}Cs and unsupported ^{210}Pb by mineral soils and sediments. *J. Environ. Radioact.* 30, 117–137. doi:10.1016/0265-931X(96)89275-7
- Inn, K.G.W., Lin, Z., Liggett, W.S., Schima, F.J., Krey, P., Feiner, M., Liu, C.-K., Holloway, R., Harvey, J., Larsen, I.L., Beasley, T., Huh, C.A., McCurdy, D., Germain, P., Yamamoto, M., Handl, J., Popplewell, D.S., Woods, M.J., Jerome, S., Bates, T.H., Holms, A., Harvey, B.R., Odell, K.J., Warren, B.B., Young, P., 1996. Low-level radioactivity ocean sediment standard reference material. *Appl. Radiat. Isot.* 47, 967–970. doi:10.1016/S0969-8043(96)00094-2
- Kemp, A.C., Sommerfield, C.K., Vane, C.H., Horton, B.P., Chenery, S., Anisfeld, S.C., Nikitina, D.L., 2012. Use of lead isotopes for developing chronologies in recent salt-marsh sediments. *Quat. Geochronol.* 12, 40–49. doi:10.1016/j.quageo.2012.05.004
- Kim, G., Hussain, N., Scudlark, J.R., Church, T.M., 2000. Factors influencing the atmospheric depositional fluxes of stable Pb, ^{210}Pb , and ^7Be into Chesapeake Bay. *J. Atmos. Chem.* 36, 65–79. doi:10.1023/A:1006383030362

- Kolker, A.S., Goodbred, S.L., Hameed, S., Cochran, J.K., 2009. High-resolution records of the response of coastal wetland systems to long-term and short-term sea-level variability. *Estuar. Coast. Shelf Sci.* 84, 493–508. doi:10.1016/j.ecss.2009.06.030
- Leslie, C., Hancock, G.J., 2008. Estimating the date corresponding to the horizon of the first detection of ^{137}Cs and $^{239+240}\text{Pu}$ in sediment cores. *J. Environ. Radioact.* 99, 483–490. doi:10.1016/j.jenvrad.2007.08.016
- McCaffrey, R.J., Thomson, J., 1980. A record of the accumulation of sediment and trace metals in a Connecticut salt marsh, in: Saltzman, B. (Ed.), *Advances in Geophysics*. Academic Press, New York, pp. 165–236.
- McCraith, B.J., Gardner, L.R., Wethey, D.S., Moore, W.S., 2003. The effect of fiddler crab burrowing on sediment mixing and radionuclide profiles along a topographic gradient in a southeastern salt marsh. *J. Mar. Res.* 61, 359–390. doi:10.1357/002224003322201232
- Monetti, M.A., 1996. Worldwide Deposition of Strontium-90 through 1990. Environmental Monitoring Laboratory Report-579. New York.
- Norris, R.S., 1996. French and Chinese nuclear weapon testing. *Secur. Dialogue* 27, 39–54. doi:10.1177/0967010696027001006
- Olsen, C.R., Simpson, H.J., Peng, T.-H., Bopp, R.F., Trier, R.M., 1981. Sediment mixing and accumulation rate effects on radionuclide depth profiles in Hudson Estuary sediments. *J. Geophys. Res.* 86, 11020–11028.
- Perkins, R.W., Thomas, C.W., 1980. Worldwide fallout, in: Hanson, W.C. (Ed.), *Transuranic Elements in the Environment*. US DOE, Washington, D.C., pp. 53–82. doi:10.1017/CBO9781107415324.004
- Ritchie, J.C., McHenry, J.R., 1990. Application of radioactive fallout cesium-137 for measuring soil erosion and sediment accumulation rates and patterns: a review. *J. Environ. Qual.* 19, 215. doi:10.2134/jeq1990.00472425001900020006x
- Robbins, J.A., 1978. Geochemical and geophysical applications of radioactive lead, in: Nriagu, J.O. (Ed.), *The Biogeochemistry of Lead in the Environment*. Elsevier, Amsterdam, pp. 285–393.
- Sanchez-Cabeza, J.A., Ruiz-Fernández, A.C., 2012. ^{210}Pb sediment radiochronology: an integrated formulation and classification of dating models. *Geochim. Cosmochim. Acta* 82, 183–200. doi:10.1016/j.gca.2010.12.024

- Shukla, B.S., Joshi, S.R., 1989. An evaluation of the CIC model of ^{210}Pb dating of sediments. *Environ. Geol. Water Sci.* 14, 73–76. doi:10.1007/BF01740587
- Thomson, J., Dyer, F.M., Croudace, I.W., 2002. Records of radionuclide deposition in two salt marshes in the United Kingdom with contrasting redox and accumulation conditions. *Geochim. Cosmochim. Acta* 66, 1011–1023. doi:10.1016/S0016-7037(01)00825-0
- Turekian, K.K., Benninger, L.K., Dion, E.P., 1983. ^7Be and ^{210}Pb total deposition fluxes at New Haven, Connecticut and at Bermuda. *J. Geophys. Res.* 88, 5411. doi:10.1029/JC088iC09p05411
- Wahlberg, J.S., Fishman, M.J., 1962. Adsorption of cesium on clay minerals. U.S. Geological Survey Bulletin 1140-A, U.S. Dept. of the Interior, pp 40.

Chapter 4

CAPTURE AND BURIAL OF ^{210}Pb AND ^{137}Cs IN SALT MARSHES

4.1 Abstract

A study of ^{210}Pb and ^{137}Cs capture and burial in salt marsh soils was conducted to document variations in activity associated with atmospheric and tidal mechanisms of radionuclide transport. Organic-rich salt marsh soils from Barnegat Bay, a coastal lagoon estuary, were compared to mineral-rich soils from Delaware Bay, a coastal plain estuary. Aboveground plant biomass and size-fractionated soil solids were analyzed to determine the relative contributions of organic matter and mineral sediment to bulk radionuclide activities. Bulk soil (0-6 cm depth) was separated into macro-organic ($>125\ \mu\text{m}$), micro-organic (125-63 μm), silt (63-4 μm), and clay ($<4\ \mu\text{m}$) size fractions, and analyzed for excess ^{210}Pb and ^{137}Cs activity via gamma spectroscopy. All soil size fractions contained excess ^{210}Pb activity suggesting that organic as well as mineral solids are carriers for radionuclides in the soil. A majority of ^{137}Cs activity was associated with the micro-organic soil-fraction at several sites indicating that plant uptake or tidal import of ^{137}Cs -laden organic material may influence surface ^{137}Cs activities. A direct relationship between excess ^{210}Pb activity aboveground and belowground was observed indicating that excess ^{210}Pb can be buried with surface organic matter. These results along with the high excess ^{210}Pb activity of organic soil solids indicate that organic capture and burial of fallout and should be considered in studies using these fallout radionuclides in chronological studies. Future work on the post-depositional mobility and plant uptake of ^{210}Pb and

^{137}Cs is needed to understand how radionuclide inventories form and are preserved in mineral- and organic-rich marsh soils.

4.2 Introduction and Background

The radionuclides ^{210}Pb and ^{137}Cs are widely used as sediment tracers and chronometers in tidal wetland and estuarine environments, and along with radionuclide transport models are capable of providing age dates for soils and sediments (McCaffrey and Thomson, 1980; DeLaune et al., 1981; Cundy et al., 1997; Kim et al., 2004, Unger et. al, submitted). An important boundary condition in geochronology is the initial activity or “zero age” of the sediment column (see Chapter 3), which is influenced by processes of radionuclide transport to the sediment surface and the composition of the dated material. In tidal wetlands, ^{210}Pb and ^{137}Cs are delivered to waterways, intertidal flats, and marsh platforms by direct atmospheric deposition, and indirectly from fluvial and estuarine sources, mostly in particulate form. It is generally acknowledged that partitioning of the total radionuclide flux among mineral sediment, particulate organic matter, and living plant matter determine the activity concentration of radionuclides in suspended particulate matter and in sediments and soils. However, because of the long chain of transport and physicochemical processes involved, initial activities of ^{210}Pb and ^{137}Cs activity are virtually impossible to predict from first principles.

Despite the enormous amount of information on ^{210}Pb and ^{137}Cs geochronology in the tidal wetland and estuarine literature, there has not been an authoritative study of radionuclide sequestration that considers the mechanisms of radionuclide delivery to marsh soils and compositional factors that influence the

activity of radionuclide upon deposition. This sentiment is echoed by He and Walling (1996):

“However, it is recognized that further study of the effects of soil mineralogy on the interaction between ^{137}Cs and unsupported ^{210}Pb and mineral soils is required. It is also emphasized that investigations of the distribution of fallout ^{137}Cs and ^{210}Pb between the organic and mineral fractions of a soil are needed to understand fully their interaction with soils. Soil organic matter will also adsorb radionuclides, although the amount adsorbed commonly comprises only a small fraction of the total (cf. Livens & Baxter, 1988a, 1988b).” – (He and Walling, 1996)

In the vast majority of chronological studies, it is merely assumed that the initial activity or depositional flux of the radionuclide is steady state without independent verification. Observational studies make clear that the atmospheric flux of ^{210}Pb is non-steady state (e.g., Graustein and Turekian, 1986; Baskaran et al., 1993; Kim et al., 2000), thus it can be assumed that the atmospheric supply of ^{210}Pb to marsh soils is non-steady, particularly in systems with a significant fraction of tidally supplied ^{210}Pb . However, how atmospheric and tidally derived radionuclide fluxes are distributed between the marsh canopy, ground surface, and subsurface is largely unknown. Advancing our understanding of these processes is important not only for purposes of geochronology, but also for characterizing the transport and fate of radionuclides released to coastal and estuarine waters from wastewater treatment facilities and nuclear power plants.

In this study the capture and burial of ^{210}Pb and ^{137}Cs in salt marshes was investigated for insight on dynamical and compositional factors that influence the initial activity of radionuclides. For two salt marsh systems of the U.S. Mid-Atlantic region, activities of ^{210}Pb and ^{137}Cs in plant matter and size-fractionated soils were measured to elucidate how radionuclide sequestration varies within and among salt

marshes. Although the focus was ^{210}Pb and ^{137}Cs and the context geochronology, results of this study have broader implications to the sequestration of other radionuclides and waterborne contaminants in tidal wetlands. The specific objectives were to:

1. quantify radionuclide activity associated with aboveground living and dead plant biomass;
2. quantify activities of the mineral (sand, silt, and clay) and organic (macro- and micro-organic) soil size-fractions; and
3. determine the relative contributions of plant, organic, and mineral fractions to the initial radionuclide activity of the marsh soil.

The guiding hypotheses of this study were as follows:

1. aboveground plant biomass captures radionuclide derived from direct atmospheric fallout and supplies it to soil upon death and burial; and
2. mineral sediment, especially clays, retain the majority of the radionuclide activity due to the high affinity of ^{210}Pb and ^{137}Cs affinity for mineral particles.

A conceptualized model of ^{210}Pb delivery and capture in the estuary-marsh system was used in to formulate the former hypothesis (Figure 4.1). While ^{137}Cs is not shown in the model, transport and capture mechanisms can be assumed to be similar to those of ^{210}Pb . Mechanisms of delivery and capture of both radionuclides are discussed further below.

4.2.1 Sources of $^{210}\text{Pb}_u$ and ^{137}Cs in tidal marsh systems

The radionuclide ^{210}Pb ($t_{1/2} = 22.2$ y) is a member of the Uranium-238 (^{238}U) decay series, and is produced primarily in the atmosphere by decay of gaseous ^{222}Rn emanating

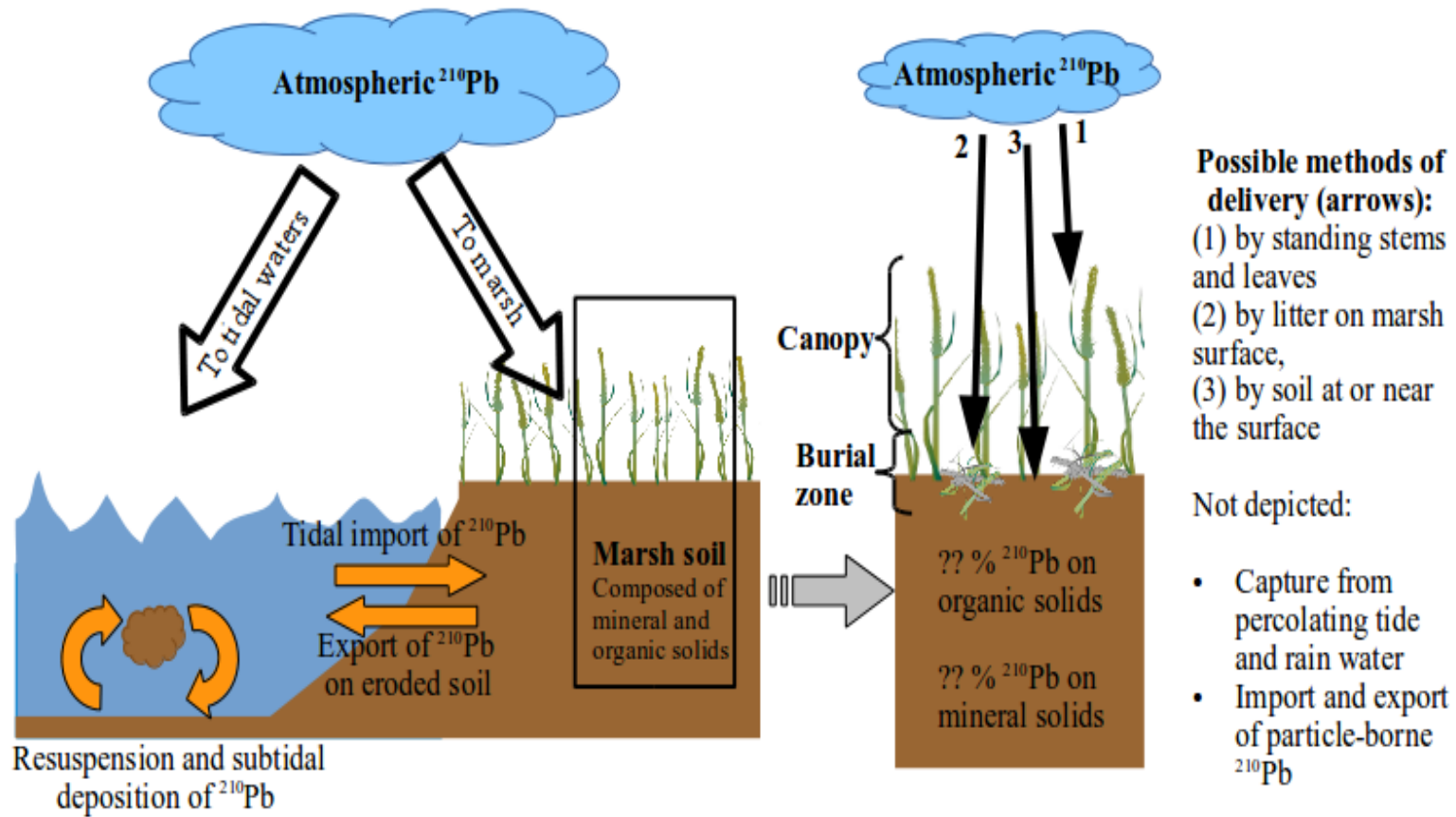


Figure 4.1. Conceptualized model of ^{210}Pb delivery to tidal marshes and methods of incorporation into marsh soils.

from the Earth's surface. Atmospheric ^{210}Pb is scavenged by aerosols and deposited on the Earth's surface by wet and dry deposition (Robbins, 1978). Additionally, in natural waters, sediments, and soils ^{210}Pb is produced by *in-situ* decay of mineralogenic ^{222}Rn . Supported and unsupported ^{210}Pb activity can be distinguished by measurement of ^{238}U or its daughters in secular equilibrium with $^{210}\text{Pb}_s$, for example, ^{214}Pb and ^{214}Bi . In a column of accumulating soil or sediment, $^{210}\text{Pb}_u$ is referred to as the "excess" activity of ^{210}Pb and is determined by subtracting $^{210}\text{Pb}_s$ from the total measured activity ($^{210}\text{Pb}_u = ^{210}\text{Pb}_{\text{total}} - ^{214}\text{Pb}$ or ^{214}Bi).

The anthropogenic radionuclide ^{137}Cs ($t_{1/2} = 30.7$ y) is a fission product whose main source to the environment was thermonuclear weapons testing in the mid-20th Century. In the Northern Hemisphere, this testing resulted in peak atmospheric fallout in 1963-1964 followed by decreasing levels following the test ban treaty. The identification of this peak in the sediment record provides an age-depth relationship that is used as a dating technique in many environments including salt marshes (DeLaune et al., 1978).

Tidal marshes sequester atmospherically sourced radionuclides by direct fallout when exposed, and indirectly by tidal transport when flooded (Figure 4.1). Because the surface area of tidal marshes is frequently smaller than that of the marsh watershed and adjoining coastal and estuarine waters, the potential exists for marshes to accumulate radionuclides indirectly due to tidal transport and deposition. The standing crop of a radionuclide in tidal waters depends on the atmospheric flux over the water body, rate of adsorption by particles, rate of removal by sedimentation, radioactive decay, among other factors. Hence, the amount of indirectly sourced

radionuclide available for deposition on the marsh platform is determined mostly by these external factors.

Watershed inputs of $^{210}\text{Pb}_u$ to estuaries and tidal wetlands are generally low as soils sequester much of the atmospheric fallout. Atmospheric $^{210}\text{Pb}_u$ supplied to rivers is quickly scavenged by suspended matter (Rama et al., 1961). Input from groundwater to marshes is also presumed to be negligible as ^{210}Pb is adsorbed by aquifer sediments and rock (Krishnaswami et al., 1982). Due to low particle concentrations, surface ocean water contains significant dissolved $^{210}\text{Pb}_u$, but in the coastal zone it is rapidly removed to bottom sediments by particle scavenging and deposition (Santschi et al., 1983). Measurements in Long Island Sound by Benninger et al. (1975) indicated a direct relationship between $^{210}\text{Pb}_u$ and suspended sediment concentration with negligible dissolved $^{210}\text{Pb}_u$. A reduction of dissolved ^{210}Pb with an increase in particulate ^{210}Pb was observed in the Delaware and Chesapeake estuaries (Marsan et al., 2014). Benninger (1978) concluded that atmospheric fallout and riverine sediment were the main sources of ^{210}Pb to the Long Island Sound with all other sources being negligible. Hence, given the particle-reactivity of ^{210}Pb , most of the $^{210}\text{Pb}_u$ transported to estuarine marshes is liable to be in the particulate phase.

4.2.2 ^{210}Pb and ^{137}Cs accumulation by plants and soils

Salt marshes have complex geochemical fluxes and thus ^{210}Pb and ^{137}Cs mobility and bioavailability can vary both spatially and temporally (Thomson et al., 2002; Sundby et al., 2005). Possible biotic and organic influences on radionuclide inventories in soils include (1) physical capture of fallout on the canopy and (or) exposed roots (Figure 4.1), (2) adsorption by aboveground structures and burial of those structures, (3) translocation from aboveground biomass to belowground, (4)

translocation from belowground roots to the aboveground stems and leaves, (5) scavenging of dissolved or trapping of particle-associated radionuclides, (6) liberation of radionuclides due to decomposition or redox conditions, and (7) downwash of radionuclides due to percolation of porewater.

There exists an extensive literature on the accumulation of heavy metals by halophytes and other plants relevant to ^{210}Pb uptake and adsorption. In most cases, Pb ions preferentially associate with mineral sediments and organic matter making them unavailable for plant uptake (Zimdahl, 1976). It is generally accepted that Pb accumulated in roots is not transported to aerial structures at an appreciable rate (Peterson, 1978). Aboveground stems and leaves could physically trap ^{210}Pb in the waxy cuticle and (or) uptake it into tissue. Pietrzak-Flis and Skowrońska-Smolak (1995), working with a variety of food and fodder crops, determined that the main source of ^{210}Pb to aboveground plant structures was atmospheric deposition and not translocation of soil ^{210}Pb from belowground to aboveground biomass. After treatment of leaves and fruit with lead aerosols, Pb was easily removed by rinsing and not present in tissues. This suggested that surface trapping, not uptake, was the mechanism of ^{210}Pb sequestration (Arvik and Zimdahl, 1974). In summary, ^{210}Pb uptake by roots is minimal and translocation from the roots to the aerial plant structures is negligible. Based on the available data, ^{210}Pb desorption and uptake are assumed to be minor processes and any uptake is not translocated to other parts of the plants.

Incorporation of ^{137}Cs into soils was reviewed by Ritchie and McHenry (1990) and is summarized here. Uptake by plants from soils is low and further reduced by the availability of nutrients (Davis, 1963), especially potassium (Delvaux et al., 2000) and clay minerals (Dahlman et al., 1975; Shand et al., 1994). Indeed, Oldfield et al. (1979)

attributed the anomalously high ^{137}Cs surface activities and profile shape to plant uptake in low-nutrient, ombrotrophic peats. Due to its particle affinity in freshwater, ^{137}Cs associates with the mineral component of soils and can become irreversible “fixed” in micaceous clays (Davis, 1963; Comans and Hockley, 1992). Seawater can cause desorption of ^{137}Cs due to competition from other cations, particularly K^+ and Na^+ (Aston and Duursma, 1973; Atun et al., 1996; Johnson-Pyrtle and Scott, 2001). Immobility of deposited ^{137}Cs in anoxic, marine sediments has been observed (Sugai et al., 1994). Desorption experiments near the Fukushima Daiichi Nuclear Power Plant resulted in only 3.4% of ^{137}Cs being leached from estuarine sediments (Yamasaki et al., 2016). Additionally, independent verification of ^{137}Cs chronology in estuaries, bays, and salt marshes further indicates that a large portion of ^{137}Cs remains geochemically fixed in cation-rich conditions. In summary, while ^{137}Cs is more easily desorbed than ^{210}Pb in saline waters, its strong affinity for clay minerals make it largely immobile in soils.

4.3 Methods

4.3.1 Sample collection and processing

Three marshes within the Barnegat Bay estuary and three in the Delaware Bay estuary were sampled in summer 2012. At each site standing stems and leaves and litter from a 0.25 m² quadrat were collected, as well as two ~ 1 m push cores from within the quadrat. The locations of the coring sites are listed in Table 4.1. Cores were transported to the laboratory, split vertically, and stored at 4°C.

The 0–2, 2–4, and 4–6 cm depth intervals of one core from each site were analyzed for ^{137}Cs , ^{210}Pb , and ^{214}Bi activities, and physical properties. Water content,

Table 4.1: Core locations and bulk soil properties and radionuclide activities for the 0–6 cm surface soils from Chapter 2.

Core	Layer age (y)	LOI (% mass)	Bulk Density (g cm ⁻³)	²¹⁰ Pb		²¹⁴ Bi		¹³⁷ Cs		Excess ²¹⁰ Pb	
				(Bq kg ⁻¹)	(Bq m ⁻²)	(Bq kg ⁻¹)	(Bq m ⁻²)	(Bq kg ⁻¹)	(Bq m ⁻²)	(Bq kg ⁻¹)	(Bq m ⁻²)
DN-1	16.9	30	0.40	159 (6)	3800 (88)	14 (1)	344 (19)	6.4 (0.7)	153 (9)	145 (8)	3456 (107)
DN-2	9.1	26	0.38	230 (7)	5179 (86)	13 (1)	285 (18)	3.7 (0.6)	84 (8)	217 (8)	4894 (103)
DN-3	7.0	29	0.28	162 (6)	2707 (60)	11 (1)	181 (12)	4.1 (0.6)	68 (6)	151 (8)	2526 (72)
DV-1	13.5	24	0.32	161 (6)	3125 (70)	14 (1)	277 (14)	4.1 (0.6)	80 (7)	147 (7)	2848 (84)
DV-2	8.3	22	0.40	86 (4)	2069 (62)	22 (2)	529 (23)	3.3 (0.6)	80 (8)	64 (6)	1540 (85)
DV-3	17.5	48	0.17	176 (7)	1840 (40)	8 (1)	83 (8)	2.8 (0.7)	29 (4)	168 (8)	1757 (48)
MR-1	6.3	22	0.51	124 (5)	3807 (87)	26 (2)	792 (31)	3.5 (0.6)	106 (11)	98 (7)	3015 (118)
MR-2	4.7	20	0.38	117 (5)	2688 (69)	23 (2)	535 (24)	3.1 (0.7)	71 (9)	93 (7)	2154 (93)
MR-3	3.8	17	0.43	141 (5)	3677 (74)	49 (2)	1286 (35)	4.7 (0.7)	121 (10)	92 (7)	2391 (109)
CC-1	22.5	34	0.32	366 (8)	7097 (91)	12 (1)	236 (16)	3.6 (0.7)	70 (7)	354 (9)	6861 (107)
CC-2	19.2	35	0.32	237 (7)	4524 (75)	10 (1)	200 (14)	3.5 (0.6)	66 (7)	227 (8)	4324 (89)
CC-3	19.0	38	0.28	198 (6)	3370 (67)	11 (1)	181 (12)	3.8 (0.5)	64 (5)	188 (8)	3189 (79)
IB-1	19.5	57	0.15	162 (6)	1509 (33)	8 (2)	77 (9)	1.6 (0.5)	15 (4)	154 (8)	1432 (42)
IB-2	20.8	65	0.12	188 (8)	1394 (37)	15 (1)	113 (7)	2.1 (0.4)	16 (3)	173 (9)	1281 (44)
IB-3	23.6	71	0.18	305 (10)	3249 (61)	7 (2)	74 (10)	0.5 (0.2)	5 (2)	298 (11)	3175 (71)
RC-1	28.3	53	0.18	358 (8)	3774 (49)	9 (2)	96 (10)	8.0 (1)	84 (6)	349 (10)	3678 (59)
RC-2	32.5	58	0.13	423 (10)	3316 (44)	5 (1)	39 (6)	14.2 (1.4)	112 (6)	418 (11)	3278 (50)
RC-3	23.1	62	0.14	450 (11)	3778 (52)	11 (3)	88 (13)	7.2 (1.3)	61 (6)	440 (13)	3690 (65)

porosity, and dry bulk density were determined gravimetrically following the methodology of Bennett and Lambert (1971). The proportions of mineral and organic solids were determined by loss-on-ignition analysis. Bulk soil radionuclide activities and physical properties presented in Table 4.1 are the average of the 0–2, 2–4, and 4–6 cm intervals weighted by bulk density. The age of the 6-cm depth surface was estimated via ^{137}Cs mass accumulation rates determined in Chapter 1. These ages were used to calculate theoretical $^{210}\text{Pb}_u$ inventories based on measurements of ^{210}Pb atmospheric flux published for the region. Bismuth-214 was used as a proxy for $^{210}\text{Pb}_s$ to calculate $^{210}\text{Pb}_u$ from $^{210}\text{Pb}_{\text{total}}$.

4.3.2 Separation of soil solids

The second core was vertically split and sampled from 0 to 6 cm. This bulk material, composed of mineral sediment and organic matter, was placed in a 1-L jar and filled with a solution of 1% sodium hexametaphosphate to disaggregate the material. The jar was first agitated by shaking and then placed in an ultrasonic bath for 1 hour. Macro-organic (>1 mm), micro-organic (1 mm –125 μm), and sand-sized (125–63 μm) organic particles were separated via wet sieving; the sand-sized fraction was almost exclusively organic matter. Solids that passed through the sieves consisted of a mixture of mineral and finely disseminated organic solids, and were separated into silt-sized (63–2 μm) and clay-sized (< 2 μm) fractions by centrifugation. The following equation described by Genrich and Bremner (1974) was used for this purpose:

$$T = \frac{(63 \times 10^8) n \log_{10} \frac{R}{S}}{N^2 D^2 (S_p - S_l)} \quad (4.1)$$

where T is the time for sedimentation (minutes), N is the viscosity of water (poises), R is the radius of rotation to top of sediment (cm), S is the radius of rotation to top of suspension (cm), N is the speed of centrifuge (RPM), D is particle diameter (microns), S_p is the specific gravity of particles (g cm^{-3}), and S_l is the specific gravity of water (g cm^{-3}). Using Equation 4.1, the silt-sized fraction was separated from suspension by centrifuging 8 minutes at 800 RPM and decanting off the supernatant. The supernatant was dried at 100°C until sample mass was constant (12–24 h) and the remaining solid classified as the clay-sized fraction. Based on sample mass and volume, the two size fractions were packed into either 60-ml jars or 6-ml vials for radionuclide analysis.

It should be noted that the soil fraction classification used in this study is purely based on size determined mechanically and centrifugation. The composition of the fractions was not determined analytically; however, the sand size fraction appeared to be composed exclusively of organic matter. Previous work in Delaware Bay marsh soils found the total organic content of the sand (63–125 μm), silt (2–63 μm) and clay (<2 μm) to be 34 ± 9 , 9 ± 6 , and 10 ± 7 % mass (Tucker, 2016). Thus, in this chapter use of the terms sand, silt, and clay refers to particle size alone and does not imply mineralogy.

4.3.3 Aboveground biomass samples

The aboveground biomass was characterized as standing biomass or litter, rinsed of mineral sediment and detritus, and dried at 70°C until sample weight was constant. The biomass mass per unit area was determined as part of a related study (Table 4.2; Unger et al, submitted). Two steps were required to reduce the volume of the biomass and create a uniform powder for radionuclide analysis. First, dried stems and leaves were ground to small pieces using a conventional blender (Waring Pro) to

Table 4.2: Aboveground biomass concentrations and radionuclide activities. Hyphens indicate where samples were not analyzed.

Core	Standing stems and leaves						Litter					
	Mass (g m ⁻²)	²¹⁰ Pb (Bq kg ⁻¹)	²¹⁴ Bi (Bq kg ⁻¹)	¹³⁷ Cs (Bq kg ⁻¹)	Excess ²¹⁰ Pb (Bq kg ⁻¹)	Excess ²¹⁰ Pb (Bq m ⁻²)	Mass (g m ⁻²)	²¹⁰ Pb (Bq kg ⁻¹)	²¹⁴ Bi (Bq kg ⁻¹)	¹³⁷ Cs (Bq kg ⁻¹)	Excess ²¹⁰ Pb (Bq kg ⁻¹)	Excess ²¹⁰ Pb (Bq m ⁻²)
DN-1	308	11 (3)	0	0	11 (3)	3.2 (1)	86	57 (4)	3 (1)	1.1 (0.6)	54 (4)	4.6 (0.4)
DN-2	330	8 (4)	0	0	8 (4)	2.6 (1.5)	119	35 (5)	3 (2)	0	31 (5)	3.7 (0.6)
DN-3	423	-	-	-	-	-	97	-	-	-	-	-
DV-1	265	14 (4)	0	0	14 (4)	3.6 (1)	48	56 (9)	13 (3)	0	43 (10)	2.1 (0.5)
DV-2	85	10 (4)	0	0	10 (4)	0.8 (0.3)	20	0	0	0	0	0
DV-3	352	7 (3)	0	0	7 (3)	2.4 (0.9)	33	45 (7)	0	0	45 (7)	1.5 (0.2)
MR-1	487	-	-	-	-	-	103	51 (4)	5 (2)	0	46 (4)	4.7 (0.4)
MR-2	780	6 (3)	0	0	6 (3)	4.9 (2.3)	69	42 (7)	0	0	42 (7)	2.9 (0.5)
MR-3	726	8 (4)	0	0	8 (4)	5.7 (2.8)	196	0	4 (2)	0	0	0

Table 4.2 continued.

CC-1	415	15 (4)	0	0	15 (4)	6.4 (1.6)	488	-	-	-	-	-
CC-2	383	18 (5)	6 (3)	1.6 (0.8)	13 (6)	4.8 (2.2)	310	220 (9)	0	0	220 (9)	68.3 (2.8)
CC-3	287	14 (3)	0	0	14 (3)	3.9 (0.9)	153	118 (5)	3 (1)	0	115 (6)	17.6 (0.9)
IB-1	10	0	0	0	0	0	11	112 (32)	0	0	112 (32)	1.2 (0.3)
IB-2	0	0	0	0	0	0	0	0	0	0	0	0
IB-3	270	0	2 (1)	0	0	0	261	154 (6)	0	0	154 (6)	40.2 (1.7)
RC-1	75	11 (4)	0	0	11 (4)	0.8 (0.3)	159	233 (7)	0	2.6 (0.9)	233 (7)	37.1 (1.1)
RC-2	67	0	0	0	0	0	267	246 (6)	8 (1)	1.3 (0.6)	239 (6)	63.8 (1.7)
RC-3	194	11 (3)	0	0	11 (3)	2.2 (0.6)	590	241 (7)	0	3.1 (0.7)	241 (7)	141.9 (4)

facilitate further milling. Second, a batch mill (IKA M-20) outfitted with a sharpened, four-blade cutter was used to mill the material into a powder, which was packed into 60-ml jars for radionuclide analysis. Standing biomass for DN-3 and MR-1 and litter for DN-3 and CC-1 was not analyzed.

4.3.4 Plant-radionuclide standard preparation

To quantify the radionuclide activity in plant biomass, a grass standard was prepared using milled *Spartina alterniflora* leaves and stems previously determined not to contain $^{210}\text{Pb}_s$. The milled biomass sample (33.67 g) was spiked with 0.0135 g of Reference Uranium Ore BL-5 available from the Canada Center for Mineral and Energy Technology. Given the relatively high ^{238}U radioactivity of the ore (866 Bq g⁻¹) only a small amount was required, less than 0.05% of the mass of the biomass matrix. The relatively small mass of the spike and the use of sample material as a matrix eliminated the need for self-attenuation corrections. A grass standard in a 6 ml vial was created in an identical fashion using 2.18 g milled biomass and 1.5 mg BL-5 for use in a well-type gamma detector.

The grass standard was counted three times for 24 h, rotating 120° each time, and averaged. Activity efficiencies for ^{210}Pb and ^{214}Bi were calculated spectroscopically using the 43.6 keV and 609 keV gamma photopeaks, respectively. Since no ^{137}Cs activity is present in the BL-5 reference material, and because the detector efficiency at 661.1 keV (^{137}Cs) is similar to that of ^{214}Bi at 609 keV, the activity efficiency of ^{137}Cs ($\varepsilon_{137\text{Cs}}$) was determined from the ^{214}Bi as follows:

$$\varepsilon_{137\text{Cs}} = \frac{\varepsilon_{214\text{Bi}}}{\gamma_{214\text{Bi}}} \cdot \gamma_{137\text{Cs}} \quad (4.2)$$

where the ε is the activity efficiency for the detector, and γ is the gamma-ray yield (branching ratio) corresponding to the emission energy of interest (609 keV ^{214}Bi emission = 46.1% and 661.6 keV ^{137}Cs emission = 85.2%). It should be noted that ^{137}Cs itself does not emit a gamma during beta-decay; rather, the 661.6 keV photopeak is produced by decay of its metastable daughter, $^{137\text{m}}\text{Ba}$.

4.3.5 Radionuclide analysis

A total of 36 aboveground biomass and 84 soil samples were prepared for gamma spectroscopy. Activities of ^{137}Cs , ^{210}Pb , and ^{214}Bi were determined via counting for 24 h using either a well- or planar-type, high-purity Ge detector (Canberra Models GCW2523, BE2825, GL2020R), interfaced with a Canberra DSA-1000 or Desktop Inspector multi-channel analyzer. For soil samples the detectors were calibrated using a natural matrix standard (SRM 4353A Rocky Flats Soil; Nour et al. 2008), and for the aboveground biomass samples using the grass standard described above. Uncertainties are calculated as the 1σ counting error.

Using the aboveground biomass samples, areal activities of ^{137}Cs and $^{210}\text{Pb}_u$ (Bq m^{-2}) were calculated as the product of massic activity (Bq kg^{-1}) and biomass area concentration (kg m^{-2}) and are referred to as aboveground inventory. Similarly, areal activities for the bulk soil samples were calculated as the product of massic activity and dry bulk density; these data were summed over the 0-6 cm depth intervals to determine the belowground, partial inventory of ^{137}Cs and $^{210}\text{Pb}_u$. Size-fraction contributions (I_{fract} in %) to the partial inventories were calculated as follows:

$$I_{fract} = 100 \cdot \frac{MA_{fract} \cdot m_{fract}}{A_{bulk}} \quad (4.3)$$

where MA_{fract} is the massic activity (Bq kg^{-1}) of the soil fraction, m_{fract} is the mass (kg) of the soil fraction in the 0–6 cm soil sample, and A_{bulk} (Bq) is the total activity of the 0–6 cm bulk soil sample. Theoretical partial inventories for $^{210}\text{Pb}_u$ (I_{theo}) were calculated for the soil samples as follows:

$$I_{theo} = (P \cdot A)e^{-\lambda A} \quad (4.4)$$

where P ($165 \text{ Bq m}^{-2} \text{ y}^{-1}$) is the literature-average atmospheric flux of ^{210}Pb for the U.S. Mid-Atlantic region ($130 \text{ Bq m}^{-2} \text{ y}^{-1}$: Turekian et al., 1983; $200 \text{ Bq m}^{-2} \text{ y}^{-1}$: Kim et al., 2000), A is the age (y) of the sediment layer based on ^{137}Cs chronology (Table 4.1) and λ is the decay constant of ^{210}Pb (0.03114 y^{-1}).

4.4 Results

4.4.1 Aboveground activities

Excess ^{210}Pb was detected on both canopy (standing stems and leaves) and litter (Table 4.3). No biomass was present at IB-2, thus, activities for that site were zero. On average, the $^{210}\text{Pb}_u$ activity of the canopy was 14% that of the litter. Only two sites had higher specific activities on canopy when compared to litter, DV-2 and MR-3. There was no $^{210}\text{Pb}_u$ detected in litter at DV-2, MR-3, and CC-1 and canopy at RC-2. One canopy (CC-2) and three litter (DN-1, RC-1, RC-2, RC-3) samples contained ^{137}Cs . For samples in which $^{210}\text{Pb}_u$ was detected on both types of aboveground biomass, the activity was 3–21 times greater on the litter. Interestingly, the aboveground inventory (Bq m^{-2}) associated with litter was 0.5–65 times greater than the inventory associated with the canopy, despite the higher mass of canopy biomass (Table 4.2). In nine of the thirty biomass samples, ^{214}Bi was detected, indicative of

Table 4.3: Massic activities (Bq kg^{-1}) for the soil size-fractions. Activity error is shown in parentheses. The size fractions are as follows: clay ($<2\mu\text{m}$), silt ($>2\mu\text{m}$ and $<63\mu\text{m}$), sand ($>63\mu\text{m}$ and $<125\mu\text{m}$), micro-organic ($>125\mu\text{m}$ and $<1\text{mm}$), and macro-organic ($>1\text{mm}$).

Core	Clay			Silt			Sand			Micro-organic			Macro-organic		
	^{210}Pb	^{214}Bi	^{137}Cs												
DN-1	90 (11)	0	9 (2)	96 (4)	15 (1)	8 (1)	108 (10)	17 (3)	5 (1)	124 (13)	21 (5)	10 (2)	53 (4)	3 (2)	0
DN-2	99 (10)	16 (3)	4 (1)	115 (4)	15 (1)	5 (1)	132 (10)	12 (3)	3 (1)	190 (12)	16 (4)	6 (2)	171 (12)	0	0
DN-3	110 (11)	8 (4)	8 (1)	101 (5)	13 (2)	5 (1)	151 (10)	18 (3)	5 (1)	211 (17)	20 (6)	10 (3)	40 (5)	0	0
DV-1	80 (10)	14 (3)	6 (1)	79 (4)	14 (1)	2 (1)	72 (11)	8 (4)	0	126 (15)	24 (6)	5 (3)	164 (30)	22 (10)	0
DV-2	53 (12)	16 (4)	6 (2)	59 (4)	13 (2)	10 (1)	75 (16)	0	19 (3)	84 (15)	44 (5)	27 (3)	45 (20)	0	10 (4)
MR-1	205 (12)	22 (3)	5 (1)	80 (4)	23 (1)	4 (1)	61 (14)	0	8 (2)	77 (17)	31 (7)	0	54 (11)	10 (4)	0
MR-2	166 (12)	20 (3)	7 (1)	74 (4)	20 (1)	3 (1)	71 (12)	21 (4)	7 (2)	65 (10)	25 (3)	3 (1)	-	-	-
MR-3	188 (14)	39 (3)	7 (1)	72 (4)	31 (2)	2 (1)	89 (11)	24 (4)	4 (1)	152 (11)	64 (4)	5 (2)	174 (17)	44 (7)	6 (3)
CC-1	262 (11)	0	7 (1)	135 (4)	15 (1)	4 (1)	228 (11)	9 (3)	4 (1)	183 (12)	23 (4)	6 (2)	240 (17)	0	7 (3)

CC-2	189 (12) 10 (3) 4 (2)	82 (4) 11 (1) 2 (1)	130 (10) 13 (3) 4 (1)	256 (12) 11 (4) 8 (2)	168 (11) 0 0
------	-----------------------	---------------------	-----------------------	-----------------------	--------------

Table 4.3 continued.

CC-3	184 (10) 0 9 (1)	87 (4) 12 (1) 5 (1)	117 (12) 15 (4) 6 (1)	150 (12) 17 (4) 8 (2)	115 (12) 8 (4) 0
------	------------------	---------------------	-----------------------	-----------------------	------------------

IB-1	167 (17) 0 5 (2)	110 (6) 3 (1) 3 (0)	185 (12) 0 8 (1)	261 (12) 11 (4) 7 (2)	175 (10) 0 0
------	------------------	---------------------	------------------	-----------------------	--------------

IB-2	152 (24) 0 0	142 (11) 9 (4) 4 (1)	174 (15) 16 (5) 5 (2)	297 (16) 0 8 (2)	143 (12) 0 0
------	--------------	----------------------	-----------------------	------------------	--------------

IB-3	255 (19) 0 0	248 (11) 10 (3) 3 (1)	340 (14) 8 (4) 4 (2)	434 (13) 18 (4) 7 (2)	254 (14) 0 0
------	--------------	-----------------------	----------------------	-----------------------	--------------

RC-1	264 (14) 0 18 (2)	150 (7) 12 (3) 10 (2)	259 (12) 15 (3) 17 (2)	308 (11) 18 (3) 20 (2)	333 (25) 0 0
------	-------------------	-----------------------	------------------------	------------------------	--------------

RC-2	323 (23) 15 (8) 15 (3)	314 (11) 6 (3) 9 (1)	382 (14) 0 13 (2)	513 (14) 16 (4) 23 (2)	273 (27) 0 0
------	------------------------	----------------------	-------------------	------------------------	--------------

RC-3	279 (18) 11 (6) 7 (3)	373 (12) 11 (3) 11 (1)	419 (14) 8 (4) 10 (1)	555 (14) 6 (3) 17 (2)	326 (22) 16 (7) 0
------	-----------------------	------------------------	-----------------------	-----------------------	-------------------

supported ^{210}Pb activity most likely associated with mineral sediment; seven of these nine samples were litter.

The $^{210}\text{Pb}_u$ activity of aboveground biomass was lower than that of the bulk soil (Figure 4.2). The bulk soil activity was between one and seven times higher than the activity of litter. In the organic-rich Barnegat Bay marshes, the $^{210}\text{Pb}_u$ of litter was more similar to the bulk soil than in the mineral-rich Delaware Bay marshes. Two Barnegat Bay marsh sites, CC-2 and IB-1, had bulk soil and litter activities that were equal (Figure 4.2).

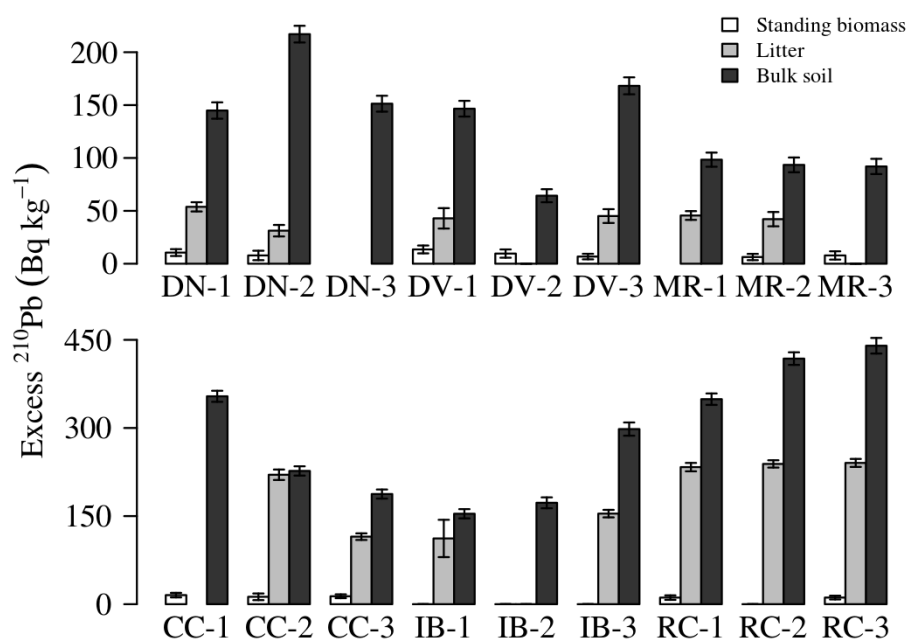


Figure 4.2: The excess ^{210}Pb activities of aboveground biomass – standing and litter – and the underlying bulk soil (0–6 cm).

Assuming that aboveground biomass is a substrate for deposition of atmospherically derived ^{210}Pb , the atmospheric flux was compared to the surface inventory of this material. Combining the inventories associated with living and dead biomass (Table 4.2) for each site gives the total aerial inventory (Bq m^{-2}). Aerial inventories determined in this manner accounted for 20.6% (range: 0.5–87%) of the mean annual atmospheric flux of ^{210}Pb (165 Bq m^{-2}) reported for the region (Turekian et al., 1983; Kim et al., 2000).

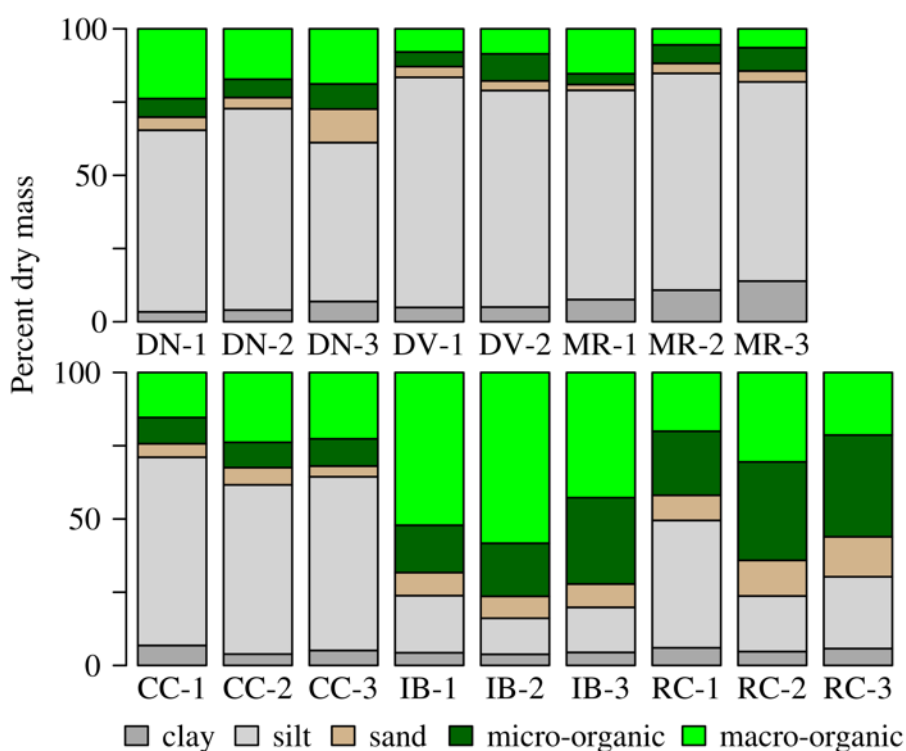


Figure 4.3: Bar plot showing the percent mass contribution of the soil-size fractions to the bulk soil (0-6cm). The top row are sites from marshes in Delaware Bay and the bottom row from marshes in Barnegat Bay. The volume contribution showed higher organic contribution and lower mineral contribution due to the low particle density of organic matter (1.14 g cm^{-3}) relative to mineral sediment (2.61 g cm^{-3}).

4.4.2 Marsh soil composition and radionuclide activity

As expected, the majority of the 0-6 cm marsh soil by mass (60-88%) and volume (78-93%) consisted of pore water. Silt-sized solids comprised the main mineral component in all of the core samples (12-78%), whereas clay- and sand-sized solids contributed least to the total mass (Figure 4.3). Five cores (IB-1, IB-2, IB-3, RC-2, and RC-3) had soils with organic matter contents >50% of the total mass. Overall, the mass of the size-separated organic solids corresponded well with bulk organic matter content determined by the LOI method (Figure 4.4).

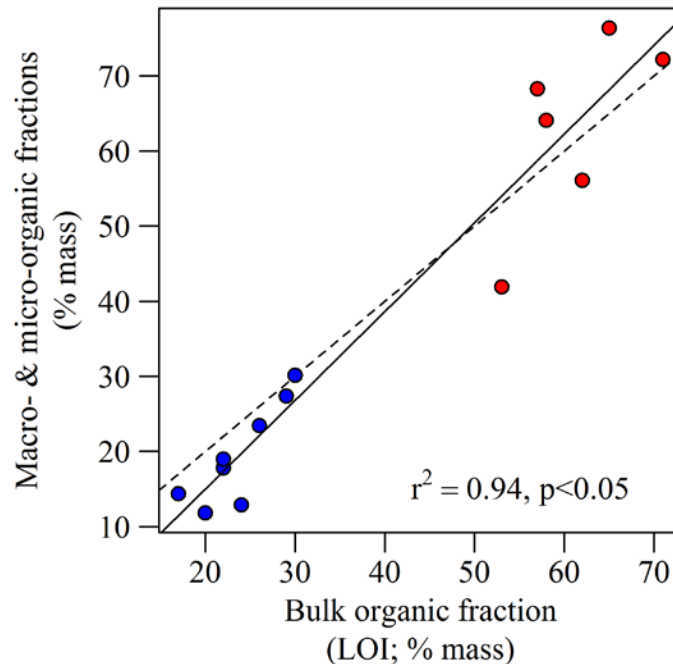


Figure 4.4: Regression of the mass contribution of organic soil-fraction (macro- and micro-) and the organic fraction of the bulk sediment sample. Data from Delaware Bay is shown in blue and from Barnegat Bay in red. Confidence in the physical separation used in size fraction methods is supported by the good agreement between the physical separation and the loss-on-ignition (LOI) method use on the bulk soil. The dashed line represents a 1:1 relationship.

Size fraction activities are presented in Table 4.3.

Detectable ^{214}Bi activity was mostly associated with the silt-sized fraction of soils (15-83%) and micro-organics (0-75%). Significantly, ^{214}Bi was not detected on the macro-organic samples at ten of the seventeen coring locations, suggesting that ^{210}Pb associated with this material is unsupported and derived exclusively from atmospheric deposition.

Size-fraction $^{210}\text{Pb}_u$ activities (Bq kg^{-1}) are presented in Figure 4.5.

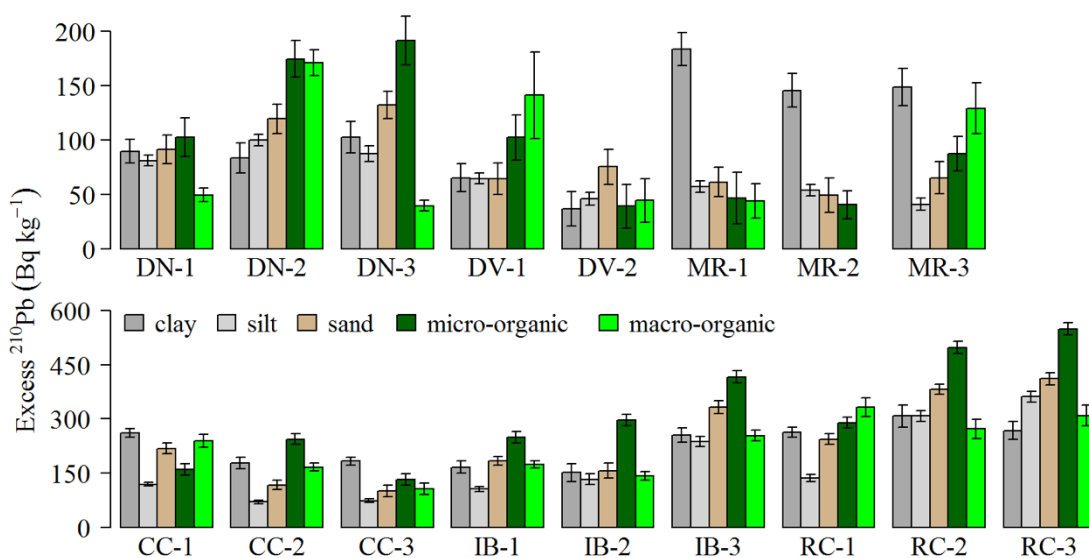


Figure 4.5: The excess ^{210}Pb activities of the clay, silt, sand, micro-organic, and macro-organic size fractions from 0–6 cm depth. Note the different scales for the top row, sites from marshes in Delaware Bay, and the bottom row, sites from marshes in Barnegat Bay.

All size fractions of the soil at all sampling sites contained detectable excess ^{210}Pb .

The organic solids (macro- and micro-organic) explained the majority of the $^{210}\text{Pb}_u$ 0-6cm inventory at coring sites CC-2, IB-1, IB-2, IB-3, RC-1, RC-2, and RC-3 (Fig.

4.6). With the exception of CC-2, all of those sites had soils consisting of at least 50% organic content by mass (Table 4.1).

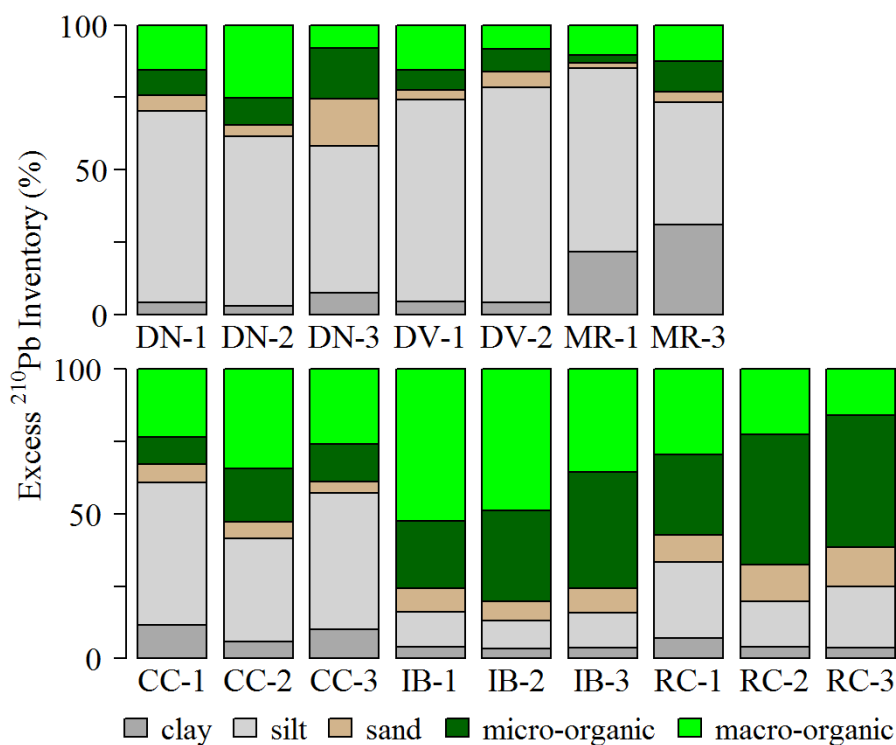


Figure 4.6: The percent of the bulk excess ^{210}Pb inventory held by each soil fraction. The top row are sites from marshes in Delaware Bay and the bottom row from marshes in Barnegat Bay.

Cesium-137 was detected in the macro-organic fraction at DV-2, MR-2, and CC-1 (Figure 4.7). It could be that incomplete separation of ^{137}Cs -laden mineral solids from the organic fraction is the source of this ^{137}Cs . Erosion and delivery of “legacy” ^{137}Cs is the only possible source in these estuaries. However, ^{214}Bi was not detected in

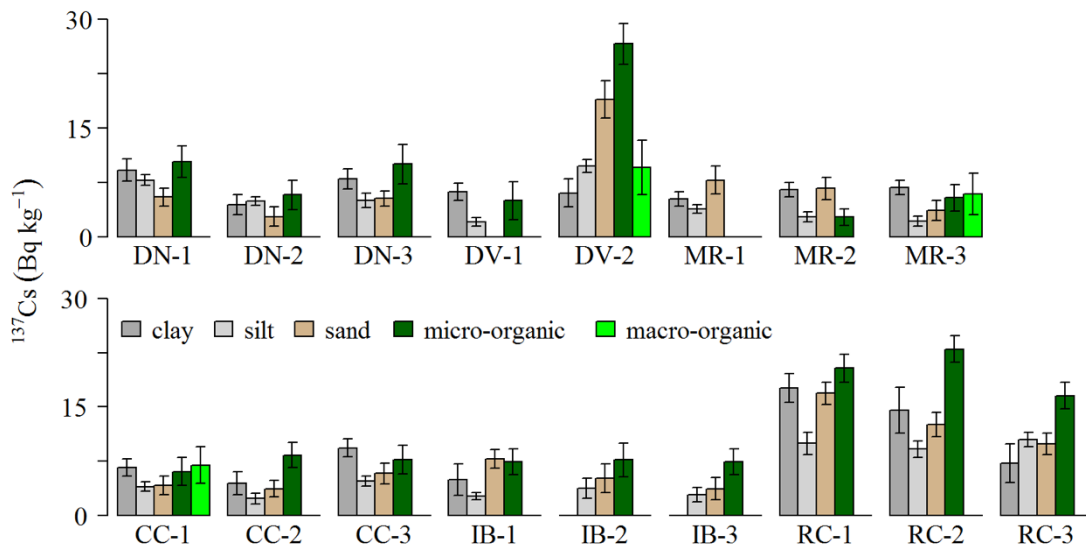


Figure 4.7: The ^{137}Cs activity of the clay, silt, sand, micro-organic, and macro-organic soil size fractions from 0–6 cm depth. The top row are sites from marshes in Delaware Bay and the bottom row are sites from marshes in Barnegat Bay.

the macro-organic fraction at DV-2 and CC-1 suggesting that no mineral material was present. The micro-organic fraction had higher activities than any other fraction at thirteen locations (Figure 4.8). The organic fraction, primarily micro-organic, contributed 0–28% of the 0-6cm ^{137}Cs inventory for the Delaware Bay samples and 17–74% of those for Barnegat Bay. The silt-sized fraction had low specific activities of ^{137}Cs (2-10 Bq kg⁻¹) but, due to its relative mass, contributed most to the inventory at sites consisting of mineral-rich soil (Figure 4.8). As with $^{210}\text{Pb}_u$, clay-sized fraction had similar or higher activities compared to silt and sand fractions (Figure 4.7), but contributed 0–28% of the 0-6 cm inventory due to its low relative mass (Figure 4.8).

With knowledge of the ^{210}Pb activity of the soil organic solids (sand + micro- + macro-organic), comparison of the aboveground biomass and soil organic material is

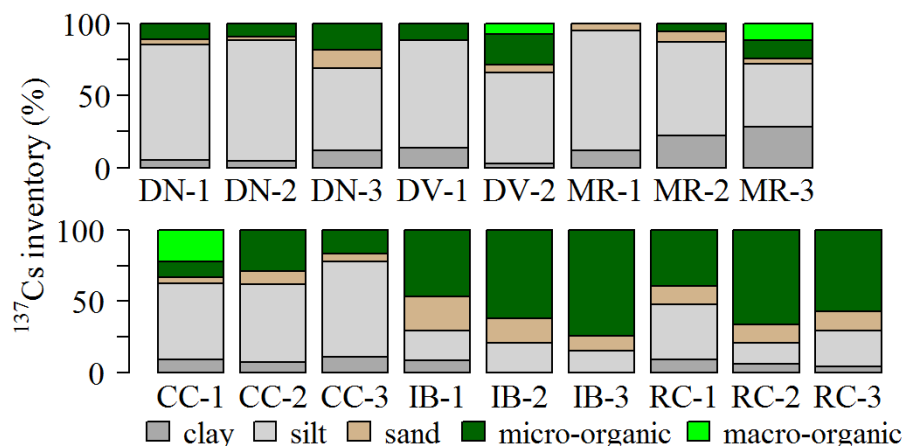


Figure 4.8: The percent of the bulk ^{37}Cs inventory held by each soil fraction. The top row are sites from marshes in Delaware Bay and the bottom row from marshes in Barnegat Bay.

possible (Figure 4.9). If the activities of the above- and below-ground solids are similar, it could indicate capture and burial of ^{210}Pb by litter. The activity of the aboveground litter was more similar to the underlying organic solids than it was to the bulk soil (organic solids + mineral solids; Figure 4.1). In many cases the activity of the soil organic-solids was still higher than the aboveground litter. This suggests that some other mechanism may be concentrating ^{210}Pb activity in the surface soil, such as decomposition, or scavenging from percolating tide or rain water.

4.4.3 Soil inventories of excess ^{210}Pb

To quantify non-atmospheric additions to the $^{210}\text{Pb}_u$ inventory, it was necessary to determine theoretical inventories based solely on atmospheric fallout measurements (Equation 4.4). Theoretical partial $^{210}\text{Pb}_u$ inventories based on an average flux of $165 \text{ Bq m}^{-2} \text{ y}^{-1}$ and layer age are presented in Figure 4.10. For all coring sites except for IB-1 and IB-2, the measured partial inventory was greater than

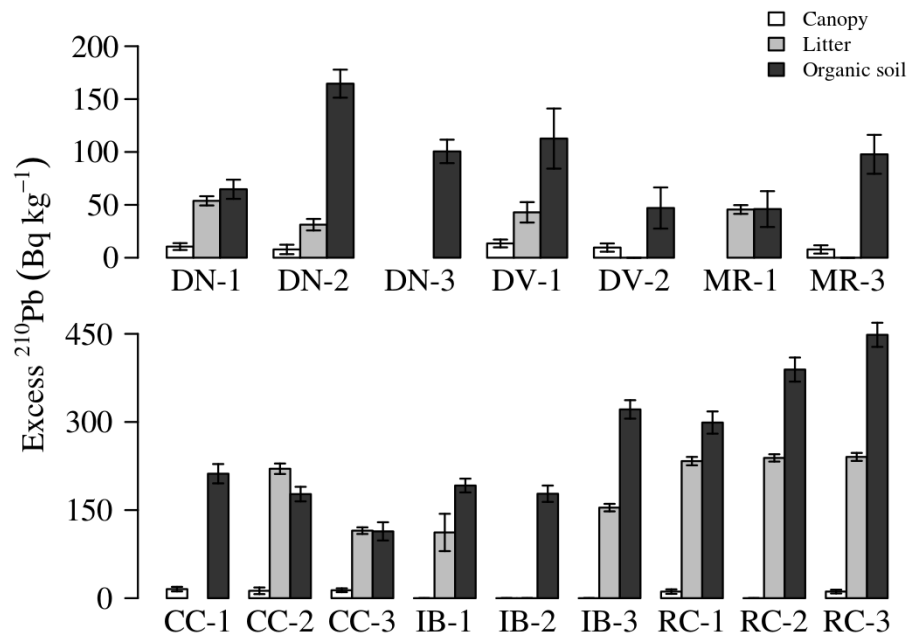


Figure 4.9: The excess ^{210}Pb activities of aboveground biomass – canopy and litter – and the underlying organic soil (sand + micro- + macro-organic; 0–6 cm).

what would be expected solely from atmospheric sources. A surplus inventory indicates one or more non-atmospheric sources of $^{210}\text{Pb}_u$ to the soils. The direct relationship between soil mass inventory and $^{210}\text{Pb}_u$ inventory in these marshes indicates that sediment focusing could be responsible for surplus inventory to these locations (Chapter 3). The deficit partial inventories found at IB-1 and IB-2 suggest that ^{210}Pb activity is incompletely captured on the marsh platform or that it is lost perhaps through surface erosion and redistribution of ^{210}Pb -laden particles.

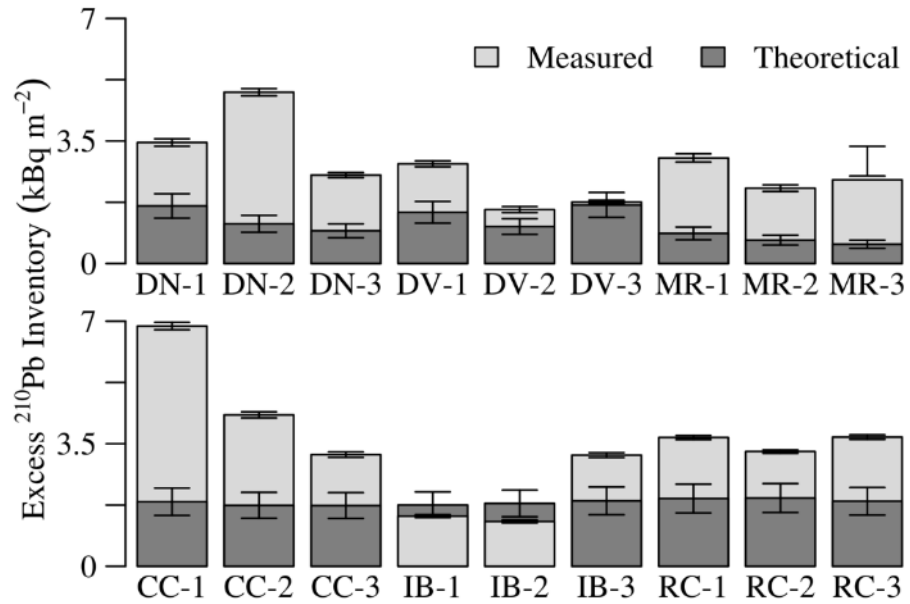


Figure 4.10: Theoretical and measured partial (0–6 cm) inventories of excess ^{210}Pb . The theoretical inventories are based on the age of the surface layer from ^{137}Cs dating (Chapter 1) and an average literature ^{210}Pb flux of $165 \text{ Bq m}^{-2} \text{ y}^{-1}$ (Turekian et al. 1983; Kim et al. 2000). All measured inventories were found to be enriched compared to theoretical inventories except for sites IB-1 and IB-2.

Although there is no direct method to differentiate between atmospheric and tidal sources of ^{210}Pb in marsh soils, a simple test can be used to estimate how much of the theoretical inventory can be accounted for by one or more soil-size fractions. Using the $^{210}\text{Pb}_u$ activities shown in Figure 4.5 and the theoretical inventories from Figure 4.10, the percentage of theoretical inventory contributed by the individual size fractions was calculated (Figure 4.11). Accordingly, the organic solids can account for 24–149% of the theoretical inventory and the mineral solids 14–334%. For eight of the sixteen sites, the organic solids of this soil accounted for 1–1.5 times the theoretical inventory, and for ten of the sites mineral solids accounted for 1–3.3 times the theoretical inventory. At four sites (DN-2, MR-3, CC-1, and CC-2) the theoretical

inventory can be explained by mineral or organic soil-fractions. These results demonstrate that both organic and mineral solids contribute to burial of $^{210}\text{Pb}_u$.

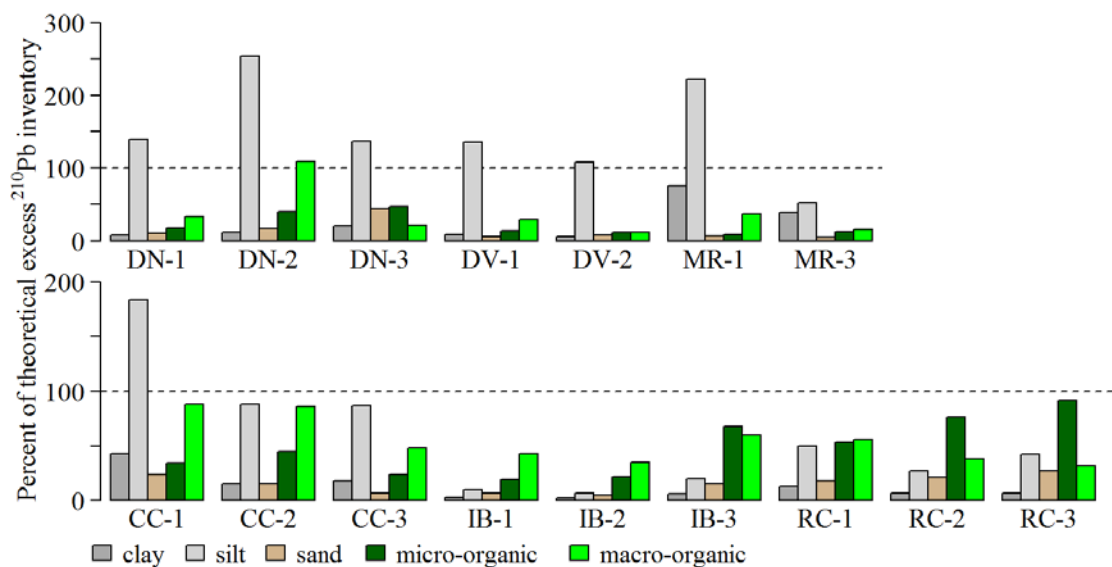


Figure 4.11: The theoretical excess ^{210}Pb inventory that could be explained by the clay, silt, sand, micro-organic, and macro-organic soil size fractions. The theoretical inventory (Figure 4.10) was calculated based on atmospheric flux of ^{210}Pb ($165 \text{ Bq m}^{-2} \text{ y}^{-1}$) and soil layer (0–6 cm) age (Table 4.1). Note the different scales for the top row, sites from marshes in Delaware Bay, and the bottom row, sites from marshes in Barnegat Bay.

Regression analysis revealed a direct relationship between specific activities of the organic fraction of soil and aboveground biomass (Figure 4.12), and similar direct relationship ($r^2=0.72$, $p<0.05$) was found between the aboveground and soil inventories associated with organic solids (Bq m^{-2}). Although these results do not convey process per se, they suggest that the aboveground biomass factors into the capture and burial of $^{210}\text{Pb}_u$.

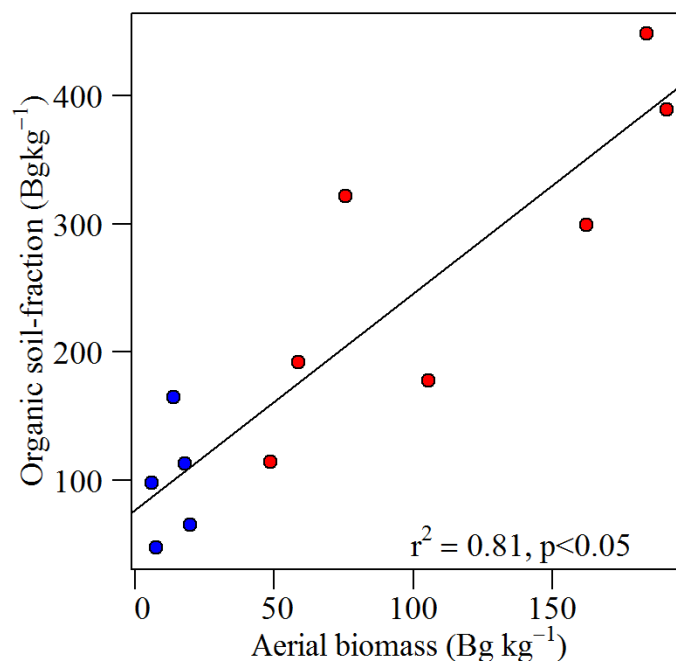


Figure 4:12: Regression of the excess ^{210}Pb activities of the organic soil-fraction (sand + macro- + micro-organic) and total aboveground biomass (standing + litter). Data from Delaware Bay is shown in blue and from Barnegat Bay in red. The positive direct relationship suggests that the activity of the plant biomass aboveground has some influence on the activity of organic matter belowground, possibly through burial of decomposed leaf and stem litter.

In summary, it appears that when mineral sediment is a large component of marsh soil, such as in Delaware Bay marshes, it accounts for the majority of the $^{210}\text{Pb}_u$ inventory (Figures 4.3 and 4.6). In this case the $^{210}\text{Pb}_u$ inventory tends to be larger than the expected value because of sediment focusing, i.e., delivery of ^{210}Pb to the marsh by sediment transport (Figure 4.10). In contrast, in organic-rich marsh soils of Barnegat Bay the majority of the $^{210}\text{Pb}_u$ inventory is associated with organic particles, at least some of which originated as aboveground biomass (Figure 4.6). While the association of $^{210}\text{Pb}_u$ with mineral sediment is not surprising given the affinity of ^{210}Pb

for fine-grained silt and clay, the large fraction of $^{210}\text{Pb}_u$ associated with organic matter was not expected (Figure 4.6). This finding demonstrates that organic matter can be a more important vector of $^{210}\text{Pb}_u$ burial in some marsh soils. As such the hypothesis that mineral sediment will contribute the majority of the $^{210}\text{Pb}_u$ activity to the soil inventory can be rejected.

4.5 Discussion

4.5.1 Plant capture and burial of excess ^{210}Pb in marsh soils

The association of belowground $^{210}\text{Pb}_u$ with soil organics could be the result of trapping by the canopy and subsequent burial or direct deposition onto aerial or exposed roots on the marsh surface. Excess ^{210}Pb was found on both the living and dead aboveground biomass (Table 4.2), making burial of aeri ally trapped fallout a possible mechanism. While not a usual component of radionuclide studies in marshes, aboveground biomass is capable of capturing fallout (Olsen et al., 1985; Olid et al., 2008; Krmar et al., 2014). Aboveground inventories measured by Olsen et al., (1985) on marsh grass collected in the Delaware ($22\pm 11 \text{ Bq m}^{-2}$) and Chesapeake ($33\pm 11 \text{ Bq m}^{-2}$) estuaries were similar to those measured here (Table 4.2). In this study, the aboveground inventories explained 1–87% of the annual atmospheric flux (165 Bq m^{-2}), so it seems that the efficiency of trapping by the marsh canopy is variable. Even so, the positive relationship between and the activity of aboveground biomass and soil organics leads to the assumption that there is some relationship between above and belowground inventories (Figure 4.12). Additionally, the similar $^{210}\text{Pb}_u$ activities of litter and soil organics suggest that litter could be contributing to the soil inventory but

the higher activities of soil organics suggest that some post-depositional process is increasing $^{210}\text{Pb}_u$ of organic solids (Figure 4.9).

Based on the strong particle association that has been observed for ^{210}Pb (Santschi et al., 1983), it is assumed that aboveground $^{210}\text{Pb}_u$ is a direct result of plant capture of atmospheric fallout. The biomass samples in question were rinsed of mineral material, so it would seem the ^{210}Pb is either absorbed into the tissue or adsorbed on the plant surface. The higher activities associated with dead biomass, with its longer time of atmospheric exposure could indicate that physical trapping and not biological incorporation is the predominant mechanism of ^{210}Pb sequestration. Landis et al. (2014) found that atmospherically deposited ^{210}Pb was permanently retained by the leaves of deciduous and coniferous vegetation, thus linking the cycling of ^{210}Pb and leaf matter.

The notion that the marsh canopy traps atmospheric ^{210}Pb is intuitive, but what is not immediately clear is how leaf- and stem-associated ^{210}Pb enters the soil and contributes to the belowground inventory. If the canopy excluded fallout from the inventory, an inverse relationship between canopy and biomass $^{210}\text{Pb}_u$ inventories would be expected, but this was not observed in this study (Figure 4.12). For *Spartina* saltmarshes, it is generally assumed that most of the organic matter retained in soils originates from belowground production of roots and rhizomes, because aboveground litter fall decomposes rapidly and thus is poorly preserved (Valiela et al., 1985). One explanation is that the aboveground inventory of ^{210}Pb is buried with a refractory component of the litter after decomposition or disaggregation by microbes or benthic organisms. This process would also concentrate of $^{210}\text{Pb}_u$ activity by reducing plant

mass, and could explain why the $^{210}\text{Pb}_u$ specific associated with soil organic matter is higher than that of the aboveground biomass (Figure 4.12).

Since the aboveground and belowground pools of $^{210}\text{Pb}_u$ are indistinguishable, tracing the possible burial pathways of $^{210}\text{Pb}_u$ associated with dead biomass is complex. Nonetheless, it is important to make the distinction between direct and indirect organic burial of radionuclides. The aboveground $^{210}\text{Pb}_u$ activities described here are due to direct adherence to, or possibly absorbed by, the plant. Additionally, based on the mineral sediment activities measured, it is reasonable to assume that mineral mass associated with aboveground structures would have some inherent radionuclide activity. Church et al. (1986), working in a Delaware salt marsh, found ^{210}Pb activities of $17.8 \pm 0.7 \text{ Bq kg}^{-1}$ in the solids trapped on *S. alterniflora* stems, which amounted to less than half of the $^{210}\text{Pb}_u$ found on any soil fraction in this study. If this trapped material is organically buried, it would represent an indirect organic control on the formation of marsh radionuclide inventories. Additionally, the standing stems may reduce flow velocity (Nepf, 1999), leading to lower rates of resuspension and higher rates of particle deposition (Yang et al., 2008). This effect could lead to the enrichment of the inventory by trapping of $^{210}\text{Pb}_u$ laden-particles as well as protection of inventory loss due to erosion of particles.

4.5.2 Implications to marsh geochronology

A common practice in radionuclide geochronology is normalize activities to clay and silt size fractions to remove the mass contributed by quartz grains (e.g., McCraith et al. 2003), which contributes mass to the sample but little to no radionuclide activity. However, normalizing activities to the clay and silt fraction would overestimate activities if radionuclides were absorbed to organic soils. Physical

separation of mineral fractions from the bulk soil for analysis would also remove roots and some organic particles. Results of this study indicate that soil-fractional contributions to the total radionuclide inventory must be taken into account when attempting to relate soil inventories to atmospheric and tidal fluxes of radionuclides.

4.5.3 Methodological and analytical considerations

Results of ultra-low background gamma spectroscopy applied in this study demonstrates the ability to analyze marsh soil radioactivity associated with different soil pools, and there are several methodological considerations offer. The amount of sample material presented to the detector to acquire significant counts is fundamental. This includes both collection of adequate sample mass and reduction of that mass to the smallest volume possible for analysis. Milling of aboveground and soil organic material provided uniform sample densities and resulted in significant counts. The uncertainties in the resulting counts might be reduced by concentrating radionuclide activity in organic samples through ashing or chemical digestion. Larger sample masses would have provided more clay and sand-sized fraction masses, which were generally lower than the mass of silt, and possibly have reduced the associated gamma counting uncertainties. These considerations are specific to the radionuclide and soil composition and should be addressed using material collected during field reconnaissance, if possible.

4.6 Conclusions

Results of this study indicate that organic matter and mineral sediment are of equal importance in the sequestration of $^{210}\text{Pb}_u$ and ^{137}Cs in salt marsh soils, depending on the type of marsh and the composition of its soils. The marsh canopy, aboveground

biomass in the form of standing stems and leaves, captured atmospheric $^{210}\text{Pb}_u$ deposition at specific activities of 0–15 Bq kg⁻¹. Litter had higher $^{210}\text{Pb}_u$ activity than the canopy and therefore despite its lower mass, was responsible for as much as 65 times the inventory provided by the canopy. Low activities of ^{137}Cs were detected in five aboveground biomass samples possibly due to trapping of particle-borne ^{137}Cs or biological uptake from soils. In mineral-rich marsh soils, the majority of $^{210}\text{Pb}_u$ and ^{137}Cs activity present was associated with mineral solids, though soil organic matter can have similar or even higher specific activities than the mineral sediment. In organic-rich soils, the belowground radionuclide inventory was mostly associated with organic solids. Radionuclide activities of aboveground biomass and soil organic solids were directly related, which suggests (but does not identify) a mechanism of plant-mediated burial of radionuclides. Based on the available data, it is possible that the aboveground inventory of ^{210}Pb is buried with a refractory component of the litter after mechanical breakdown and decomposition. This process would also effectively concentrate $^{210}\text{Pb}_u$ activity in the soil by reducing plant mass. Additional work is required to fully elucidate capture and burial of radionuclides in salt marsh soils, as it will contribute to our understanding of the fate of radionuclides discharged to estuaries by wastewater treatment facilities and nuclear power plants.

REFERENCES

- Arvik, J.H., Zimdahl, R.L., 1974. Barriers to the foliar uptake of lead. *J. Environ. Qual.* 3, 369. doi:10.2134/jeq1974.00472425000300040015x
- Aston, S., Duursma, E., 1973. Concentration effects on ^{137}Cs , ^{65}Zn , ^{60}Co and ^{106}Ru sorption by marine sediments, with geochemical implications. *Netherlands J. Sea Res.* 6, 225–240. doi:10.1016/0077-7579(73)90015-X
- Atun, G., Bilgin, B., Mardinli, A., 1996. Sorption of cesium on montmorillonite and effects of salt concentration. *J. Radioanal. Nucl. Chem. Artic.* 211, 435–442. doi:10.1007/BF02039709
- Baskaran, M., Coleman, C.H. and Santschi, P.H., 1993. Atmospheric depositional fluxes of ^7Be and ^{210}Pb at Galveston and College Station, Texas. *J. Geophys. Res. Atmos.* 98(D11): 20555-20571. doi:10.1029/93JD02182
- Bennett, R.H., Lambert, D.N., 1971. Rapid and reliable technique for determining unit weight and porosity of deep-sea sediments. *Mar. Geol.* 11, 201–207. doi:10.1016/0025-3227(71)90007-7
- Benninger, L.K., 1978. ^{210}Pb balance in Long Island Sound. *Geochim. Cosmochim. Acta* 42, 1165–1174. doi:10.1016/0016-7037(78)90111-4
- Benninger, L.K., Lewis, D.M., Turekian, K.K., 1975. The use of natural Pb-210 as a heavy metal tracer in the river-estuarine system, in: Church, T.M. (Ed.), *Marine Chemistry in the Coastal Environment*. American Chemical Society, pp. 202–210. doi:10.1021/bk-1975-0018.ch012
- Church, T.M., Bernat, M., Sharma, P., 1986. Distribution of natural uranium, thorium, lead, and polonium radionuclides in tidal phases of a Delaware salt marsh. *Estuaries* 9, 2–8. doi:10.2307/1352187
- Comans, R.N.J., Hockley, D.E., 1992. Kinetics of cesium sorption on illite. *Geochim. Cosmochim. Acta* 56, 1157–1164. doi:10.1016/0016-7037(92)90053-L

- Cundy, A.B., Croudace, I.W., Thomson, J., Lewis, J.T., 1997. Reliability of salt marshes as “geochemical recorders” of pollution Input: a case study from contrasting estuaries in Southern England. *Environ. Sci. Technol.* 31, 1093–1101. doi:10.1021/es960622d
- Dahlman, R.C., Francis, C.W., Tamura, T., 1975. Radiocesium cycling in vegetation and soil, in: Howell, F.G., Gentry, J.E., Smith, M.H. (Eds.), *Mineral Cycling in Southeastern Ecosystems*. ERDA Symposium Series. (CONF-740513), pp. 462–481.
- Davis, J.J., 1963. Cesium and its relationship to potassium in ecology, in: Schultz, V., Klement, A. (Eds.), *Radioecology*. Reinhold, New York, pp. 539–556.
- DeLaune, R., Reddy, C.N., Patrick Jr., W., 1981. Accumulation of plant nutrients and heavy metals through sedimentation processes and accretion in a Louisiana salt marsh. *Estuaries* 4, 328. doi:10.2307/1352157
- DeLaune, R.D., Patrick Jr., W.H., Buresh, R.J., 1978. Sedimentation rates determined by ^{137}Cs dating in a rapidly accreting salt marsh. *Nature* 275, 532–533. doi:doi:10.1038/275532a0
- Delvaux, B., Kruyts, N., Cremers, A., 2000. Rhizospheric mobilization of radiocesium in soils. *Environ. Sci. Technol.* 34, 1489–1493. doi:10.1021/es990658g
- Genrich, D.A., Bremner, J.M., 1974. Isolation of soil particle-size fractions. *Soil Sci. Soc. Am. J.* 38, 222–225. doi:10.2136/sssaj1974.03615995003800020009x
- Graustein, W.C., Turekian, K.K., 1986. ^{210}Pb and ^{137}Cs in air and soils measure the rate and vertical profile of aerosol scavenging. *J. Geophys. Res.* 91, 14355–143369. doi:10.1029/JD091iD13p14355
- He, Q., Walling, D., 1996. Interpreting particle size effects in the adsorption of ^{137}Cs and unsupported ^{210}Pb by mineral soils and sediments. *J. Environ. Radioact.* 30, 117–137. doi:10.1016/0265-931X(96)89275-7
- Johnson-Pyrtle, A., Scott, M.R., 2001. Distribution of ^{137}Cs in the Lena River Estuary–Laptev Sea System. *Mar. Pollut. Bull.* 42, 912–926. doi:10.1016/S0025-326X(00)00237-X
- Kim, G., Alleman, L., Church, T., 2004. Accumulation records of radionuclides and trace metals in two contrasting Delaware salt marshes. *Mar. Chem.* 87, 87–96. doi:10.1016/j.marchem.2004.02.002

- Kim, G., Hussain, N., Scudlark, J.R., Church, T.M., 2000. Factors influencing the atmospheric depositional fluxes of stable Pb, ^{210}Pb , and ^7Be into Chesapeake Bay. *J. Atmos. Chem.* 36, 65–79. doi:10.1023/A:1006383030362
- Krishnaswami, S., Graustein, W.C., Turekian, K.K., Dowd, J.F., 1982. Radium, thorium and radioactive lead isotopes in groundwaters: application to the in situ determination of adsorption-desorption rate constants and retardation factors. *Water Resour. Res.* 18, 1663–1675. doi:10.1029/WR018i006p01663
- Krmar, M., Radnović, D., Hansman, J., 2014. Correlation of unsupported ^{210}Pb activity in soil and moss. *J. Environ. Radioact.* 129, 23–26. doi:10.1016/j.jenvrad.2013.11.009
- Landis, J., Renshaw, C., Kaste, J., 2014. Quantitative retention of atmospherically-deposited elements by native vegetation is traced by the fallout radionuclides ^7Be and ^{210}Pb . *Environ. Sci. Technol.* 48, 12022–12030.
- Livens, F.R., Baxter, M.S., 1988a. Chemical associations of artificial radionuclides in Cumbrian soils. *J. Environ. Radioact.* 7, 75–86. doi:10.1016/0265-931X(88)90043-4
- Livens, F.R., Baxter, M.S., 1988b. Particle size and radionuclide levels in some west Cumbrian soils. *Sci. Total Environ.* 70, 1–17. doi:10.1016/0048-9697(88)90248-3
- Marsan, D., Rigaud, S., Church, T., 2014. Natural radionuclides ^{210}Po and ^{210}Pb in the Delaware and Chesapeake Estuaries: modeling scavenging rates and residence times. *J. Environ. Radioact.* 138C, 447–455. doi:10.1016/j.jenvrad.2014.08.014
- McCaffrey, R.J., Thomson, J., 1980. A record of the accumulation of sediment and trace metals in a Connecticut salt marsh, in: Saltzman, B. (Ed.), *Advances in Geophysics*. Academic Press, New York, pp. 165–236.
- McCraith, B.J., Gardner, L.R., Wethey, D.S., Moore, W.S., 2003. The effect of fiddler crab burrowing on sediment mixing and radionuclide profiles along a topographic gradient in a southeastern salt marsh. *J. Mar. Res.* 61, 359–390. doi:10.1357/002224003322201232
- Nepf, H.M., 1999. Drag, turbulence, and diffusion in flow through emergent vegetation. *Water Resour. Res.* 35, 479–489. doi:10.1029/1998WR900069

- Oldfield, F., Appleby, P.G., Cambray, R.S., Eakins, J.D., Barber, K.E., Battarbee, R.W., Pearson, G.R., Williams, J.M., 1979. ^{210}Pb , ^{137}Cs and ^{239}Pu profiles in ombrotrophic peat. *Oikos* 33, 40–45. doi:10.2307/3544509
- Olid, C., Garcia-Orellana, J., Martínez-Cortizas, A., Masqué, P., Peiteado, E., Sanchez-Cabeza, J.-A., 2008. Role of surface vegetation in ^{210}Pb -dating of peat cores. *Environ. Sci. Technol.* 42, 8858–8864. doi:10.1021/es801552v
- Olsen, C.R., Larsen, I.L., Lowry, P.D., Cutshall, N.H., Todd, J.F., Wong, G.T.F., Casey, W.H., 1985. Atmospheric fluxes and marsh-soil inventories of ^7Be and ^{210}Pb . *J. Geophys. Res.* 90, 10487–10495. doi:10.1029/JD090iD06p10487
- Peterson, P.J., 1978. Lead and vegetation, in: Nriagu, J. (Ed.), *The Biogeochemistry Of Lead In The Environment. Part B Biological Effects*. Elsevier/North-Holland Biomedical Press, Amsterdam, p. 384.
- Pietrzak-Flis, Z., Skowrońska-Smolak, M., 1995. Transfer of ^{210}Pb and ^{210}Po to plants via root system and above-ground interception. *Sci. Total Environ.* 162, 139–147. doi:10.1016/0048-9697(95)04445-7
- Rama, Koide, M., Goldberg, E.D., 1961. Lead-210 in natural waters. *Science*. 134, 98–99. doi:10.1126/science.134.3472.98
- Ritchie, J.C., McHenry, J.R., 1990. Application of radioactive fallout cesium-137 for measuring soil erosion and sediment accumulation rates and patterns: a review. *J. Environ. Qual.* 19, 215. doi:10.2134/jeq1990.00472425001900020006x
- Robbins, J.A., 1978. Geochemical and geophysical applications of radioactive lead, in: Nriagu, J.O. (Ed.), *The Biogeochemistry of Lead in the Environment*. Elsevier, Amsterdam, pp. 285–393.
- Rogowski, A., Tamura, T., 1970. Environmental mobility of cesium-137. *Radiat. Bot.* I, 35–45. doi:10.1016/S0033-7560(70)80050-3
- Santschi, P.H., Li, Y.-H., Adler, D.M., Amdurer, M., Bell, J., Nyffeler, U.P., 1983. The relative mobility of natural (Th, Pb and Po) and fallout (Pu, Am, Cs) radionuclides in the coastal marine environment: results from model ecosystems (MERL) and Narragansett Bay. *Geochim. Cosmochim. Acta* 47, 201–210. doi:10.1016/0016-7037(83)90133-3
- Shand, C.A., Cheshire, M.V., Smith, S., Vidal, M., Rauret, G., 1994. Distribution of radiocaesium in organic soils. *J. Environ. Radioact.* 23, 285–302. doi:10.1016/0265-931X(94)90067-1

- Sugai, S.F., Alperin, M.J., Reeburgh, W.S., 1994. Episodic deposition and ^{137}Cs immobility in Skan Bay sediments: a ten-year ^{210}Pb and ^{137}Cs time series. *Mar. Geol.* 116, 351–372. doi:10.1016/0025-3227(94)90051-5
- Sundby, B., Caetano, M., Vale, C., Gobeil, C., Luther, G.W., Nuzzio, D.B., 2005. Root-induced cycling of lead in salt marsh sediments. *Environ. Sci. Technol.* 39, 2080–2086. doi:10.1021/es048749n
- Thomson, J., Dyer, F.M., Croudace, I.W., 2002. Records of radionuclide deposition in two salt marshes in the United Kingdom with contrasting redox and accumulation conditions. *Geochim. Cosmochim. Acta* 66, 1011–1023. doi:10.1016/S0016-7037(01)00825-0
- Tucker, K.J., 2016. Variability of organic carbon accumulation on a tidal wetland coast. M.S. thesis. University of Delaware.
- Turekian, K.K., Benninger, L.K., Dion, E.P., 1983. ^7Be and ^{210}Pb total deposition fluxes at New Haven, Connecticut and at Bermuda. *J. Geophys. Res.* 88, 5411. doi:10.1029/JC088iC09p05411
- Unger, V., Elsey-Quirk, T., Sommerfield, C.K., and Velinsky, D.J. Stability of organic carbon accumulating in *Spartina alterniflora*-dominated salt marshes of the Mid-Atlantic U.S. Manuscript in review.
- Valiela, I., Teal, J.M., Allen, S.D., Van Etten, R., Goehring, D., Volkmann, S., 1985. Decomposition in salt marsh ecosystems: the phases and major factors affecting disappearance of above-ground organic matter. *J. Exp. Mar. Bio. Ecol.* 89, 29–54. doi:10.1016/0022-0981(85)90080-2
- Yamasaki, S., Imoto, J., Furuki, G., Ochiai, A., Ohnuki, T., Sueki, K., Nanba, K., Ewing, R.C., Utsunomiya, S., 2016. Radioactive Cs in the estuary sediments near Fukushima Daiichi Nuclear Power Plant. *Sci. Total Environ.* 551-552, 155–162. doi:10.1016/j.scitotenv.2016.01.155
- Yang, S.L., Li, H., Ysebaert, T., Bouma, T.J., Zhang, W.X., Wang, Y.Y., Li, P., Li, M., Ding, P.X., 2008. Spatial and temporal variations in sediment grain size in tidal wetlands, Yangtze Delta: on the role of physical and biotic controls. *Estuar. Coast. Shelf Sci.* 77, 657–671. doi:10.1016/j.ecss.2007.10.024
- Zimdahl, R.L., 1976. Entry and movement in vegetation of lead derived from air and soil sources. *J. Air Pollut. Control Assoc.* 26, 655–660. doi:10.1080/00022470.1976.10470298

Chapter 5

POTENTIAL USE OF ^{241}Am AS A SEDIMENT CHRONOMETER IN NORTH AMERICAN TIDAL MARSHES

5.1 Abstract

In this chapter use of the radionuclide Americium-241 (^{241}Am) as geochronometer in tidal wetlands is examined. The study was motivated by the knowledge that ^{137}Cs concentrations currently sequestered in wetland sediments and soils will decay to extinction during the next century. At the same time, ingrowth of ^{241}Am from decay of fallout ^{241}Pu will yield maximum inventories in 2036, and its 432-yr half-life ensures that it will remain detectable for centuries. Measurements of ^{241}Am in soils from tidal marshes in Delaware Bay and Barnegat Bay were made to assess variations in ^{241}Am activity across a range of estuarine and coastal marsh types. Activities of ^{241}Am were similar in mineral- and organic-rich soils indicating that soil composition did not appear to influence the initial capture of ^{241}Pu or retention of its ^{241}Am daughter. Depth profiles of ^{241}Am broadly mirrored those of ^{137}Cs , indicating that the input function of ^{241}Pu fallout and ^{241}Am ingrowth was not disturbed by transport between wetland waterways and the marsh surface. Moreover, given that ^{241}Am has a significantly greater affinity for particles than ^{137}Cs , the concordance of ^{137}Cs and ^{241}Am profiles indicates that ^{137}Cs has not experienced significant post-depositional chemical mobility. The findings of this study suggest that ^{241}Am has great potential as a particle tracer and geochronometer in tidal wetland systems.

5.2 Introduction

5.2.1 Motivation

During a study of sediment accumulation in U.S. Mid-Atlantic salt marshes (Chapter 2), Americium-241 (^{241}Am) was detected in samples analyzed for ^{210}Pb and ^{137}Cs activity by standard gamma spectroscopy. Knowing that ^{241}Am activity concentrations in the environment will increase due to ingrowth from decay of ^{241}Pu , a product of 1952-1963 nuclear weapons testing and atmospheric fallout, ^{241}Am sources and its potential use as geochronometer in tidal marshes were investigated. This chapter describes a study in which down-core activities of ^{241}Am in salt marsh soils were compared to those of ^{137}Cs , another fallout radionuclide deposited during the nuclear weapons testing era. Results indicated that decay of ^{241}Pu can explain the presence of ^{241}Am in the soils, and that activities are suitable for chronometry with acceptable confidence limits. Given that fallout ^{137}Cs will decay to below detection limits within the next century, ^{241}Am has potential to serve as a replacement chronometer given its high affinity for sedimentary particles, long half-life, and convenient measurement by gamma spectroscopy.

5.2.2 Sources of ^{241}Am in the environment

The artificial radionuclide ^{241}Am ($t_{1/2}=432.2$ y) is a transuranic element produced by decay of ^{241}Pu ($t_{1/2}=14.4$ y). Decay of ^{241}Am occurs primarily through alpha emission at 5.486 MeV (yield 85%) followed by a weak gamma emission at 59.5 keV (yield 36%), which allows it to be detected via alpha (destructive) as well as gamma (nondestructive) spectroscopy. While virtually no ^{241}Am is produced in the ^{238}U fission reaction, it later ingrows via decay of deposited ^{241}Pu . Because most of the ^{241}Pu present in the environment is a consequence of global fallout following Northern

Hemisphere thermonuclear atmospheric weapons testing (AWT), virtually all ^{241}Am in the environment was produced by AWT fallout, although there can be local sources from nuclear power plant releases and fuel reprocessing facilities. The source function of ^{241}Pu in the environment parallels that of the more abundant ^{137}Cs , thus with time and ingrowth in sediments and soils ^{241}Am has potential to provide absolute age markers concordant with the first occurrence (1952-1954) and peak (1963-1964) of AWT fallout.

Americum-241 is largely immobile in soils and sediments, more so than other radionuclides like ^{137}Cs . In soils, ^{241}Am adsorbs to clays and organic matter (Kazinskaya et al., 2012; Lujanienė et al., 2012), and soil-to-root transfer rates are low (Kozhakhanov et al., 2014). The partitioning coefficient, also known as the distribution coefficient, (K_d) can be used to compare the particle reactivity (or immobility) of radionuclides adsorbed to particles and is calculated as the ratio of radionuclide concentration of solids (Bq kg^{-1}) to radionuclide dissolved in solution (Bq L^{-1}). In the Irish Sea, K_d values determined using natural sediment were 10^3 , 10^4 – 10^6 , and 10^6 for Cs, Pu, and Am (Kershaw et al., 1992 and references therein). Similarly, in mesocosm experiments Santschi et al. (1983) found that ^{241}Am was more particle reactive than ^{236}Pu , ^{210}Pb , and ^{137}Cs and concluded that the chemical mobility of these radionuclides is as follows: $^{241}\text{Am} < ^{236}\text{Pu} < ^{210}\text{Pb} < ^{137}\text{Cs}$.

As detailed in Chapter 3, the most commonly used fallout radionuclide for geochronometry of soils and sediments is ^{137}Cs ($t_{1/2}=30.2$ y). Fallout ^{137}Cs was delivered to Earth's surface in relatively large amounts, thus despite its relatively short half-life it has been abundant in sediments and soils since the time of peak fallout in 1963-1964. The main disadvantage of ^{137}Cs as a particle tracer and chronometer is its

relatively low particle affinity in brackish and salt water, and chemical mobility in soils and sedimentary deposits (Dahlman et al., 1975; Delvaux et al., 2000; Johnson-Pyrtle and Scott 2001). This mobility can complicate identification of the depth of ^{137}Cs first occurrence in the sediment column (Leslie and Hancock, 2008). Both ^{241}Pu and ^{241}Am are considerably more particle reactive and thus less chemically mobile than ^{137}Cs , measurements of ^{241}Am can be used to validate ^{137}Cs and ^{210}Pb geochronologies (Appleby et al., 1991; Dyer et al., 2002; Olid et al., 2008; Olid et al., 2016).

5.2.3 ^{241}Am as a particle tracer and chronometer

Fallout ^{241}Am has been detected in a broad range of aquatic environments including lakes (Appleby et al., 1991), coastal waters (Koide et al., 1981) oceanic waters (Fowler et al., 1983; Cochran et al., 1987), continental margin sediments (Koide et al., 1980; Beasley et al., 1982; Koide and Goldberg, 1982; Carpenter et al., 1987), and tidal marsh soils and sediments (Dyer et al., 2002; Olid et al., 2008, Olid et al., 2016). Early work with ^{241}Am focused on its use as a tracer of atmosphere-ocean exchange and physiochemical processes. For example, studies on the North American Pacific shelf and slope have used ^{241}Am to determine rates of scavenging and to relate changes in nuclide inventories and ratios to patterns of AWT (Beasley et al., 1982; Carpenter et al., 1987). Fallout ^{241}Am has not been widely used as a geochronometer, partly because the activity of ^{241}Pu in fallout was relatively small, ~17% that of ^{137}Cs (Appleby et al., 1991), and because time was required for ingrowth to detectable levels in soils and sediments. Near the Nevada Test Site (where AWT took place), Appleby et al. (1991) detected ^{241}Am activities in lake-bottom sediments with depth profiles that mirrored the atmospheric source function preserved by down-core ^{137}Cs activities.

Peat marshes in Europe have been shown to preserve AWT-sourced ^{241}Am , and the radionuclide has been often used to verify ^{210}Pb age-dates (Olid et al., 2016). Additionally, ^{241}Am geochronometry has been performed in estuarine environments where ^{241}Pu and ^{241}Am releases from nuclear fuel reprocessing plants (Sellafield, UK) and power plants (Chernobyl) provided sufficient activity for detection (Thomson et al., 2002). However, ^{241}Am geochronometry has not been widely employed in estuarine and tidal wetland environments.

5.3 Methods

5.3.1 Measurement of radionuclides and soil physical properties

Eighteen marsh sediment cores from tidal marshes in Delaware Bay and Barnegat Bay were collected and vertically subsampled into 2-cm layers, to measure rates of marsh accumulation and accretion via ^{210}Pb and ^{137}Cs chronometry (Chapter 2). As described in Chapter 2, loss-on-ignition (LOI) and gravimetric methods were used to determine the mass of organic and mineral solids in the soils. Samples were gamma counted for 24 h using Canberra Low Energy Germanium (LEGe) detectors affixed with low-background components (Canberra Model GL2020R). Photopeak counts, as shown in Figure 5.1, at 59.5 keV (^{241}Am) and 661.6 keV (^{137}Cs) were converted to activities after calibrating the detectors using a natural-matrix standard (National Institute of Standards and Technology Ocean Sediment, SRM 4357) with certified (^{137}Cs) and uncertified (^{241}Am) activities. Because the soil samples were counted in a geometry identical to that of the standard (60-ml jar), a matrix self-adsorption correction for ^{241}Am , a low-energy radionuclide like ^{210}Pb (46.5 keV), was not required. Activity errors were calculated as the 1σ counting error. For the detector

system and sample geometry used in this study, the theoretical minimum detectable activity (MDA) for ^{137}Cs and ^{241}Am were 0.09 ± 0.02 and 0.02 ± 0.01 Bq, respectively.

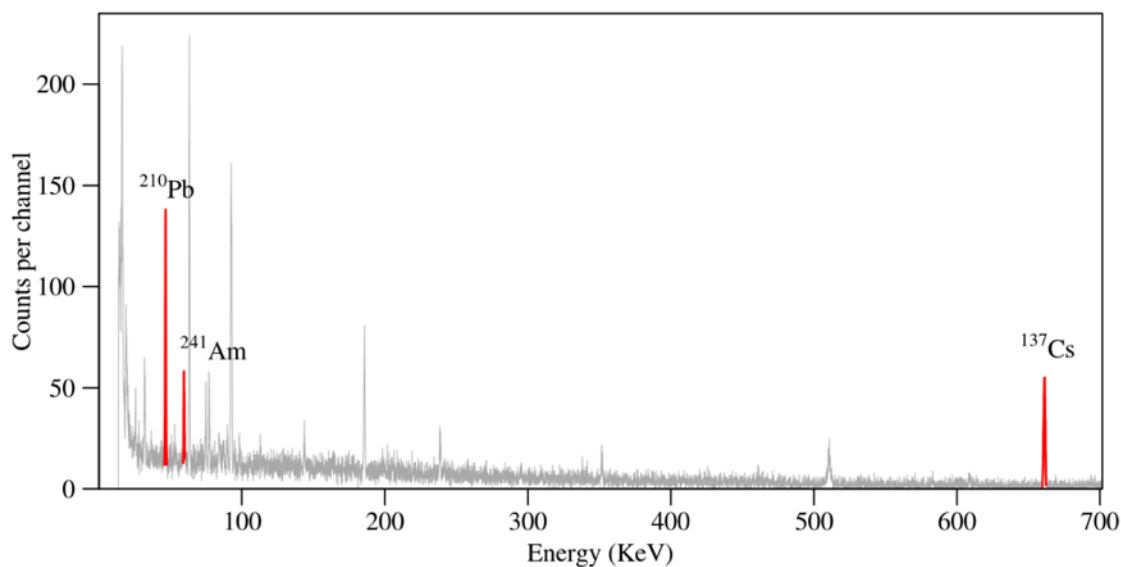


Figure 5.1: Energy spectrum showing gamma photopeaks generated from a sediment sample from core RC-3 at 14-16 cm depth. Photopeaks produced by ^{210}Pb , ^{241}Am , and ^{137}Cs are shown in red.

5.3.2 Fallout and theoretical ^{241}Am inventory

To estimate steady-state soil inventories of ^{137}Cs , ^{241}Pu , and ^{241}Am from AWT fallout, ground-level fallout measurements of Strontium-90 (^{90}Sr) at New York, New York available from the Environmental Measurements Laboratory were accessed (EML, 1999). This was necessary because fallout records of ^{137}Cs and ^{241}Pu are not available for the U.S. Mid-Atlantic region. Atmospheric fluxes of ^{137}Cs and ^{241}Pu were based on the ratios measured in nuclear debris for $^{137}\text{Cs}:^{90}\text{Sr}$ (1.45; Harley et al., 1965 as cited in Bowen et al., 1974) and $^{241}\text{Pu}:^{137}\text{Cs}$ (0.177; Appleby et al., 1991). The theoretical inventories of ^{137}Cs and ^{241}Pu were based on the atmospheric flux and

radionuclide decay. The theoretical ^{241}Am inventory was based on ingrowth from ^{241}Pu decay and decay of ^{241}Am itself. These estimated inventories assume complete capture, burial, and retention of fallout in the soil with no horizontal focusing by atmospheric or ground-level transport processes. There are no known non-fallout sources of ^{241}Pu , ^{241}Am , or ^{137}Cs in the study area, thus AWT deposition should be the sole source for these radionuclides. In general, the soil inventory (I ; Bq m^{-2}) of an atmospherically derived radionuclide is related to the deposition rate (P ; $\text{Bq m}^{-2} \text{y}^{-1}$) by its decay constant ($\lambda = \ln(2)/\text{half-life}$; 0.0229 y^{-1} for ^{137}Cs). In the case of ^{137}Cs , this relationship is as follows:

$$P = \lambda_{137\text{Cs}} \times I_{137\text{Cs}} \quad (5.1)$$

5.4 Results

5.4.1 Activities and profiles of ^{241}Am and ^{137}Cs

Among the eighteen soil cores, ^{241}Am was present above detection limits in 83 of 485 core subsamples. By comparison, ^{137}Cs was detected in 417 of the 485 subsamples. Activities of ^{241}Am and ^{137}Cs were directly correlated, albeit weakly (Figure 5.2), which supports an AWT fallout source for ^{241}Am . A peak in ^{137}Cs activity corresponding to 1963-1964 AWT was identified in seventeen of the eighteen cores, and of these nine had a discernable ^{241}Am peak composed of at least three depth intervals with activities above detection.

Down-core profiles of ^{137}Cs and ^{241}Am activity for four of the nine cores with ^{241}Am peaks, two from Delaware Bay and two from Barnegat Bay, are shown in Figure 5.3. Activities of ^{137}Cs were roughly twenty times greater than ^{241}Am due to the larger production of ^{137}Cs compared to the ^{241}Am parent, ^{241}Pu , and slow ingrowth of

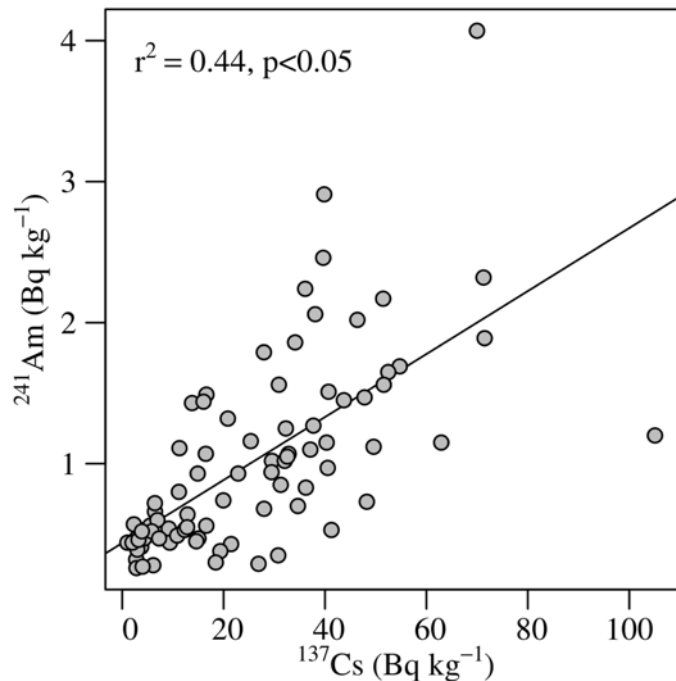


Figure 5.2: Scatterplot of ^{241}Am and ^{137}Cs activities ($n = 83$) measured in 2-cm depth intervals from eighteen marsh cores collected in marshes located in the Delaware and Barnegat bays. The direct relationship, higher ^{241}Am activity associated with higher ^{137}Cs activity, suggests that these radionuclides have a similar input function, likely Northern Hemisphere atmospheric weapons testing fallout.

^{241}Am from ^{241}Pu decay. As shown in the Figure 5.3, ^{241}Am peaks were concordant with ^{137}Cs peak. In addition to ^{241}Am and ^{137}Cs peak agreement, the shapes of the radionuclide profiles were in broad agreement. In the Delaware Bay marsh cores, ^{241}Am was present in the near surface in layers with ^{137}Cs dates corresponding to the years 2006 and 2008, well after AWT fallout ceased (Figure 5.3). Soil inventories calculated by integration of the ^{241}Am profiles were 51 ± 17 , 16 ± 3 , 24 ± 6 , and 22 ± 5 Bq m^{-2} for DN-2, DV-3, IB-2, and RC-3, respectively. As determined in Chapter 2, the

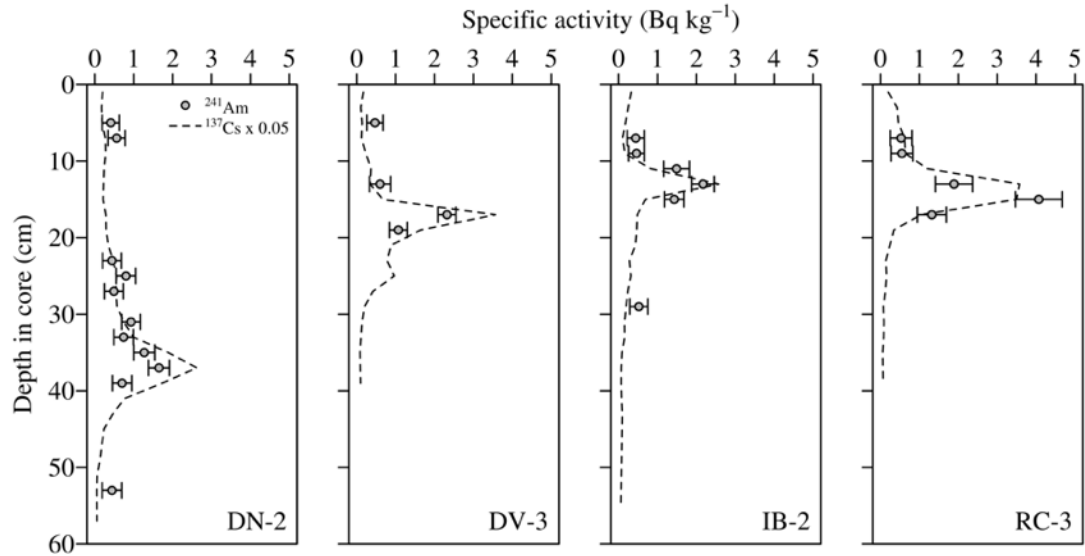


Figure 5.3: Depth profiles of ^{137}Cs and ^{241}Am activity measured in marsh cores from the Delaware (DN-2 and DV-3) and Barnegat (IB-2 and RC-3) bay estuaries. The depth of the ^{137}Cs and ^{241}Am activity peaks is attributed to the 1963-1964 maximum fallout of Northern Hemisphere atmospheric weapons testing. Note different scales for ^{137}Cs and ^{241}Am .

organic content (% dry mass) of these cores was 26 ± 3 , 52 ± 6 , 38 ± 16 , and 45 ± 16 for DN-2, DV-3, IB-2, and RC-3, respectively.

5.4.2 Soil inventory of ^{241}Am

As shown in Figure 5.4, over half of the total AWT fallout of ^{137}Cs and ^{241}Pu occurred between 1961 and 1964. The larger AWT release of ^{137}Cs compared to ^{241}Pu resulted in a larger atmospheric depositional flux to Earth's surface as the total flux of ^{137}Cs and ^{241}Pu based on ^{90}Sr fallout is estimated at 5.75 and 0.98 kBq m^{-2} , respectively.

Estimated changes in the theoretical soil inventory of ^{241}Pu , ^{137}Cs , and ^{241}Am through time due to atmospheric deposition, radioactive decay, and in the case of ^{241}Am , ingrowth are shown in Figure 5.5. From 1954 to 1965, the ^{241}Pu inventory grew to 729

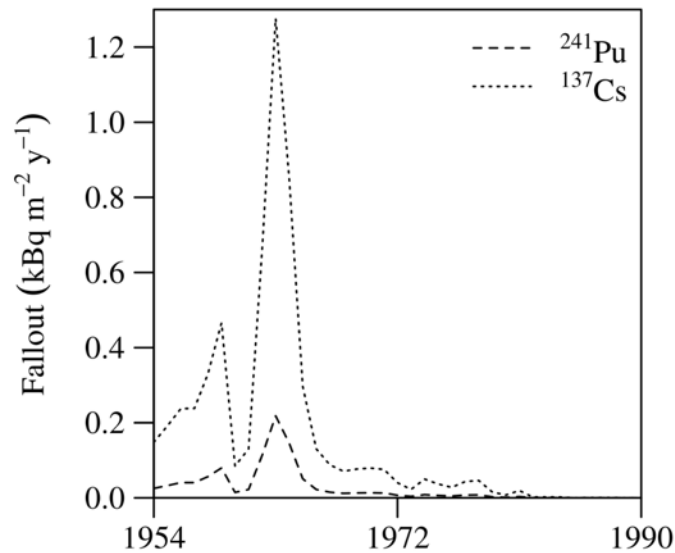


Figure 5.4: Fallout history of ^{241}Pu and ^{137}Cs due to atmospheric weapons testing. The record is based on the ^{90}Sr fallout measured at New York, New York, USA and the concentrations of ^{241}Pu and ^{137}Cs in fallout debris. See text for further discussion.

Bq m^{-2} after which it decreased rapidly due to the decreasing atmospheric flux coupled with radioactive decay (Figure 5.5). Only 5% of the 1965 ^{241}Pu inventory will remain by 2033. The ^{137}Cs inventory grew to its maximum in 1966 at 4.5 kBq m^{-2} and only 10% of this will remain by 2075.

In the case of ^{241}Am , the inventory time course was initially a consequence of ingrowth by decay of ^{241}Pu followed by decay of ^{241}Am itself. Assuming no additional sources, the theoretical ^{241}Am inventory will reach a maximum of 30 Bq m^{-2} in 2036 and it will decay to extinction in the late 4100s. At the time the marsh cores were collected in 2012, the ^{241}Pu inventory was 97 Bq m^{-2} and, due to its larger atmospheric flux and longer half-life, the ^{137}Cs inventory was 1860 Bq m^{-2} (Figure 5.5). The

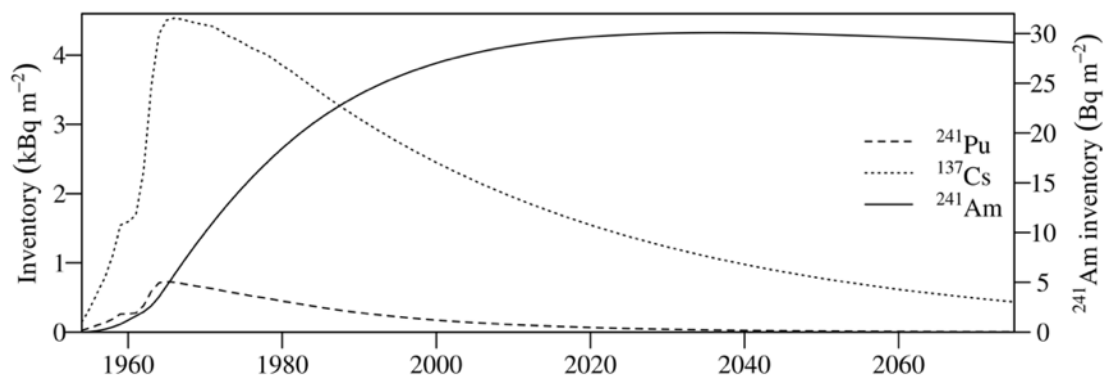


Figure 5.5: Theoretical soil inventories of ^{241}Pu , ^{137}Cs , and ^{241}Am from the time these radionuclides were introduced to the environment in 1954 to 2075. The inventory record for ^{241}Pu and ^{137}Cs is based on the estimated atmospheric flux (Figure 5.4) and radioactive decay. The ^{241}Am inventory is based on ingrowth from ^{241}Pu and decay. Note the different scale (right) for ^{241}Am .

theoretical 2012 inventory of ^{241}Am was estimated at 29 Bq m^{-2} , which is broadly comparable to the measured inventories ($16\text{-}51 \text{ Bq m}^{-2}$).

5.5 Discussion

5.5.1 Attribution of ^{241}Am to AWT fallout

Detection of a ^{241}Am activity peak in the soil column at a depth coincident with the ^{137}Cs peak confirms that the source of ^{241}Am was AWT fallout and decay of ^{241}Pu (Figure 5.3). Near-surface activities of ^{241}Am in cores DN-2 and DV-3 are high considering the length of time that has passed between 1963 and 2012, suggesting that ingrowth from ^{241}Pu is not the sole source of ^{241}Am to the marsh soils (Figure 5.3). Similarly, ^{137}Cs detected near the marsh surface suggests that direct atmospheric deposition over the marsh platform was not (and currently is not) the only source of ^{137}Cs to the soil. Sediment focusing has been shown to increase $^{210}\text{Pb}_u$ and ^{137}Cs

inventories in these marshes (see Chapter 3), thus particulate ^{241}Am redistributed within the wetland system by erosion and redeposition can explain the shape of the activity profiles. Similarly, focusing can explain measured ^{241}Am inventories greater than those supported by direct atmospheric deposition.

As shown here and in other studies of tidal marsh soils (e.g., Dyer et al., 2002; Olid et al., 2008), ^{241}Am activities are lower than those of ^{137}Cs but nonetheless detectable using standard low-background gamma detectors. Gamma spectroscopy has major advantages over alpha spectrometric methods (e.g., Livingston et al., 1975), which are destructive and more time consuming.

5.5.2 Advantages of ^{241}Am as a geochronometer

Advantages of ^{241}Am over ^{137}Cs as a geochronometer include not only its relatively long half-life but its relative chemical immobility in sediments and soils (Appleby et al., 1991). The affinity of ^{241}Am for particles in seawater is three orders of magnitude greater than that of ^{137}Cs (Kershaw et al., 1992 and references therein). In a study on soil transfer of radionuclides, Kozhakhonov et al. (2014) found that ^{241}Am accumulated a rate 140 times less than that of ^{137}Cs in a variety of agricultural crops including grasses. Immobility of ^{241}Am in marsh peats has led some investigators to place more emphasis on ^{241}Am than ^{137}Cs when identifying the 1963-1964 AWT peak (Gallagher et al., 2001; Dyer et al., 2002; Olid et al., 2008). Carpenter and Beasley (1981) found similar ^{241}Am inventories in oxic and anoxic marine sediments suggesting that ^{241}Am should remain fixed in soils where anoxic conditions can be prevalent. These results imply that ^{241}Am and ^{137}Cs can be used in unison for the immediate future, thus providing two geochemically different tracers with identical input functions. In tidal marshes, use of these radionuclides together

could be used to identify processes of trace metal and radionuclide sequestration, including plant uptake and bioavailability.

5.6 Conclusions

Americium-241 detected in salt marsh soils from Delaware Bay and Barnegat Bay can be attributed to ingrowth by in-situ decay of fallout ^{241}Pu . Comparison with ^{137}Cs activity-depth profiles for the same soils indicates that the ^{241}Am follows a distribution consistent with the record of fallout due to Northern Hemisphere AWT. Activities of ^{241}Am were highest in relatively organogenic marshes suggesting that organic marsh soils can retain ^{241}Am as has been observed in peatlands. These results indicate that ^{241}Am is largely immobile in marsh soils and has potential use as a particle tracer and geochronometer in estuarine and tidal wetland environments. Significantly, results of this study demonstrate that AWT-sourced ^{241}Am has reached levels of detection achievable by commercially available High Purity Germanium detectors.

REFERENCES

- Appleby, P.G., Richardson, N., Nolan, P.J., 1991. ^{241}Am dating of lake sediments. *Hydrobiologia* 214, 35–42. doi:10.1007/BF00050929
- Beasley, T.M., Carpenter, R., Jennings, C.D., 1982. Plutonium, ^{241}Am and ^{137}Cs ratios, inventories and vertical profiles in Washington and Oregon continental shelf sediments. *Geochim. Cosmochim. Acta* 46, 1931–1946. doi:10.1016/0016-7037(82)90131-4
- Bowen, V.T., Noshkin, V.E., Volchok, H.L., Livingston, H.D., Wong, K.M., 1974. Cesium 137 to strontium 90 ratios in the Atlantic Ocean 1966 through 1972. *Limnol. Oceanogr.* 19, 670–681. doi:10.4319/lo.1974.19.4.0670
- Carpenter, R., Beasley, T.M., 1981. Plutonium and americium in anoxic marine sediments: evidence against remobilization. *Geochim. Cosmochim. Acta* 45, 1917–1930. doi:10.1016/0016-7037(81)90022-3
- Carpenter, R., Beasley, T.M., Zahnle, D., Somayajulu, B.L.K., 1987. Cycling of fallout (Pu, ^{241}Am , ^{137}Cs) and natural (U, Th, ^{210}Pb) radionuclides in Washington continental slope sediments. *Geochim. Cosmochim. Acta* 51, 1897–1921. doi:10.1016/0016-7037(87)90181-5
- Cochran, J.K., Livingston, H.D., Hirschberg, D.J., Surprenant, L.D., 1987. Natural and anthropogenic radionuclide distributions in the northwest Atlantic Ocean. *Earth Planet. Sci. Lett.* 84, 135–152. doi:10.1016/0012-821X(87)90081-1
- Dahlman, R.C., Francis, C.W., Tamura, T., 1975. Radiocesium cycling in vegetation and soil, in: Howell, F.G., Gentry, J.E., Smith, M.H. (Eds.), *Mineral Cycling in Southeastern Ecosystems*. ERDA Symposium Series. (CONF-740513), pp. 462–481.
- Delvaux, B., Kruyts, N., Cremers, A., 2000. Rhizospheric mobilization of radiocesium in soils. *Environ. Sci. Technol.* 34, 1489–1493. doi:10.1021/es990658g
- Dyer, F.M., Thomson, J., Croudace, I.W., Cox, R., Wadsworth, R.A., 2002. Records of change in salt marshes: a radiochronological study of three Westerschelde (SW Netherlands) marshes. *Environ. Sci. Technol.* 36, 854–861. doi:10.1021/es0110527

- Environmental Measurements Laboratory (EML), 1999. Global Fallout Program. New York, New York.
- Fowler, S.W., Ballestra, S., La Rosa, J., Fukai, R., 1983. Vertical transport of particulate-associated plutonium and americium in the upper water column of the Northeast Pacific. *Deep Sea Res.* 30, 1221–1233. doi:10.1016/0198-0149(83)90081-X
- Gallagher, D., McGee, E.J., Mitchell, P.I., 2001. A recent history of C-14, Cs-137, Pb-210, and Am-241 accumulation at two Irish peat bog sites: An east versus west coast comparison. *Radiocarbon* 43, 517–525.
- Harley, N., Fisenne, I., Ong, D., Harley, J.H., 1965. Fission yield and fission product decay. USAEC Health Safety Lab. Fallout Program Quart. Summ. Rep. HASL-264, pp. 251–260.
- Johnson-Pyrtle, A., Scott, M.R., 2001. Distribution of ^{137}Cs in the Lena River Estuary–Laptev Sea System. *Mar. Pollut. Bull.* 42, 912–926. doi:10.1016/S0025-326X(00)00237-X
- Kazinskaya, I.E., Goryachenkova, T.A., Novikov, A.P., Vinokurov, S.E., Tkachev, V.V., 2012. Association of radionuclides with components of fulvic acids isolated from soils. *Radiochemistry* 54, 87–91. doi:10.1134/S1066362212010134
- Kershaw, P.J., Pentreath, R.J., Woodhead, D.S., Hunt, G.J., 1992. A review of radioactivity in the Irish Sea - A report prepared for the Marine Pollution Monitoring Management Group. Lowestoft.
- Koide, M., Goldberg, E.D., 1982. Transuranic nuclides in two coastal marine sediments off Peru. *Earth Planet. Sci. Lett.* 57, 263–277. doi:10.1016/0012-821X(82)90149-2
- Koide, M., Goldberg, E.D., Hodge, V.F., 1980. ^{241}Pu and ^{241}Am in sediments from coastal basins off California and Mexico. *Earth Planet. Sci. Lett.* 48, 250–256. doi:10.1016/0012-821X(80)90188-0
- Koide, M., Williams, P.W., Goldberg, E.D., 1981. Am-241/Pu-239 + 240 ratios in the marine environment. *Mar. Environ. Res.* 5, 241–246. doi:10.1016/0141-1136(81)90007-6
- Kozhakhyanov, T.E., Lukashenko, S.N., Larionova, N. V., 2014. Accumulation of artificial radionuclides in agricultural plants in the area used for surface nuclear tests. *J. Environ. Radioact.* 137, 217–226. doi:10.1016/j.jenvrad.2014.06.026

- Leslie, C., Hancock, G.J., 2008. Estimating the date corresponding to the horizon of the first detection of ^{137}Cs and $^{239+240}\text{Pu}$ in sediment cores. *J. Environ. Radioact.* 99, 483–490. doi:10.1016/j.jenvrad.2007.08.016
- Lujanienė, G., Beneš, P., Štamberg, K., Ščiglo, T., 2012. Kinetics of plutonium and americium sorption to natural clay. *J. Environ. Radioact.* 108, 41–49. doi:10.1016/j.jenvrad.2011.07.012
- Olid, C., Diego, D., Garcia-Orellana, J., Cortizas, A.M., Klaminder, J., 2016. Modeling the downward transport of ^{210}Pb in peatlands: initial penetration-constant rate of supply (IP-CRS) model. *Sci. Total Environ.* 541, 1222–1231. doi:10.1016/j.scitotenv.2015.09.131
- Olid, C., Garcia-Orellana, J., Martínez-Cortizas, A., Masqué, P., Peiteado, E., Sanchez-Cabeza, J.-A., 2008. Role of surface vegetation in ^{210}Pb -dating of peat cores. *Environ. Sci. Technol.* 42, 8858–8864. doi:10.1021/es801552v
- Santschi, P.H., Li, Y.-H., Adler, D.M., Amdurer, M., Bell, J., Nyffeler, U.P., 1983. The relative mobility of natural (Th, Pb and Po) and fallout (Pu, Am, Cs) radionuclides in the coastal marine environment: results from model ecosystems (MERL) and Narragansett Bay. *Geochim. Cosmochim. Acta* 47, 201–210. doi:10.1016/0016-7037(83)90133-3
- Thomson, J., Dyer, F.M., Croudace, I.W., 2002. Records of radionuclide deposition in two salt marshes in the United Kingdom with contrasting redox and accumulation conditions. *Geochim. Cosmochim. Acta* 66, 1011–1023. doi:10.1016/S0016-7037(01)00825-0

Chapter 6

SUMMARY AND CONCLUSIONS

The goal of this dissertation research was to apply radionuclide tracer and geochronological methods (^{210}Pb , ^{137}Cs , and ^{241}Am) to the study of salt marsh sedimentary processes. This was undertaken through a comparative study of salt marsh systems associated with Delaware Bay and Barnegat Bay, US Mid-Atlantic region. The main conclusions of this research are detailed below.

6.1 Summary

The first component of this work (Chapter 2) investigated the geomorphic controls on tidal marsh accretion by relating mineral and organic accumulation to the hydrologic and topographic characteristics of marshes in two geologic settings. This comparison was aided by the fact that the marshes were selected from the same regional area minimizing meteorological and oceanographic variables affecting both physical and biotic processes in the marsh. The coastal lagoonal Barnegat Bay marshes are likely to be submerged based on comparisons with sea-level rise from tide gage records.

The second component of this work (Chapter 3) investigated the application of ^{137}Cs and ^{210}Pb chronology in salt marshes. The fallout record of ^{90}Sr was used as a proxy for ^{137}Cs and theoretical profiles were generated for comparison with measured activity profiles. This comparison showed that while inventories were in agreement with atmospheric flux peak shape was not. This disagreement indicated that post-

depositional processes such as erosion and deposition of remobilized ^{137}Cs is likely occurring in these marshes. The CFCS, CRS, and CIC models of ^{210}Pb accumulation were applied to the eighteen cores to determine which, if any model was most appropriate in the tidal marsh setting. Comparison of inventories and theoretical flux suggest that sediment focusing is a dominant mechanism of radionuclide inventory formation in these marshes. No one dating model was determined as appropriate for all marshes. The organogenic marshes of Barnegat Bay suit the assumptions of CRS model, where organic matter and atmospheric flux are the primary controls of the marsh radionuclide inventory. Whereas the CIC model better suited the minerogenic marshes of the Delaware Bay, due to the variation in mineral accumulation spatially and temporally and the import of ^{210}Pb on particles as well as due to atmospheric flux. The CFCS model does not suit most scenarios in tidal marshes where accretion due to sediment accumulation is a time-variable process. This model does however yield reasonable core averaged rates of mass accumulation.

The third component of this work (Chapter 4) investigated how plants and organic material trap radionuclides and the contribution of organic-adsorbed radionuclides to the sediment record. The aerial plant biomass and litter trapped some portion of the annual atmospheric flux which was directly related to the organically held inventory belowground. Aboveground dead biomass had higher radionuclide activities perhaps to either time of exposure to atmospheric flux, decomposition reducing plant mass and increasing radionuclide concentration, or both. Organic and mineral particles were found to be associated with ^{137}Cs in these shallow (0-6 cm) and therefore young layers indicating focusing of previous deposited ^{137}Cs both on organic matter and mineral sediment.

The fourth component of this work (Chapter 5) identified a known, but not commonly used fallout tracer, ^{241}Am , in the marsh sediment record. The comparison of ^{137}Cs and ^{241}Am activities and activities peaks suggest that this radionuclide can be used a direct replacement for ^{137}Cs in marsh soils. Perhaps of more interest is that for the near future, two measurable fallout tracers are present in the soil record – ^{137}Cs is known to incorporate into tissue and ^{241}Am is known to be fairly immobile. The coupled use of these nuclides could reveal how uptake by plants affects distribution of similar soil contaminants.

6.2 Conclusions

The estuarine Delaware Bay marshes are less likely to be inundated and this is attributed to the higher rates of mineral sediment accumulation. However, mineral sediment accumulation is not related to flooding frequency, duration, or elevation as has been shown in other system measuring rates of accumulation over the shorter time scales. This lack of a relationship between sediment accumulation and hydrogeomorphic variables suggests that mineral sediment availability, specifically the suspended sediment concentrations of flood waters possibly during storm events, is the factor controlling sediment accumulation in these systems.

No single chronological model is appropriate in tidal marshes, which are both spatially and temporally variable. Application of ^{137}Cs and ^{210}Pb methods requires knowledge of the marsh history and possible radionuclide sources. Agreement of these independent methods shows that ^{137}Cs and ^{210}Pb chronology are suited for tidal marshes. The range of radionuclide inventories in a small geographic region suggests that these tools can also be used to investigate how sediment (and particle associated compounds) are remobilized in the estuary-marsh system. Successful chronology

starts before samples are analyzed by careful selection and sampling of field sites according to the goals of the study.

The ^{137}Cs and ^{210}Pb are associated with organic matter above and belowground suggest that plants have a direct or indirect role in the soil radionuclide inventory formation and, in organic-rich marshes, the majority of the inventory was associated with organic matter. A common practice in chronological and contaminant studies is to normalize or analyze just the silt and clay size fraction of the record under the assumption that these particles hold the majority of the inventory. The results of this work suggest that should not be a primary assumption in tidal marshes. Aerial biomass traps atmospherically deposited radionuclides and is related to the organic soil inventory but the exact mechanism connecting above and belowground inventories is still unclear, but burial of aerial biomass is a likely mechanism.

6.3 Implications and applications

The results of these studies have implications for marsh viability in the face of sea-level rise and applications into the refinement of dating and geomorphic models. The conclusions from Chapter 2 show that while tidal marshes can accrete through primarily organic accumulation, mineral sediment enhances accretionary processes. The reduction of sediment to systems on the tipping point of persistence or submergence should be a primary concern. A better understanding of how natural and anthropogenic change affects mineral sediment availability in estuaries and deliver to the marsh surface would aid in assessing marsh viability in these and other systems.

The mechanism for burial, if any, of radionuclides trapped on aerial plant structures is unclear. Collection and quantification of radionuclides in litter at various stages of decomposition could determine if the fate of organically trapped

radionuclides are associated with the litter itself. Preliminarily, detection of ^{137}Cs on organic particles in the near surface suggest the two are linked. Since no recent source of ^{137}Cs exists, the organically bound ^{137}Cs in the near surface could have been imported on organic particles.

6.4 Future work

The results of these studies highlight areas of future work. The complexities of the organic and mineral accumulation in marshes are still unclear. It is clear that a great degree of variability exists in marsh accumulation and accretion over small distances. Investigation of the trapping efficiency of marshes by relating topographic and hydrographic characteristics with sediment fluxes as done here could explain some of this variance.

The conclusions of Chapters 2, 3, and 4 support the notion of a biophysical feedback in tidal marsh sedimentation. Radionuclide analysis of the soil component of the entire core could show how the relationship between organic and mineral sediment changes over depth and time in the soil mass and radionuclide inventories. Repeat surveys of marshes artificially nourished with mineral sediment could provide insight into how organic production stabilizes mineral sediment and contributes to soil volume.

Additionally, the ability to construct chronologies is based on the known flux and behavior after burial. Monitoring of atmospheric radionuclide flux must continue to produce reliable records for both comparisons to the soil record and for the determination of spatial and temporal variability. A field effort to better constrain the flux of radionuclides in the marsh system and, specifically, in organic or mineral associated form would improve the models currently used that are predicated on a

sole, atmospheric flux and assume mineral association of radionuclides is preferred. Field monitoring stations, perhaps with vegetated and unvegetated marsh plots, would reveal more about radionuclide incorporation into the soil and possible mechanisms of marsh soil formation.

REFERENCES

- Allen, J.R.L., 1990. Salt-marsh growth and stratification: a numerical model with special reference to the Severn Estuary, southwest Britain. *Mar. Geol.* 95, 77–96. doi:10.1016/0025-3227(90)90042-I
- Allen, J.R.L., 2000. Morphodynamics of Holocene salt marshes: a review sketch from the Atlantic and Southern North Sea coasts of Europe. *Quat. Sci. Rev.* 19, 1155–1231. doi:10.1016/S0277-3791(99)00034-7
- Appleby, P.G., 2001. Chronostratigraphic techniques in recent sediments, in: Last, W.M., Smol, J.P. (Eds.), *Tracking Environmental Change Using Lake Sediments. Volume 1: Basin Analysis, Coring, and Chronological Techniques.* Kluwer Academic Publishers, Dordrecht, The Netherlands, pp. 171–203.
- Appleby, P.G., Oldfield, F., 1983. The assessment of ^{210}Pb data from sites with varying sediment accumulation rates. *Hydrobiologia* 103, 29–35. doi:10.1007/BF00028424
- Appleby, P.G., Richardson, N., Nolan, P.J., 1991. ^{241}Am dating of lake sediments. *Hydrobiologia* 214, 35–42. doi:10.1007/BF00050929
- Armentano, T., Woodwell, G., 1975. Sedimentation rates in a Long Island marsh determined by ^{210}Pb dating. *Limnol. Oceanogr.* 20, 452–456.
- Arvik, J.H., Zimdahl, R.L., 1974. Barriers to the foliar uptake of lead. *J. Environ. Qual.* 3, 369. doi:10.2134/jeq1974.00472425000300040015x
- Aston, S., Duursma, E., 1973. Concentration effects on ^{137}Cs , ^{65}Zn , ^{60}Co and ^{106}Ru sorption by marine sediments, with geochemical implications. *Netherlands J. Sea Res.* 6, 225–240. doi:10.1016/0077-7579(73)90015-X
- Atun, G., Bilgin, B., Mardinli, A., 1996. Sorption of cesium on montmorillonite and effects of salt concentration. *J. Radioanal. Nucl. Chem. Artic.* 211, 435–442. doi:10.1007/BF02039709
- Baskaran, M., Coleman, C.H. and Santschi, P.H., 1993. Atmospheric depositional fluxes of ^7Be and ^{210}Pb at Galveston and College Station, Texas. *J. Geophys. Res. Atmos.* 98(D11): 20555-20571. doi:10.1029/93JD02182

- Beasley, T.M., Carpenter, R., Jennings, C.D., 1982. Plutonium, ^{241}Am and ^{137}Cs ratios, inventories and vertical profiles in Washington and Oregon continental shelf sediments. *Geochim. Cosmochim. Acta* 46, 1931–1946. doi:10.1016/0016-7037(82)90131-4
- Bennett, R.H., Lambert, D.N., 1971. Rapid and reliable technique for determining unit weight and porosity of deep-sea sediments. *Mar. Geol.* 11, 201–207. doi:10.1016/0025-3227(71)90007-7
- Benninger, L.K., 1978. ^{210}Pb balance in Long Island Sound. *Geochim. Cosmochim. Acta* 42, 1165–1174. doi:10.1016/0016-7037(78)90111-4
- Benninger, L.K., Lewis, D.M., Turekian, K.K., 1975. The use of natural Pb-210 as a heavy metal tracer in the river-estuarine system, in: Church, T.M. (Ed.), *Marine Chemistry in the Coastal Environment*. American Chemical Society, pp. 202–210. doi:10.1021/bk-1975-0018.ch012
- Biggs, R.B., Beasley, E.L., 1988. Bottom and suspended sediments in the Delaware River and Estuary, in: Majumdar, S.K., Miller, E.W., Sage, L.E. (Eds.), *Ecology and Restoration of the Delaware River Basin*. The Pennsylvania Academy of Science, pp. 116–131.
- Binford, M.W., Kahl, J.S., Norton, S. a., 1993. Interpretation of ^{210}Pb profiles and verification of the CRS dating model in PIRLA project lake sediment cores. *J. Paleolimnol.* 9, 275–296. doi:10.1007/BF00677218
- Boorman, L.A., Hazelden, J., Boorman, M. 2001. The effect of rates of sedimentation and tidal submersion regimes on the growth of salt marsh plants. *Cont. Shelf Res.* 21, 2155-2165.
- Bouma, T.J., De Vries, M.B., Herman, P.M.J., 2010. Comparing ecosystem engineering efficiency of two plant species with contrasting growth strategies. *Ecology* 91, 2696–704.
- Bowen, V.T., Noshkin, V.E., Volchok, H.L., Livingston, H.D., Wong, K.M., 1974. Cesium 137 to strontium 90 ratios in the Atlantic Ocean 1966 through 1972. *Limnol. Oceanogr.* 19, 670–681. doi:10.4319/lo.1974.19.4.0670
- Bricker-Urso, S., Nixon, S.W., Cochran, J.K., Hirschberg, D.J., Hunt, C., 1989. Accretion rates and sediment accumulation in Rhode Island salt marshes. *Estuaries* 12, 300–317. doi:10.2307/1351908

- Cahoon, D.R., 2015. Estimating relative sea-level rise and submergence potential at a coastal wetland. *Estuaries and Coasts* 38, 1077–1084. doi:10.1007/s12237-014-9872-8
- Cahoon, D.R., Reed, D.J., 1995. Relationships among marsh surface topography, hydroperiod, and soil accretion in a deteriorating Louisiana salt marsh. *J. Coast. Res.* 11, 357–369.
- Cahoon, D.R., Turner, R.E., 1989. Accretion and canal impacts in a rapidly subsiding wetland II. feldspar marker horizon technique. *Estuaries* 12, 260–268. doi:10.2307/1351905
- Callaway, J.C., Borgnis, E.L., Turner, R.E., Milan, C.S., 2012. Carbon sequestration and sediment accretion in San Francisco Bay tidal wetlands. *Estuaries and Coasts* 35, 1163–1181. doi:10.1007/s12237-012-9508-9
- Callaway, J.C., DeLaune, R.D., Patrick, W.H., Patrick Jr., W., 1996. Chernobyl Cs-137 used to determine sediment accretion rates at selected northern European coastal wetlands. *Limnol. Oceanogr.* 41, 444–450. doi:10.4319/lo.1996.41.3.0444
- Callaway, J.C., DeLaune, R., Patrick Jr., W., 1997. Sediment accretion rates from four coastal wetlands along the Gulf of Mexico. *J. Coast. Res.* 13, 181–191.
- Calvo-Cubero, J., Ibáñez, C., Rovira, A., Sharpe, P.J., Reyes, E., 2013. Mineral versus organic contribution to vertical accretion and elevation change in restored marshes (Ebro Delta, Spain). *Ecol. Eng.* 61, 12–22. doi:10.1016/j.ecoleng.2013.09.047
- Cambay, R.S., Cawse, P.A., Garland, J.A., Gibson, J.A.B., Johnson, P., Lewis, G.N.J., Newton, D., Salmon, L., Wade, B.O., 1987. Observations on radioactivity from the Chernobyl accident. *Nucl. Energy* 26, 77–101.
- Carpenter, R., Beasley, T.M., 1981. Plutonium and americium in anoxic marine sediments: evidence against remobilization. *Geochim. Cosmochim. Acta* 45, 1917–1930. doi:10.1016/0016-7037(81)90022-3
- Carpenter, R., Beasley, T.M., Zahnle, D., Somayajulu, B.L.K., 1987. Cycling of fallout (Pu, ²⁴¹Am, ¹³⁷Cs) and natural (U, Th, ²¹⁰Pb) radionuclides in Washington continental slope sediments. *Geochim. Cosmochim. Acta* 51, 1897–1921. doi:10.1016/0016-7037(87)90181-5
- Chmura, G.L., Hung, G.A., 2004. Controls on salt marsh accretion: a test in salt marshes of Eastern Canada. *Estuaries* 27, 70–81. doi:10.1007/BF02803561

- Church, T.M., Bernat, M., Sharma, P., 1986. Distribution of natural uranium, thorium, lead, and polonium radionuclides in tidal phases of a Delaware salt marsh. *Estuaries* 9, 2–8. doi:10.2307/1352187
- Church, T., Lord III, C., Somayajulu, B., 1981. Uranium, thorium and lead nuclides in a Delaware salt marsh sediment. *Estuar. Coast. Shelf Sci.* 13, 267–275. doi:10.1016/S0302-3524(81)80025-4
- Cochran, J.K., Livingston, H.D., Hirschberg, D.J., Surprenant, L.D., 1987. Natural and anthropogenic radionuclide distributions in the northwest Atlantic Ocean. *Earth Planet. Sci. Lett.* 84, 135–152. doi:10.1016/0012-821X(87)90081-1
- Comans, R.N.J., Hockley, D.E., 1992. Kinetics of cesium sorption on illite. *Geochim. Cosmochim. Acta* 56, 1157–1164. doi:10.1016/0016-7037(92)90053-L
- Cook, T.L., Sommerfield, C.K., Wong, K.-C., 2007. Observations of tidal and springtime sediment transport in the upper Delaware Estuary. *Estuar. Coast. Shelf Sci.* 72, 235–246. doi:10.1016/j.ecss.2006.10.014
- Corbett, D.R., Walsh, J.P., 2015. 210-lead and 137-cesium: establishing a chronology for the last century, in: Shennan, I., Long, A.J., Horton, B.P. (Eds.), *Handbook of Sea-Level Research*. John Wiley and Sons, pp. 361–372. doi:10.1002/9781118452547.ch24
- Crusius, J., Anderson, R.F., 1995. Sediment focusing in six small lakes inferred from radionuclide profiles. *J. Paleolimnol.* 13, 143–155. doi:10.1007/BF00678103
- Cundy, A.B., Croudace, I.W., Thomson, J., Lewis, J.T., 1997. Reliability of salt marshes as “geochemical recorders” of pollution Input: a case study from contrasting estuaries in Southern England. *Environ. Sci. Technol.* 31, 1093–1101. doi:10.1021/es960622d
- Dahlman, R.C., Francis, C.W., Tamura, T., 1975. Radiocesium cycling in vegetation and soil, in: Howell, F.G., Gentry, J.E., Smith, M.H. (Eds.), *Mineral Cycling in Southeastern Ecosystems*. ERDA Symposium Series. (CONF-740513), pp. 462–481.
- Darmody, R.G., Foss, J.E., 1979. Soil-landscape relationships of the tidal marshes of Maryland. *Soil Sci. Soc. Am. J.* 43, 534–541.
- Davis, J.J., 1963. Cesium and its relationship to potassium in ecology, in: Schultz, V., Klement, A. (Eds.), *Radioecology*. Reinhold, New York, pp. 539–556.

- Defne, Z., Ganju, N.K., 2015. Quantifying the residence time and flushing characteristics of a shallow, back-barrier estuary: application of hydrodynamic and particle tracking models. *Estuaries and Coasts* 38, 1719–1734. doi:10.1007/s12237-014-9885-3
- DeLaune, R.D., Patrick Jr., W.H., Buresh, R.J., 1978. Sedimentation rates determined by ^{137}Cs dating in a rapidly accreting salt marsh. *Nature* 275, 532–533. doi:doi:10.1038/275532a0
- DeLaune, R., Reddy, C.N., Patrick Jr., W., 1981. Accumulation of plant nutrients and heavy metals through sedimentation processes and accretion in a Louisiana salt marsh. *Estuaries* 4, 328. doi:10.2307/1352157
- Delvaux, B., Kruyts, N., Cremers, A., 2000. Rhizospheric mobilization of radiocesium in soils. *Environ. Sci. Technol.* 34, 1489–1493. doi:10.1021/es990658g
- Deng, Z., An, S., Zhao, C., Chen, L., Zhou, C., Zhi, Y., Li, H., 2008. Sediment burial stimulates the growth and propagule production of *Spartina alterniflora* Loisel. *Estuar. Coast. Shelf Sci.* 76, 818–826. doi:10.1016/j.ecss.2007.08.008
- Dyer, F.M., Thomson, J., Croudace, I.W., Cox, R., Wadsworth, R.A., 2002. Records of change in salt marshes: a radiochronological study of three Westerschelde (SW Netherlands) marshes. *Environ. Sci. Technol.* 36, 854–861. doi:10.1021/es0110527
- Environmental Measurements Laboratory (EML), 1999. Global Fallout Program. New York, New York.
- Ezer, T., Atkinson, L.P., Corlett, W.B., Blanco, J.L., 2013. Gulf Stream's induced sea level rise and variability along the U.S. Mid-Atlantic coast. *J. Geophys. Res. Ocean.* 118, 685–697. doi:10.1002/jgrc.20091
- Fagherazzi, S., Kirwan, M.L., Mudd, S.M., 2012. Numerical models of salt marsh evolution: Ecological, geomorphic, and climatic factors. *Rev. Geophys.* 50, 1–28. doi:10.1029/2011RG000359.1.INTRODUCTION
- Fletcher, III, C.H., Knebel, H.J., Kraft, J.C., 1990. Holocene evolution of an estuarine coast and tidal wetlands. *Geol. Soc. Am. Bull.* 102, 283–297. doi:10.1130/0016-7606(1990)102<0283:HEOAEC>2.3.CO;2
- Fletcher, III, C., Knebel, H., Kraft, J.C., 1992. Holocene depocenter migration and sediment accumulation in Delaware Bay: a submerging marginal marine sedimentary basin. *Mar. Geol.* 103, 165–183.

- Fowler, S.W., Ballestra, S., La Rosa, J., Fukai, R., 1983. Vertical transport of particulate-associated plutonium and americium in the upper water column of the Northeast Pacific. *Deep Sea Res.* 30, 1221–1233. doi:10.1016/0198-0149(83)90081-X
- French, J.R., 1993. Numerical simulation of vertical marsh growth and adjustment to accelerated sea-level rise, North Norfolk, U.K. *Earth Surf. Process. Landforms* 18, 63–81. doi:10.1002/esp.3290180105
- French, J.R., 2006. Tidal marsh sedimentation and resilience to environmental change: Exploratory modelling of tidal, sea-level and sediment supply forcing in predominantly allochthonous systems. *Mar. Geol.* 235, 119–136. doi:10.1016/j.margeo.2006.10.009
- French, J.R., Spencer, T., 1993. Dynamics of sedimentation in a tide-dominated backbarrier salt marsh, Norfolk, UK. *Mar. Geol.* 110, 315–331. doi:10.1016/0025-3227(93)90091-9
- Frey, R., Basan, P., 1985. Coastal Salt Marshes, in: Davis, R. (Ed.), *Coastal Sedimentary Environments*. Springer-Verlag, New York, p. 716. doi:10.1007/978-1-4612-5078-4
- Friedrichs, C.T., Perry, J.E., 2001. Tidal salt marsh morphodynamics: a synthesis. *J. Coast. Res.* 81, 7–37.
- Gallagher, D., McGee, E.J., Mitchell, P.I., 2001. A recent history of C-14, Cs-137, Pb-210, and Am-241 accumulation at two Irish peat bog sites: An east versus west coast comparison. *Radiocarbon* 43, 517–525.
- Genrich, D.A., Bremner, J.M., 1974. Isolation of soil particle-size fractions. *Soil Sci. Soc. Am. J.* 38, 222–225. doi:10.2136/sssaj1974.03615995003800020009x
- Gleason, M.L., Elmer, D.A., Pien, N.C., Fisher, J.S., 1979. Effects of Stem Density upon Sediment Retention by Salt Marsh Cord Grass, *Spartina alterniflora* Loisel. *Estuaries* 2, 271. doi:10.2307/1351574
- Goldberg, E.D., 1963. Geochronology with lead-210, in: *Radioactive Dating*. IAEA, Vienna, pp. 121–131.
- Graustein, W.C., Turekian, K.K., 1986. ^{210}Pb and ^{137}Cs in air and soils measure the rate and vertical profile of aerosol scavenging. *J. Geophys. Res.* 91, 14355–143369. doi:10.1029/JD091iD13p14355

- Harley, N., Fisenne, I., Ong, D., Harley, J.H., 1965. Fission yield and fission product decay. USAEC Health Safety Lab. Fallout Program Quart. Summ. Rep. HASL-264, pp. 251–260.
- He, Q., Walling, D., 1996. Interpreting particle size effects in the adsorption of ^{137}Cs and unsupported ^{210}Pb by mineral soils and sediments. *J. Environ. Radioact.* 30, 117–137. doi:10.1016/0265-931X(96)89275-7
- Heiri, O., Lotter, A.F., Lemcke, G., 2001. Loss on ignition as a method for estimating organic and carbonate content in sediments: reproducibility and comparability of results. *J. Paleolimnol.* 25, 101–110. doi:10.1023/A:1008119611481
- Horton, B.P., Engelhart, S.E., Hill, D.F., Kemp, A.C., Nikitina, D., Miller, K.G., Peltier, W.R., 2013. Influence of tidal-range change and sediment compaction on Holocene relative sea-level change in New Jersey, USA. *J. Quat. Sci.* 28, 403–411. doi:10.1002/jqs.2634
- Inn, K.G.W., Lin, Z., Liggett, W.S., Schima, F.J., Krey, P., Feiner, M., Liu, C.-K., Holloway, R., Harvey, J., Larsen, I.L., Beasley, T., Huh, C.A., McCurdy, D., Germain, P., Yamamoto, M., Handl, J., Popplewell, D.S., Woods, M.J., Jerome, S., Bates, T.H., Holms, A., Harvey, B.R., Odell, K.J., Warren, B.B., Young, P., 1996. Low-level radioactivity ocean sediment standard reference material. *Appl. Radiat. Isot.* 47, 967–970. doi:10.1016/S0969-8043(96)00094-2
- Johnson-Pyrtle, A., Scott, M.R., 2001. Distribution of ^{137}Cs in the Lena River Estuary–Laptev Sea System. *Mar. Pollut. Bull.* 42, 912–926. doi:10.1016/S0025-326X(00)00237-X
- Kazinskaya, I.E., Goryachenkova, T.A., Novikov, A.P., Vinokurov, S.E., Tkachev, V.V., 2012. Association of radionuclides with components of fulvic acids isolated from soils. *Radiochemistry* 54, 87–91. doi:10.1134/S1066362212010134
- Kemp, A.C., Horton, B.P., Vane, C.H., Bernhardt, C.E., Corbett, D.R., Engelhart, S.E., Anisfeld, S.C., Parnell, A.C., Cahill, N., 2013. Sea-level change during the last 2500 years in New Jersey, USA. *Quat. Sci. Rev.* 81, 90–104. doi:10.1016/j.quascirev.2013.09.024
- Kemp, A.C., Sommerfield, C.K., Vane, C.H., Horton, B.P., Chenery, S., Anisfeld, S.C., Nikitina, D.L., 2012. Use of lead isotopes for developing chronologies in recent salt-marsh sediments. *Quat. Geochronol.* 12, 40–49. doi:10.1016/j.quageo.2012.05.004

- Kennish, M.J., 2001. Physical description of the Barnegat Bay—Little Egg Harbor estuarine system. *J. Coast. Res.* SI 32, 13–27.
- Kershaw, P.J., Pentreath, R.J., Woodhead, D.S., Hunt, G.J., 1992. A review of radioactivity in the Irish Sea - A report prepared for the Marine Pollution Monitoring Management Group. Lowestoft.
- Kim, G., Alleman, L., Church, T., 2004. Accumulation records of radionuclides and trace metals in two contrasting Delaware salt marshes. *Mar. Chem.* 87, 87–96. doi:10.1016/j.marchem.2004.02.002
- Kim, G., Hussain, N., Scudlark, J.R., Church, T.M., 2000. Factors influencing the atmospheric depositional fluxes of stable Pb, ^{210}Pb , and ^7Be into Chesapeake Bay. *J. Atmos. Chem.* 36, 65–79. doi:10.1023/A:1006383030362
- Kirwan, M.L., Guntenspergen, G.R., D'Alpaos, A., Morris, J.T., Mudd, S.M., Temmerman, S., 2010. Limits on the adaptability of coastal marshes to rising sea level. *Geophys. Res. Lett.* 37, 1–5. doi:10.1029/2010GL045489
- Kirwan, M.L., Temmerman, S., Skeeahan, E.E., Guntenspergen, G.R., Fagherazzi, S., 2016. Overestimation of marsh vulnerability to sea level rise. *Nat. Clim. Chang.* 6, 253–260. doi:10.1038/nclimate2909
- Koide, M., Goldberg, E.D., 1982. Transuranic nuclides in two coastal marine sediments off Peru. *Earth Planet. Sci. Lett.* 57, 263–277. doi:10.1016/0012-821X(82)90149-2
- Koide, M., Goldberg, E.D., Hodge, V.F., 1980. ^{241}Pu and ^{241}Am in sediments from coastal basins off California and Mexico. *Earth Planet. Sci. Lett.* 48, 250–256. doi:10.1016/0012-821X(80)90188-0
- Koide, M., Williams, P.W., Goldberg, E.D., 1981. Am-241/Pu-239 + 240 ratios in the marine environment. *Mar. Environ. Res.* 5, 241–246. doi:10.1016/0141-1136(81)90007-6
- Kolker, A.S., Goodbred, S.L., Hameed, S., Cochran, J.K., 2009. High-resolution records of the response of coastal wetland systems to long-term and short-term sea-level variability. *Estuar. Coast. Shelf Sci.* 84, 493–508. doi:10.1016/j.ecss.2009.06.030
- Kozhakhyanov, T.E., Lukashenko, S.N., Larionova, N. V., 2014. Accumulation of artificial radionuclides in agricultural plants in the area used for surface nuclear tests. *J. Environ. Radioact.* 137, 217–226. doi:10.1016/j.jenvrad.2014.06.026

- Kraft, J.C., Yi, H., Khalequzzaman, M., 1992. Geologic and human factors in the decline of the tidal salt marsh lithosome: the Delaware estuary and Atlantic coastal zone. *Sediment. Geol.* 80, 233–246. doi:10.1016/0037-0738(92)90043-Q
- Krishnaswami, S., Graustein, W.C., Turekian, K.K., Dowd, J.F., 1982. Radium, thorium and radioactive lead isotopes in groundwaters: application to the in situ determination of adsorption-desorption rate constants and retardation factors. *Water Resour. Res.* 18, 1663–1675. doi:10.1029/WR018i006p01663
- Krmar, M., Radnović, D., Hansman, J., 2014. Correlation of unsupported ^{210}Pb activity in soil and moss. *J. Environ. Radioact.* 129, 23–26. doi:10.1016/j.jenvrad.2013.11.009
- Krone, R., 1987. A method for simulating historic marsh elevations, in: Krause, N. (Ed.), *Coastal Sediments '87*. American Society of Civil Engineers, New York, New York, pp. 316–323.
- Landis, J., Renshaw, C., Kaste, J., 2014. Quantitative retention of atmospherically-deposited elements by native vegetation is traced by the fallout radionuclides ^7Be and ^{210}Pb . *Environ. Sci. Technol.* 48, 12022–12030.
- Langlois, E., Bonis, A., Bouzillé, J.B., 2001. The response of *Puccinellia maritima* to burial: a key to understanding its role in salt-marsh dynamics? *J. Veg. Sci.* 12, 289–297. doi:10.2307/3236613
- Lathrop Jr., R., Bognar, J., 2001. Habitat loss and alteration in the Barnegat Bay region. *J. Coast. Res.* 212–228.
- Leslie, C., Hancock, G.J., 2008. Estimating the date corresponding to the horizon of the first detection of ^{137}Cs and $^{239+240}\text{Pu}$ in sediment cores. *J. Environ. Radioact.* 99, 483–490. doi:10.1016/j.jenvrad.2007.08.016
- Livens, F.R., Baxter, M.S., 1988a. Chemical associations of artificial radionuclides in Cumbrian soils. *J. Environ. Radioact.* 7, 75–86. doi:10.1016/0265-931X(88)90043-4
- Livens, F.R., Baxter, M.S., 1988b. Particle size and radionuclide levels in some west Cumbrian soils. *Sci. Total Environ.* 70, 1–17. doi:10.1016/0048-9697(88)90248-3
- Livingston, H.D., Schneider, D.L., Bowen, V.T., 1975. ^{241}Pu in the marine environment by a radiochemical procedure. *Earth Planet. Sci. Lett.* 25, 361–367. doi:10.1016/0012-821X(75)90254-X

- Lujanienė, G., Beneš, P., Štamberg, K., Ščiglo, T., 2012. Kinetics of plutonium and americium sorption to natural clay. *J. Environ. Radioact.* 108, 41–49. doi:10.1016/j.jenvrad.2011.07.012
- Luo, W., 1998. Short note hypsometric analysis with a geographic information system. *Comput. Geosci.* 24, 815–821. doi:10.1016/S0098-3004(98)00076-4
- Marsan, D., Rigaud, S., Church, T., 2014. Natural radionuclides ^{210}Po and ^{210}Pb in the Delaware and Chesapeake Estuaries: modeling scavenging rates and residence times. *J. Environ. Radioact.* 138C, 447–455. doi:10.1016/j.jenvrad.2014.08.014
- Matisoff, G., Bonniwell, E.C., Whiting, P.J., 1999. Soil erosion and sediment sources in an Ohio watershed using beryllium-7, cesium-137, and lead-210. *J. Environ. Qual.* 31, 54–61. doi:10.2134/jeq2002.5400
- McCaffrey, R.J., Thomson, J., 1980. A record of the accumulation of sediment and trace metals in a Connecticut salt marsh, in: Saltzman, B. (Ed.), *Advances in Geophysics*. Academic Press, New York, pp. 165–236.
- McCraith, B.J., Gardner, L.R., Wethey, D.S., Moore, W.S., 2003. The effect of fiddler crab burrowing on sediment mixing and radionuclide profiles along a topographic gradient in a southeastern salt marsh. *J. Mar. Res.* 61, 359–390. doi:10.1357/002224003322201232
- McSweeney, J.M., Chant, R.J., Sommerfield, C.K., 2016. Lateral variability of sediment transport in the Delaware Estuary. *J. Geophys. Res. Ocean.* 121, 725–744. doi:10.1002/2015JC010974
- Monetti, M.A., 1996. *Worldwide Deposition of Strontium-90 through 1990*. Environmental Monitoring Laboratory Report-579. New York.
- Morris, J.T., Sundareshwar, P. V., Nietch, C.T., Kjerfve, B., Cahoon, D.R., 2002. Responses of Coastal Wetlands To Rising Sea Level. *Ecology* 83, 2869–2877. doi:10.1890/0012-9658(2002)083[2869:ROCWTR]2.0.CO;2
- Moskalski, S.M., Sommerfield, C.K., 2012. Suspended sediment deposition and trapping efficiency in a Delaware salt marsh. *Geomorphology* 139-140, 195–204. doi:10.1016/j.geomorph.2011.10.018
- Moskalski, S.M., Sommerfield, C.K., 2013. Effects of northeaster storms on water level and turbidity in a Delaware Bay subestuary. *J. Coast. Res.* doi:10.2112/JCOASTRES-D-12-00222.1

- Moskalski, S.M., Sommerfield, C.K., and Wong, K.C., 2011. Oceanic and hydrologic influences on flow and water properties in the St. Jones River Estuary, Delaware. *Estuaries and Coasts*, doi: 10.1007/s12237-011-9407-5.
- Mudd, S.M., Howell, S.M., Morris, J.T., 2009. Impact of dynamic feedbacks between sedimentation, sea-level rise, and biomass production on near-surface marsh stratigraphy and carbon accumulation. *Estuar. Coast. Shelf Sci.* 82, 377–389. doi:10.1016/j.ecss.2009.01.028
- Murtaugh, P.A., 2007. Simplicity and complexity in ecological data analysis. *Ecology* 88, 56–62. doi:10.1890/0012-9658(2007)88[56:SACIED]2.0.CO;2
- National Oceanic and Atmospheric Administration (NOAA), 1985. National estuarine inventory: data atlas. Volume 1: physical and hydrologic characteristics. Washington, D.C.
- National Oceanic and Atmospheric Administration (NOAA) /National Ocean Service (NOS)/Center for Operational Oceanographic Products and Services(CO-OPS), 2013. Sea levels online: sea level variations of the United States derived from National Water Level Observation Network stations. <http://tidesandcurrents.noaa.gov/sltrends/sltrends.html> (accessed 1.1.2014).
- Nepf, H.M., 1999. Drag, turbulence, and diffusion in flow through emergent vegetation. *Water Resour. Res.* 35, 479–489. doi:10.1029/1998WR900069
- Neubauer, S., 2008. Contributions of mineral and organic components to tidal freshwater marsh accretion. *Estuar. Coast. Shelf Sci.* 78, 78–88. doi:10.1016/j.ecss.2007.11.011
- Neubauer, S., Anderson, I., Constantine, J., Kuehl, S., 2002. Sediment deposition and accretion in a mid-Atlantic (USA) tidal freshwater marsh. *Estuar. Coast. Shelf Sci.* 54, 713–727. doi:10.1006/ecss.2001.0854
- Nicholls, R.J., Hoozemans, F.M.J., Marchand, M., 1999. Increasing flood risk and wetland losses due to global sea-level rise: regional and global analyses. *Glob. Environ. Chang.* 9. doi:10.1016/S0959-3780(99)00019-9
- Nichols, M.M., 1989. Sediment accumulation rates and relative sea-level rise in lagoons. *Mar. Geol.* 88, 201–219. doi:10.1016/0025-3227(89)90098-4
- Nikitina, D., Kemp, A.C., Engelhart, S.E., Horton, B.P., Hill, D.F., Kopp, R.E., 2015. Sea-level change and subsidence in the Delaware Estuary during the last ~2200 years. *Estuar. Coast. Shelf Sci.* 164, 506–519. doi:10.1016/j.ecss.2015.08.012

- Nikitina, D.L., Kemp, A.C., Horton, B.P., Vane, C.H., van de Plassche, O., Engelhart, S.E., 2014. Storm erosion during the past 2000 years along the north shore of Delaware Bay, USA. *Geomorphology* 208, 160–172. doi:10.1016/j.geomorph.2013.11.022
- Norris, R.S., 1996. French and Chinese nuclear weapon testing. *Secur. Dialogue* 27, 39–54. doi:10.1177/0967010696027001006
- Nour, S., Inn, K., Filliben, J., 2008. Development of the NIST Rocky Flats Soil Standard. *J. Radioanal. Nucl. Chem.* 277, 161–168. doi:10.1007/s10967-008-0725-4
- Nyman, J., DeLaune, R., Roberts, H., Patrick Jr., W., 1993. Relationship between vegetation and soil formation in a rapidly submerging coastal marsh. *Mar. Ecol. Prog. Ser.* 96, 269–279.
- Nyman, J.A., Walters, R.J., Delaune, R.D., Patrick Jr., W.H., 2006. Marsh vertical accretion via vegetative growth. *Estuar. Coast. Shelf Sci.* 69, 370–380. doi:10.1016/j.ecss.2006.05.041
- Odum, W., 1988. Comparative ecology of tidal freshwater and salt marshes. *Annu. Rev. Ecol. Syst.* 19, 147–176.
- Oenema, O., DeLaune, R.D., 1988. Accretion rates in salt marshes in the Eastern Scheldt, South-west Netherlands. *Estuar. Coast. Shelf Sci.* 26, 379–394. doi:10.1016/0272-7714(88)90019-4
- Oertel, G.F., Kraft, J.C., 1994. New Jersey and Delmarva Barrier Islands, in: Davis, R.A. (Ed.), *Geology of Holocene Barrier Island Systems*. Springer, Berlin, pp. 207–232. doi:10.1007/978-3-642-78360-9_6
- Oldfield, F., Appleby, P.G., Cambray, R.S., Eakins, J.D., Barber, K.E., Battarbee, R.W., Pearson, G.R., Williams, J.M., 1979. ^{210}Pb , ^{137}Cs and ^{239}Pu profiles in ombrotrophic peat. *Oikos* 33, 40–45. doi:10.2307/3544509
- Olid, C., Diego, D., Garcia-Orellana, J., Cortizas, A.M., Klaminder, J., 2016. Modeling the downward transport of ^{210}Pb in peatlands: initial penetration-constant rate of supply (IP-CRS) model. *Sci. Total Environ.* 541, 1222–1231. doi:10.1016/j.scitotenv.2015.09.131
- Olid, C., Garcia-Orellana, J., Martínez-Cortizas, A., Masqué, P., Peiteado, E., Sanchez-Cabeza, J.-A., 2008. Role of surface vegetation in ^{210}Pb -dating of peat cores. *Environ. Sci. Technol.* 42, 8858–8864. doi:10.1021/es801552v

- Olsen, C.R., Larsen, I.L., Lowry, P.D., Cutshall, N.H., Todd, J.F., Wong, G.T.F., Casey, W.H., 1985. Atmospheric fluxes and marsh-soil inventories of ^7Be and ^{210}Pb . *J. Geophys. Res.* 90, 10487–10495. doi:10.1029/JD090iD06p10487
- Olsen, C.R., Simpson, H.J., Peng, T.-H., Bopp, R.F., Trier, R.M., 1981. Sediment mixing and accumulation rate effects on radionuclide depth profiles in Hudson Estuary sediments. *J. Geophys. Res.* 86, 11020–11028.
- Perkins, R.W., Thomas, C.W., 1980. Worldwide fallout, in: Hanson, W.C. (Ed.), *Transuranic Elements in the Environment*. US DOE, Washington, D.C., pp. 53–82. doi:10.1017/CBO9781107415324.004
- Peterson, P.J., 1978. Lead and vegetation, in: Nriagu, J. (Ed.), *The Biogeochemistry Of Lead In The Environment. Part B Biological Effects*. Elsevier/North-Holland Biomedical Press, Amsterdam, p. 384.
- Pethick, J.S., 1981. Long-term accretion rates on tidal salt marshes. *J. Sediment. Petrol.* 51, 0571–0577. doi:10.1306/212F7CDE-2B24-11D7-8648000102C1865D
- Pietrzak-Flis, Z., Skowrońska-Smolak, M., 1995. Transfer of ^{210}Pb and ^{210}Po to plants via root system and above-ground interception. *Sci. Total Environ.* 162, 139–147. doi:10.1016/0048-9697(95)04445-7
- Rama, Koide, M., Goldberg, E.D., 1961. Lead-210 in natural waters. *Science.* 134, 98–99. doi:10.1126/science.134.3472.98
- Redfield, A.C., 1972. Development of a New England Salt Marsh. *Ecol. Monogr.* 42, 201–237. doi:10.2307/1942263
- Reed, D.J., Bishara, D.A., Cahoon, D.R., Donnelly, J.P., Kearney, M.S., Kolker, A.S., Leonard, L.L., Orson, R.A., Stevenson, J.C., 2008. Site-Specific Scenarios for Wetlands Accretion as Sea Level Rises in the Mid-Atlantic Region, in: Titus, J.G., Strange, E.M. (Eds.), *Background Documents Supporting Climate Change Science Program Synthesis and Assessment Product 4.1*. U.S. EPA, Washington, D.C., pp. 134–174.
- Reed, D.J., de Luca, N., Foote, A.L., 1997. Effect of Hydrologic Management on Marsh Surface Sediment Deposition in Coastal Louisiana. *Estuaries* 20, 301. doi:10.2307/1352345

- Ritchie, J.C., McHenry, J.R., 1990. Application of Radioactive Fallout Cesium-137 for Measuring Soil Erosion and Sediment Accumulation Rates and Patterns: A Review. *J. Environ. Qual.* 19, 215.
doi:10.2134/jeq1990.00472425001900020006x
- Robbins, J.A., 1978. Geochemical and geophysical applications of radioactive lead, in: Nriagu, J.O. (Ed.), *The Biogeochemistry of Lead in the Environment*. Elsevier, Amsterdam, pp. 285–393.
- Rogers, Golden, Halpern, 1990. Profile of the Barnegat Bay: final report for the Barnegat Bay Study Group. New Jersey Dept. of Environmental Protection, Trenton, New Jersey.
- Rogowski, A., Tamura, T., 1970. Environmental mobility of cesium-137. *Radiat. Bot.* I, 35–45. doi:10.1016/S0033-7560(70)80050-3
- Roman, C.T., Daiber, F.C., 1984. Aboveground and belowground primary production dynamics of two Delaware Bay tidal marshes. *Bull. Torrey Bot. Club* 111, 34–41. doi:10.2307/2996208
- Rooth, J.E., Stevenson, J.C., Cornwell, J.C., 2003. Increased sediment accretion rates following invasion by *Phragmites australis*: The role of litter. *Estuaries* 26. doi:10.1007/BF02823724
- Sanchez-Cabeza, J.A., Ruiz-Fernández, A.C., 2012. ^{210}Pb sediment radiochronology: an integrated formulation and classification of dating models. *Geochim. Cosmochim. Acta* 82, 183–200. doi:10.1016/j.gca.2010.12.024
- Sanford, L.P., Halka, J.P., 1993. Assessing the paradigm of mutually exclusive erosion and deposition of mud, with examples from upper Chesapeake Bay. *Mar. Geol.* 114, 37–57. doi:10.1016/0025-3227(93)90038-W
- Santschi, P.H., Li, Y.-H., Adler, D.M., Amdurer, M., Bell, J., Nyffeler, U.P., 1983. The relative mobility of natural (Th, Pb and Po) and fallout (Pu, Am, Cs) radionuclides in the coastal marine environment: results from model ecosystems (MERL) and Narragansett Bay. *Geochim. Cosmochim. Acta* 47, 201–210. doi:10.1016/0016-7037(83)90133-3
- Shand, C.A., Cheshire, M.V., Smith, S., Vidal, M., Rauret, G., 1994. Distribution of radiocaesium in organic soils. *J. Environ. Radioact.* 23, 285–302. doi:10.1016/0265-931X(94)90067-1
- Shukla, B.S., Joshi, S.R., 1989. An evaluation of the CIC model of ^{210}Pb dating of sediments. *Environ. Geol. Water Sci.* 14, 73–76. doi:10.1007/BF01740587

- Snedden, G.A., Cretini, K., Patton, B., 2015. Inundation and salinity impacts to above- and belowground productivity in *Spartina patens* and *Spartina alterniflora* in the Mississippi River deltaic plain: implications for using river diversions as restoration tools. *Ecol. Eng.* 81, 133–139. doi:10.1016/j.ecoleng.2015.04.035
- Sommerfield, C.K., Wong, K.-C., 2011. Mechanisms of sediment flux and turbidity maintenance in the Delaware Estuary. *J. Geophys. Res.* 116, 1–16. doi:10.1029/2010JC006462
- Strahler, A.N., 1952. Hypsometric (area-altitude) analysis of erosional topography. *Geol. Soc. Am. Bull.* 63, 1117. doi:10.1130/0016-7606(1952)63[1117:HAAOET]2.0.CO;2
- Stumpf, R.P., 1983. The process of sedimentation on the surface of a salt marsh. *Estuar. Coast. Shelf Sci.* 17, 495–508. doi:10.1016/0272-7714(83)90002-1
- Sugai, S.F., Alperin, M.J., Reeburgh, W.S., 1994. Episodic deposition and ¹³⁷Cs immobility in Skan Bay sediments: a ten-year ²¹⁰Pb and ¹³⁷Cs time series. *Mar. Geol.* 116, 351–372. doi:10.1016/0025-3227(94)90051-5
- Sundby, B., Caetano, M., Vale, C., Gobeil, C., Luther, G.W., Nuzzio, D.B., 2005. Root-induced cycling of lead in salt marsh sediments. *Environ. Sci. Technol.* 39, 2080–2086. doi:10.1021/es048749n
- Temmerman, S., Govers, G., Meire, P., Wartel, S., 2003. Modelling long-term tidal marsh growth under changing tidal conditions and suspended sediment concentrations, Scheldt estuary, Belgium. *Mar. Geol.* 193, 151–169. doi:10.1016/S0025-3227(02)00642-4
- Temmerman, S., Govers, G., Wartel, S., Meire, P., 2004. Modelling estuarine variations in tidal marsh sedimentation: response to changing sea level and suspended sediment concentrations. *Mar. Geol.* 212, 1–19. doi:10.1016/j.margeo.2004.10.021
- Thomson, J., Dyer, F.M., Croudace, I.W., 2002. Records of radionuclide deposition in two salt marshes in the United Kingdom with contrasting redox and accumulation conditions. *Geochim. Cosmochim. Acta* 66, 1011–1023. doi:10.1016/S0016-7037(01)00825-0
- Tucker, K.J., 2016. Variability of organic carbon accumulation on a tidal wetland coast. M.S. thesis. University of Delaware.

- Turekian, K.K., Benninger, L.K., Dion, E.P., 1983. ^7Be and ^{210}Pb total deposition fluxes at New Haven, Connecticut and at Bermuda. *J. Geophys. Res.* 88, 5411. doi:10.1029/JC088iC09p05411
- Turner, R.E., Swenson, E.M., Milan, C.S., 2000. Organic and inorganic contributions to vertical accretion in salt marsh sediments, in: Weinstien, M.P., Kreeger, D.A. (Eds.), *Concepts and Controversies in Tidal Marsh Ecology*. Kluwer Academic Publishers, Dordrecht, pp. 583–595. doi:10.1007/0-306-47534-0_27
- U. S. Fish and Wildlife Service (USFWS), 2010. National Wetlands Inventory. <http://www.fws.gov/wetlands/> (accessed 1.1.2014)
- Unger, V., Elsey-Quirk, T., Sommerfield, C.K., and Velinsky, D.J. Stability of organic carbon accumulating in *Spartina alterniflora*-dominated salt marshes of the Mid-Atlantic U.S. Manuscript in review.
- Valiela, I., Teal, J.M., Allen, S.D., Van Etten, R., Goehringer, D., Volkmann, S., 1985. Decomposition in salt marsh ecosystems: the phases and major factors affecting disappearance of above-ground organic matter. *J. Exp. Mar. Bio. Ecol.* 89, 29–54. doi:10.1016/0022-0981(85)90080-2
- van Proosdij, D., Davidson-Arnott, R.G.D., Ollerhead, J., Vanproosdij, D., 2006. Controls on spatial patterns of sediment deposition across a macro-tidal salt marsh surface over single tidal cycles. *Estuar. Coast. Shelf Sci.* 69, 64–86. doi:10.1016/j.ecss.2006.04.022
- Velinsky, D.J., Sommerfield, C.K., Enache, M., Charles, D.F., 2011. Nutrient and ecological histories in Barnegat Bay, New Jersey. New Jersey Depart. of Environmental Protection PCER Report No. 10-05. Philadelphia, PA.
- Voulgaris, G., Meyers, S.T., 2004. Temporal variability of hydrodynamics, sediment concentration and sediment settling velocity in a tidal creek. *Cont. Shelf Res.* 24, 1659–1683. doi:10.1016/j.csr.2004.05.006
- Wahlberg, J.S., Fishman, M.J., 1962. Adsorption of cesium on clay minerals. U.S. Geological Survey Bulletin 1140-A, U.S. Dept. of the Interior, pp 40.
- Watts, C.W., Tolhurst, T.J., Black, K.S., Whitmore, A.P., 2003. In situ measurements of erosion shear stress and geotechnical shear strength of the intertidal sediments of the experimental managed realignment scheme at Tollesbury, Essex, UK. *Estuar. Coast. Shelf Sci.* 58, 611–620. doi:10.1016/S0272-7714(03)00139-2

- Windham, L., 2001. Comparison of biomass production and decomposition between *Phragmites australis* (common reed) and *Spartina patens* (salt hay grass) in brackish tidal marshes of New Jersey, USA. *Wetlands* 21, 179–188.
doi:10.1672/0277-5212(2001)021[0179:COBPAD]2.0.CO;2
- Zhang, X., Walling, D., 2005. Characterizing land surface erosion from cesium-137 profiles in lake and reservoir sediments. *J. Environ. Qual.* 34, 514–523.
doi:10.2134/jeq2005.0514

Appendix A

SOIL PHYSICAL PROPERTIES AND RADIONUCLIDE ACTIVITIES

Tabulated soil physical properties and radionuclide activities for the eighteen marsh cores used in this study. Water content is % mass and loss-on-ignition (LOI) is % solid mass. Dry bulk density (DBD) is in units of kg m^{-3} . Radionuclide activities are in units of Bq kg^{-1} .

Core	Depth		Physical Properties				Radionuclide activities				
	cm	kg m^{-2}	Water content	LOI	Fractional porosity	DBD	Sample mass (g)	^{210}Pb	^{241}Am	^{214}Bi	^{137}Cs
DN-1	1	3.8	68	32	0.82	384	43.61	206 (7)	-	14 (1)	6.7 (0.6)
DN-1	3	11.8	66	28	0.81	415	47.87	146 (6)	-	14 (1)	7 (0.6)
DN-1	5	19.9	67	31	0.82	394	38.54	128 (6)	-	16 (1)	5.6 (0.7)
DN-1	7	27.8	68	27	0.82	395	41.08	126 (6)	-	16 (1)	5.2 (0.7)
DN-1	9	35.2	71	29	0.84	347	39.39	127 (6)	-	16 (1)	7.7 (0.7)
DN-1	11	42.3	70	25	0.84	357	41.07	111 (6)	0.5 (0.2)	19 (1)	9.2 (0.7)
DN-1	13	49	73	27	0.86	316	35.59	111 (6)	-	17 (1)	10.6 (0.8)
DN-1	15	55	76	31	0.87	281	35.48	117 (5)	-	14 (1)	15 (0.9)
DN-1	17	60.1	80	38	0.89	228	30.36	120 (6)	0.4 (0.2)	14 (2)	21.5 (1.1)
DN-1	19	64.2	83	43	0.91	185	20.63	82 (7)	1.4 (0.3)	14 (2)	43.7 (1.8)
DN-1	21	67.9	83	39	0.91	190	22.62	64 (5)	1.2 (0.3)	13 (2)	105.1 (2.4)
DN-1	23	71.4	86	44	0.92	151	14.87	50 (6)	1.7 (0.3)	13 (2)	54.7 (2.3)

Core	Depth		Physical Properties				Radionuclide activities				
	cm	kg m ⁻²	Water content	LOI	Fractional porosity	DBD	Sample mass (g)	²¹⁰ Pb	²⁴¹ Am	²¹⁴ Bi	¹³⁷ Cs
DN-1	25	74.2	88	49	0.93	131	14.11	50 (6)	1 (0.3)	11 (2)	29.5 (1.8)
DN-1	27	76.8	87	48	0.93	134	14.82	73 (6)	-	11 (2)	14.9 (1.4)
DN-1	29	79.6	87	46	0.93	142	16.45	86 (6)	1.1 (0.3)	13 (2)	11.3 (1.2)
DN-1	31	82.4	87	49	0.93	138	17.53	111 (7)	-	8 (2)	8.4 (1.1)
DN-1	33	85.1	87	51	0.93	137	16.58	57 (5)	-	10 (2)	5.9 (0.9)
DN-1	35	88.5	82	50	0.89	198	32.06	89 (6)	-	10 (1)	4.4 (0.7)
DN-1	37	92.5	81	47	0.89	205	33.49	39 (5)	-	14 (1)	3.6 (0.6)
DN-1	39	95.9	87	54	0.92	138	17.7	33 (4)	-	7 (2)	4.6 (0.8)
DN-1	41	98.6	88	53	0.93	127	16.63	18 (5)	-	10 (2)	-
DN-1	43	101.2	87	47	0.93	135	14.55	30 (7)	-	11 (2)	-
DN-1	45	103.8	88	51	0.93	124	16.09	28 (7)	-	10 (2)	3.4 (1)
DN-1	47	106.2	89	55	0.93	119	14.9	19 (7)	-	9 (2)	-
DN-1	49	108.5	90	56	0.94	108	13.18	16 (7)	-	12 (2)	-
DN-2	1	3.9	68	23	0.83	391	49.43	272 (7)	-	12 (1)	4 (0.6)
DN-2	3	11.6	69	28	0.83	376	47.27	223 (7)	-	14 (1)	3.5 (0.6)
DN-2	5	18.9	70	28	0.84	360	40.61	191 (6)	0.4 (0.2)	12 (1)	3.7 (0.6)
DN-2	7	26	71	29	0.84	349	44.45	186 (6)	0.6 (0.2)	13 (1)	5.5 (0.6)
DN-2	9	33.1	70	27	0.84	354	42.05	137 (5)	-	11 (1)	5.6 (0.6)
DN-2	11	40.1	71	24	0.85	346	40.07	124 (5)	-	9 (2)	4.8 (0.7)
DN-2	13	47.1	70	26	0.84	357	37.94	152 (6)	-	11 (1)	4.5 (0.7)
DN-2	15	53.9	73	26	0.85	323	34.66	121 (5)	-	10 (1)	4.2 (0.7)
DN-2	17	59.8	76	30	0.88	270	33.59	118 (5)	-	14 (1)	5.7 (0.7)
DN-2	19	65.4	75	30	0.87	293	42.6	114 (5)	-	8 (1)	5.8 (0.7)

Core	Depth		Physical Properties				Radionuclide activities				
	cm	kg m ⁻²	Water content	LOI	Fractional porosity	DBD	Sample mass (g)	²¹⁰ Pb	²⁴¹ Am	²¹⁴ Bi	¹³⁷ Cs
DN-2	21	71.3	75	26	0.87	296	42.2	104 (5)	-	14 (1)	7 (0.7)
DN-2	23	76.9	77	28	0.88	264	28.61	105 (5)	0.4 (0.2)	9 (2)	9.4 (0.9)
DN-2	25	82.4	76	26	0.87	281	30.69	111 (5)	0.8 (0.2)	11 (2)	11.2 (1)
DN-2	27	88.3	74	27	0.86	310	31.98	95 (5)	0.5 (0.2)	16 (2)	10.8 (0.9)
DN-2	29	94.4	74	26	0.86	304	31.64	81 (5)	-	15 (1)	11.4 (1)
DN-2	31	100.4	75	24	0.87	296	35.1	83 (5)	0.9 (0.2)	12 (1)	14.9 (1)
DN-2	33	106.5	73	21	0.86	315	37.44	90 (5)	0.7 (0.2)	17 (1)	19.9 (1)
DN-2	35	112.6	75	23	0.87	297	36.14	91 (5)	1.3 (0.3)	13 (1)	37.7 (1.3)
DN-2	37	118.5	75	24	0.87	286	29.99	87 (5)	1.6 (0.3)	17 (2)	52.5 (1.6)
DN-2	39	123.8	78	30	0.89	245	32.71	67 (5)	0.7 (0.2)	13 (1)	34.6 (1.3)
DN-2	41	129	76	29	0.87	278	41.66	60 (5)	-	16 (1)	15.4 (0.9)
DN-2	43	134.1	79	31	0.89	237	26.27	47 (5)	-	15 (2)	9.3 (0.9)
DN-2	45	139.1	77	28	0.88	261	32.82	51 (4)	-	16 (2)	4.7 (0.7)
DN-2	47	144.1	79	29	0.89	241	33.23	54 (4)	-	11 (1)	3.6 (0.6)
DN-2	49	149.3	77	27	0.88	270	35.72	63 (4)	-	13 (1)	2.6 (0.6)
DN-2	51	155.6	70	22	0.84	368	46.29	56 (5)	-	17 (1)	1.2 (0.6)
DN-2	53	163	69	20	0.84	372	48.76	48 (4)	0.4 (0.2)	17 (2)	1 (0.5)
DN-2	55	170.9	67	20	0.82	410	46.29	35 (5)	-	20 (1)	-
DN-2	57	178.6	70	23	0.84	362	47.63	41 (5)	-	18 (1)	1.1 (0.4)
DN-2	59	185.5	72	28	0.85	325	45	39 (5)	-	16 (1)	-
DN-3	1	2.7	77	29	0.88	269	40.3	180 (6)	-	12 (1)	4.3 (0.6)
DN-3	3	8.1	77	29	0.88	269	33.07	163 (6)	-	10 (1)	3.8 (0.6)
DN-3	5	13.7	74	29	0.86	297	39.88	145 (6)	-	10 (1)	4.2 (0.6)

Core	Depth		Physical Properties				Radionuclide activities				
	cm	kg m ⁻²	Water content	LOI	Fractional porosity	DBD	Sample mass (g)	²¹⁰ Pb	²⁴¹ Am	²¹⁴ Bi	¹³⁷ Cs
DN-3	7	19.9	73	28	0.86	316	41.69	132 (6)	-	13 (1)	5.5 (0.6)
DN-3	9	25.9	75	29	0.87	284	35.71	138 (6)	-	14 (1)	5.6 (0.6)
DN-3	11	31.5	75	29	0.87	283	32.29	110 (6)	-	14 (1)	7.6 (0.7)
DN-3	13	37.5	73	26	0.86	318	40.74	113 (6)	-	15 (1)	6.3 (0.7)
DN-3	15	44.1	72	25	0.85	333	39.07	113 (6)	-	16 (1)	7.1 (0.7)
DN-3	17	50.2	76	26	0.88	277	37.41	115 (6)	-	13 (1)	7.5 (0.7)
DN-3	19	55.7	76	27	0.87	280	38.33	100 (6)	-	12 (1)	6.2 (0.7)
DN-3	21	61.3	76	27	0.87	281	34.6	98 (6)	-	14 (1)	7.9 (0.8)
DN-3	23	67.2	74	25	0.87	300	38.26	113 (6)	-	14 (1)	11 (0.8)
DN-3	25	73.2	74	24	0.87	300	36.06	112 (6)	-	17 (1)	12.1 (0.8)
DN-3	27	79.3	73	23	0.86	317	41.78	86 (6)	-	18 (1)	14.3 (0.9)
DN-3	29	85.4	75	26	0.87	287	36.46	79 (6)	-	15 (1)	17.6 (1)
DN-3	31	91.9	70	23	0.84	363	48.39	100 (6)	-	19 (1)	19.1 (0.9)
DN-3	33	99.2	69	20	0.84	372	42.96	87 (6)	-	15 (2)	24.9 (1.1)
DN-3	35	106.5	70	21	0.84	357	45.03	91 (6)	1.5 (0.3)	17 (1)	47.8 (1.3)
DN-3	37	113.7	70	20	0.84	360	45.02	79 (6)	1.6 (0.3)	18 (1)	51.6 (1.4)
DN-3	39	121.1	68	18	0.84	385	44.04	78 (6)	-	19 (1)	29 (1.1)
DN-3	41	129.2	66	18	0.82	419	43.57	76 (6)	1.2 (0.3)	21 (1)	25.4 (1)
DN-3	43	137.9	64	17	0.81	449	48.21	81 (6)	-	20 (1)	14.6 (0.9)
DN-3	45	147	64	17	0.8	462	54.21	87 (6)	-	23 (2)	7.6 (0.6)
DN-3	47	156	65	16	0.81	446	49.75	75 (6)	-	21 (1)	3.2 (0.5)
DN-3	49	165	64	16	0.81	450	45.23	58 (6)	0.3 (0.2)	22 (1)	2.8 (0.4)
DN-3	51	173.7	66	17	0.82	417	47.77	70 (6)	-	19 (1)	0.9 (0.5)

Core	Depth		Physical Properties				Radionuclide activities				
	cm	kg m ⁻²	Water content	LOI	Fractional porosity	DBD	Sample mass (g)	²¹⁰ Pb	²⁴¹ Am	²¹⁴ Bi	¹³⁷ Cs
DN-3	53	181.7	69	18	0.84	383	44.52	64 (6)	-	17 (1)	1.1 (0.4)
DN-3	55	189	71	18	0.85	348	44.82	61 (6)	-	19 (1)	-
DN-3	57	196.5	67	16	0.83	405	48.25	60 (6)	-	22 (1)	-
DN-3	59	204.9	65	16	0.82	438	47.17	49 (6)	-	23 (1)	-
DN-3	61	214.4	61	14	0.79	508	53.58	55 (6)	-	22 (1)	-
DV-1	1	2.9	75	20	0.87	294	42.74	154 (6)	-	14 (1)	3.9 (0.6)
DV-1	3	9.2	72	25	0.85	334	45.19	171 (6)	-	15 (1)	4.1 (0.6)
DV-1	5	16	71	28	0.84	344	42.08	157 (6)	-	13 (1)	4.4 (0.6)
DV-1	7	23.1	69	25	0.84	368	48.12	133 (5)	-	19 (1)	5.1 (0.6)
DV-1	9	30.6	69	22	0.83	382	45.11	122 (6)	-	14 (1)	3.3 (0.6)
DV-1	11	37.8	72	22	0.85	338	56.91	137 (7)	-	17 (1)	5.9 (0.6)
DV-1	13	44.7	71	23	0.85	349	49.34	118 (6)	0.7 (0.3)	16 (1)	6.5 (0.6)
DV-1	15	51.3	73	27	0.86	313	48.61	124 (6)	-	14 (1)	10.6 (0.7)
DV-1	17	57.4	75	30	0.86	295	50.64	107 (6)	-	15 (1)	17.9 (0.8)
DV-1	19	63.5	73	27	0.86	313	57.4	129 (6)	-	18 (1)	29.3 (1)
DV-1	21	69.1	78	32	0.88	255	44.52	81 (5)	0.7 (0.2)	15 (1)	48.2 (1.3)
DV-1	23	73.8	81	35	0.9	208	29.65	54 (6)	0.5 (0.3)	13 (1)	41.3 (1.5)
DV-1	25	78.2	79	29	0.89	236	37.37	54 (6)	1.1 (0.3)	14 (1)	40.3 (1.3)
DV-1	27	82.8	80	26	0.9	221	34.73	58 (5)	0.8 (0.3)	13 (2)	31.3 (1.2)
DV-1	29	87.1	81	29	0.9	212	29.28	42 (6)	-	13 (1)	16.9 (1)
DV-1	31	91.7	78	23	0.89	247	38.15	60 (6)	-	17 (1)	5.7 (0.7)
DV-1	33	96.8	77	22	0.89	260	38.76	45 (4)	-	18 (1)	3.5 (0.6)
DV-1	35	102	77	24	0.88	267	48.01	76 (6)	-	14 (1)	2.4 (0.5)

Core	Depth		Physical Properties				Radionuclide activities				
	cm	kg m ⁻²	Water content	LOI	Fractional porosity	DBD	Sample mass (g)	²¹⁰ Pb	²⁴¹ Am	²¹⁴ Bi	¹³⁷ Cs
DV-1	37	106.9	80	29	0.9	222	36.8	55 (5)	-	12 (1)	-
DV-1	39	111.5	79	25	0.89	236	40.8	62 (6)	-	13 (1)	1.2 (0.5)
DV-1	41	117.1	73	21	0.86	323	45.59	46 (6)	-	16 (1)	-
DV-1	43	122.9	77	25	0.88	260	46.01	55 (5)	-	13 (1)	-
DV-1	45	127.9	79	24	0.89	241	35.6	34 (4)	-	13 (1)	-
DV-1	47	132.6	80	24	0.9	222	34.73	41 (4)	-	15 (1)	-
DV-1	49	138.2	71	17	0.85	345	47.21	41 (4)	-	18 (1)	-
DV-1	51	145.4	69	16	0.84	374	47.23	37 (4)	-	21 (1)	-
DV-1	53	152.9	69	17	0.84	377	42.23	36 (5)	-	18 (1)	-
DV-1	55	159.9	73	20	0.86	322	45.46	39 (4)	-	19 (1)	-
DV-1	57	166.1	75	20	0.87	297	44.87	36 (4)	-	19 (1)	-
DV-1	59	172.1	74	20	0.87	301	45.96	43 (4)	-	16 (1)	-
DV-1	61	178.1	74	19	0.87	304	-	-	-	-	-
DV-1	63	184.5	72	18	0.86	330	-	-	-	-	-
DV-1	65	191.3	70	18	0.85	355	-	-	-	-	-
DV-1	67	-	67	-	-	-	-	-	-	-	-
DV-1	69	-	66	-	-	-	-	-	-	-	-
DV-1	71	-	67	-	-	-	-	-	-	-	-
DV-1	73	-	67	-	-	-	-	-	-	-	-
DV-1	75	-	69	-	-	-	-	-	-	-	-
DV-2	1	3.7	69	21	0.84	373	40.8	90 (5)	-	33 (2)	3.2 (0.6)
DV-2	3	11.4	68	23	0.83	394	41.53	89 (5)	-	11 (1)	3.9 (0.6)
DV-2	5	19.7	65	22	0.81	431	40.69	81 (4)	-	23 (2)	3 (0.6)

Core	Depth		Physical Properties				Radionuclide activities				
	cm	kg m ⁻²	Water content	LOI	Fractional porosity	DBD	Sample mass (g)	²¹⁰ Pb	²⁴¹ Am	²¹⁴ Bi	¹³⁷ Cs
DV-2	7	28.4	65	22	0.81	442	45.06	82 (5)	-	15 (1)	3.3 (0.6)
DV-2	9	37.2	65	19	0.81	436	40.32	81 (4)	-	18 (2)	4.8 (0.7)
DV-2	11	45.8	65	20	0.81	430	58.91	89 (5)	-	19 (2)	4.2 (0.6)
DV-2	13	54.2	67	21	0.82	405	46.22	80 (4)	-	16 (2)	4.1 (0.7)
DV-2	15	62.2	68	20	0.83	396	46.85	78 (4)	-	14 (2)	3.6 (0.6)
DV-2	17	69.9	69	18	0.84	378	50.39	71 (4)	0.5 (0.2)	18 (2)	3.4 (0.7)
DV-2	19	77.4	69	19	0.84	372	51.68	73 (4)	-	19 (2)	3.8 (0.6)
DV-2	21	85.2	68	16	0.83	400	41.34	69 (4)	0.5 (0.2)	15 (2)	4.3 (0.7)
DV-2	23	93.3	67	17	0.82	413	39.94	68 (4)	-	16 (2)	4.4 (0.6)
DV-2	25	101.2	69	18	0.84	374	42.42	68 (4)	-	14 (1)	4.5 (0.6)
DV-2	27	108.5	70	20	0.84	361	51.14	67 (4)	-	20 (2)	3.4 (0.6)
DV-2	29	115.3	73	21	0.86	313	41.4	47 (4)	0.3 (0.1)	14 (2)	2.8 (0.6)
DV-2	31	121.2	76	25	0.88	280	40.78	61 (4)	-	12 (2)	3.6 (0.6)
DV-2	33	126.5	78	25	0.89	252	37.42	73 (4)	-	10 (2)	6.4 (0.7)
DV-2	35	131.5	78	26	0.89	245	35.1	76 (4)	-	13 (2)	11.2 (0.9)
DV-2	37	135.5	85	51	0.92	157	22.46	70 (5)	-	7 (2)	48.6 (1.8)
DV-2	39	138.7	85	45	0.92	161	28.23	71 (5)	-	9 (2)	106.9 (2.4)
DV-2	41	142.6	79	30	0.89	238	44.43	44 (4)	-	14 (1)	46.7 (1.4)
DV-2	43	147.6	78	31	0.88	255	36.57	41 (4)	-	13 (2)	11.2 (0.9)
DV-2	45	153.2	74	26	0.86	307	50.71	42 (4)	-	21 (2)	6.5 (0.7)
DV-2	47	160.1	69	20	0.83	383	49.43	36 (4)	0.6 (0.3)	21 (2)	2.3 (0.6)
DV-2	49	166.6	77	29	0.88	268	39.08	32 (4)	-	11 (2)	1.2 (0.6)
DV-2	51	172.2	75	28	0.87	294	45.05	30 (4)	-	15 (2)	-

Core	Depth		Physical Properties				Radionuclide activities				
	cm	kg m ⁻²	Water content	LOI	Fractional porosity	DBD	Sample mass (g)	²¹⁰ Pb	²⁴¹ Am	²¹⁴ Bi	¹³⁷ Cs
DV-2	53	177.9	76	29	0.87	274	37.95	19 (4)	-	16 (1)	-
DV-2	55	183.3	77	31	0.88	266	41.28	27 (3)	-	13 (1)	-
DV-2	57	188.5	78	31	0.88	251	35.83	20 (4)	-	17 (2)	2.6 (0.6)
DV-2	59	193.3	79	31	0.89	235	33.5	18 (4)	-	12 (2)	-
DV-3	1	1.7	84	49	0.91	168	20.4	176 (7)	-	7 (2)	3.5 (0.7)
DV-3	3	5.1	84	52	0.91	176	26.21	184 (7)	-	9 (1)	2.1 (0.7)
DV-3	5	8.7	84	43	0.91	179	25.21	169 (7)	0.5 (0.2)	7 (1)	2.8 (0.7)
DV-3	7	12.2	84	48	0.91	174	19.09	168 (7)	-	8 (2)	2.5 (0.9)
DV-3	9	16.2	79	42	0.88	230	21.87	130 (6)	-	12 (1)	4.7 (0.8)
DV-3	11	20.4	83	54	0.9	186	22.62	108 (5)	-	10 (2)	7.4 (0.8)
DV-3	13	23.5	88	67	0.93	122	14.52	60 (5)	0.6 (0.3)	6 (2)	6.9 (1.2)
DV-3	15	25.7	90	68	0.94	105	13.7	100 (6)	-	7 (2)	13.4 (1.3)
DV-3	17	28.7	82	60	0.89	192	29.49	203 (7)	2.3 (0.2)	6 (1)	71.3 (1.9)
DV-3	19	32.2	85	55	0.91	161	23.59	63 (5)	1.1 (0.2)	9 (1)	32.8 (1.4)
DV-3	21	35.2	87	54	0.93	134	15.74	52 (5)	-	11 (2)	17.6 (1.4)
DV-3	23	37.8	88	52	0.93	126	15.21	41 (6)	-	11 (2)	15.6 (1.4)
DV-3	25	40.2	88	47	0.94	123	17.14	31 (5)	-	11 (2)	19.3 (1.3)
DV-3	27	42.8	87	46	0.93	138	20.23	35 (5)	-	11 (2)	8.4 (1)
DV-3	29	45.6	87	51	0.93	138	18.77	32 (5)	-	11 (2)	4 (0.8)
DV-3	31	48.4	87	49	0.92	143	19.62	13 (4)	-	6 (2)	2.8 (0.8)
DV-3	33	51.3	86	54	0.92	145	24.45	14 (3)	-	7 (1)	-
DV-3	35	54.2	87	52	0.92	141	21.57	16 (4)	-	9 (1)	1.7 (0.7)
DV-3	37	57.2	85	51	0.91	162	27.21	9 (3)	-	5 (1)	-

Core	Depth		Physical Properties				Radionuclide activities				
	cm	kg m ⁻²	Water content	LOI	Fractional porosity	DBD	Sample mass (g)	²¹⁰ Pb	²⁴¹ Am	²¹⁴ Bi	¹³⁷ Cs
DV-3	39	60	89	58	0.93	121	17.13	18 (6)	-	7 (2)	2 (0.8)
DV-3	41	62.2	91	58	0.95	96	12.5	14 (5)	-	6 (2)	-
DV-3	43	-	90	-	-	-	-	-	-	-	-
DV-3	45	-	90	-	-	-	-	-	-	-	-
DV-3	47	-	91	-	-	-	-	-	-	-	-
DV-3	49	-	92	-	-	-	-	-	-	-	-
DV-3	51	-	83	-	-	-	-	-	-	-	-
DV-3	53	-	92	-	-	-	-	-	-	-	-
DV-3	55	-	90	-	-	-	-	-	-	-	-
DV-3	57	-	89	-	-	-	-	-	-	-	-
DV-3	59	-	88	-	-	-	-	-	-	-	-
MR-1	1	5	61	21	0.78	498	51.94	140 (5)	-	31 (2)	3.5 (0.6)
MR-1	3	15	61	23	0.78	503	48.61	118 (5)	-	26 (2)	4.2 (0.6)
MR-1	5	25.3	59	21	0.77	531	50.55	115 (5)	-	22 (2)	2.8 (0.6)
MR-1	7	36	59	23	0.77	534	52.48	112 (5)	-	26 (2)	4 (0.7)
MR-1	9	46.4	60	23	0.78	511	47.84	93 (5)	-	23 (2)	4.5 (0.6)
MR-1	11	56.8	60	21	0.77	524	55.12	92 (4)	-	29 (2)	4 (0.6)
MR-1	13	67.1	60	22	0.78	511	50.49	92 (4)	-	30 (2)	4.8 (0.6)
MR-1	15	77.5	60	21	0.77	524	49.01	78 (4)	-	27 (2)	5.9 (0.6)
MR-1	17	87.5	62	20	0.79	481	49.81	85 (5)	-	23 (2)	6.8 (0.7)
MR-1	19	97.5	60	18	0.78	512	52.21	77 (5)	-	28 (2)	5.8 (0.7)
MR-1	21	107.9	59	17	0.78	530	48.74	73 (5)	-	30 (2)	7.1 (0.8)
MR-1	23	118	62	17	0.79	483	47.53	80 (4)	-	28 (2)	9.4 (0.8)

Core	Depth		Physical Properties				Radionuclide activities				
	cm	kg m ⁻²	Water content	LOI	Fractional porosity	DBD	Sample mass (g)	²¹⁰ Pb	²⁴¹ Am	²¹⁴ Bi	¹³⁷ Cs
MR-1	25	127.5	64	18	0.8	462	46.08	67 (4)	-	24 (2)	9 (0.8)
MR-1	27	136.7	64	18	0.81	456	43.05	61 (5)	-	28 (2)	9.6 (0.8)
MR-1	29	146.1	62	17	0.79	486	50.04	61 (5)	-	30 (2)	10.8 (0.9)
MR-1	31	156.4	59	15	0.77	541	54.23	62 (5)	-	33 (2)	10.3 (0.8)
MR-1	33	167.4	57	15	0.76	567	51.85	68 (4)	0.4 (0.2)	34 (2)	14.6 (0.9)
MR-1	35	178.6	58	15	0.77	550	50.56	69 (4)	-	32 (2)	17.6 (1)
MR-1	37	189.4	59	15	0.78	531	50.02	61 (5)	0.4 (0.2)	33 (2)	19.4 (1)
MR-1	39	200.1	59	14	0.78	535	49.69	53 (4)	-	33 (2)	20.5 (1)
MR-1	41	210.6	60	14	0.78	518	48.62	57 (4)	-	30 (2)	25.8 (1.1)
MR-1	43	221	60	14	0.78	521	44.78	53 (5)	0.9 (0.3)	25 (2)	29.4 (1.2)
MR-1	45	231.7	59	13	0.77	547	44.62	57 (4)	0.4 (0.2)	27 (2)	30.8 (1.2)
MR-1	47	242.6	59	15	0.77	547	48.16	59 (4)	-	30 (2)	28.8 (1.1)
MR-1	49	253.8	57	13	0.77	567	47.65	57 (4)	-	29 (2)	22.4 (1)
MR-1	51	264.9	58	13	0.77	552	47.81	52 (4)	-	29 (2)	17.4 (1)
MR-1	53	275.3	62	13	0.8	486	45.37	58 (4)	-	30 (2)	20.4 (1)
MR-1	55	285	63	13	0.8	477	45.23	56 (4)	-	26 (2)	18.4 (1)
MR-1	57	294.6	62	13	0.8	489	41.87	47 (4)	-	27 (2)	13.9 (1)
MR-1	59	304.6	61	13	0.79	506	47.16	43 (4)	-	32 (2)	15.1 (0.9)
MR-1	61	314.5	62	14	0.8	490	41.31	42 (4)	-	28 (2)	16.5 (1.1)
MR-1	63	324.9	58	13	0.77	549	50.03	46 (4)	-	33 (2)	13.7 (0.8)
MR-1	65	335.6	60	14	0.78	521	52.91	57 (4)	-	32 (2)	14.8 (0.9)
MR-1	67	345.7	62	13	0.8	493	47.87	50 (4)	-	33 (2)	13.4 (0.9)
MR-1	69	355.8	60	14	0.79	515	49.26	46 (4)	-	29 (2)	10.2 (0.8)

Core	Depth		Physical Properties				Radionuclide activities				
	cm	kg m ⁻²	Water content	LOI	Fractional porosity	DBD	Sample mass (g)	²¹⁰ Pb	²⁴¹ Am	²¹⁴ Bi	¹³⁷ Cs
MR-1	71	366.4	59	13	0.78	542	50.97	41 (4)	-	30 (2)	9.4 (0.8)
MR-1	73	377.1	59	13	0.78	534	53.36	55 (4)	-	32 (2)	8.5 (0.8)
MR-2	1	3.2	73	24	0.86	319	26.5	116 (6)	-	20 (2)	3.1 (0.8)
MR-2	3	10.6	66	19	0.82	418	35.67	115 (5)	-	24 (2)	3.5 (0.7)
MR-2	5	18.9	66	19	0.82	416	47.15	119 (5)	-	25 (2)	2.7 (0.6)
MR-2	7	27	67	21	0.83	399	44.84	111 (5)	-	26 (2)	4.3 (0.6)
MR-2	9	34.7	70	25	0.84	365	39.24	58 (4)	-	22 (2)	5 (0.7)
MR-2	11	42.1	69	22	0.83	382	47.91	80 (4)	-	24 (2)	5.3 (0.7)
MR-2	13	50.3	65	19	0.81	434	48.26	112 (5)	-	24 (2)	7 (0.7)
MR-2	15	59.3	63	17	0.8	466	42.24	88 (5)	-	22 (2)	6 (0.7)
MR-2	17	68.9	61	16	0.79	496	48.49	78 (4)	-	28 (2)	5.3 (0.8)
MR-2	19	78.6	63	18	0.8	474	46.84	93 (5)	-	30 (2)	8.5 (0.8)
MR-2	21	88	64	17	0.8	461	52.51	94 (5)	-	28 (2)	8.8 (0.8)
MR-2	23	97.1	64	19	0.8	454	46.11	82 (5)	-	25 (2)	7.6 (0.8)
MR-2	25	105.9	66	17	0.82	420	45.37	76 (5)	-	25 (2)	10.3 (0.9)
MR-2	27	114.4	66	16	0.82	430	46.74	68 (5)	-	27 (2)	11.5 (0.8)
MR-2	29	123	65	17	0.81	438	44.5	83 (5)	-	28 (2)	9.6 (0.8)
MR-2	31	131.7	66	19	0.82	426	44.15	84 (5)	-	33 (2)	13.5 (0.9)
MR-2	33	141.3	59	15	0.78	531	49.59	78 (5)	-	37 (2)	12.1 (0.8)
MR-2	35	151.6	61	14	0.79	504	48.99	68 (5)	-	36 (2)	13.2 (0.8)
MR-2	37	161.8	60	14	0.79	517	49.46	73 (5)	-	38 (2)	15.2 (0.9)
MR-2	39	172.3	59	14	0.78	537	49.64	72 (5)	-	36 (2)	15.5 (0.9)
MR-2	41	182.9	60	14	0.79	514	49.64	78 (4)	-	42 (2)	17.9 (0.9)

Core	Depth		Physical Properties				Radionuclide activities				
	cm	kg m ⁻²	Water content	LOI	Fractional porosity	DBD	Sample mass (g)	²¹⁰ Pb	²⁴¹ Am	²¹⁴ Bi	¹³⁷ Cs
MR-2	43	193.5	59	13	0.77	547	52.58	67 (4)	0.3 (0.2)	38 (2)	18.4 (1)
MR-2	45	204.3	59	13	0.78	533	53.06	74 (4)	-	47 (2)	17.4 (1)
MR-2	47	214.9	60	13	0.78	530	49.58	57 (5)	-	40 (2)	25.3 (1.1)
MR-2	49	225.6	59	14	0.77	545	49.22	65 (4)	-	40 (2)	31.2 (1.2)
MR-2	51	236.4	60	13	0.78	530	48.7	64 (4)	-	40 (2)	34 (1.3)
MR-2	53	247	59	10	0.78	534	45.82	57 (4)	0.3 (0.2)	34 (2)	26.9 (1.2)
MR-2	55	257.5	60	10	0.79	516	49.06	63 (4)	-	41 (2)	24 (1.1)
MR-2	57	268.1	59	11	0.78	545	49.64	66 (4)	-	39 (2)	20 (1)
MR-2	59	279.4	57	12	0.76	576	47.21	57 (4)	-	39 (2)	19.6 (1)
MR-2	61	291	56	11	0.76	591	46.1	61 (4)	-	36 (2)	15.1 (1)
MR-2	63	303	55	12	0.75	611	53.4	53 (4)	-	32 (2)	15.8 (0.9)
MR-2	65	314.5	59	13	0.78	536	50.49	55 (4)	-	33 (2)	14.1 (0.9)
MR-2	67	325.1	60	13	0.78	522	50.95	53 (4)	-	34 (2)	15.1 (0.9)
MR-2	69	335.6	60	14	0.78	528	52.29	59 (4)	-	35 (2)	11.3 (0.8)
MR-2	71	346.1	60	13	0.78	528	51.97	49 (4)	-	35 (2)	10.7 (0.8)
MR-2	73	357.1	57	14	0.76	570	50	46 (4)	-	37 (2)	7.8 (0.8)
MR-2	75	368.3	59	14	0.77	546	50.87	53 (4)	0.3 (0.2)	36 (2)	6.1 (0.7)
MR-2	77	379.4	57	14	0.76	571	46.89	52 (4)	-	37 (2)	6.1 (0.7)
MR-3	1	4.1	67	17	0.83	407	48.23	149 (5)	-	47 (2)	5.6 (0.7)
MR-3	3	12.3	66	19	0.82	416	48.1	126 (5)	-	42 (2)	3.7 (0.7)
MR-3	5	21.2	63	15	0.8	477	53.25	149 (5)	-	58 (2)	4.7 (0.6)
MR-3	7	30.8	62	15	0.8	481	48.54	125 (5)	-	57 (2)	4.4 (0.7)
MR-3	9	40.4	63	16	0.8	477	55.18	118 (5)	0.3 (0.2)	57 (2)	4 (0.7)

Core	Depth		Physical Properties				Radionuclide activities				
	cm	kg m ⁻²	Water content	LOI	Fractional porosity	DBD	Sample mass (g)	²¹⁰ Pb	²⁴¹ Am	²¹⁴ Bi	¹³⁷ Cs
MR-3	11	50.2	61	14	0.79	503	47.79	96 (5)	-	49 (2)	4.1 (0.6)
MR-3	13	60.4	60	14	0.79	514	49.14	120 (5)	-	42 (2)	4 (0.6)
MR-3	15	70.3	62	15	0.8	484	49.61	121 (5)	-	47 (2)	5 (0.7)
MR-3	17	80.3	61	15	0.79	512	50.06	108 (5)	-	49 (2)	5 (0.7)
MR-3	19	90	64	16	0.81	458	47.34	107 (5)	-	46 (2)	5.8 (0.7)
MR-3	21	99.7	61	18	0.78	507	46.74	121 (5)	-	51 (2)	5.5 (0.7)
MR-3	23	110.3	58	14	0.77	552	52.22	106 (5)	-	52 (2)	4.8 (0.7)
MR-3	25	121.1	60	13	0.78	531	48.77	99 (5)	-	42 (2)	4.5 (0.6)
MR-3	27	131.3	62	15	0.79	492	50.92	93 (5)	-	49 (2)	3.5 (0.7)
MR-3	29	140.8	64	15	0.81	459	43.12	90 (5)	-	49 (2)	3.9 (0.7)
MR-3	31	150.5	61	14	0.79	505	50.03	94 (5)	-	51 (2)	4.7 (0.7)
MR-3	33	160.4	62	14	0.8	486	42.98	98 (5)	-	47 (2)	6 (0.7)
MR-3	35	170.1	62	16	0.8	483	49.52	93 (4)	-	51 (2)	5.5 (0.7)
MR-3	37	179.7	62	15	0.8	482	56.91	103 (5)	-	49 (2)	4.5 (0.6)
MR-3	39	189.2	63	14	0.8	470	51.24	97 (5)	-	50 (2)	5.8 (0.6)
MR-3	41	198.9	61	15	0.79	497	46.15	93 (5)	-	50 (2)	3.7 (0.7)
MR-3	43	208.5	63	14	0.81	465	49.68	92 (5)	-	39 (2)	4.5 (0.7)
MR-3	45	217.7	64	15	0.81	453	44.06	85 (5)	-	42 (2)	5.3 (0.7)
MR-3	47	226.6	65	17	0.81	441	45.21	80 (5)	-	40 (2)	5.5 (0.7)
MR-3	49	235.6	64	15	0.81	454	46.22	84 (5)	-	44 (2)	5.3 (0.7)
MR-3	51	244.9	63	14	0.8	476	47.92	91 (5)	-	47 (2)	5.5 (0.7)
MR-3	53	254.5	62	14	0.8	488	50.02	85 (5)	-	44 (2)	6.3 (0.7)
MR-3	55	264.2	63	13	0.8	477	44.48	92 (4)	-	46 (2)	7.6 (0.7)

Core	Depth		Physical Properties				Radionuclide activities				
	cm	kg m ⁻²	Water content	LOI	Fractional porosity	DBD	Sample mass (g)	²¹⁰ Pb	²⁴¹ Am	²¹⁴ Bi	¹³⁷ Cs
MR-3	57	274.2	60	13	0.78	520	45.57	92 (4)	-	50 (2)	5.9 (0.8)
MR-3	59	284.3	62	14	0.8	490	45.44	92 (5)	-	48 (2)	7.2 (0.7)
MR-3	61	293.6	65	16	0.81	441	43.4	85 (4)	-	49 (2)	7.7 (0.8)
MR-3	63	302.4	65	19	0.81	441	48.47	82 (5)	-	52 (2)	8.8 (0.8)
MR-3	65	312	60	13	0.79	517	55.8	81 (5)	-	58 (2)	7.1 (0.8)
MR-3	67	322.5	59	13	0.78	534	48.52	89 (5)	-	52 (2)	8.2 (0.8)
MR-3	69	333.7	56	12	0.76	586	47.01	77 (4)	-	51 (2)	8.5 (0.8)
MR-3	71	345.3	57	12	0.76	574	49.24	74 (5)	-	54 (2)	8.7 (0.8)
MR-3	73	356.8	57	12	0.76	580	51.24	76 (4)	-	51 (2)	10.1 (0.8)
MR-3	75	368.2	58	12	0.77	557	55.55	81 (5)	-	60 (2)	10.8 (0.8)
CC-1	1	3.6	70	29	0.83	362	27.74	428 (9)	-	14 (2)	3.3 (0.7)
CC-1	3	10.1	75	38	0.86	289	28.12	256 (7)	-	9 (1)	3.4 (0.7)
CC-1	5	16.2	73	36	0.85	319	39.22	394 (8)	-	14 (1)	4.1 (0.6)
CC-1	7	22.3	75	39	0.86	288	33.12	219 (6)	-	13 (1)	4.7 (0.7)
CC-1	9	27.3	81	49	0.89	212	25.6	117 (6)	-	10 (1)	4.7 (0.8)
CC-1	11	31.9	78	38	0.88	253	30.58	114 (6)	1 (0.3)	46 (2)	32 (1.3)
CC-1	13	36.7	80	41	0.89	222	25.87	84 (5)	0.5 (0.2)	8 (1)	15 (1)
CC-1	15	41.3	78	36	0.88	242	26.98	59 (5)	-	8 (1)	34.4 (1.4)
CC-1	17	49.4	58	16	0.76	563	64.38	191 (7)	1.5 (0.3)	31 (2)	40.7 (1.1)
CC-1	19	60.6	58	17	0.76	555	57.89	102 (5)	0.8 (0.3)	21 (1)	36.2 (1.1)
CC-1	21	70.8	63	18	0.8	465	58.38	102 (5)	-	23 (2)	16.1 (0.8)
CC-1	23	79.9	64	19	0.81	452	56.3	72 (5)	-	23 (1)	9.4 (0.7)
CC-1	25	88.8	65	19	0.81	435	52.16	42 (4)	-	20 (1)	5.5 (0.6)

Core	Depth		Physical Properties				Radionuclide activities				
	cm	kg m ⁻²	Water content	LOI	Fractional porosity	DBD	Sample mass (g)	²¹⁰ Pb	²⁴¹ Am	²¹⁴ Bi	¹³⁷ Cs
CC-1	27	97.1	68	21	0.83	398	46.94	50 (5)	-	20 (1)	2.4 (0.6)
CC-1	29	104.2	74	23	0.86	311	39.56	76 (5)	-	24 (2)	3.7 (0.6)
CC-1	31	110.4	73	22	0.86	314	34.3	60 (5)	-	24 (2)	1.8 (0.6)
CC-1	33	116.4	76	24	0.88	280	28.57	46 (4)	-	18 (2)	1.8 (0.7)
CC-1	35	122.6	71	22	0.85	344	42.5	42 (4)	-	16 (1)	-
CC-1	37	130.1	67	20	0.83	400	54.5	50 (5)	-	16 (1)	-
CC-1	39	137.9	69	20	0.83	383	48.27	45 (4)	-	17 (1)	-
CC-1	41	146.2	65	18	0.81	441	54.66	36 (4)	-	18 (1)	1.1 (0.5)
CC-2	1	3.6	70	29	0.84	357	38.04	298 (7)	-	13 (1)	3.3 (0.6)
CC-2	3	10.1	74	38	0.85	298	36.03	208 (7)	-	9 (1)	4.1 (0.6)
CC-2	5	16.1	74	39	0.85	298	42.55	195 (6)	0.4 (0.2)	9 (1)	3 (0.6)
CC-2	7	21.7	76	42	0.87	268	36.32	109 (5)	-	11 (1)	2.5 (0.6)
CC-2	9	26.5	81	52	0.89	210	25.19	105 (5)	-	8 (1)	2.7 (0.7)
CC-2	11	31	79	45	0.88	238	33.9	185 (6)	0.5 (0.2)	7 (1)	5.8 (0.7)
CC-2	13	35.8	78	42	0.88	245	29.01	147 (5)	0.6 (0.2)	8 (1)	12.9 (0.9)
CC-2	15	40.5	80	36	0.89	222	22.57	78 (5)	0.9 (0.2)	10 (2)	22.9 (1.3)
CC-2	17	47.8	61	16	0.79	504	56.42	123 (6)	1 (0.3)	24 (1)	40.5 (1.1)
CC-2	19	56.7	68	20	0.83	395	40.34	71 (5)	1.1 (0.2)	14 (1)	32.6 (1.3)
CC-2	21	65.2	64	19	0.8	455	51.87	52 (5)	-	21 (1)	19.5 (0.9)
CC-2	23	74.1	66	21	0.81	428	48.51	68 (5)	0.5 (0.2)	17 (1)	7.3 (0.6)
CC-2	25	82.8	65	21	0.81	439	49.91	73 (6)	-	18 (1)	2 (0.6)
CC-2	27	89.7	77	33	0.88	258	24.47	41 (4)	-	13 (2)	1.7 (0.9)
CC-2	29	94.7	78	31	0.89	244	22.63	32 (4)	-	10 (2)	-

Core	Depth		Physical Properties				Radionuclide activities				
	cm	kg m ⁻²	Water content	LOI	Fractional porosity	DBD	Sample mass (g)	²¹⁰ Pb	²⁴¹ Am	²¹⁴ Bi	¹³⁷ Cs
CC-2	31	99.5	79	32	0.89	233	22.68	34 (4)	-	12 (2)	-
CC-2	33	104.1	80	33	0.9	221	16.26	36 (6)	-	12 (2)	-
CC-2	35	108.4	81	31	0.9	217	25.89	39 (4)	-	10 (1)	-
CC-2	37	113.2	77	29	0.88	260	24.12	47 (5)	-	13 (2)	-
CC-2	39	118.2	79	30	0.89	239	28.9	38 (4)	-	11 (1)	-
CC-2	41	123.4	75	25	0.87	286	31.72	29 (4)	-	11 (1)	-
CC-2	43	-	67	-	-	-	-	-	-	-	-
CC-2	45	-	63	-	-	-	-	-	-	-	-
CC-2	47	-	64	-	-	-	-	-	-	-	-
CC-2	49	-	62	-	-	-	-	-	-	-	-
CC-2	51	-	64	-	-	-	-	-	-	-	-
CC-3	1	3.1	73	30	0.86	314	34.38	380 (8)	-	12 (1)	3.7 (0.5)
CC-3	3	9	76	40	0.86	274	36.84	100 (5)	-	10 (1)	3.8 (0.6)
CC-3	5	14.4	77	45	0.87	262	31.44	83 (5)	-	9 (1)	3.7 (0.5)
CC-3	7	19.3	79	46	0.88	231	27.37	57 (5)	-	7 (1)	2.3 (0.6)
CC-3	9	23.9	80	42	0.89	227	24.4	68 (6)	-	10 (1)	5.9 (0.8)
CC-3	11	28.6	79	38	0.88	241	28.93	130 (6)	-	11 (1)	8.8 (0.8)
CC-3	13	33.3	79	39	0.89	234	30.95	168 (7)	-	11 (1)	15 (1)
CC-3	15	38	79	34	0.89	231	28.21	105 (6)	0.7 (0.3)	12 (1)	28 (1.3)
CC-3	17	43	76	28	0.88	270	32.9	106 (6)	1.1 (0.3)	13 (1)	62.9 (1.6)
CC-3	19	48.8	73	23	0.86	314	36.04	83 (6)	1.1 (0.3)	15 (1)	49.6 (1.5)
CC-3	21	55.5	71	22	0.85	353	42.59	86 (6)	1.1 (0.3)	15 (1)	37.1 (1.3)
CC-3	23	62.9	68	23	0.83	392	44.45	72 (6)	0.6 (0.3)	19 (1)	16.6 (0.9)

Core	Depth		Physical Properties				Radionuclide activities				
	cm	kg m ⁻²	Water content	LOI	Fractional porosity	DBD	Sample mass (g)	²¹⁰ Pb	²⁴¹ Am	²¹⁴ Bi	¹³⁷ Cs
CC-3	25	71	67	18	0.82	413	46.88	50 (6)	-	18 (1)	8.3 (0.7)
CC-3	27	80	62	18	0.79	487	56.61	70 (6)	-	14 (1)	2.6 (0.5)
CC-3	29	89.7	62	18	0.79	483	57.01	51 (6)	-	19 (1)	1.7 (0.4)
CC-3	31	98.8	65	21	0.81	434	49.77	48 (5)	-	14 (1)	1.4 (0.4)
CC-3	33	106.6	71	23	0.85	346	40.17	34 (5)	-	15 (1)	-
CC-3	35	112.8	77	29	0.88	265	31.99	28 (5)	-	13 (1)	1 (0.5)
CC-3	37	118.9	71	21	0.85	351	41.55	40 (5)	-	15 (1)	-
CC-3	39	126.7	66	20	0.82	426	52.49	49 (6)	-	17 (1)	-
CC-3	41	135.9	61	18	0.79	496	55.96	29 (6)	-	17 (1)	-
IB-1	1	1.4	87	49	0.93	139	11.81	269 (7)	-	13 (2)	2.8 (0.9)
IB-1	3	4.4	84	61	0.9	167	20.14	119 (6)	-	6 (2)	-
IB-1	5	7.7	85	61	0.91	159	19.43	115 (6)	-	7 (2)	2.3 (0.8)
IB-1	7	10.7	87	91	0.89	137	17.07	91 (5)	-	6 (2)	-
IB-1	9	13.5	86	63	0.91	144	17.07	119 (6)	-	6 (2)	3.6 (0.9)
IB-1	11	16.4	86	59	0.92	145	17.55	113 (6)	-	6 (2)	5 (1)
IB-1	13	19.4	85	52	0.91	159	20.34	129 (6)	-	7 (2)	21.4 (1.4)
IB-1	15	22.9	83	48	0.9	189	24.96	168 (6)	1.6 (0.3)	8 (1)	30.9 (1.4)
IB-1	17	27	80	44	0.89	224	32.14	161 (5)	1.1 (0.3)	7 (1)	16.5 (1)
IB-1	19	32	76	39	0.87	271	31.93	99 (5)	-	10 (1)	11.7 (0.9)
IB-1	21	36.8	81	47	0.89	211	25.56	44 (4)	-	9 (2)	7.9 (1)
IB-1	23	40.8	83	43	0.9	189	23.47	34 (4)	-	6 (2)	7.6 (1)
IB-1	25	44.6	83	39	0.91	187	19.61	23 (5)	-	9 (2)	7.2 (1.1)
IB-1	27	48.2	84	36	0.91	179	20.26	21 (5)	-	14 (2)	11.6 (1.1)

Core	Depth		Physical Properties				Radionuclide activities				
	cm	kg m ⁻²	Water content	LOI	Fractional porosity	DBD	Sample mass (g)	²¹⁰ Pb	²⁴¹ Am	²¹⁴ Bi	¹³⁷ Cs
IB-1	29	51.8	83	34	0.91	183	22	30 (4)	-	12 (2)	8.7 (1)
IB-1	31	55.6	83	38	0.91	188	19.87	38 (5)	-	6 (2)	6.5 (0.9)
IB-1	33	59.5	81	35	0.9	207	24.04	26 (4)	-	10 (2)	2.6 (0.8)
IB-1	35	63.6	82	33	0.91	201	24.2	20 (4)	-	10 (2)	4.2 (0.9)
IB-1	37	68.3	76	23	0.88	276	33.35	22 (4)	-	11 (2)	2.1 (0.6)
IB-1	39	73.4	79	32	0.89	232	24.76	27 (4)	-	12 (2)	3.4 (0.8)
IB-1	41	78.2	78	34	0.89	242	32.55	22 (4)	-	10 (1)	3.2 (0.7)
IB-1	43	83.1	78	36	0.88	250	34.58	14 (4)	-	9 (1)	3.7 (0.6)
IB-1	45	88.2	77	34	0.88	262	31.81	-	-	8 (1)	3.1 (0.7)
IB-2	1	1.2	89	60	0.93	120	17.22	365 (11)	-	47 (3)	6.5 (1.2)
IB-2	3	3.7	88	68	0.92	125	12.5	106 (7)	-	-	-
IB-2	5	6.2	88	67	0.92	126	13.73	100 (7)	-	-	-
IB-2	7	8.6	88	68	0.92	122	18.7	261 (8)	0.4 (0.2)	3 (1)	2 (0.7)
IB-2	9	11.1	88	65	0.92	128	23.4	159 (6)	0.5 (0.2)	2 (1)	3.2 (0.7)
IB-2	11	13.9	86	59	0.92	145	15.45	191 (8)	1.5 (0.3)	4 (2)	16.6 (1.6)
IB-2	13	17.1	83	52	0.9	181	20.2	221 (7)	2.2 (0.3)	7 (1)	51.5 (1.9)
IB-2	15	21.1	80	48	0.89	218	28.64	216 (7)	1.4 (0.2)	9 (1)	13.8 (0.9)
IB-2	17	25.5	80	45	0.89	217	22.63	121 (7)	-	7 (2)	9.6 (1)
IB-2	19	29.5	83	43	0.9	188	20.75	77 (5)	-	9 (2)	9.3 (1)
IB-2	21	33.1	84	44	0.91	175	22.27	66 (6)	-	8 (1)	8.6 (1)
IB-2	23	36.9	82	42	0.9	204	38.33	38 (4)	-	8 (1)	5.6 (0.7)
IB-2	25	41.5	77	34	0.88	258	29.64	43 (4)	-	15 (1)	6.3 (0.8)
IB-2	27	47.3	73	28	0.86	313	41.79	32 (5)	-	14 (1)	4.8 (0.7)

Core	Depth		Physical Properties				Radionuclide activities				
	cm	kg m ⁻²	Water content	LOI	Fractional porosity	DBD	Sample mass (g)	²¹⁰ Pb	²⁴¹ Am	²¹⁴ Bi	¹³⁷ Cs
IB-3	1	1.9	82	66	0.88	194	15.51	467 (12)	-	8 (2)	-
IB-3	3	5.6	84	73	0.89	169	15.37	220 (9)	-	9 (2)	-
IB-3	5	9	84	74	0.89	169	20.18	204 (8)	-	4 (1)	1.6 (0.7)
IB-3	7	12.9	79	74	0.85	223	20.35	373 (9)	-	3 (1)	6.4 (0.8)
IB-3	9	17.1	82	70	0.88	195	22.32	215 (7)	1.2 (0.3)	7 (1)	32.3 (1.5)
IB-3	11	21.6	76	68	0.84	261	21.48	131 (6)	2.1 (0.3)	6 (1)	38.1 (1.6)
IB-3	13	25.9	84	60	0.9	168	16.5	97 (7)	0.7 (0.3)	5 (2)	6.4 (1.1)
IB-3	15	29.3	85	52	0.91	165	19.96	67 (6)	-	4 (2)	5.7 (0.8)
IB-3	17	32.6	84	46	0.91	171	15.16	64 (7)	-	12 (2)	4.8 (0.9)
IB-3	19	37.1	76	27	0.87	282	29.56	59 (5)	-	23 (2)	4.3 (0.7)
IB-3	21	42.4	78	31	0.89	246	28.65	68 (6)	-	21 (2)	5.4 (0.7)
IB-3	23	48.2	72	19	0.86	336	34.42	48 (5)	-	26 (2)	3.5 (0.6)
IB-3	25	54.7	74	20	0.87	311	31.58	38 (5)	-	23 (2)	3.6 (0.6)
IB-3	27	60.3	78	28	0.89	250	29.65	38 (5)	-	28 (2)	2.9 (0.6)
IB-3	29	65.9	74	29	0.86	307	43.69	31 (5)	-	17 (1)	3.9 (0.5)
IB-3	31	71.8	75	26	0.87	286	29.22	41 (5)	-	17 (2)	3 (0.6)
IB-3	33	76.6	82	38	0.91	195	21.55	13 (6)	-	13 (2)	2.5 (0.7)
IB-3	35	80.2	85	45	0.92	164	17.73	20 (6)	-	12 (2)	3.6 (0.8)
IB-3	37	83.9	82	34	0.9	200	23.38	22 (6)	-	12 (2)	4.6 (0.7)
IB-3	39	88	81	31	0.9	216	25.67	21 (5)	-	10 (1)	4.8 (0.7)
IB-3	41	92.5	79	30	0.89	233	31.66	21 (5)	-	13 (1)	4.1 (0.7)
RC-1	1	1.7	84	50	0.91	175	23.37	393 (8)	-	9 (2)	8 (1)
RC-1	3	5.3	84	54	0.9	177	23.04	336 (8)	-	11 (2)	8 (1)

Core	Depth		Physical Properties				Radionuclide activities				
	cm	kg m ⁻²	Water content	LOI	Fractional porosity	DBD	Sample mass (g)	²¹⁰ Pb	²⁴¹ Am	²¹⁴ Bi	¹³⁷ Cs
RC-1	5	8.8	84	54	0.9	174	23.42	345 (8)	-	8 (2)	7.9 (1)
RC-1	7	12.1	85	56	0.91	158	21.51	187 (7)	-	7 (2)	15 (1.2)
RC-1	9	15.1	87	54	0.92	142	20.58	131 (6)	-	9 (2)	45.5 (1.9)
RC-1	11	17.9	87	54	0.93	135	20.2	106 (6)	-	10 (2)	69 (2.2)
RC-1	13	20.6	87	52	0.93	134	16.84	103 (6)	2.9 (0.4)	9 (2)	39.8 (1.9)
RC-1	15	23.1	88	51	0.93	123	15.09	70 (6)	1.4 (0.4)	10 (2)	16 (1.7)
RC-1	17	25.4	90	56	0.94	102	12.16	59 (6)	-	-	11.6 (1.5)
RC-1	19	27.3	91	58	0.95	90	11.23	64 (7)	-	10 (2)	8.3 (1.4)
RC-1	21	29.3	90	54	0.94	108	12.65	72 (7)	-	6 (2)	6.6 (1.4)
RC-1	23	31.7	87	50	0.93	134	17.2	79 (6)	-	10 (2)	6.7 (1)
RC-1	25	34.9	83	38	0.91	184	27.38	51 (4)	-	10 (2)	2.8 (0.7)
RC-1	27	39.1	79	34	0.89	236	36.5	34 (4)	-	14 (2)	1.3 (0.7)
RC-1	29	43.9	78	36	0.88	248	37.65	31 (4)	-	16 (2)	-
RC-1	31	49.2	75	36	0.86	284	39.23	29 (4)	-	19 (1)	1.3 (0.6)
RC-1	33	55.2	73	34	0.85	312	38.06	25 (4)	-	17 (2)	1.6 (0.6)
RC-1	35	61.3	74	37	0.86	294	44.16	16 (3)	-	13 (1)	-
RC-1	37	66.7	78	40	0.88	250	35.42	22 (3)	-	15 (2)	-
RC-1	39	71.9	76	35	0.87	276	39.77	27 (4)	-	14 (2)	-
RC-1	41	78.4	70	26	0.84	367	51.38	17 (4)	-	22 (2)	-
RC-2	1	1.3	87	56	0.93	133	17.35	464 (10)	-	9 (2)	11.4 (1.4)
RC-2	3	4	88	58	0.93	129	15.61	429 (10)	-	-	10 (1.2)
RC-2	5	6.5	88	60	0.92	130	19.22	375 (9)	-	5 (2)	21.4 (1.5)
RC-2	7	9.1	88	61	0.93	126	15.68	402 (10)	2.5 (0.5)	11 (2)	39.6 (2)

Core	Depth		Physical Properties				Radionuclide activities				
	cm	kg m ⁻²	Water content	LOI	Fractional porosity	DBD	Sample mass (g)	²¹⁰ Pb	²⁴¹ Am	²¹⁴ Bi	¹³⁷ Cs
RC-2	9	11.6	88	61	0.93	122	14.31	341 (9)	2 (0.5)	6 (2)	46.4 (2.2)
RC-2	11	14.1	88	60	0.93	126	11.41	280 (10)	1.9 (0.6)	8 (2)	34.1 (2.3)
RC-2	13	16.6	88	61	0.93	123	14.87	219 (8)	2.2 (0.4)	7 (2)	36.1 (2)
RC-2	15	19	88	67	0.92	125	13.63	164 (7)	1.8 (0.4)	8 (2)	27.9 (1.8)
RC-2	17	21.7	87	44	0.93	139	18.42	86 (5)	-	6 (2)	9.1 (1.1)
RC-2	19	24.6	86	54	0.92	151	20.85	70 (4)	-	8 (2)	9.7 (0.9)
RC-2	21	27.9	83	49	0.9	183	23.91	64 (4)	-	7 (2)	6.4 (0.8)
RC-2	23	32.1	79	40	0.88	239	30.68	28 (4)	-	12 (2)	2.5 (0.6)
RC-2	25	37.1	77	38	0.87	259	31.69	27 (4)	-	15 (1)	2.4 (0.6)
RC-2	27	42.5	76	36	0.87	274	34.47	31 (4)	-	12 (2)	-
RC-2	29	47.9	76	38	0.87	267	34.52	28 (4)	-	14 (1)	1.4 (0.6)
RC-2	31	53.1	77	42	0.87	254	41.55	24 (3)	-	11 (1)	1.6 (0.5)
RC-2	33	58.4	76	38	0.86	279	40.65	28 (4)	-	14 (1)	1.2 (0.5)
RC-2	35	64	75	40	0.86	281	40.96	28 (4)	-	14 (1)	1.4 (0.5)
RC-2	37	70.4	70	35	0.83	353	53.18	22 (4)	-	17 (1)	1.4 (0.4)
RC-2	39	79	60	21	0.78	511	62.19	29 (4)	-	26 (2)	-
RC-2	41	89.5	59	17	0.77	536	59.37	32 (4)	-	24 (2)	-
RC-2	43	98.6	69	23	0.83	380	52.86	19 (4)	-	17 (2)	1.1 (0.4)
RC-2	45	106	70	23	0.84	359	44.81	19 (4)	-	19 (2)	-
RC-2	47	114	65	19	0.81	440	54.65	27 (4)	0.3 (0.1)	25 (2)	-
RC-2	49	122.7	66	20	0.81	428	48.74	21 (4)	-	22 (2)	-
RC-2	51	131.5	64	19	0.81	454	46.81	20 (4)	-	21 (2)	-
RC-2	53	140.7	63	19	0.8	463	55.86	20 (4)	-	21 (2)	-

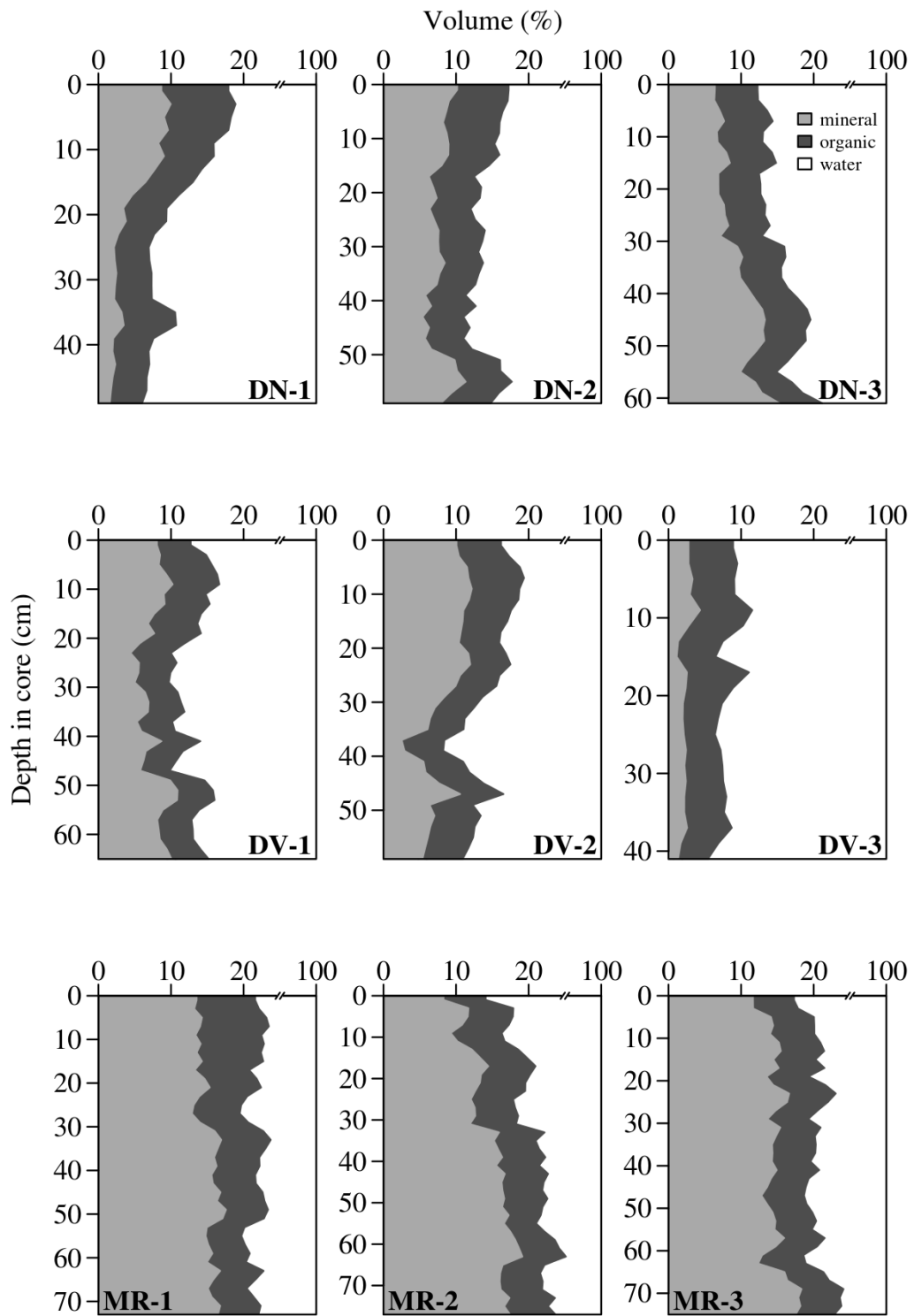
Core	Depth		Physical Properties				Radionuclide activities				
	cm	kg m ⁻²	Water content	LOI	Fractional porosity	DBD	Sample mass (g)	²¹⁰ Pb	²⁴¹ Am	²¹⁴ Bi	¹³⁷ Cs
RC-2	55	-	66	-	-	-	-	-	-	-	-
RC-2	57	-	64	-	-	-	-	-	-	-	-
RC-2	59	-	66	-	-	-	-	-	-	-	-
RC-2	61	-	69	-	-	-	-	-	-	-	-
RC-2	63	-	61	-	-	-	-	-	-	-	-
RC-3	1	1.4	87	63	0.92	141	16.17	355 (9)	-	14 (2)	4 (1)
RC-3	3	4.2	87	60	0.92	140	11.95	525 (12)	-	8 (3)	8.6 (1.3)
RC-3	5	7	87	63	0.92	139	13.72	472 (11)	-	10 (3)	9.2 (1.5)
RC-3	7	9.7	87	61	0.92	135	12.05	484 (12)	0.5 (0.3)	10 (3)	12.3 (1.5)
RC-3	9	12.4	88	66	0.92	127	11.1	334 (11)	0.6 (0.3)	7 (3)	12.8 (1.6)
RC-3	11	14.9	88	61	0.93	125	13.48	381 (10)	-	13 (3)	24.1 (1.8)
RC-3	13	17.4	88	61	0.92	129	15.58	254 (8)	1.9 (0.5)	9 (3)	71.5 (2.5)
RC-3	15	20	87	58	0.92	134	11.46	191 (9)	4.1 (0.6)	-	70 (2.9)
RC-3	17	22.7	87	59	0.92	135	19.52	119 (6)	1.3 (0.4)	11 (2)	20.8 (1.4)
RC-3	19	25.5	86	60	0.92	145	14.93	103 (6)	-	7 (3)	6.9 (1.2)
RC-3	21	28.8	83	46	0.9	186	18.52	52 (5)	-	19 (2)	4.8 (1)
RC-3	23	32.8	81	43	0.89	211	25.71	39 (4)	-	12 (2)	2.8 (0.7)
RC-3	25	37.4	78	36	0.88	246	28.41	32 (4)	-	17 (2)	3.1 (0.6)
RC-3	27	42.5	77	36	0.87	265	30.58	29 (4)	-	15 (2)	2.6 (0.6)
RC-3	29	47.7	77	36	0.87	261	32.66	24 (3)	-	15 (2)	1.4 (0.7)
RC-3	31	53	77	35	0.87	266	30.73	19 (3)	-	18 (2)	1.8 (0.6)
RC-3	33	59.5	68	25	0.83	382	48.3	13 (3)	-	20 (2)	1.7 (0.5)
RC-3	35	68.4	61	18	0.78	507	52.48	18 (4)	-	23 (2)	1.1 (0.5)

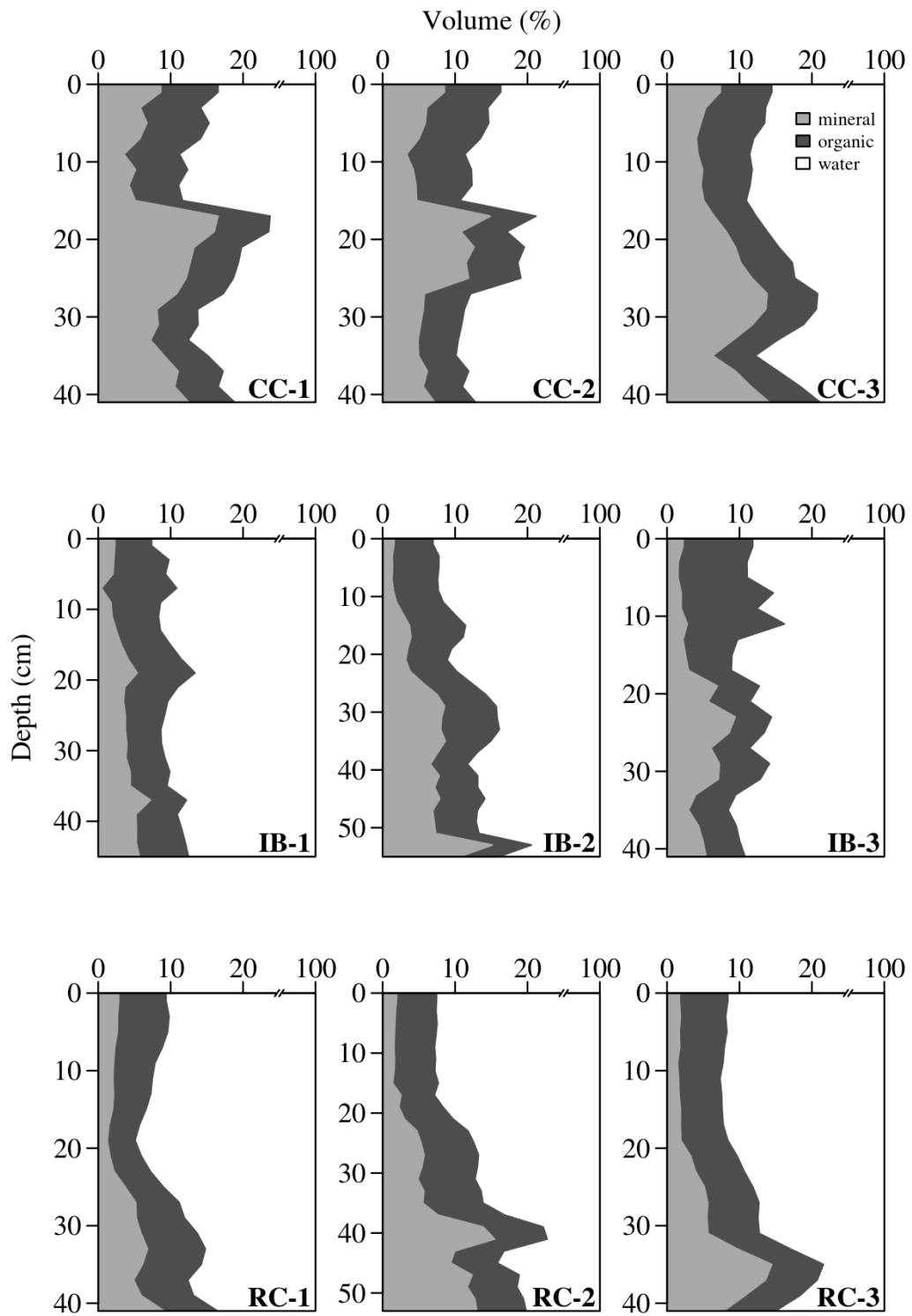
Core	Depth		Physical Properties				Radionuclide activities				
	cm	kg m ⁻²	Water content	LOI	Fractional porosity	DBD	Sample mass (g)	²¹⁰ Pb	²⁴¹ Am	²¹⁴ Bi	¹³⁷ Cs
RC-3	37	78.3	62	19	0.79	484	55.3	20 (4)	-	24 (2)	-
RC-3	39	87.3	66	24	0.82	415	49.04	17 (4)	-	21 (2)	1.3 (0.5)
RC-3	41	94.7	72	29	0.85	327	39.85	23 (4)	-	19 (2)	-

Appendix B

SOIL VOLUME PROFILES

Soil volume composition profiles for the eighteen marsh cores collected in this study. Note the broken scale on the horizontal axis.





Appendix C

RADIONUCLIDE PROFILES

Profiles of ^{210}Pb and ^{214}Bi , excess ^{210}Pb ($^{210}\text{Pb}_u$), and ^{137}Cs and ^{241}Am for the eighteen marsh cores in this study. Excess ^{210}Pb activities were linearly extrapolated for those cores that did not extend past the maximum penetration of $^{210}\text{Pb}_u$.

